Structural and Mechanistic Studies on *N*-Hydroxylating Monooxygenases Involved in Siderophore Biosynthesis

Reeder McNeil Robinson

Dissertation submitted to the faculty of the Virginia Polytechnic Institute and State University in partial fulfillment of the requirements for the degree of

Doctor of Philosophy
In
Biochemistry

Pablo Sobrado, Chair
David R. Bevan
Florian D. Schubot
Robert H. White

March 24, 2015
Blacksburg, VA

Keywords: flavin-dependent monooxygenases, *N*-hydroxylating, C4a-hydroperoxyflavin, siderophore, enzyme mechanism, X-ray crystallography

Structural and Mechanistic Studies on *N*-Hydroxylating Monooxygenases Involved in Siderophore Biosynthesis

Reeder McNeil Robinson

ABSTRACT

N-Hydroxylating monooxygenases (NMOs) are flavin dependent enzymes that primarily catalyze the hydroxylation of L-ornithine or L-lysine. This is the first, committed step to siderophore biosynthesis. Pathogenic microbes including *Aspergillus fumigatus* and *Mycobacterium tuberculosis* secrete these low molecular weight compounds in order to uptake Fe^{III} from their hosts for their metabolic needs when establishing infection. Therefore, members of this family of enzymes represent novel drug targets for the development of antibiotics. Here, we present the detailed functional and structural analysis of the L-ornithine monooxygenase SidA from *Aspergillus fumigatus* and the L-lysine monooxygenases MbsG from *Mycobacterium smegmatis* and NbtG from *Nocardia farcinica*. The detailed chemical mechanism for flavin oxidation in SidA was elucidated for formation of the C4a-hydroperoxyflavin, deprotonation of L-ornithine, and for the chemical steps of hydrogen peroxide elimination and water elimination. This was performed through a combination of kinetic isotope effect, pH, and density functional theory studies. Also, important residues involved in substrate binding and catalysis were characterized using site-directed mutagenesis for both SidA and NbtG. These include residues involved in coenzyme selectivity, substrate binding, and residues important in C4a-hydroperoxyflavin stabilization and flavin oxidation. The kinetic mechanisms of the L-lysine monooxygenases MbsG and NbtG were characterized which show unique differences with SidA. These include differences in coenzyme selectivity, and C4a-

hydroperoxyflavin stabilization. Lastly, the three-dimensional structure of NbtG was solved using X-ray crystallography which is the first structure of a lysine monooxygenase. The structure shows the NADPH-binding domain is rotated ~30 º relative to the FAD-binding domain which occludes $NADP^+$ binding in NbtG. Unlike SidA, NbtG does not stabilize a C4a-hydroperoxyflavin and this occlusion observed in the structure might explain this difference. This highlights both the structural and mechanistic diversities among NMOs and the data presented here provides valuable information for the future development of specific inhibitors of NMOs.

ACKNOWLEDGEMENTS

I would like to thank the many people who have helped me over the years as I pursued my Ph.D. I would like to first thank my advisor, Dr. Pablo Sobrado, who guided me along my research path as a graduate student and gave me the opportunity to flourish in his laboratory. I will be forever grateful to him in facilitating my development as a scientist. I would also like to thank my undergraduate mentor Wyatt Chocklett; without his time and patience in my training I would not be in the position where I am today. I would also like to thank the many lab members who contributed to my work and provided advice including, Dr. Michelle Oppenheimer, Dr. Jun Qi, Dr. Karina Kizjakina, Dr. Yumin Qi, Dr. Isabel da Fonseca, Dr. Somaye Badieyan, Dr. Elvira Romero, Dr. Julia Martin del Campo, Dr. Nancy Vogelaar, Mike Fedkenheuer, Nick Keul, Carolyn Shirey, Pedro Rodriguez, Catherine Klancher, and Jacob Ellerbrock. I would also like to thank my committee members Dr. David Bevan, Dr. Florian Schubot, and Dr. Robert White for the time they have provided over the years and their willingness to help me. My work would not be as comprehensive and detailed without the help of our collaborators Dr. Andrea Mattevi, Dr. Claudia Binda, and Dr. Stefano Franceschini. I am very appreciative for their generous contributions of their time and efforts.

TABLE OF CONTENTS

LIST OF FIGURES

LIST OF SCHEMES

LIST OF TABLES

ATTRIBUTIONS

Several chapters of this dissertation were done in collaboration with others both in research and writing. The contributing coauthors include: Associate Professor Pablo Sobrado and Dr. Somaye Badieyan from the Department of Biochemistry at Virginia Tech; Dr. Andrea Mattevi and Dr. Claudia Binda from the Department of Biology and Biotechnology at the University of Pavia. Each chapter explains the specific contributions of each collaborator for that section. Each published chapter has the original work cited. All work on this thesis, unless noted, is my own.

CHAPTER 1

Introduction

Flavin-dependent monooxygenases are a family of enzymes that can either perform the electrophilic or nucleophilic oxygenation of substrates through generation of a C4a-hydroperoxyflavin or C4a-peroxyflavin, respectively [1]. This family catalyzes a wide range of reactions including regioselective hydroxylations and enantioselective sulfoxidations [2]. One subclass of the flavin monooxygenase family is the Class B monooxygenases which include the flavin-containing monooxygenases, Baeyer-Villiger monooxygenases, and the microbial *N*-hydroxylating monooxygenases. The microbial *N*-hydroxylating monooxygenases (NMOs) perform the hydroxylation of long chain amines including L-ornithine and L-lysine which is the first step in hydroxamate-containing siderophore biosynthesis [3, 4]. Hydroxamate-containing siderophores are essential for Fe^{III} uptake in a number of pathogenic organisms such as *Aspergillus fumigatus*, *Pseudomonas aeruginosa*, and *Mycobacterium tuberculosis* among others and are virulence factors [3, 5, 6]. Therefore, NMOs are potential drug targets as humans acquire Fe^{III} through their diet and do not possess similar enzymes. This dissertation reviews the literature on NMOs and their roles in virulence and presents structural and mechanistic studies on the L-ornithine monooxygenase SidA from *Aspergillus fumigatus* and the L-lysine monooxygenases NbtG from *Nocardia farcinica* and MbsG from *Mycobacterium smegmatis*.

Chapter 2 introduces NMOs and how they are involved in iron uptake. This starts with an introduction on how iron is an essential, but scarce nutrient and then highlights how microbes overcome this thermodynamic barrier through the biosynthesis of siderophores which have a very high affinity for Fe^{III}. Then, the catalytic cycle of NMOs is discussed along with their three-dimensional structure. This is tied in with their substrate specificity and the mechanism by which

they stabilize a C4a-hydroperoxyflavin. This chapter is then concluded by discussion of a high-throughput screening assay developed by our lab to identify inhibitors of NMOs.

Chapters 3 and 4 focus on the chemical steps of flavin oxidation in the L-ornithine monooxygenase SidA. First, we show that the C4a-hydroperoxyflavin forms first through a proton transfer from the 2'-OH of the nicotinamide ribose of $NADP^+$. L-Ornithine then binds in its deprotonated form through an altered pK_a value for the N^5 in the active site of SidA which allows for electrophilic oxygenation. The resulting C4a-hydroxyflavin is then dehydrated through a single proton transfer from the N5 of the flavin, consistent with the chemical mechanism for hydrogen peroxide elimination.

Chapters 5 – 7 highlight key residues in SidA involved in substrate binding and catalysis. Arg279 was determined to be the residue that provides selectivity for NADPH over NADH. Lys107, Asn293, Asn323, and Ser469 were determined to all coordinate binding of ornithine. Asn323 was also determined to help regulate NADP(H) sliding in the active site, which is important for its role as both a source of a hydride equivalent and to provide stabilizing interactions to the C4a-hydroperoxyflavin. Finally, Met101, Gln102, and Arg144 were all determined to be important for flavin oxidation. This includes proper positioning of the isoalloxazine ring of the flavin, stabilization of the C4a-hydroperoxyflavin, and facilitating proton transfer in water elimination.

Chapters 8 – 10 provide mechanistic and structural characterization for the L-lysine monooxygenases MbsG and NbtG. These chapters highlight the differences between the L-lysine monooxygenases and the L-ornithine monooxygenases where they are non-selective between NADPH and NADH, have different rate-limiting steps than SidA and other Class B monooxygenases, and do not stabilize C4a-hydroperoxyflavins. Also, the first three-dimensional

structure of an L-lysine monooxygenase, NbtG, was solved. This structure shows unique differences with SidA where the NADPH-binding domain is rotated so that $NADP^+$ cannot adopt the necessary conformation to provide interactions to stabilize a C4a-hydroperoxyflavin.

The work presented here is important for understanding the chemical mechanism of flavin oxidation in NMOs, determining important residues involved in substrate binding and catalysis, and for providing the first detailed structural and mechanistic analysis of L-lysine monooxygenases. This work will aid in the rational design of inhibitors of NMOs which will lead to new antibiotics against diseases such as aspergillosis and tuberculosis.

1. References

[1] V. Massey, J Biol Chem 269 (1994) 22459-22462.
[2] W.J. van Berkel, N.M. Kamerbeek, M.W. Fraaije, J Biotechnol 124 (2006) 670-689.
[3] A.H. Hissen, A.N. Wan, M.L. Warwas, L.J. Pinto, M.M. Moore, Infect Immun 73 (2005) 5493-5503.
[4] M.D. McMahon, J.S. Rush, M.G. Thomas, J Bacteriol 194 (2012) 2809-2818.
[5] H. Takase, H. Nitanai, K. Hoshino, T. Otani, Infect Immun 68 (2000) 1834-1839.
[6] J.J. De Voss, K. Rutter, B.G. Schroeder, H. Su, Y. Zhu, C.E. Barry, 3rd, Proc Natl Acad Sci U S A 97 (2000) 1252-1257.

CHAPTER 2

Flavin-dependent monooxygenases in siderophore biosynthesis

Reprinted from Handbook of Flavoproteins, Robinson, R. M., and Sobrado, P. "Flavin-dependent monooxygenases in siderophore biosynthesis" *Handbook of Flavoproteins: Complex Flavoproteins, Dehydrogenases and Physical Methods*. Hille, R., Miller, S., and Palfey, B. (eds.) 2013 Vol 2: 29-50.

Author Contributions:
Reeder M. Robinson wrote the chapter.

Pablo Sobrado oversaw and directed the writing.

Abstract

Microbial *N*-hydroxylating monooxygenases (NMOs) are a class of flavin-dependent enzymes involved in the biosynthesis of hydroxamate-containing siderophores. These flavoenzymes catalyze the NADPH- and oxygen-dependent *N*-hydroxylation of a narrow group of substrates that include L-ornithine, L-lysine, and primary aliphatic amines. Siderophores are essential for microbial pathogenesis, and the activities of NMOs are specifically required for their function. To date, only a small number NMOs have been characterized. While the biochemical properties of NMOs vary, two common characteristics have been observed. These include a high degree of substrate specificity, and the stabilization of a long-lived C4a-hydroperoxyflavin intermediate. This ensures efficient hydroxylation of the appropriate substrate and minimal release of hydrogen peroxide. Recent mechanistic and structural studies have provided insight into the molecular mechanism for these two traits. The high substrate specificity has been attributed to a unique "molecular ruler mechanism," and stabilization of the C4a-hydroperoxyflavin is achieved by specific interactions with $NADP^+$. In addition, a high-throughput screening assay that allows for the identification of NMO inhibitors from small

molecule libraries has been developed. This, compounded with rational drug design, holds promise for the identification of inhibitors to combat increasingly virulent microbes.

1. Iron, an essential but scarce nutrient

Iron is an essential element required by most living organisms [1]. The need for this metal originates from its requirement as a cofactor in a wide range of biological reactions. The functional diversity of iron results from its inherent nature as a reductant or an oxidant, depending on whether it is present in a ferrous (Fe^{II}) or ferric state (Fe^{III}), respectively. Although these two oxidation states dominate in biological systems, when iron is bound to certain proteins, the reaction between Fe^{II} and molecular oxygen can lead to the formation of high-valent iron-oxo species, which catalyze a number of oxygenation reactions.

One important role of iron is demonstrated by the oxygen transport protein hemoglobin [2]. Here, iron is complexed with a porphyrin ring, which allows oxygen to be transported to different tissues of the body for use in aerobic respiration pathways. In plants, iron plays an essential role in photosynthesis. Chloroplast ferredoxin is an iron-containing protein that acts as a carrier of electrons that are produced from absorbed sunlight [3]. In microorganisms, perhaps the most important iron-containing reaction is seen with nitrogenase, which catalyzes the reduction of dinitrogen to ammonia [4]. The resulting "fixed nitrogen" can be utilized in the nitrogen cycle where it is used for the biosynthesis of amino and nucleic acids, as well as other nitrogen-containing biomolecules.

In vivo, free iron is toxic [5]. The reaction of iron in its ferrous or ferric form with hydrogen peroxide, termed the Fenton reaction, can lead to the generation of reactive oxygen species such as superoxide and hydroxyl radicals [6]. Effects of these oxidative by-products

include lipid peroxidation, protein denaturation, and DNA strand breaks, all of which are deleterious to the cell [7].

Mammals have evolved several mechanisms to lower the concentration of free iron to minimize the level of toxic oxidative by-products. Iron-binding proteins such as transferrin, lactoferrin, and ferritin store excess iron and make it available during periods of iron limitation [8,9]. Iron sequestration in mammals also has antimicrobial activity as it limits the availability of this essential nutrient in serum [10]. This, compounded with the fact that free Fe^{III} forms insoluble iron-hydroxide complexes (10^{-18} M at pH 7), represents a fundamental problem of iron deficiency that pathogenic microbes must overcome [11]. In response, pathogens have evolved a mechanism to scavenge iron from mammalian hosts by synthesizing and secreting low-molecular weight iron chelators termed siderophores (Greek for "iron carrier") [12].

2. Siderophores

Siderophores provide a unique mechanism for pathogens to acquire iron where they can utilize it for their own metabolic needs in a non-toxic fashion. Siderophores competitively acquire iron from the bacterial host as they possess a remarkably high affinity for Fe^{III}. For example, the catechol siderophore enterobactin produced by the bacterium *Escherichia coli* possesses a K_d value on the order of 10^{-49} M [13]. The high affinity allows pathogens to proliferate by scavenging iron from hosts. Siderophores vary in their structures and denticity for iron that ranges from bi- to hexadentate [14]. Siderophores can contain a number of functional groups that chelate Fe^{III}, including catechols, phenols, hydroxamates, and carboxylates [15]. Examples of siderophores from different organisms are shown in Fig. 2.1, and a list of siderophores along with their respective affinity constants for Fe^{III} is given in Table 2.1.

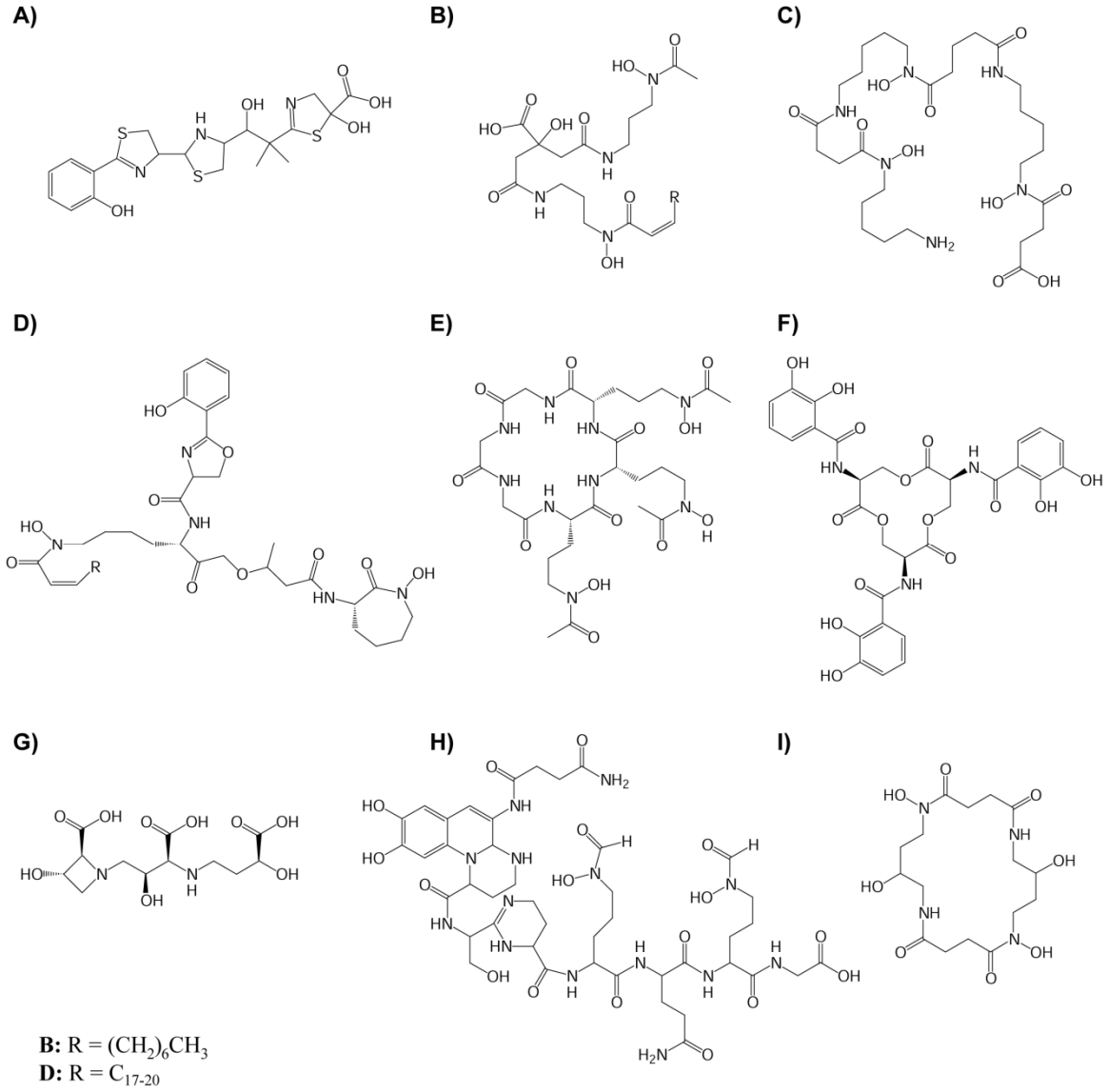

Figure 2.1 The structural diversity of siderophores. (A) Yersiniabactin from *Yersenia pestis*. (B) Rhizobactin 1021 from *Rhizobium meliloti.* (C) Desferrioxamine G_1 from *Streptomyces* spp. (D) Mycobactin T from *Mycobacterium tuberculosis*. (E) Ferricrocin from *Aspergillus fumigatus*. (F) Enterobactin from *Escherichia coli*. (G) Mugineic acid from *Hordium vulgare.* (H) Pyoverdin from *Pseudomonas aeruginosa*. (I) Alcaligin from *Bordetella pertussis.*

Table 2.1 Siderophores and their respective affinities for Fe^{III}.

Organism	Siderophore	Type	K_{FeIII} (M)	Ref.
Alteromonas luteoviolacea	Alterobactin	Carboxylate/Catechol	10^{-53}	[15]
Escherichia coli	Enterobactin	Catechol	10^{-49}	[13]
Yersinia pestis	Yersiniabactin	Mixed	10^{-36}	[16]
Hordium vulgare	Mugineic acid	Carboxylate	10^{-33}	[17]
Streptomyces griseus	Desferrioxamine E	Hydroxamate	10^{-32}	[18]
Bordetella pertussis	Alcaligin	Hydroxamate	10^{-32}	[19]
Pseudomonas syringae	Pyoverdin	Catechol/Hydroxamate	10^{-32}	[20]
Neurospora crassa	Ferrichrome	Hydroxamate	10^{-29}	[21]
Rhizopus microsporus	Rhizoferrin	Carboxylate	10^{-25}	[22]
Azotobacter vinelandii	Azotobactin	Catechol/Hydroxamate	10^{-22}	[23]

2.1 Siderophores are important virulence factors. Siderophores have been shown to be linked to virulence in many human pathogens. For instance, deletion of the gene cluster involved in the biosynthesis of the siderophore anthrachelin in *Bacillus anthracis* resulted in both attenuated growth and virulence in macrophages and mice [25]. A similar effect was demonstrated in *Pseudomonas aeruginosa* where pyoverdin- and pyochelin-deficient mutants grew poorly in immunosuppressed mice. Lethality in mice was reduced from 100% in wild-type to 0% in the double mutant 48 hours post inoculation [26]. Effects on virulence were also observed in *Aspergillus fumigatus* and *Burkholderia cepacia* upon deletion of genes involved in siderophore biosynthesis [27-29]. In *Aspergillus fumigatus*, disruption of the biosynthesis of the siderophores triacetylfusarinine C and ferricrocin resulted in a mutant strain with diminished growth in low-iron media. In mice, though, the mutant fungus was unable to establish infection, indicating the necessity for siderophores in virulence. Similarly, by targeting the biosynthesis of mycobactin through gene disruption, the rate of growth of *Mycobacterium tuberculosis* was significantly decreased in iron-deficient media as well as macrophage like THP-1 cells in one study, whereas in a similar study, a mycobactin-deficient strain failed to grow in low-iron media [30,31].

2.2 Structural diversity of siderophores. Siderophores are structurally diverse molecules that can contain one, or many, of several functional groups important for their iron-chelating properties. Amino acids are the precursors for the functional groups and are incorporated by an assembly line of domains called non-ribosomal peptide synthetases [14]. These synthetases link amino acids through thioester intermediates, and have different amino acid substrate specificities across different organisms [32,33]. The amino acid selectivity of the synthetases contributes to siderophore diversity (Fig. 2.1).

Siderophores such as alcaligin from *Bordetella pertussis* and ferricrocin from *Aspergillus fumigatus* are predominately composed of a heterocyclic ring with hydroxamates that function as the chelating groups. On the other hand, siderophores such as mycobactin T from *Mycobacterium tuberculosis*, and yersiniabactin from *Yersinia pestis*, contain a number of functional groups that include oxazoline/thiozoline rings, phenols, hydroxamates, and carboxylates.

Because siderophores are important for virulence, the enzymes involved in siderophore biosynthesis are considered potential drug targets. In particular, flavin dependent microbial *N*-hydroxylating monooxygenases (NMOs) have emerged as ideal systems for drug development due to their central role in the biosynthesis of hydroxamate-containing siderophores [26-31].

3. Flavin-dependent *N*-hydroxylating monooxygenases

NMOs are flavin-containing monooxygenases involved in the biosynthesis of hydroxamate-containing siderophores. These enzymes target the soft nucleophilic terminal amine groups of L-ornithine, L-lysine, and the primary aliphatic diamines 1,3-diaminopropane, putrescine, and cadaverine (Fig. 2.2) [28,34-42].

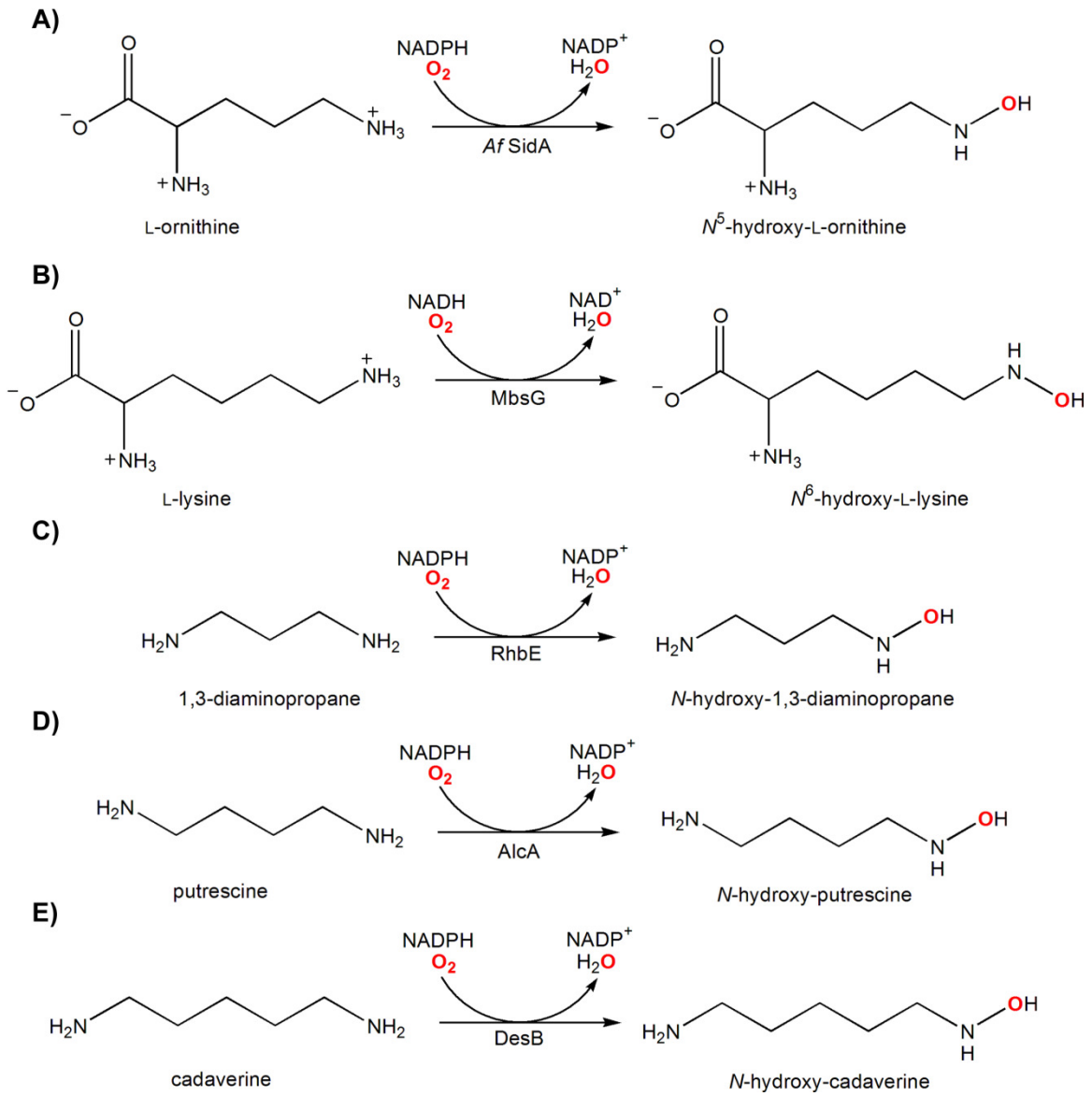

Figure 2.2 Reactions catalyzed by NMOs. The oxygen atoms involved in the reaction are shown in red. The amino acids L-ornithine and L-lysine are *N*-hydroxylated by *Af* SidA (A) and MbsG (B), respectively. The *N*-hydroxylation of the aliphatic diamines 1,3-diaminopropane, putrescine, and cadaverine are catalyzed by RhbE (C) AlcA (D), and DesB (E), respectively.

NMOs are members of the Class B flavoprotein monooxygenase family which include Baeyer-Villiger monooxygenases (BVMOs) and the bacterial and microsomal flavin-containing monooxygenases (bFMO and mFMO, respectively) [43]. Enzymes in this family are encoded by

a single gene, bind flavin adenine dinucleotide (FAD), utilize NADPH as a coenzyme, keep $NADP^+$ bound throughout the catalytic cycle, and contain two dinucleotide binding domains.

Many members of the NMO family have previously been identified through the characterization of gene clusters involved in the biosynthesis of several hydroxamate-containing siderophores. IucD from *Escherichia coli* was the first NMO to be characterized. The function of IucD was determined by gene knockout studies and direct detection of hydroxylated L-lysine [44]. Similar studies to identify related NMOs were also performed in *Burkholderia cepacia, Mycobacterium tuberculosis*, *Omphalotus olearius*, *Ustilago maydi*s, *Pseudomonas aeruginosa*, and *Aspergillus* spp., among others [28,34,36,37,45,46].

Several NMOs have been specifically linked to virulence through gene knockout studies. Upon deletion of the L-ornithine monooxygenase gene, *sidA,* in *Aspergillus fumigatus*, the mutant strain was unable to produce triacetylfusarinine C and ferricrocin, and was unable to cause infection in mice [27]. Similar results were obtained when the L-ornithine monooxygenase gene, *pvdA,* from *Burkholderia cepacia* was deleted [28]. Here, the mutant bacteria were unable to establish infection in rats. These results show the function of NMOs as essential for virulence in both bacteria and fungi. Thus, NMOs clearly represent potential drug targets.

Despite the NMOs identified to date, relatively few have been characterized in detail. NMOs that have been expressed, purified, and characterized include the L-ornithine monooxygenases, *Pseudomonas aeruginosa* pyoverdin A (*Pa* PvdA), *Aspergillus fumigatus* siderophore A (*Af* SidA), *Streptomyces coelicolor* coelichelin B (CchB), *Rhizobium leguminosarum* vicibactin synthase O (VbsO), and the L-lysine monooxygenases from *Escherichia coli* iron uptake chelate D (IucD), and *Mycobacterium smegmatis* G (MbsG) [35,39,47-50].

4. Catalytic cycle of NMOs

Af SidA and *Pa* PvdA are the two most comprehensively characterized NMOs to date. Their kinetic mechanisms have been studied by steady-state and stopped-flow spectrophotometric methods [47,48,51-54]. As with other flavin-containing monooxygenases, the catalytic cycle of microbial NMOs can be divided into two half-reactions. The first of these is the reductive half-reaction where NADH or NADPH transfers a hydride to reduce the flavin cofactor [55]. The second is the oxidative half-reaction where reduced flavin reacts with molecular oxygen and substrate is hydroxylated.

A general kinetic mechanism of NMOs, particularly that of *Af* SidA, is depicted in Fig. 2.3 [51]. The first step involves the reaction of the oxidized flavin with NADPH (Fig. 2.3B). This produces reduced flavin and $NADP^+$, which remains bound to the enzyme, a characteristic common among Class B monooxygenases [43]. The reduced enzyme-$NADP^+$ complex then reacts with molecular oxygen to form a C4a-hydroperoxyflavin, the hydroxylating species (Figs. 2.3C* and 2.3D). The presence of $NADP^+$ plays a critical role in the stabilization of this intermediate. The C4a-hydroperoxyflavin is long-lived and the enzyme turns over rapidly only when substrate binds to the active site. In NMOs, substrate hydroxylation is highly specific and the enzyme predominately produces hydrogen peroxide if an inappropriate substrate binds, such as in the case of L-lysine binding in *Af* SidA [47,48,51-54]. Hydroxylation is followed by dehydration of the flavin to produce the oxidized cofactor (Fig. 2.3F). Release of the hydroxylated product, and lastly, $NADP^+$, completes the catalytic cycle (Fig. 2.3G). The two most important questions that emerged from this general catalytic cycle pertain to the mechanism of stabilization of the C4a-hydroperoxyflavin and the structural characteristics that lead to the

high degree of substrate selectivity. Recent mechanistic and structural information on members of the NMO family addressing these questions has recently been made available.

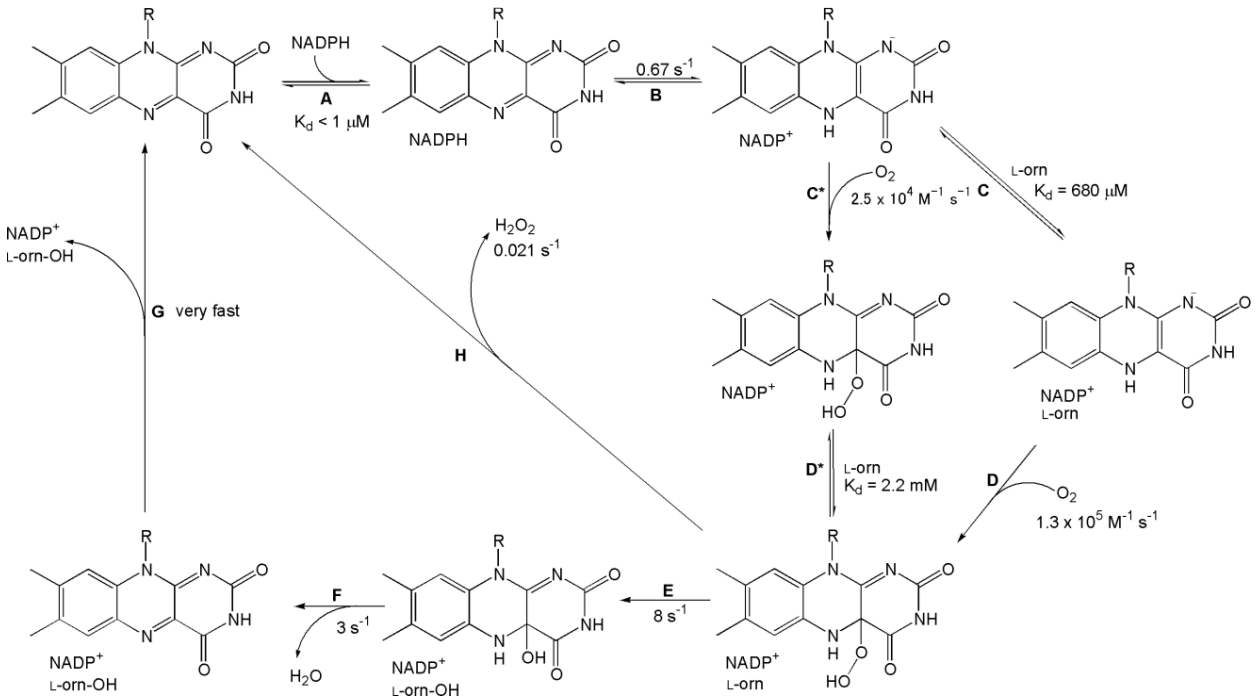

Figure 2.3 Kinetic mechanism of *Af* SidA [51]. NADPH first binds to the oxidized form of the enzyme (A) which then reduces FAD to yield $FADH^-$ (B). After reduction two kinetic pathways are possible. The first and preferred pathway is where L-ornithine can bind to the $NADP^+$-enzyme complex (C) which then reacts with molecular oxygen to form a C4a-hydroperoxyflavin (D). Alternatively, molecular oxygen can first react with $FADH^-$ to form a C4a-hydroperoxyflavin (C*) after which the binding of L-ornithine occurs (D*). After the formation of a stable C4a-hydroperoxyflavin and when L-ornithine is bound, hydroxylation occurs resulting in a C4a-hydroxyflavin (E). The flavin is then dehydrated (F) to regenerate oxidized FAD which then allows for release of $NADP^+$ and hydroxylated L-ornithine (G). In the absence of substrate, the C4a-hydroperoxyflavin slowly decays to hydrogen peroxide and oxidized flavin (H).

4.1 Flavin reduction in NMOs. Direct measurement of the rates of flavin reduction in *Af* SidA and *Pa* PvdA show this to be the rate-limiting step in the catalytic cycle (Fig. 2.3) [51,52,54]. This is consistent with previous studies by Macheroux and coworkers where FAD analogs with IucD were used [49]. Studies with *Af* SidA show a biphasic reduction of the flavin with

NAD(P)H [51,54]. This was originally analyzed by Dubois and coworkers as corresponding to NADPH binding followed by hydride transfer. Recent primary kinetic isotope effect (KIE) studies with NADPH resulted in KIE values for k_{red} of 5.5 for both phases of reduction [54]. These results show that hydride transfer is rate-limiting in reduction and occurs in both phases, suggesting that NADPH is reacting with different enzyme forms. The concentration dependence of these two phases could not accurately be measured with NADPH due to its high affinity to *Af* SidA. In contrast, with NADH, only the fast phase was dependent on the concentration of the coenzyme. A KIE value of 4.7 was measured in this phase, suggesting that it corresponds to hydride transfer. The slow phase was concentration and isotope independent. Thus, with NADH, the first phase corresponds to flavin reduction while the second phase most likely is NAD^+ release. These studies also showed that *Af* SidA is specific for transfer of the *pro*-R hydrogen at the C-4 position of the nicotinamide ring in both NADPH and NADH, an observation consistent with other flavin-containing monooxygenases [56]. Lastly, the rates of the reductive steps in *Pa* PvdA and *Af* SidA are independent of L-ornithine [51,52]. This lack of an effect by substrate contrasts with that of *p*-hydroxybenzoate hydroxylase (PHBH). Here, substrate enhances reduction by ~1.4 x 10^5-fold and highlights one mechanistic difference among flavin-containing monooxygenases [57].

4.2 Flavin oxidation in NMOs. In solution, the activation of molecular oxygen involves the single electron transfer from reduced flavin to oxygen, which produces a caged radical pair that leads to formation of the C4a-peroxyflavin [58]. This reaction is relatively slow (~250 M^{-1} s^{-1}) due to spin inversion of triplet oxygen reacting with singlet reduced flavin. In contrast, flavoproteins can accelerate this reaction to a range of 10^3-10^6 $M^{-1}s^{-1}$ [59]. Following oxygen

activation, the reaction can proceed in various ways: a) destabilization of the caged radical pair and release of the superoxide anion, b) release of hydrogen peroxide after the collapse of the caged radical pair, or c) stabilization of a C4a-hydroperoxyflavin intermediate [58]. Flavin oxidases react with oxygen and form hydrogen peroxide; however, flavin monooxygenases must stabilize the oxygenated flavin intermediate for an efficient oxygenation reaction to occur. This intermediate can exist as a C4a-peroxyflavin or C4a-hydroperoxyflavin depending if the enzyme performs a nucleophilic or electrophilic reaction, respectively.

The first electron transfer step in NMOs has not been observed to date, as the caged radical pair rapidly collapses to form the C4a-peroxyflavin [51,52]. In NMOs, the rate of activation of molecular oxygen is moderately enhanced by L-ornithine binding. Reduced *Af* SidA reacts with molecular oxygen on the order of 10^4 M^{-1} s^{-1} and 10^5 M^{-1} s^{-1} in the absence and presence of L-ornithine, respectively [51].

After oxygen addition, a C4a-peroxyflavin is formed, however the hydroxylation of L-ornithine requires the protonated form of this intermediate, the C4a-hydroperoxyflavin [55]. In *Pa* PvdA, a species at 361 nm is observed immediately after oxygen addition in the absence of L-ornithine. In the presence of L-ornithine the intermediate shifts to 376 nm [52]. The intermediate observed at 361 nm is similar to the C4a-peroxyflavin intermediate observed in cyclohexanone monooxygenase [60]. Thus, it was suggested that this species corresponded to the C4a-peroxyflavin that became protonated upon binding of L-ornithine [52]. In *Af* SidA though, a species is observed at 382 nm immediately after oxygen addition, indicative of a C4a-hydroperoxyflavin. This species remains unchanged over a pH range of 6-10 and does not shift upon L-ornithine binding [51,61]. This indicates that in *Af* SidA, the pK_a value of the C4a-hydroperoxyflavin is high (>10). Therefore, it appears that *Af* SidA rapidly forms and stabilizes

the C4a-hydroperoxyflavin [61]. It is not clear why these two related enzymes differ in the steps of formation of their oxygenated flavin intermediates.

In order to efficiently catalyze the electrophilic insertion of oxygen into substrate, NMOs depend on $NADP^+$. As previously mentioned, $NADP^+$ remains bound after reduction where the enzyme-$NADP^+$ complex then reacts with molecular oxygen to form a stable, long-lived C4a-hydroperoxyflavin. The longevity of the C4a-hydroperoxyflavin ensures hydroxylation of L-ornithine which prevents the release of hydrogen peroxide and regeneration of oxidized flavin (Fig. 2.3H). NADH can effectively reduce *Af* SidA; however, upon reaction with oxygen the intermediate is less stable [48]. These results indicate a specific role of NADP(H) in the stabilization of the C4a-hydroperoxyflavin, which will be discussed in Section 7.

5. Three-dimensional structure of NMOs

Determination of the three-dimensional structure of NMOs has been hampered by the lack of stable proteins that contain a tightly bound flavin cofactor [47,49]. The structure of the first NMO, *Pa* PvdA, was only recently solved (Fig. 2.4) [62]. Conditions were obtained where the protein was co-crystallized with FAD, $NADP^+$, and L-ornithine. Furthermore, the crystallized protein complex could be chemically reduced. Thus, the structures of the oxidized (1.9 Å) and reduced enzymes (3.03 Å) are available (PDB codes 3S5W and 3S61, respectively). The structure of *Pa* PvdA contains three domains, including two α/β-Rossmann-like domains for FAD- and NADPH-binding, and a small helical domain for L-ornithine-binding (Fig. 2.4) [62]. Amino acid sequence alignment among members of the NMO family predicts that all contain the three-domain architecture (Fig. 2.5). We will discuss the structure of *Pa* PvdA in detail; however, the analysis is also applicable to *Af* SidA as our group has recently solved the structure.

Our analysis revealed and that the three-dimensional structures of these two enzymes are virtually identical.

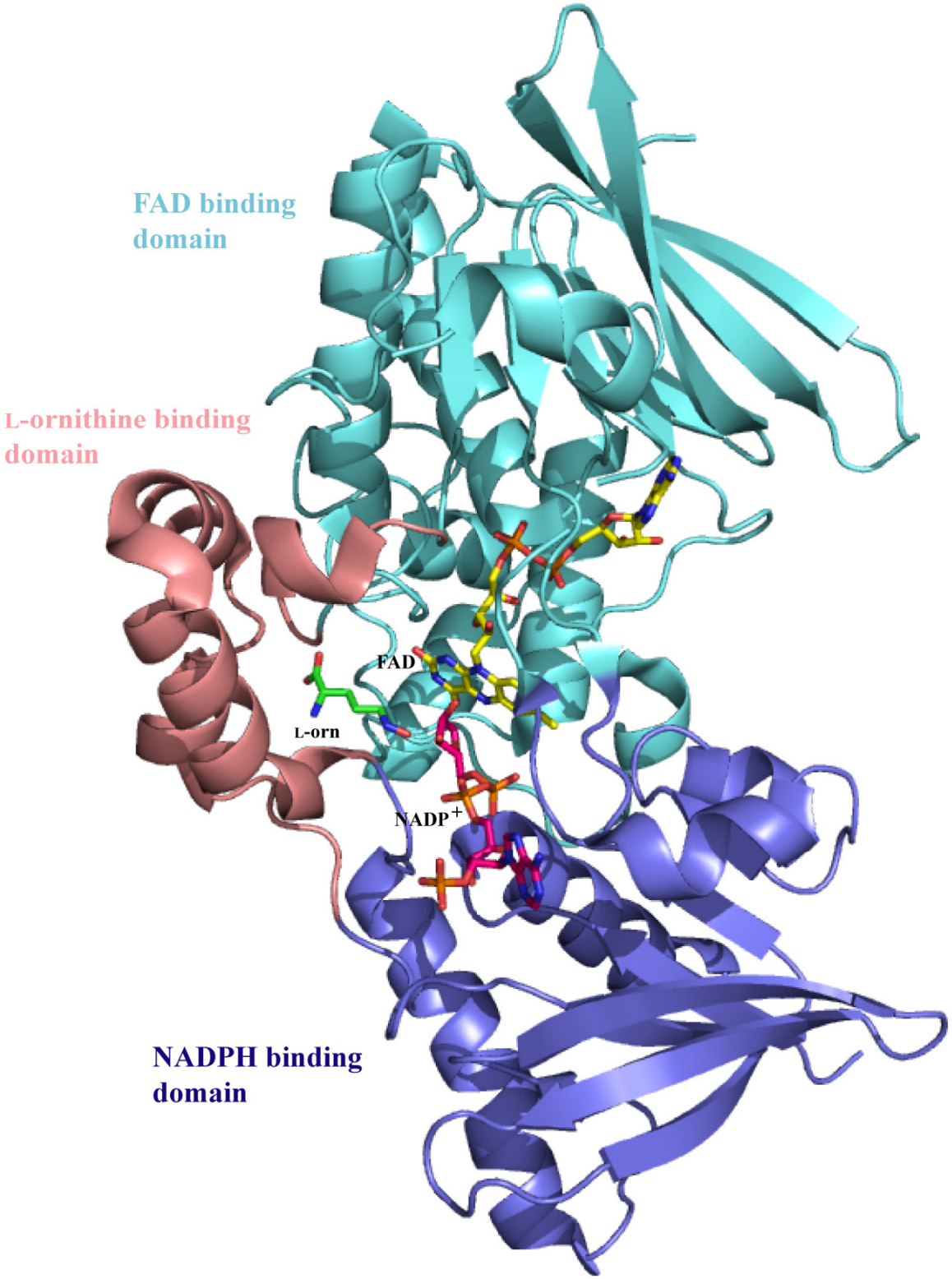

Figure 2.4 Overall structure of *Pa* PvdA (PDB code 3S5W). The FAD-binding domain is shown in cyan, the NADPH-binding domain in slate blue, and the L-ornithine-binding domain in salmon. FAD carbons are shown in yellow, $NADP^+$ carbons in pink, and L-ornithine carbons in green.

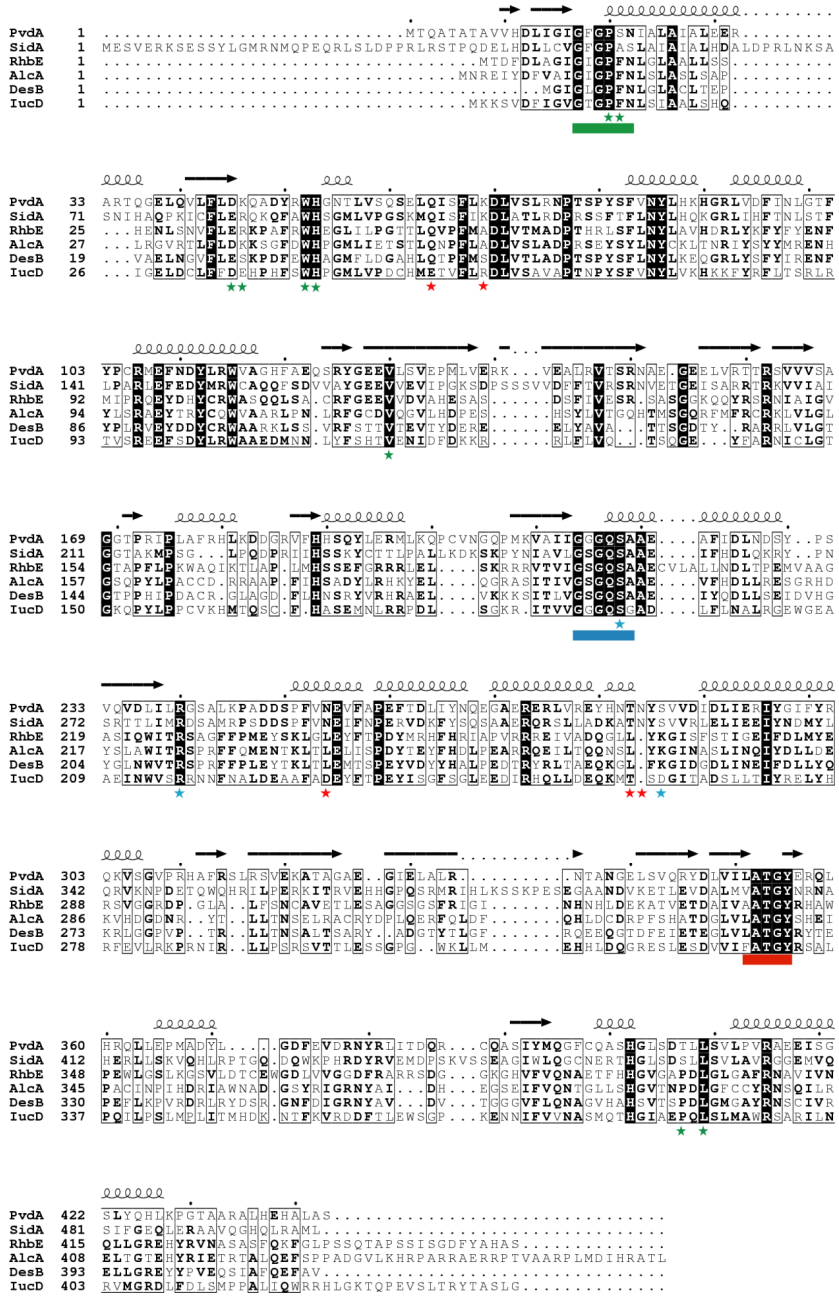

Figure 2.5 Primary sequence alignment of NMOs with different substrate specifities. The L-ornithine monooxygenases *Pa* PvdA and *Af* SidA, the 1,3-diaminopropane monooxygenase RhbE, the putrescine monooxygenase AlcA, the cadaverine monooxygenase DesB, and the L-lysine monooxygenase IucD are aligned. Sequence identities to *Pa* PvdA are 38% for *Af* SidA, 27% for RhbE, 26% for AlcA, 30% for DesB, and 29% for IucD. The green bar indicates the FAD-binding motif, the blue bar the NADPH binding motif, and the red bar the L/FATGY motif. Residues starred in green, blue, and red are proposed to be involved in FAD, NADPH, and L-ornithine binding, respectively, in *Pa* PvdA. The secondary structure of *Pa* PvdA (PDB code 3S5W) is threaded to the alignment. Loops represent α-helices, arrows represent β-sheets, and spaces represent loops. The alignment was performed with Multalin and ESpript.

5.1 FAD-binding domain. The FAD-binding domain in *Pa* PvdA is the largest and is composed of residues 1-171, 356-396, and 405-443 [62]. The FAD-binding motif is located near the N-terminus in *Pa* PvdA (Fig. 2.5, green bar). This classic GXGXXG flavin-binding motif is conserved in phenylacetone monooxygenase (PAMO), cyclohexanone monooxygenase (CHMO), and the bFMO monooxygenase from *Methylophaga* sp. strain SK1 [63-65]. In NMOs, the last glycine is replaced by a proline. It was proposed that this amino acid change was partially responsible for the weak affinity for FAD among some members of this class of enzymes [66]. Upon solving the structure of *Pa* PvdA, the identification of a unique FAD binding motif in NMOs that consists of GXGXXN is observed which originates through a shift of two amino acids to the C-terminus from the previously proposed motif. As seen in Fig. 2.5, this motif is conserved among NMOs, although in *Af* SidA the asparagine is replaced by a serine.

The recombinant forms of *Pa* PvdA and IucD are purified in an inactive apo-state in the absence of bound FAD. This is due to their relatively low affinities for FAD (~25 μM) [47,49]. In these cases, excess FAD is added to obtain an active, holo-enzyme. Interestingly, *Af* SidA and MbsG have been isolated with approximately > 50% of FAD bound per monomer, suggesting tight binding of the FAD [48,50]. Crystallographic analysis shows that interactions between the protein and the flavin are mediated by hydrogen bonding with the backbone and several side chains of *Pa* PvdA. Comparison of the FAD-binding residues with that of bFMO, which contains a tightly bound cofactor, indicates there are no significant differences, and the hydrogen bonds, which hold the FAD in place are almost identical (Fig. 2.6). Olucha et al. suggested that the weak affinity of *Pa* PvdA for FAD results from the exposed nature of the cofactor in its respective binding site as opposed to the solvent sequestered FAD in bFMO [62,65]. As mentioned, the structure of *Af* SidA is almost identical to *Pa* PvdA[1]. There are no significant

differences in the FAD-binding cleft in *Af* SidA when compared to *Pa* PvdA. This indicates that the tight-binding observed with *Af* SidA is likely due to a reason that cannot be determined by x-ray crystallographic analysis. Further work is needed to elucidate the cause of this key difference between these two highly similar NMOs.

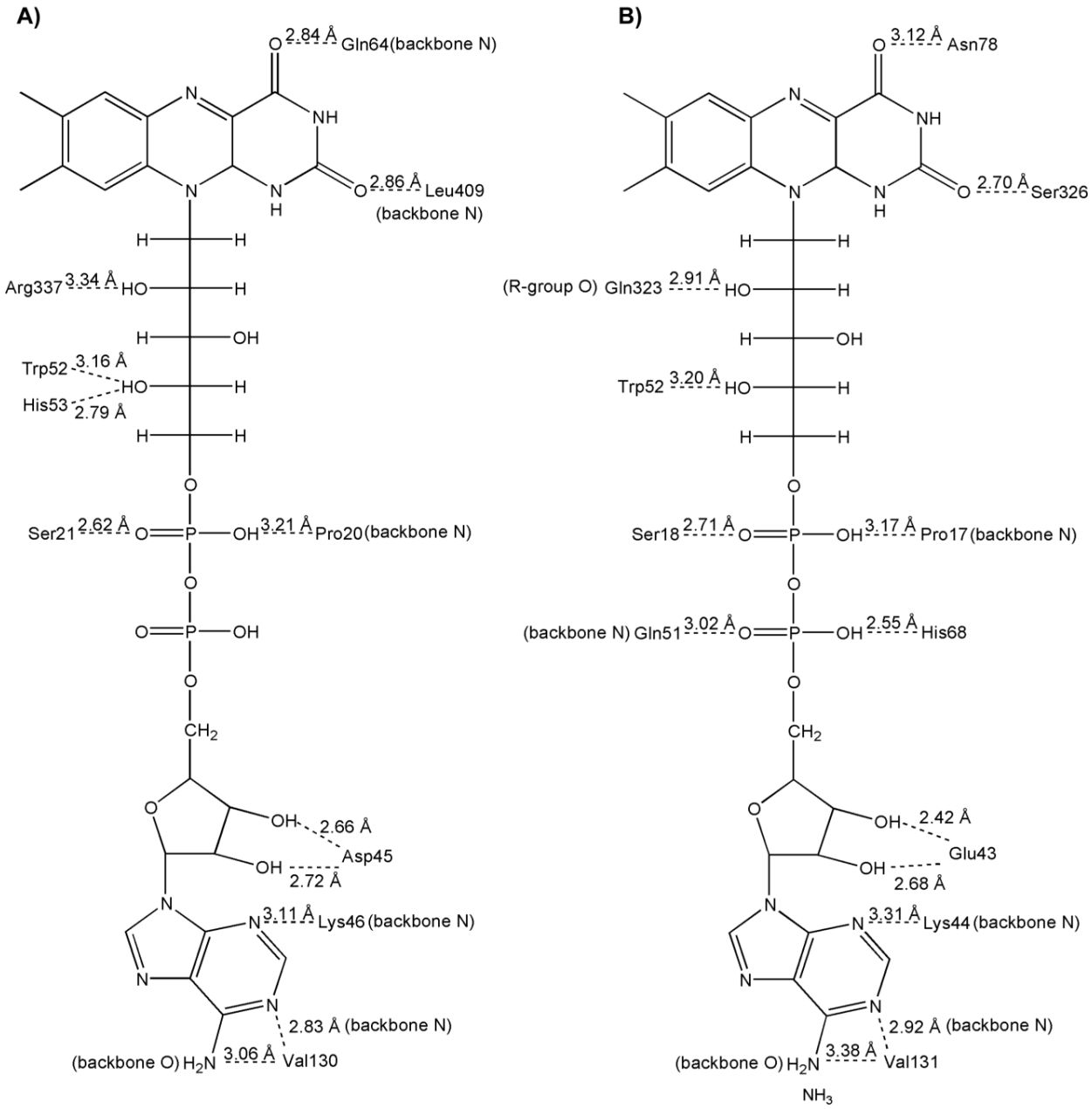

Figure 2.6 FAD interactions among Class B monooxygenases. Interactions of FAD with residues of *Pa* PvdA (A) and bFMO (B).

5.2 NADPH-binding domain. The NADPH-binding domain in *Pa* PvdA is composed of residues 170-245 and 285-355 [66]. The second nucleotide-binding motif, GXGXXG/A, is present in this domain and is located in the middle of the polypeptide chain (Fig. 2.5, blue bar). NMOs, such as CchB, *Pa* PvdA, and IucD, are specific to NADPH as no turnover with NADH is observed [39,47,67]. In contrast, *Af* SidA and MbsG are more promiscuous as they are active with both coenzymes [48,50]. Although, *Af* SidA preferentially utilizes NADPH, MbsG appears to be slightly more specific for NADH. The crystal structure of *Pa* PvdA provides structural evidence for the specificity of NADPH over NADH. Olucha and co-authors report that Arg-240 forms two hydrogen bonds with the phosphate group of the adenine ribose. This residue is conserved among NMOs (Fig. 2.5) and presumably, in all of these enzymes, interaction of this Arg residue with the phosphate of NADPH is partially responsible for the selectivity for this coenzyme.

5.3 L-Ornithine-binding domain. In *Pa* PvdA, the L-ornithine-binding domain is the third, and smallest domain, which is composed of residues 248-285 and 398-404 [66]. It was first proposed that the L/FATGY motif was predominately involved in substrate-binding (Fig. 2.5, red bar). This hydrophobic sequence is conserved among Class B monooxygenases, but after determination of the crystal structure of *Pa* PvdA, the L/FATGY sequence was found to not be involved in any significant interactions with L-ornithine and is located in the NADPH-binding domain [62]. Instead, Asn-254 and Thr-283, and Lys-69 interact with the α-carboxylate and amino groups, respectively, providing structural evidence for the steroselectivity for L-ornithine over D-ornithine [47]. The residues Gln-64 and Asn-284 provide interactions with the N^5-amine of L-ornithine that hold it near the C4a of the isoalloxazine ring in a favorable position for hydroxylation [62].

Primary amino acid sequence alignment of NMOs with different substrate specificities indicates that key residues that interact with L-ornithine in *Pa* PvdA are not conserved (Fig. 2.5). In particular, amino acids Lys-69, Asn-254, and Asn-283, which help provide specificity for L-ornithine in *Pa* PvdA, are conserved in *Af* SidA but not in all NMOs with different substrate specificities. Perhaps these structural differences are responsible for the accommodation of substrates other than L-ornithine.

6. Mechanism of substrate specificity in NMOs

As mentioned, NMOs are highly specific for hydroxylation of substrate. For example, *Af* SidA and *Pa* PvdA are highly specific for the hydroxylation of L-ornithine [47,48]. When in the presence of structurally similar analogs such as D-ornithine, L-lysine, L-arginine, and 1,4-diaminobutane, these NMOs yield little or no hydroxylated products. Similar stringent selectivity has been observed with the L-lysine monooxygenases IucD and MbsG [49,50].

While both *Af* SidA and *Pa* PvdA are very specific for hydroxylation of L-ornithine, substrate analogs stimulate turnover by causing a "misfiring" of the C4a-hydroperoxyflavin, producing solely hydrogen peroxide [47,48]. The most dramatic is with L-lysine, a non-substrate effector that causes nearly complete uncoupling of the reaction. The structure of *Pa* PvdA complexed with L-ornithine and $NADP^+$ provides some insight into the effector role of L-lysine (Fig. 2.7). As suggested by Olucha and coworkers, since L-lysine is longer than L-ornithine, the N^6-amine might protrude too far into the active site to allow for favorable positioning and stabilization of the C4a-hydroperoxyflavin upon binding (Fig. 2.7) [62]. Thus, a structural "ruler mechanism" is employed by NMOs to select the proper substrate for hydroxylation.

In contrast to the substrate selectivity of NMOs, mammalian FMOs have a broad substrate specificity as they will oxygenate a range of drugs and xenobiotics [68]. In particular, microsomal liver FMO can catalyze the hydroxylation of a number of soft nucleophiles including secondary and tertiary amines, thiols, hydrazines, sulfides, thiocarbamides, and thioamides [69-72]. Similarly, PAMO and CHMO can catalyze the oxygenation of several ketones and alkyl sulfides [73,74].

In *Af* SidA, the reaction of the C4a-hydroperoxyflavin and L-ornithine is concentration dependent and saturates at high concentrations of L-ornithine, suggesting formation of a complex [51]. In contrast, the reactivity of the C4a-hydroperoxyflavin intermediate with bFMO has been shown to occur as a second-order reaction. Here, the intermediate is in a "cocked-gun" state where the protein is ready to fire upon substrate binding [75]. This could suggest that formation of a complex in NMOs leads to another layer of substrate selectivity where only the appropriate substrate is hydroxylated.

7. Mechanism of stabilization of the C4a-hydroperoxyflavin by $NADP^+$

Insights into the stabilization mechanism of the C4a-hydroperoxyflavin by NADP(H) in NMOs became evident when the three-dimensional structure of *Pa* PvdA in complex with $NADP^+$ was solved by Lamb and coworkers [62]. The reduced structure shows $NADP^+$ in a position that is not optimal for hydride transfer. Instead, binding was proposed to be optimal for stabilization of the C4a-hydroperoxyflavin (Fig. 2.7A). Furthermore, binding of L-ornithine predicts that the N^5-amine will be located in the precise position to attack the distal oxygen of the flavin intermediate (Fig. 2.7A). This analysis is consistent with the results and the proposal of the "moonlighting" effect of NADPH in bFMO reported by Mattevi and Fraaije [65]. In this related enzyme, $NADP^+$ is bound in the active site in a position optimal for stabilization of a C4a-

hydroperoxyflavin, similar to *Pa* PvdA. Recently, site-directed mutagenesis of residues that are predicted to stabilize the binding of $NADP^+$ produced mutant enzymes that are highly uncoupled in bFMO [76]. This supports the proposal that the observed position of $NADP^+$ in the active site of these enzymes is important for stabilization of the C4a-hydroperoxyflavin.

The importance of stabilization of the C4a-hydroperoxyflavin by $NADP^+$ was demonstrated as chemical reduction of *Af* SidA with dithionite and exposure to oxygen in the presence of L-ornithine produces only hydrogen peroxide [51]. Thus, the binding of $NADP^+$ is essential in the oxidative-half reaction. The observed conformation of $NADP^+$ in the active site of *Pa* PvdA shows that it creates a pocket for the formation of the C4a-hydroperoxyflavin (Fig. 2.7B). Thus, shielding it from solvent and providing hydrogen-bonding partners for stabilization. This pocket also plays a role in the selectivity for L-ornithine, since larger substrates (e.g, L-lysine) protrude too far and displace the interaction of $NADP^+$ with the C4a-hydroperoxide (Fig. 2.7C).

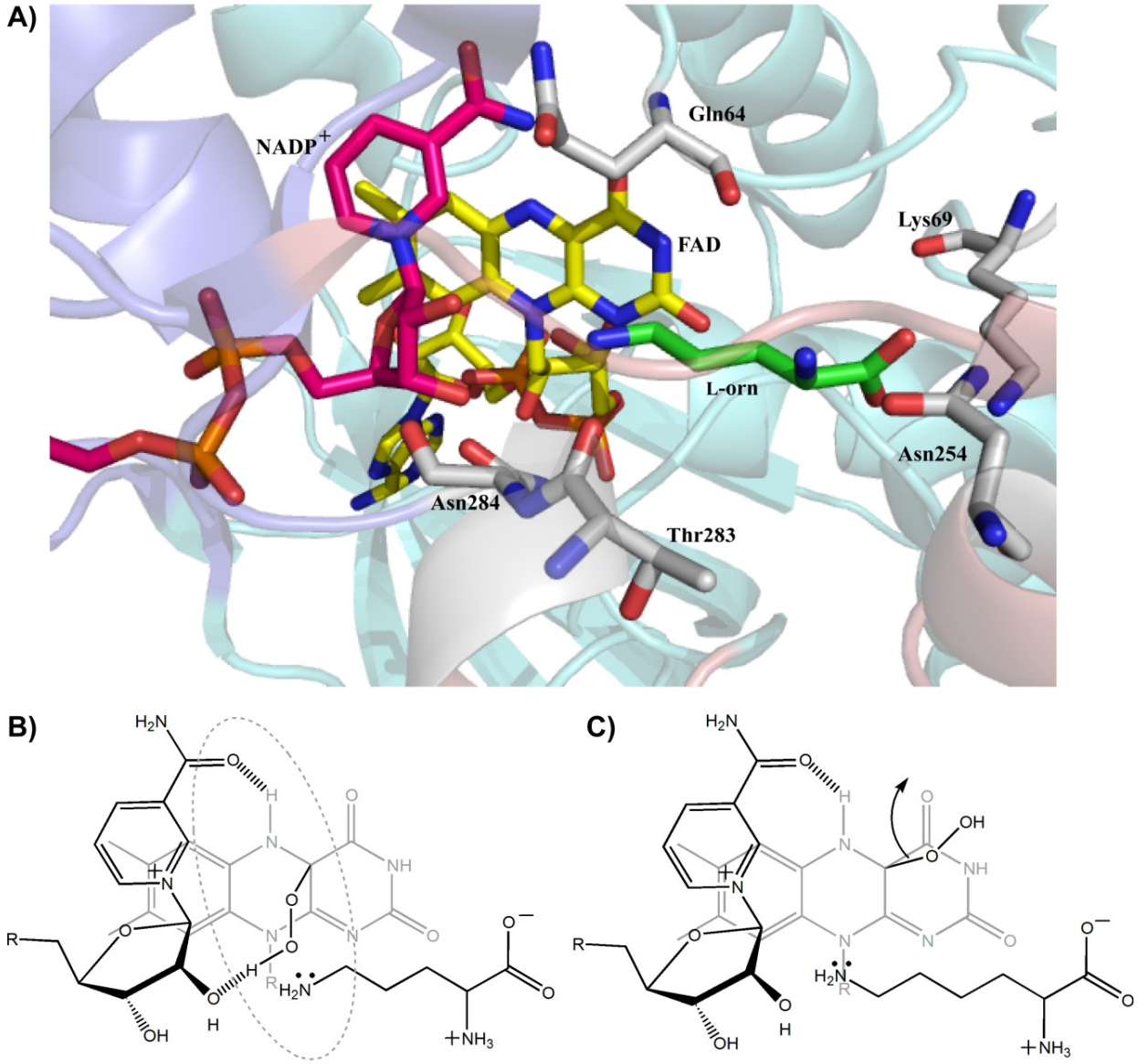

Figure 2.7 Stabilization of the C4a-hydroperoxyflavin in the active site of *Pa* PvdA (PDB code 3S61). The active site of *Pa* PvdA (A) where FAD carbons are shown in yellow, $NADP^+$ carbons in pink, L-ornithine carbons in green, and side chain carbons in gray. This provides a role of stabilization for the C4a-hydroperoxyflavin by $NADP^+$ along with the pocket (dashed circle) for dioxygen of the intermediate defined by $NADP^+$ and L-ornithine (B). When L-lysine binds the amine protrudes too far into the active site to be hydroxylated and stimulates the release of hydrogen peroxide (C).

The exact conformational changes that occur to locate $NADP^+$ in the position observed in the structures of all Class B monooxygenases is not known, mainly because the structures in the absence of $NADP^+$ have been elusive. However, biochemical evidence of coenzyme-induced

conformational changes has been reported in *Af* SidA. By monitoring the fluorescence of FAD upon binding of NAD^+, an increase in flavin fluorescence was observed while binding of $NADP^+$ produced a decrease in fluorescence [54]. These results indicate different modes of binding of the coenzymes in the active site that must be modulated by the 2'-phosphate of $NADP^+$. It was also shown that binding of $NADP^+$ protects *Af* SidA from degradation by trypsin in limited proteolysis studies. This effect was not observed in the presence of L-ornithine or NAD^+. Thus, it appears that NADP(H) induces conformational changes that modulate the interaction of the nicotinamide ring with the flavin cofactor.

8. Activation of NMOs by amino acid binding

The oxidation of the flavin in NMOs occurs in two distinct phases [51-53]. The first phase is the formation of a stable C4a-hydroperoxyflavin intermediate, while the second phase is dehydration of the flavin to form fully oxidized FAD. Formation of a stable C4a-hydroperoxyflavin occurs in *Af* SidA and *Pa* PvdA in the absence of substrate, but the rate of formation has been shown to increase in the presence of saturating levels of L-ornithine by ~80-fold and ~15-fold for *Pa* PvdA and *Af* SidA, respectively [47,48,51,52].

Binding of the amino acids L-citrulline and L-arginine also enhance the activity of *Af* SidA [53]. This effect has been observed on both reduction by NADPH and formation of the C4a-hydroperoxyflavin. L-arginine provides the highest rate enhancement with a ~10-fold increase in the rate of flavin reduction and a ~100-fold increase for the formation of the C4a-hydroperoxyflavin. Activation by L-arginine is concentration dependent and displays Michaelis-Menten kinetics with a $K_{activation}$ value for the C4a-hydroperoxyflavin of ~620 μM. It is clear that binding of L-arginine to *Af* SidA stabilizes the C4a-hydroperoxyflavin as the enzyme becomes

more coupled, changing from ~90% in the absence of L-arginine to ~100% in the presence of L-arginine.

The mechanism of oxygen activation in flavoenzymes has been studied extensively [77-80]. A common trait among flavin oxidases is the presence of a positive charge near the N5 of the isoalloxazine ring. For example, the positive charges of a lysine and histidine residue in *N*-methyltryptophan oxidase and glucose oxidase, respectively, have been shown to activate oxygen. In the absence of an L-amino acid, *Af* SidA activates oxygen ~100-fold faster than free, reduced flavin [51]. Furthermore, when saturating levels of L-arginine are present, formation of a C4a-hydroperoxyflavin occurs ~100-fold faster than in the absence of L-arginine [53]. Binding of L-arginine to *Af* SidA could play a role in oxygen activation similar to the lysine and histidine residues in flavin oxidases. Here, the positive charge of the guanidinium group in L-arginine could be involved in the activation of molecular oxygen. Further studies are needed to determine the exact mechanism of activation of *Af* SidA by L-arginine.

9. Unusual NMOs

Mycobacterium smegmatis G (MbsG), a L-lysine monooxygenase involved in mycobactin biosynthesis (Fig. 2.2B), does not share the same mechanistic features described for members of the NMO family. As discussed earlier, *Pa* PvdA and *Af* SidA contain a number of characteristics that ensure coupling and prevent the release of oxygen reactive species. These characteristics are not conserved in MbsG [50].

The most interesting aspect about MbsG is the lack of control of oxygen reactivity. When substrate is absent, the enzyme functions like an NAD(P)H oxidase producing superoxide and hydrogen peroxide [50]. Once L-lysine is introduced, superoxide and hydrogen peroxide

production decreases and product formation occurs, albeit at low levels. Under the most optimal conditions, MbsG is ~30% coupled, and under physiological conditions only ~12% coupled. While these reactive oxygen species are seemingly detrimental, in some cases they are postulated to play a role in the expression of genes regulated by the cell's redox state [68].

In the biosynthesis of hydroxamate-containing siderophores, hydroxylation is thought to be the first step in siderophore biosynthesis [35,41,49,81]. A recent report proposed that in the biosynthesis of mycobactin, hydroxylation of L-lysine occurs after its incorporation into the siderophore [31]. This conclusion was based upon lipidomic analysis that showed the presence of di/monodeoxymycobactin and mycobactin in media growth of wild-type *Mycobacterium tuberculosis*. Furthermore, in an *mbtG* knockout strain, only dideoxymycobactin was detected. Thus, it was proposed that MbtG hydroxylation of lysine at the N^6-position was the final step in mycobactin biosynthesis [31]. A recent report provided a possible explanation for the presence of dideoxymycobactin. It was determined that MbtF, a peptide synthetase involved in acylation, has specificity for N^6-hydroxy-L-lysine. However, it is also capable of acylating L-lysine, which can lead to the formation of dideoxymycobactin instead of mycobactin [82]. This could explain the accumulation of ~2% dideoxymycobactin in *mbtG* knockouts of *M. tuberculosis* compared to the wild-type. Here, mycobactin biosynthesis in the deoxy-state is still able to occur, but at a much reduced rate. These results as well as and the biochemical characterization of MbsG as a lysine hydroxylase support the hydroxylation of free L-lysine in the biosynthesis of mycobactin [50].

10. High-throughput screening assay to identify inhibitors of NMOs

As discussed previously, NMOs are essential for virulence in many human pathogens. The recent mechanistic and structural studies provide valuable information for new therapeutic

strategies. In addition to rational drug design, the screening of small molecule libraries for inhibitors of NMOs could help identify new drugs. A fluorescence polarization binding assay that can monitor the binding of small molecules to the active site of NMOs was recently developed (Fig. 2.8) [83]. This assay uses a fluorescently labeled ADP molecule. The ADP portion targets the NADPH binding site, while the fluorophore (TAMRA) is connected via a hydrophobic linker. The tricyclic rings of the fluorophore are postulated to stack with the isoalloxazine ring of the FAD, further increasing its affinity for NMOs. *Af* SidA, bFMO, and MbsG all have been shown to bind this ligand.

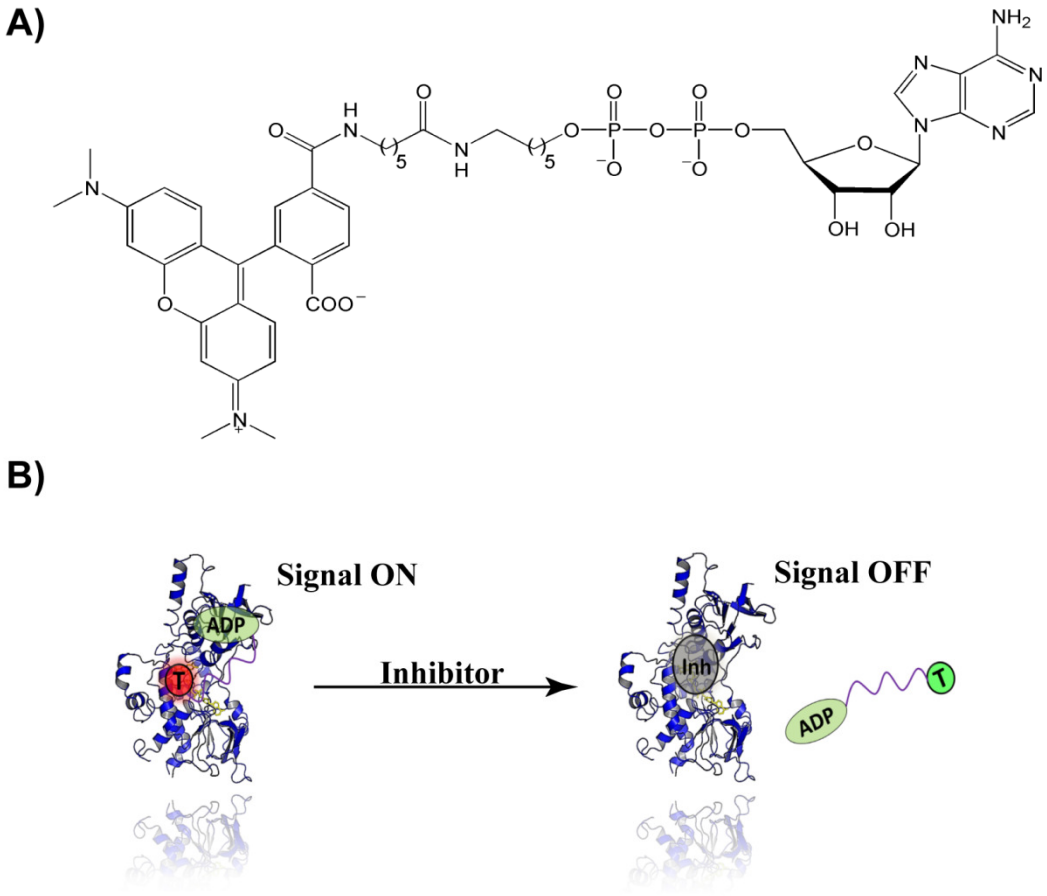

Figure 2.8 The fluorescence binding assay developed for *Af* SidA. The fluorophore used to detect inhibitors of NMOs (A) and the cartoon depiction of the detection of inhibitors with the fluorophore shown with the crystal structure of *Af* SidA (B).

Both *Af* SidA and MbsG display low K_d values for the fluorescent ligand (2-6 µM). This binding across NMOs indicates that the ligand could potentially be utilized to screen for inhibitors in a number of enzymes. The fluorophore binds to the active site of *Af* SidA as it is displaced by $NADP^+$ and NAD^+. Furthermore, L-lysine and L-ornithine can displace the fluorophore, indicating its effectiveness for identifying analogs of either substrate. A pilot screen of 160 molecules identified sanguinarine sulfate as a weak inhibitor of *Af* SidA with an IC_{50} value of ~ 500 µM [83]. These results suggest that screening of large molecule libraries will most likely identify potent and specific inhibitors of NMOs.

11. Concluding remarks

NMOs constitute a large family of flavin-dependent monooxygenases involved in the biosynthesis of hydroxamate-containing siderophores. These enzymes are linked to the virulence of several human pathogens and, thereby, represent potentially novel drug targets. Mechanistically, this family shares many similarities with other members of the Class B flavin monooxygenases with some exceptions, as with MbsG. A unique feature of NMOs is their remarkable specificity for substrate hydroxylation which is achieved by a "molecular ruler mechanism." The exact placement of substrate along with the moonlighting role of $NADP^+$ provides a well-defined pocket for a C4a-hydroperoxyflavin to be stabilized. Also, oxygen activation in NMOs is enhanced by the binding of certain amino acids. Elucidation of the three-dimensional structures along with a developed high-throughput assay to screen for inhibitors provides a solid foundation for development of drugs that target NMOs.

12. Reference list

[1] Pierre JL, Fontecave M. Iron and activated oxygen species in biology: the basic chemistry. Biometals 1999;12:195-9.

[2] Maton A, editor. Human Biology and Health. Englewood Cliffs, New Jersey, USA: Prentice Hall; 1993.

[3] Tagawa K, Tsujimoto HY, Arnon DI. Role of chloroplast ferredoxin in the energy conversion process of photosynthesis. Proc Natl Acad Sci USA 1963;49:567-72.

[4] Kim J, Rees DC. Nitrogenase and biological nitrogen fixation. Biochemistry 1994;33:389-97.

[5] Gutteridge JM, Halliwell B. Iron toxicity and oxygen radicals. Baillieres Clin Haematol 1989;2:195-256.

[6] Stohs SJ, Bagchi D. Oxidative mechanisms in the toxicity of metal ions. Free Radic Biol Med 1995;18:321-36.

[7] Schaible UE, Kaufmann SH. Iron and microbial infection. Nat Rev Microbiol 2004;2:946-53.

[8] Eisenstein RS. Iron regulatory proteins and the molecular control of mammalian iron metabolism. Annu Rev Nutr 2000;20:627-62.

[9] Ward PP, Uribe-Luna S, Conneely OM. Lactoferrin and host defense. Biochem Cell Biol 2002;80:95-102.

[10] Marx JJM. Iron and infection: Competition between host and microbes for a precious element. Best Pract Res Clin Haematol 2002;15:411-26.
[11] Andrews SC, Robinson AK, Rodriguez-Quinones F. Bacterial iron homeostasis. FEMS Microbiol Rev 2003;27:215-37.
[12] Sandy M, Butler A. Microbial iron acquisition: Marine and terrestrial siderophores. Chem Rev 2009;109:4580-95.
[13] Loomis LD, Raymond KN. Solution equilibria of enterobactin and metal-enterobactin complexes. Inorg Chem 1991;30:906-11.
[14] Hider RC, Kong X. Chemistry and biology of siderophores. Nat Prod Rep 2010;27:637-57.
[15] Neilands JB. Microbial iron compounds. Annu Rev Biochem 1981;50:715-31.
[16] Reid RT, Live DH, Faulkner DJ, Butler A. A siderophore from a marine bacterium with an exceptional ferric ion affinity constant. Nature 1993;366:455-8.
[17] Perry RD, Balbo PB, Jones HA, Fetherston JD, DeMoll E. Yersiniabactin from Yersinia pestis: biochemical characterization of the siderophore and its role in iron transport and regulation. Microbiology 1999;145 (Pt 5):1181-90.
[18] Murakami T, Ise K, Hayakawa M, Kamei S, Takagi SI. Stabilities of metal-complexes of mugineic acids and their specific affinities for iron(iii). Chem Lett 1989:2137-40.
[19] Schwarzenbach G, Anderegg G. Metal complexes with biguanide. Pharm Acta Helv 1963;38:547-52.
[20] Hou Z, Raymond KN, O'Sullivan B, Esker TW, Nishio T. A preorganized siderophore: thermodynamic and structural characterization of alcaligin and bisucaberin, microbial macrocyclic dihydroxamate chelating agents[1]. Inorg Chem 1998;37:6630-7.
[21] Torres L, Perez-Ortin JE, Tordera V, Beltran JP. Isolation and characterization of an Fe(III)-chelating compound produced by Pseudomonas syringae. Appl Environ Microbiol 1986;52:157-60.
[22] Wong GB, Kappel MJ, Raymond KN, Matzanke B, Winkelmann G. Coordination chemistry of microbial iron transport compounds .24. Characterization of coprogen and ferricrocin, 2 ferric hydroxamate siderophores. J Am Chem Soc 1983;105:810-5.
[23] Carrano CJ, Drechsel H, Kaiser D, et al. Coordination chemistry of the carboxylate type siderophore rhizoferrin: the iron(iii) complex and its metal analogs. Inorg Chem 1996;35:6429-36.
[24] Palanche T, Blanc S, Hennard C, Abdallah MA, Albrecht-Gary AM. Bacterial iron transport: coordination properties of azotobactin, the highly fluorescent siderophore of Azotobacter vinelandii. Inorg Chem 2004;43:1137-52.
[25] Cendrowski S, MacArthur W, Hanna P. Bacillus anthracis requires siderophore biosynthesis for growth in macrophages and mouse virulence. Mol Microbiol 2004;51:407-17.
[26] Takase H, Nitanai H, Hoshino K, Otani T. Impact of siderophore production on Pseudomonas aeruginosa infections in immunosuppressed mice. Infect Immun 2000;68:1834-9.
[27] Hissen AH, Wan AN, Warwas ML, Pinto LJ, Moore MM. The Aspergillus fumigatus siderophore biosynthetic gene sidA, encoding L-ornithine N5-oxygenase, is required for virulence. Infect Immun 2005;73:5493-503.

[28] Sokol PA, Darling P, Woods DE, Mahenthiralingam E, Kooi C. Role of ornibactin biosynthesis in the virulence of Burkholderia cepacia: Characterization of pvdA, the gene encoding L-ornithine N(5)-oxygenase. Infect Immun 1999;67:4443-55.
[29] Schrettl M, Bignell E, Kragl C, et al. Siderophore biosynthesis but not reductive iron assimilation is essential for Aspergillus fumigatus virulence. J Exp Med 2004;200:1213-9.
[30] De Voss JJ, Rutter K, Schroeder BG, Su H, Zhu Y, Barry CE, 3rd. The salicylate-derived mycobactin siderophores of Mycobacterium tuberculosis are essential for growth in macrophages. Proc Natl Acad Sci USA 2000;97:1252-7.
[31] Madigan CA, Cheng TY, Layre E, et al. Lipidomic discovery of deoxysiderophores reveals a revised mycobactin biosynthesis pathway in Mycobacterium tuberculosis. Proc Natl Acad Sci USA 2012;109:1257-62.
[32] Frueh DP, Arthanari H, Koglin A, et al. Dynamic thiolation-thioesterase structure of a non-ribosomal peptide synthetase. Nature 2008;454:903-6.
[33] Crosa JH, Walsh CT. Genetics and assembly line enzymology of siderophore biosynthesis in bacteria. Microbiol Mol Biol Rev 2002;66:223-49.
[34] Visca P, Ciervo A, Orsi N. Cloning and nucleotide sequence of the pvdA gene encoding the pyoverdin biosynthetic enzyme L-ornithine N5-oxygenase in Pseudomonas aeruginosa. J Bacteriol 1994;176:1128-40.
[35] Heemstra JR, Jr., Walsh CT, Sattely ES. Enzymatic tailoring of ornithine in the biosynthesis of the Rhizobium cyclic trihydroxamate siderophore vicibactin. J Am Chem Soc 2009;131:15317-29.
[36] Quadri LE, Sello J, Keating TA, Weinreb PH, Walsh CT. Identification of a Mycobacterium tuberculosis gene cluster encoding the biosynthetic enzymes for assembly of the virulence-conferring siderophore mycobactin. Chem Biol 1998;5:631-45.
[37] Mei B, Budde AD, Leong SA. sid1, a gene initiating siderophore biosynthesis in Ustilago maydis: molecular characterization, regulation by iron, and role in phytopathogenicity. Proc Natl Acad Sci USA 1993;90:903-7.
[38] Herrero M, de Lorenzo V, Neilands JB. Nucleotide sequence of the iucD gene of the pColV-K30 aerobactin operon and topology of its product studied with phoA and lacZ gene fusions. J Bacteriol 1988;170:56-64.
[39] Pohlmann V, Marahiel MA. Delta-amino group hydroxylation of L-ornithine during coelichelin biosynthesis. Org Biomol Chem 2008;6:1843-8.
[40] Lynch D, O'Brien J, Welch T, et al. Genetic organization of the region encoding regulation, biosynthesis, and transport of rhizobactin 1021, a siderophore produced by Sinorhizobium meliloti. J Bacteriol 2001;183:2576-85.
[41] Kang HY, Brickman TJ, Beaumont FC, Armstrong SK. Identification and characterization of iron-regulated Bordetella pertussis alcaligin siderophore biosynthesis genes. J Bacteriol 1996;178:4877-84.
[42] Barona-Gomez F, Wong U, Giannakopulos AE, Derrick PJ, Challis GL. Identification of a cluster of genes that directs desferrioxamine biosynthesis in Streptomyces coelicolor M145. J Am Chem Soc 2004;126:16282-3.
[43] van Berkel WJ, Kamerbeek NM, Fraaije MW. Flavoprotein monooxygenases, a diverse class of oxidative biocatalysts. J Biotechnol 2006;124:670-89.
[44] de Lorenzo V, Bindereif A, Paw BH, Neilands JB. Aerobactin biosynthesis and transport genes of plasmid ColV-K30 in Escherichia coli K-12. J Bacteriol 1986;165:570-8.

[45] Welzel K, Eisfeld K, Antelo L, Anke T, Anke H. Characterization of the ferrichrome A biosynthetic gene cluster in the homobasidiomycete Omphalotus olearius. FEMS Microbiol Lett 2005;249:157-63.
[46] Eisendle M, Oberegger H, Zadra I, Haas H. The siderophore system is essential for viability of Aspergillus nidulans: functional analysis of two genes encoding l-ornithine N 5-monooxygenase (sidA) and a non-ribosomal peptide synthetase (sidC). Mol Microbiol 2003;49:359-75.
[47] Meneely KM, Lamb AL. Biochemical characterization of a flavin adenine dinucleotide-dependent monooxygenase, ornithine hydroxylase from Pseudomonas aeruginosa, suggests a novel reaction mechanism. Biochemistry 2007;46:11930-7.
[48] Chocklett SW, Sobrado P. Aspergillus fumigatus SidA is a highly specific ornithine hydroxylase with bound flavin cofactor. Biochemistry 2010;49:6777-83.
[49] Macheroux P, Plattner HJ, Romaguera A, Diekmann H. FAD and substrate analogs as probes for lysine N6-hydroxylase from Escherichia coli EN 222. Eur J Biochem 1993;213:995-1002.
[50] Robinson R, Sobrado P. Substrate binding modulates the activity of Mycobacterium smegmatis G, a flavin-dependent monooxygenase involved in the biosynthesis of hydroxamate-containing siderophores. Biochemistry 2011;50:8489-96.
[51] Mayfield JA, Frederick RE, Streit BR, Wencewicz TA, Ballou DP, DuBois JL. Comprehensive spectroscopic, steady state, and transient kinetic studies of a representative siderophore-associated flavin monooxygenase. J Biol Chem 2010;285:30375-88.
[52] Meneely KM, Barr EW, Bollinger JM, Jr., Lamb AL. Kinetic mechanism of ornithine hydroxylase (PvdA) from Pseudomonas aeruginosa: substrate triggering of O2 addition but not flavin reduction. Biochemistry 2009;48:4371-6.
[53] Frederick RE, Mayfield JA, DuBois JL. Regulated O2 activation in flavin-dependent monooxygenases. J Am Chem Soc 2011;133:12338-41.
[54] Romero E, Fedkenheuer M, Chocklett SW, Qi J, Oppenheimer M, Sobrado P. Dual role of NADP(H) in the reaction of a flavin dependent N-hydroxylating monooxygenase. Biochim Biophys Acta 2012;1824:850-7.
[55] Ghisla S, Massey V. Mechanisms of flavoprotein-catalyzed reactions. Eur J Biochem 1989;181:1-17.
[56] Ryerson CC, Ballou DP, Walsh C. Kinetic isotope effects in the oxidation of isotopically labeled NAD(P)H by bacterial flavoprotein monooxygenases. Biochemistry 1982;21:1144-51.
[57] Husain M, Massey V. Kinetic studies on the reaction of p-hydroxybenzoate hydroxylase. Agreement of steady state and rapid reaction data. J Biol Chem 1979;254:6657-66.
[58] Massey V. Activation of molecular oxygen by flavins and flavoproteins. J Biol Chem 1994;269:22459-62.
[59] Palfey BA, McDonald CA. Control of catalysis in flavin-dependent monooxygenases. Arch Biochem Biophys 2010;493:26-36.
[60] Sheng D, Ballou DP, Massey V. Mechanistic studies of cyclohexanone monooxygenase: chemical properties of intermediates involved in catalysis. Biochemistry 2001;40:11156-67.

[61] Romero E, Avila D, Sobrado P. Effect of pH on the reductive and oxidative half-reactions of *Aspergillus fumigatus* siderophore A. In Flavins and Flavoproteins (Miller, S Ed) *In press* 2011.
[62] Olucha J, Meneely KM, Chilton AS, Lamb AL. Two structures of an N-hydroxylating flavoprotein monooxygenase: ornithine hydroxylase from Pseudomonas aeruginosa. J Biol Chem 2011;286:31789-98.
[63] Malito E, Alfieri A, Fraaije MW, Mattevi A. Crystal structure of a Baeyer-Villiger monooxygenase. Proc Natl Acad Sci USA 2004;101:13157-62.
[64] Mirza IA, Yachnin BJ, Wang S, et al. Crystal structures of cyclohexanone monooxygenase reveal complex domain movements and a sliding cofactor. J Am Chem Soc 2009;131:8848-54.
[65] Alfieri A, Malito E, Orru R, Fraaije MW, Mattevi A. Revealing the moonlighting role of NADP in the structure of a flavin-containing monooxygenase. Proc Natl Acad Sci U S A 2008;105:6572-7.
[66] Stehr M, Diekmann H, Smau L, et al. A hydrophobic sequence motif common to N-hydroxylating enzymes. Trends Biochem Sci 1998;23:56-7.
[67] Plattner HJ, Pfefferle P, Romaguera A, Waschutza S, Diekmann H. Isolation and some properties of lysine N6-hydroxylase from Escherichia coli strain EN222. Biol Met 1989;2:1-5.
[68] Krueger SK, Williams DE. Mammalian flavin-containing monooxygenases: structure/function, genetic polymorphisms and role in drug metabolism. Pharmacol Ther 2005;106:357-87.
[69] Ziegler DM, Jollow, D., and Cook, D.E. Flavins and Flavoproteins. 1971:475-97.
[70] Prough RA. The N-oxidation of alkylhydrazines catalyzed by the microsomal mixed-function amine oxidase. Arch Biochem Biophys 1973;158:442-4.
[71] Paulsen LL, Hyslop RM, Ziegler DM. S-oxidation of thioureylenes catalyzed by a microsomal flavoprotein mixed-function oxidase. Biochem Pharmacol 1974;23:3431-40.
[72] Paulsen LL, Ziegler DM. Microsomal mixed-function oxidase-dependent renaturation of reduced ribonuclease. Arch Biochem Biophys 1977;183:563-70.
[73] de Gonzalo G, Pazmino DET, Ottolina G, Fraaije MW, Carrea G. Oxidations catalyzed by phenylacetone monooxygenase from Thermobifida fusca. Tetrahedron Asymmetry 2005;16:3077-83.
[74] Branchaud BP, Walsh CT. Functional-group diversity in enzymatic oxygenation reactions catalyzed by bacterial flavin-containing cyclohexanone oxygenase. J Am Chem Soc 1985;107:2153-61.
[75] Paulsen LL, Ziegler DM. The liver microsomal FAD-containing monooxygenase. Spectral characterization and kinetic studies. J Biol Chem 1979;254:6449-55.
[76] Orru R, Pazmino DE, Fraaije MW, Mattevi A. Joint functions of protein residues and NADP(H) in oxygen activation by flavin-containing monooxygenase. J Biol Chem 2010;285:35021-8.
[77] McDonald CA, Fagan RL, Collard F, Monnier VM, Palfey BA. Oxygen reactivity in flavoenzymes: context matters. J Am Chem Soc 2011;133:16809-11.
[78] Su Q, Klinman JP. Nature of oxygen activation in glucose oxidase from Aspergillus niger: the importance of electrostatic stabilization in superoxide formation. Biochemistry 1999;38:8572-81.

[79] Roth JP, Klinman JP. Catalysis of electron transfer during activation of O2 by the flavoprotein glucose oxidase. Proc Natl Acad Sci USA 2003;100:62-7.
[80] Bruckner RC, Winans J, Jorns MS. Pleiotropic impact of a single lysine mutation on biosynthesis of and catalysis by N-methyltryptophan oxidase. Biochemistry 2011;50:4949-62.
[81] Ge L, Seah SY. Heterologous expression, purification, and characterization of an l-ornithine N(5)-hydroxylase involved in pyoverdine siderophore biosynthesis in Pseudomonas aeruginosa. J Bacteriol 2006;188:7205-10.
[82] McMahon MD, Rush JS, Thomas MG. Analyses of MbtB, MbtE, and MbtF suggest revisions to the mycobactin biosynthesis pathway in Mycobacterium tuberculosis. J Bacteriol 2012;194:2809-18.
[83] Qi J, Kizjakina K, Robinson R, Tolani K, Sobrado P. A fluorescence polarization binding assay to identify inhibitors of flavin-dependent monooxygenases. Anal Biochem 2012;425:80-7.

CHAPTER 3

C4a-hydroperoxyflavin formation in *N*-hydroxylating flavin monooxygenases is mediated by the 2'-OH of the nicotinamide ribose of $NADP^+$

Reprinted with permission from Biochemistry, Robinson, R., Badieyan, S., and Sobrado, P. "C4a-hydroperoxyflavin formation in *N*-hydroxylating flavin monooxygenases is mediated by the 2'-OH of the nicotinamide ribose of $NADP^+$" *Biochemistry*. 2013 (ID 10.1021/bi4014903) Vol 52: 9089-9091.

Author Contributions:
Reeder Robinson performed all the stopped-flow experiments, and helped write the article.

Somayesadat Badieyan performed all of the computational studies, and helped write the article.

Pablo Sobrado oversaw and directed the research, and helped write the article.

Abstract

Flavin-dependent monooxygenases must stabilize a C4a-hydroperoxyflavin intermediate to hydroxylate their respective substrates. Formation and decay of the C4a-hydroperoxyflavin was monitored under rapid reaction kinetic conditions in SidA, an *N*-hydroxylating monooxygenase involved in siderophore biosynthesis. Solvent kinetic isotope effect studies on flavin oxidation indicate that both hydrogen peroxide and water elimination occur via hydrogen abstraction from the N5 of the flavin. Kinetic isotope effect and density functional theory results are consistent with the transfer of a proton from the 2'-OH of the nicotinamide ribose of $NADP^+$ to the C4a-peroxyflavin to form the C4a-hydroperoxyflavin. This represents a novel role for $NADP^+$ in the reaction of flavin-dependent enzymes.

1. Introduction, Results, and Discussion

Flavin-dependent monooxygenases catalyze the addition of an oxygen atom in hydroxylation, epoxidation, and ester bond formation reactions. The catalytic cycle includes reduction of the flavin cofactor by NAD(P)H, activation of molecular oxygen, and formation of covalent oxygen-flavin intermediates.[1,2] Depending on the specific chemical reaction, a C4a-peroxyflavin (FAD_{OO-}) or C4a-hydroperoxyflavin (FAD_{OOH}) intermediate is stabilized.[1,2] Siderophore A (SidA) is a member of the Class B flavoprotein monooxygenases that catalyze the N5-hydroxylation of ornithine in the biosynthesis of siderophores in *Aspergillus fumigatus*.[3,4] In the catalytic cycle of SidA, $NADP^+$ is the last product released. The presence of $NADP^+$ in the active site is required for the stabilization of the oxygenated flavin intermediate.[5,6] Biochemical and structural studies on SidA suggest that the role of $NADP^+$ in the stabilization of the flavin intermediate involves movement of the nicotinamide ring after hydride transfer to create a site for the $FAD_{OO(H)}$ intermediate to form and for the assembly of hydrogen bond interactions required for its stabilization.[7] This role for $NADP^+$ is conserved in other members of the Class B flavoprotein monooxygenases.[8,9] Activation of molecular oxygen by flavin monooxygenases is initiated by a single electron transfer from reduced flavin to oxygen resulting in a flavin semiquinone and superoxide radical pair that collapses to form the FAD_{OO-} intermediate. SidA and other hydroxylating flavoprotein monooxygenases require the protonated form of this intermediate (FAD_{OOH}) for catalysis. The mechanism by which FAD_{OOH} forms in SidA is not well understood.

Formation and decay of $FAD_{OO(H)}$ in SidA were probed by measuring solvent kinetic isotope effects (SKIE) in a stopped-flow spectrophotometer (Tables 3.1 and 3.2). In the absence of ornithine, the formation of the intermediate ($k_{OO(H)}$) was monitored at 372 nm. The

intermediate is very stable and decays by the elimination of hydrogen peroxide (k_{H2O2}) to form the oxidized flavin. This process is monitored at 452 nm (Fig. 3.1). In the presence of ornithine, hydroxylation takes place and the oxidized flavin is formed via the elimination of water (k_{H2O}), which is also monitored at 452 nm (Scheme 3.1). In the absence of ornithine, a SKIE value of ~1 was determined for $k_{OO(H)}$. In contrast, a SKIE value of ~1.5 was determined for k_{H2O2}. In the presence of ornithine, the SKIE value on $k_{OO(H)}$ was also ~1. The lack of a SKIE on $k_{OO(H)}$ is consistent with no protons in flight in the transition state for formation of the oxygenated flavin intermediate, or that protonation occurs very fast. In the presence of ornithine, a significantly higher SKIE value for k_{H2O} was determined. This is consistent with previous stopped-flow experiments that show flavin oxidation to be partially rate-limiting in the catalytic cycle of SidA.[6,10]

Table 3.1 Rate constants for the oxidative steps of SidA.

	(-) ornithine	(+) ornithine
	$k_{OO(H)}$, s^{-1}	$k_{OO(H)}$, s^{-1}
Control	0.65 ± 0.06	18 ± 2
NADPD	0.56 ± 0.04	11.5 ± 0.7
95% D_2O	0.56 ± 0.06	18.1 ± 0.6
NADPD + D_2O	0.59 ± 0.07	16 ± 1
D_2O, 600 s incubation	0.48 ± 0.02	14.9 ± 0.2
	k_{H2O2}, s^{-1}	k_{H2O}, s^{-1}
Control	0.0149 ± 0.0005	1.20 ± 0.03
NADPD	0.0148 ± 0.0006	1.013 ± 0.006
95% D_2O	0.0096 ± 0.0004	0.403 ± 0.005
NADPD + D_2O	0.0065 ± 0.0002	0.278 ± 0.008
D_2O, 600 s incubation	0.0059 ± 0.0001	0.287 ± 0.001

Conditions: 100 mM sodium phosphate, pH 7.5, 25 °C.

Table 3.2 KIEs on the oxidative steps of SidA.

	(-) ornithine	(+) ornithine
	$k_{OO(H)}$, s^{-1}	$k_{OO(H)}$, s^{-1}
D_2O	1.2 ± 0.2	1.0 ± 0.1
NADPD	1.1 ± 0.1	1.2 ± 0.2
NADPD + D_2O	1.1 ± 0.2	1.1 ± 0.1
D_2O, 600 s incubation	1.3 ± 0.1	1.2 ± 0.1
	k_{H2O2}, s^{-1}	$k_{H2O,}$ s^{-1}
D_2O	1.55 ± 0.09	2.97 ± 0.09
NADPD	1.01 ± 0.05	1.18 ± 0.03
NADPD + D_2O	2.3 ± 0.1	4.3 ± 0.2
D_2O, 600 s incubation	2.5 ± 0.1	4.2 ± 0.1

Conditions: 100 mM sodium phosphate, pH 7.5, 25 °C.

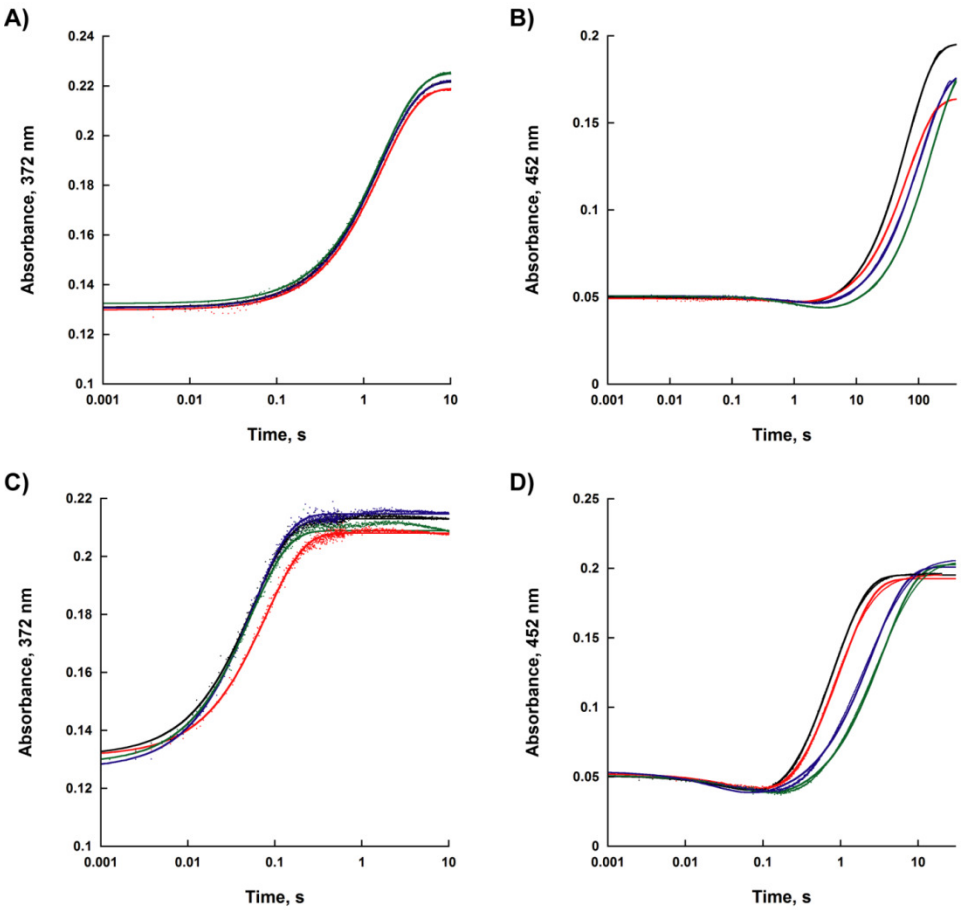

Figure 3.1 Oxidation traces of SidA (+/-) L-ornithine at 25 °C. A) Formation of the C4a-(hydro)peroxyflavin intermediate ($k_{OO(H)}$) as observed at 372 nm in the absence of ornithine. B) Flavin oxidation in the absence of ornithine (via hydrogen peroxide elimination, k_{H2O2}) monitored at 452 nm. C) Formation of the C4a-(hydro)peroxyflavin intermediate ($k_{OO(H)}$) as observed at 372 nm in the presence of ornithine with 300 µM oxygen. D) Flavin oxidation in the presence of ornithine (via flavin dehydration, k_{H2O}) monitored at 452 nm. Black traces represent oxidation performed in 100% H_2O with NADPH. Red traces represent oxidation performed in 100% H_2O with NADPD. Blue traces represent oxidation performed in 95% D_2O with NADPH. Green traces represent oxidation performed in 95% D_2O with NADPD. The concentration of oxygen was 300 µM and ornithine at 10 mM.

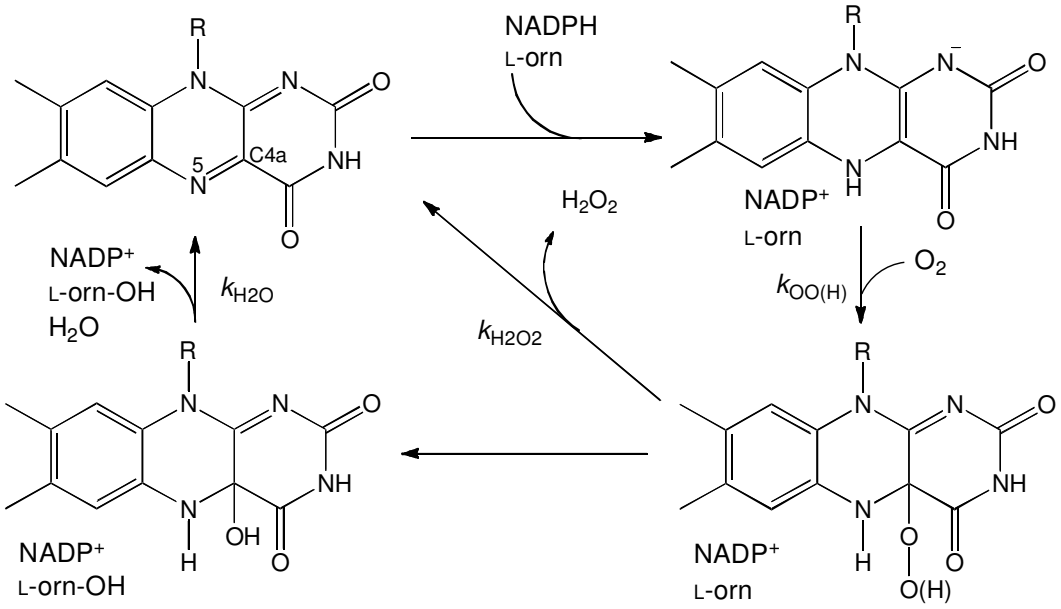

Scheme 3.1 Catalytic cycle of SidA.

In order to determine if H_2O_2 or H_2O elimination involves hydrogen atom abstraction from the N5 of FAD, we performed experiments where SidA was reduced with 4*R*-4-^{2}H-NADPH (NADPD). Upon reduction, ^{2}H-N5-FAD forms and a kinetic isotope effect (KIE) would be measured if the breaking of this bond is rate-limiting during flavin oxidation, either by H_2O or H_2O_2 elimination. A KIE value close to 1 was measured for k_{H2O2} and only a slightly higher value was measured for k_{H2O} (Table 3.2). We then measured the KIE on oxidation where SidA was reduced with NADPD in D_2O. In this experiment, the KIE for both k_{H2O2} and k_{H2O} were significantly higher than with either D_2O or NADPD alone. We hypothesized that the difference in the KIE values might originate from buffer exchange with the N5-FAD. To test whether the observed lower SKIE value for oxidation is an apparent effect influenced by proton exchange, SidA was mixed with NADPH in D_2O for 600 s (instead of 60 s) before reacting with oxygen. Under these conditions, the SKIE values for k_{H2O2} and k_{H2O} were equal to the KIE values with NADPD + D_2O. The spectra for these oxidation experiments are shown in Figs. 3.2 and 3.3.

These results indicate that the observed lower SKIE on oxidation is due to relatively slow buffer exchange between D_2O and the H-N5-FAD. Similarly, the observed KIE values with NADPD are lower due to exchange of ^{2}H-N5-FAD with H_2O. As expected the KIE values with NADPD alone or in D_2O on $k_{OO(H)}$ were close to 1. In summary, the results indicate that: 1) the observed KIEs for k_{H2O2} and k_{H2O} originate from hydrogen atom abstraction from the N5 of FAD, as shown for other flavoenzymes[11] and 2) the transition state for cleavage of this bond is more rate-limiting for H_2O elimination than for H_2O_2 elimination.

Density functional theory (DFT) analysis was performed to provide insight into the protonation mechanism of FAD_{OO-} to form the FAD_{OOH} in SidA. The DFT analysis of FAD_{OO-} (no ornithine bound) shows that the proton between the distal oxygen and the oxygen of the 2'-OH is shared based on the bond distance (Table 3.3 and Fig. 3.4A). Similarly, in the FAD_{OO-}:Orn complex (N5-ornithine uncharged) the 2'-OH proton is also clearly shared with the distal oxygen (Fig. 3.4B). Results from the FAD_{OO-}:Orn^+ (N5-ornithine positively charged) complex show that at the very early stages of the simulation, a proton is transferred from the N5-atom of ornithine to the distal oxygen of FAD_{OO-} to form a FAD_{OOH}:Orn complex (Fig. 3.5). A mechanism evoking proton transfer from ornithine to the FAD_{OO-} has been proposed in PvdA, a related N5-ornithine flavoenzyme monooxygenase from *Pseudomonas aeruginosa*. The authors proposed that an enhancement on $k_{OO(H)}$ (80-fold) in the presence of ornithine might be coupled to proton transfer from ornithine to FAD_{OO-} in PvdA.[13] In SidA, the presence of ornithine also enhances $k_{OO(H)}$. We previously attributed this enhancing effect, as well as the effect observed with lysine and arginine, to the presence of the positive charge from N5-ornithine, or other ligands, being in close proximity to the C4a-FAD. This would stabilize the flavin semiquinone and superoxide radical pair that forms prior to formation of the covalent oxygenated flavin intermediate.[7] In

order to determine if a positive charge close to the C4a-FAD is in fact required to enhance $k_{OO(H)}$, we tested the effect of norvaline on this step. Since norvaline does not have a positive charge on the side chain, it should not have an enhancement effect. However, norvaline enhances $k_{OO(H)}$ by ~7-fold. This is less than the enhancement determined for arginine (~200-fold) but similar to the enhancement observed with ornithine (~20-fold) and lysine (~10-fold) (Table 3.4). Clearly, a positive charge is not absolutely necessary to enhance the formation of $FAD_{OO(H)}$ in SidA. This is inconsistent with the mechanism of protonation of FAD_{OO-} by ornithine. Similarly, the SKIE studies presented here do not support a proton transfer from ornithine (or solvent) to the FAD_{OO-} to form $FAD_{OOH.}$ In addition, pH studies on SidA have shown that $k_{OO(H)}$ is pH independent and no changes in the spectra of the intermediate characteristic of protonation of FAD_{OO-} were observed.[12] We interpreted these data as suggesting that the intermediate observed in SidA is the FAD_{OOH}. Furthermore, the spectra of the intermediate are identical in the presence of ornithine, norvaline, or in the absence of ligand, suggesting that formation of the intermediate is independent of ornithine (or analog) binding and most likely is the FAD_{OOH} (Fig. 3.6). Structural analysis of the SidA active site fails to identify a residue in proper distance to function as an acid to protonate the flavin intermediate. Similarly, in the $FAD_{OOH}/NADP^+$/Orn complex there is not enough space to accommodate a water molecule to donate a proton (Fig. 3.7). Together, the data does not support the protonation of FAD_{OO-} by ornithine, solvent, or other amino acids in the active site of SidA and suggest that the intermediate observed in SidA is the FAD_{OOH}.

Table 3.3 Critical bond lengths (in Å) and charges (Mulliken charges in atomic unit) for different protonation states of the C4a-peroxyflavin intermediate in either the presence or absence of ornithine after geometry optimization. The geometry optimizations were performed at B3LYP/6-31+G(d) level of theory. The most considerable differences among the geometry optimized complexes belong to the distance of the hydrogen atom (HX) and the distal oxygen (OX2). HX is initially covalentally bonded to the distal oxygen in FAD_{OOH} (no ligand) and FAD_{OOH}:Orn complexes. In FAD_{OO-}:Orn^+, the hydrogen atom moves to the distal oxygen from N5-ionized ornithine. In FAD_{OO-} (no ligand) and FAD_{OO-}:Orn, this hydrogen is shared between the O2' from the nicotinamide ribose of $NADP^+$ and the distal oxygen. The negative charge on the O2' increases when the hydrogen is shared with the distal oxygen.

	Bond Length (Å)			**Charges**		
	C4(FAD)-OX1	OX1-OX2	OX2-HX	OX1	OX2	O2'
FAD_{OO-} (no ligand)	1.476	1.464	1.062	-0.336	-0.518	-0.737
FAD_{OOH} (no ligand)	1.474	1.463	0.985	-0.341	-0.426	-0.658
FAD_{OO-} :Orn	1.430	1.476	1.441	-0.339	-0.552	-0.709
FAD_{OO-}:Orn^+	1.501	1.455	1.020	-0.321	-0.484	-0.669
FAD_{OOH} :Orn	1.486	1.458	0.991	-0.304	-0.413	-0.650

OX1: Proximal oxygen
OX2: Distal oxygen
HX: Hydrogen atom covalently bonded to or shared with the distal oxygen
O2': Oxygen from nicotinamide 2'-OH ribose of $NADP^+$
Orn: ornithine neutral at the N5 atom
Orn^+: ornithine with a positive charge at the N5 atom

Table 3.4 Effect of different ligands on the formation of the C4a-(hydro)peroxyflavin intermediate in SidA.

	$k_{OO(H)}$, s^{-1}	fold-effect
no ligand	0.30 ± 0.05	
ornithine	7 ± 1	23 ± 5
lysine	3.27 ± 0.07	11 ± 2
arginine	62 ± 3	210 ± 40
norvaline	2.1 ± 0.2	7 ± 1

Conditions: 100 mM sodium phosphate, pH 7.5, 8 °C. 10 mM of each ligand was used.

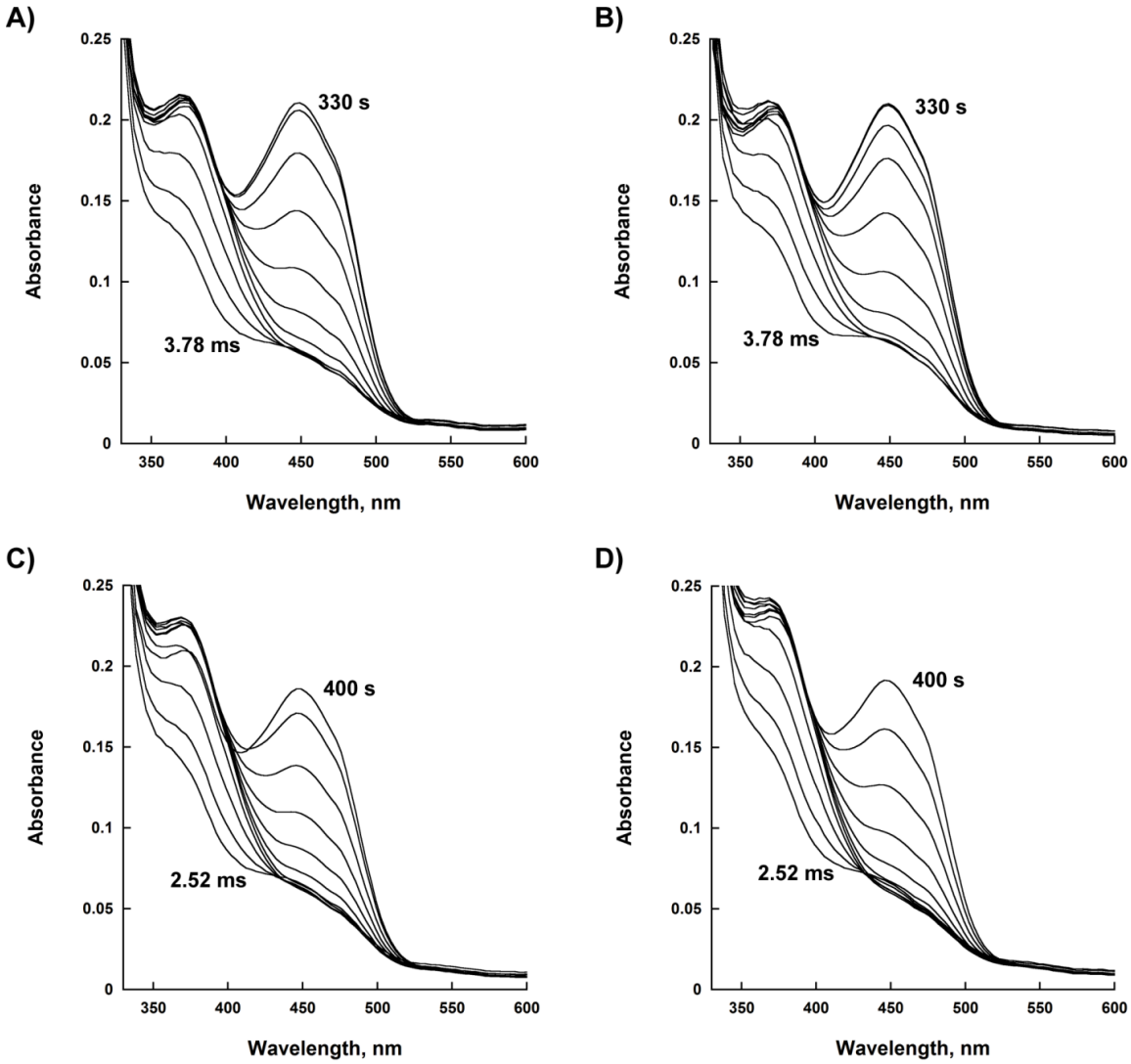

Figure 3.2 SidA flavin oxidation spectra (-) L-ornithine at 25 °C. A) Flavin oxidation in H_2O with NADPH. B) Flavin oxidation in H_2O with NADPD. C) Flavin oxidation in 95% D_2O with NADPH. D) Flavin oxidation in 95% D_2O with NADPD. In total, one thousand spectra were taken in each experiment (only selected spectra are shown in each panel).

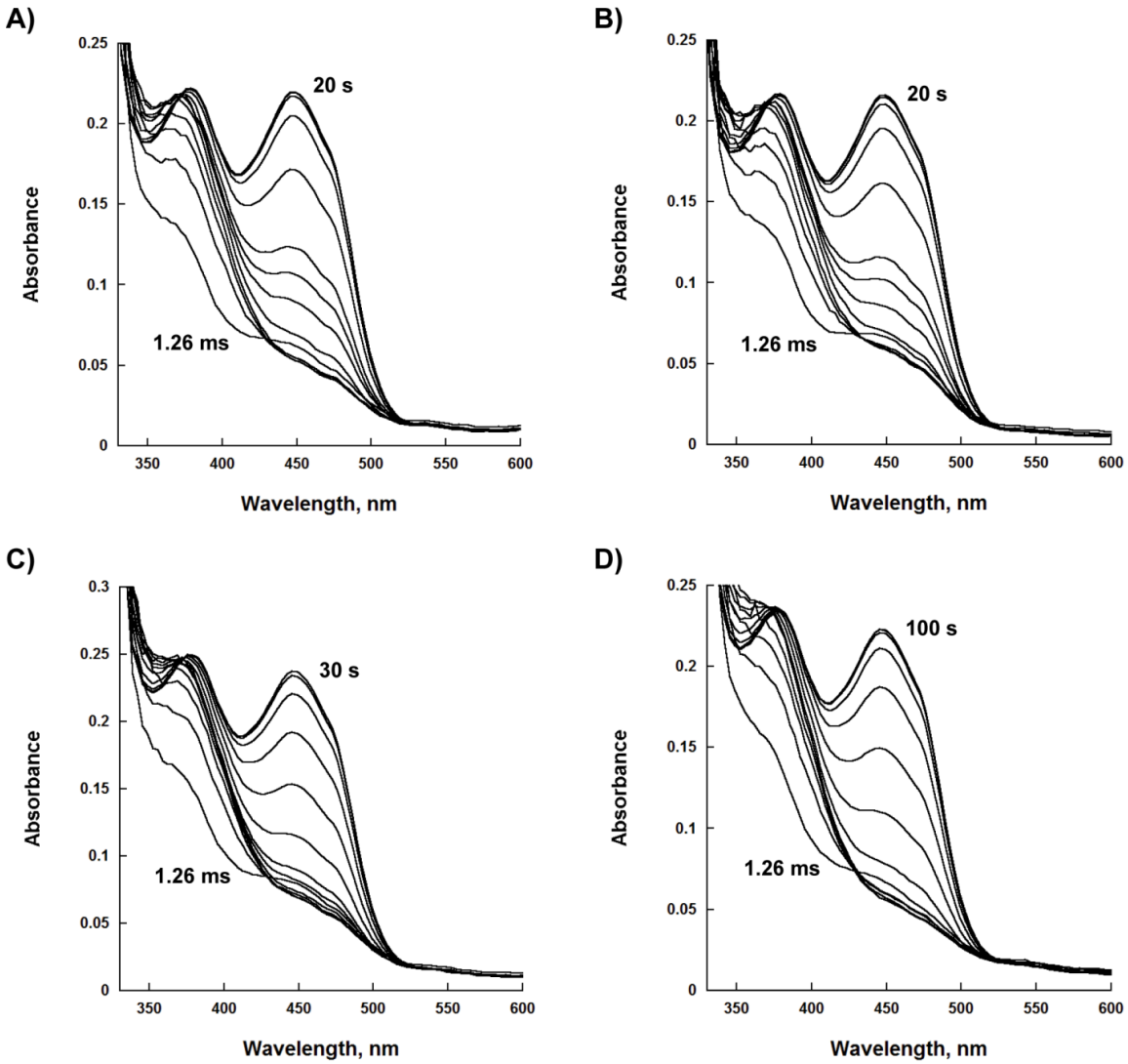

Figure 3.3 SidA flavin oxidation spectra with 10 mM L-ornithine at 25 °C. A) Flavin oxidation in H_2O with NADPH. B) Flavin oxidation in H_2O with NADPD. C) Flavin oxidation in 95% D_2O with NADPH. D) Flavin oxidation in 95% D_2O with NADPD. In total, one thousand spectra were taken in each experiment (only selected spectra are shown in each panel).

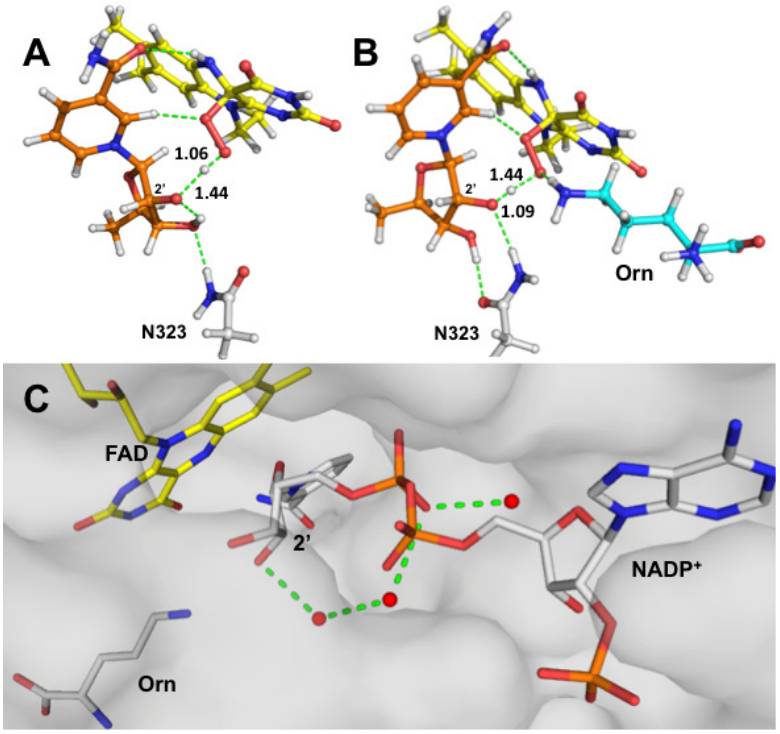

Figure 3.4 DFT optimized coordination of the intermediate formed in SidA show that the 2'-OH of the nicotinamide ribose is in transition to the distal oxygen when the starting complex is either FAD_{OO^-} (A) or the FAD_{OO^-}:Orn complex (B) (distances in Å). Panel C, shows a top view of SidA highlighting the proposed water (red spheres) and phosphate mediated proton shuttle that will facilitate protonation of FAD_{OO^-}.

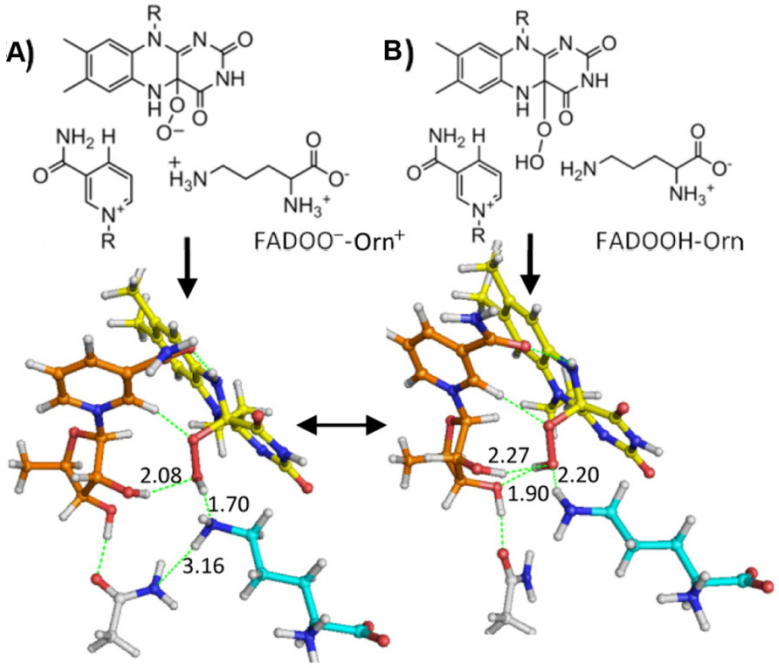

Figure 3.5 Ground state liganded complexes of SidA optimized at B3LYP/6-31+G(d) theory level, stating different protonation states of ornithine and oxygenated flavin intermediate. N323 in hydrogen binding distance from $NADP^+$ is the only residue displayed here for simplicity. The figure shows the optimized geometries of A) FAD_{OO-}:Orn^+ and B) FAD_{OOH}:Orn. Although FAD_{OOH}:Orn^+ forms a stable complex by energy optimization, this complex was not studied because it is not predicted to be an active complex since the lone electron pair of the nucleophilic heteroatom (N5) is already captured by an additional hydrogen atom. Two hydrogen binding orientations are considered for the FAD_{OOH}:Orn complex: FAD_{OOH} acting as a hydrogen bond donor and the amine group of Orn acting as hydrogen bond acceptor and vice versa (Figs. A and B). The FAD_{OOH}:Orn complex with the distal oxygen as the hydrogen bond acceptor from the amine group (B) is the least stable complex, and in this case the C4a-hydroperoxide donates a hydrogen to the O3' of the nicotinamide ribose. The differences in the energy between these two arrangements of the hydrogen atom are 2.12 kcal/mol.

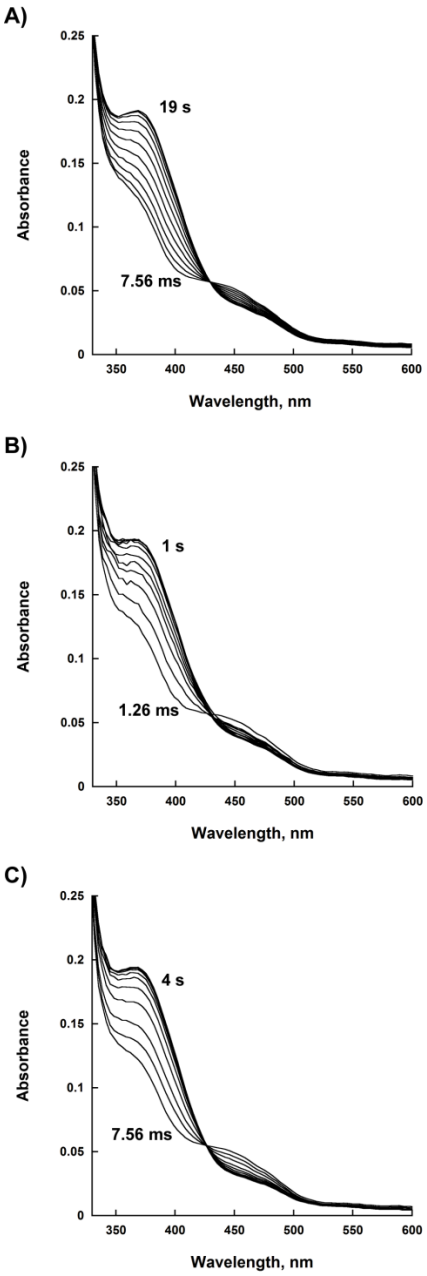

Figure 3.6 Formation of the C4a-(hydro)peroxyflavin intermediate in SidA at 8 °C. A) Formation of the intermediate with no ligands present. B) Formation of the intermediate in the presence of 10 mM ornithine. C) Formation of the intermediate in the presence of 10 mM norvaline. The observed intermediate corresponds to the increase in absorbance at 372 nm. In total, one thousand spectra were taken in each experiment (only selected spectra are shown in each panel).

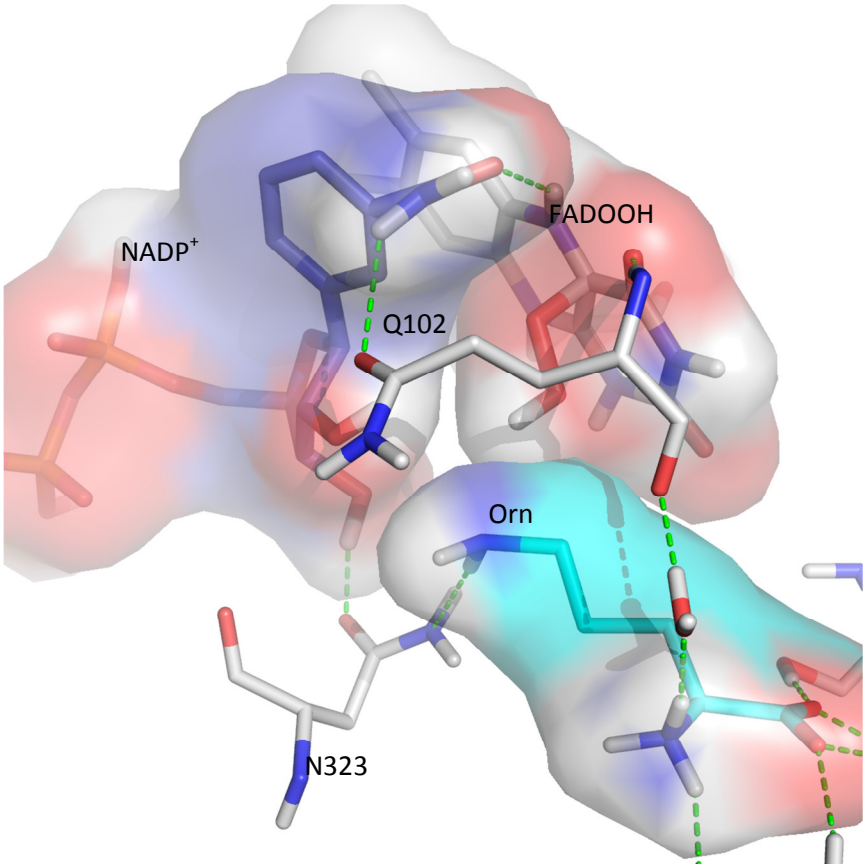

Figure 3.7 Surface presentation of the FAD_{OOH} intermediate, $NADP^+$ and Orn complex in the active site of SidA. The illustration of the electronic surface of cofactors, ligand, and active site residues (especially Q102 and N323) shows that, no water molecule(s) (or any other molecule that may work as acid/base) can be accommodated in the vicinity of the peroxide group to act as a proton donor. The figure is prepared by PyMol[13] using the default probe radius of 1.4 Å.

We favor the alternative mechanism suggested by the DFT results, where the N5-ornithine binds in the catalytically competent neutral form and formation of FAD_{OOH} is mediated by proton transfer from the 2'-OH of the nicotinamide ribose of $NADP^+$. Proton transfer might be facilitated by a water and β-phosphate-mediated proton shuttle network that connects the 2'-OH of the nicotinamide ribose to the solvent (Fig. 3.4C). We propose that the enhancement of $k_{OO(H)}$ in the presence of ornithine observed in SidA and PvdA originates from substrate induced preorganization of the active site. This would include alignment of the water molecules to form

the proton shuttle network, and proper hydrogen bonding interactions to position the 2'-OH of the nicotinamide ribose in optimal orientation for proton transfer to the distal oxygen of FAD_{OO-}.

In summary, the biochemical and computational results described here support a novel role for $NADP^+$ in the formation of FAD_{OOH} by donating a proton from the 2'-OH of the nicotinamide ribose. This is a previously unrecognized role for this cofactor in the mechanism of flavin-dependent monooxygenases and might be a general mechanism utilized for hydroxylating flavin monooxygenases that require $NADP^+$ for stabilization of the FAD_{OOH} as they all have a highly conserved mode coenzyme of binding.

2. Materials and Methods

2.1 Materials. L-ornithine, L-lysine, L-arginine, L-norvaline, buffers, and D_2O were obtained from Fisher Scientific (Pittsburg, PA). NADPH was obtained from EMD4 Biosciences (Billerica, MA). Glucose oxidase Type-X was obtained from MP Biomedical (Solon, OH). Alcohol dehydrogenase was obtained from Sigma Aldrich (St. Louis, MO). Isopropanol-*D*8 was obtained from Cambridge Isotope Laboratories, Inc. (Tewksbury, MA). SidA was expressed and purified as described previously.[15]

2.2 Synthesis of 4-pro-R-^{2}H-NADPH. 4-*pro-R*-^{2}H-NADPH (NADPD) was synthesized by the method of Jeong with some modifications as described previously.[16, 17] NADPH was synthesized by the same method as a control.

2.3 Kinetic isotope and ligand effects on flavin oxidation. The rate of flavin oxidation was determined anaerobically using an Applied Photophysics SX20 stopped-flow spectrophotometer

(Leatherhead, UK) in double mixing mode. All buffers were made anaerobic by applying vacuum for 1 hour intervals and cycling with ultra-pure argon five times for 6 hours total. The stopped-flow was made anaerobic by flushing with 1 mL of 100 µg/mL glucose oxidase and 100 mM D-glucose dissolved in 100 mM sodium acetate, pH 5.0. SidA and synthesized dinucleotides were made anaerobic by the same process as used for the buffers, but in 20 minute intervals of applying vacuum and cycling with ultra-pure argon for 1.5 hours total. Commercial NADPH and all ligands were made anaerobic by dissolving in anaerobic buffer inside of the glove box. Reactions were performed at 25 °C for the isotope effect experiments and at 8 °C for the ligand effect experiments. The temperature was lowered for the ligand effect experiments in order to more accurately determine the rate of formation of the C4a-hydroperoxyflavin when L-arginine is present. Reactions were performed in 100 mM sodium phosphate pL 7.5 in either 100% H_2O or 95% D_2O (final concentration after mixing). Oxygen saturated buffer (1.2 mM) was obtained by bubbling 100% oxygen gas into a closed vial for 30 minutes at 25 °C.[18] For reactions in H_2O, 60 µM oxidized SidA was reduced for 60 seconds with either 60 µM NADPH or NADPD and then oxidized with 300 µM oxygen (concentration after mixing). All ligands were present at a concentration of 10 mM after the second mix. For all experiments in 95% D_2O, concentrated SidA (in 100% H_2O at 300 µM) was diluted to 60 µM yielding 80% D_2O. After two sequential mixes with 100% D_2O buffer, SidA oxidation was observed in 95% D_2O. For experiments where SidA was incubated for a longer time period (after the first mix), before reacting with oxygen, the same procedure as described above was followed, but the time between the first and second mixing was varied from 60 to 600 sec, longer incubation times did not result in changes to the KIE value.

2.4 Data analysis. All data were fit using KaleidaGraph (Synergy Software, Reading, PA). The rates of formation of the C4a-(hydro)peroxyflavin intermediate were determined by fitting the increase in absorbance at 372 nm to a single exponential rise equation (eq. 1). Flavin oxidation monitored at 452 nm occurred in two phases. At this wavelength, a fast but small decrease in absorbance is observed before the increase in absorbance characteristic of flavin oxidation occurs. The fast phase is coupled to the formation of the C4a-(hydro)peroxyflavin. The absorbance changes at 452 nm best fit to a double exponential equation (eq. 2).

(1) $$v = c + a(1 - e^{-(k \times t)})$$

(2) $$v = c + a_1(1 - e^{-(k_1 \times t)}) + a_2(1 - e^{-(k_2 \times t)})$$

2.5 Protein structures and molecular dynamics (MD) simulations. The model system was based on the crystal structure of re-oxidized SidA in complex to $NADP^+$ and ornithine (PDB:4B67). The protonation states of ionizable residues in the structures were determined using H++.[19] To establish the proper hydrogen bond networking, the enzyme-reactants complexes, were subjected to conventional MD simulations while a large harmonic force constant of 1.0×10^6 (kJ mol^{-1} nm^{-2}) was applied to restrain the position of the heavy atoms of the protein, cofactors and ligands. The cofactors were simulated as they are bound to the enzyme, $NADP^+$, and hydroquinone form of FAD ($FADH^-$). The N5 of ornithine was ionized while the α-amino and α-carboxylate groups were unionized. The MD simulations were performed with Gromacs 4.5[20] including energy minimization and 500 ps of MD production at NPT ensemble. The system preparation and MD procedures were described previously.[21]

2.6 DFT analyses of SidA. The equilibrated structures from MD trajectories were used to study the reaction mechanisms quantum mechanically. In addition to ornithine FAD, and $NADP^+$, the residues in hydrogen-bonding distance of ornithine including Q102, K107, N293, N323, S469 and a water molecule that links the N5 amine group of ornithine to the side chain of Q102 were included in the final system. Apart from Q102, the side chains of the selected residues hydrogen bonding to ornithine are at least 8 Å from the reaction center and were excluded from the calculations as they do not affect the reaction significantly. Carbon atoms of the active site amino acids were constrained during the optimization. In order to reduce the computational cost, only the nicotinamide and ribose moieties from $NADP^+$ and the isoalloxazine ring along with the 1' and 2' carbons of the ribityl chain from FAD were selected for the calculations. The peroxide group was added to FAD as described by Polyak *et al*.[22] Geometry optimizations were carried out using B3LYP functional (default spin) with 6-31+G(d) basis set. A larger basis set 6-311+G(p,d) was used for single point energy calculations on the optimized geometries. No water molecules are expected to be in the proximity of the reaction center, therefore the exclusion of explicit water molecules did not have a significant impact on reaction features and parameters. All subsequent DFT calculations were conducted using the Gaussian 09 package.[23]

3. Acknowledgements

This work was supported by a grant from the NSF-MCB-1021384 (to PS).

4. References

(1) van Berkel, W. J., Kamerbeek, N. M., and Fraaije, M. W. (2012) *J. Biotechnol. 124*, 670-689.
(2) Chaiyen, P., Fraaije, M. W., and Mattevi, A. (2012) *Trends Biochem. Sci. 37*, 373-380.
(3) Eisendle, M., Oberegger, H., Zadra, I., and Haas, H. (2003) *Mol. Microbiol. 49*, 359-375.

(4) Hissen, A. H., Wan, A. N., Warwas, M. L., Pinto, L. J., and Moore, M. M. (2005) *Infect. Immun. 73*, 5493-5503.
(5) Chocklett, S. W., and Sobrado, P. (2010) *Biochemistry 49*, 6777-6783.
(6) Mayfield, J. A., Frederick, R. E., Streit, B. R., Wencewicz, T. A., Ballou, D. P., and DuBois, J. L. (2010) *J. Biol. Chem. 285*, 30375-30388.
(7) Franceschini, S., Fedkenheuer, M., Vogelaar, N. J., Robinson, H. H., Sobrado, P., and Mattevi, A. (2012) *Biochemistry 51*, 7043-7045.
(8) Alfieri, A., Malito, E., Orru, R., Fraaije, M. W., and Mattevi, A. (2008) *Proc. Natl. Acad. Sci. USA 105*, 6572-6577.
(9) Orru, R., Dudek, H. M., Martinoli, C., Torres Pazmino, D. E., Royant, A., Weik, M., Fraaije, M. W., and Mattevi, A. (2011) *J. Biol. Chem. 286,* 29284-29291.
(10) Romero, E., Fedkenheuer, M., Chocklett, S. W., Qi, J., Oppenheimer, M., and Sobrado, P. (2012) *Biochim. Biophys. Acta 1824*, 850-857.
(11) Thotsaporn, K., Chenprakhon, P., Sucharitakul, J., Mattevi, A., and Chaiyen, P. (2011) *J. Biol. Chem. 286*, 28170-28180.
(12) Romero, E., Avila, D, and Sobrado, P. (2013) In *Flavins and Flavoproteins* Miller, S., Hille, R., Palfey, B. Ed., Lulu.
(13) Meneely, K. M., Barr, E. W., Bollinger, J. M., Jr., and Lamb, A. L. (2009) *Biochemistry 48*, 4371-4376.
(14) The PyMOL Molecular Graphics System, Version 1.5.0.4 ed., Schrödinger, LLC.
(15) Franceschini, S., Fedkenheuer, M., Vogelaar, N. J., Robinson, H. H., Sobrado, P., and Mattevi, A. (2012) *Biochemistry 51*, 7043-7045.
(16) Jeong, S. S., and Gready, J. E. (1994) *Anal. Biochem. 221*, 273-277.
(17) Dhatwalia, R., Singh, H., Solano, L. M., Oppenheimer, M., Robinson, R. M., Ellerbrock, J. F., Sobrado, P., and Tanner, J. J. (2012) *J. Am. Chem. Soc. 134*, 18132-18138.
(18) Harris, C. M., and Massey, V. (1997) *J. Biol. Chem. 272*, 8370-8379.
(19) Gordon, J. C., Myers, J. B., Folta, T., Shoja, V., Heath, L. S., and Onufriev, A. (2005) *Nucleic Acids Res. 33*, W368-W371.
(20) Hess, B., Kutzner, C., van der Spoel, D., and Lindahl, E. (2008) *J. Chem. Theory Comput. 4*, 435-447.
(21) Badieyan, S., Bevan, D. R., and Zhang, C. (2012) *Biochemistry 51*, 8907-8918.
(22) Polyak, I., Reetz, M. T., and Thiel, W. (2012) *J. Am. Chem. Soc. 134*, 2732-2741.
(23) Frisch, M. J., et al. (2009) Gaussian 09, Revision A.02, Gaussian, Inc., Wallingford, CT.

CHAPTER 4

The active site of SidA lowers the pK_a value for the N^5 of ornithine to allow for deprotonation and hydroxylation

Author Contributions:
Reeder Robinson performed all the research except the experiments mentioned below and wrote the chapter.

Pedro Rodriguez performed the steady-state pH profile of oxygen consumption.

Pablo Sobrado oversaw and directed the research.

Abstract

Siderophore A (SidA) from *Aspergillus fumigatus* is a flavin-containing monooxygenase that performs the NADPH dependent hydroxylation of the N^5 of L-Orn. In order for electrophilic hydroxylation by the C4a-hydroperoxyflavin to occur, the N^5 of L-Orn must be deprotonated. The high intrinsic pK_a value for this amine provides a barrier to catalysis in SidA, but the enzyme appears to efficiently overcome this hurdle. In this study, we examined the pL dependence of SidA in the absence of a substrate, with L-Orn, L-Lys, and L-norvaline (L-Nva) in order to probe the mechanism by which SidA stabilizes the C4a-hydroperoxyflavin and hydroxylates L-Orn. In the absence of L-Orn, a high pK_a value (≥9) for flavin oxidation was observed which corresponds to the N5 of the flavin. Upon binding of L-Orn, the pH dependence of SidA oxidation shifts to yield an apparent pK_a value of 6.7 ± 0.1. This reflects an altered pK_a value for the N^5 of L-Orn in the active site which allows for deprotonation of the N^5 of L-Orn at physiological pH and subsequent hydroxylation. A pK_a value of 7.73 ± 0.09 was calculated for the N^6 of L-Lys. This change in the observed pK_a value for L-Lys is likely due to differences in the microenvironments around the terminal amine groups as L-Lys protrudes further into the

active site than L-Orn. Solvent kinetic isotope effect studies in the pL independent regions for flavin oxidation indicate that in the absence of a substrate, proton transfer from the N5 of the flavin to eliminate hydrogen peroxide is rate-limiting, but with L-Lys present, the chemical steps of hydrogen peroxide elimination are not rate-limiting. This could suggest that instead of hydrogen peroxide elimination occurring through proton transfer from the N5 of the flavin, protrusion of L-Lys near the C4a locus provides a proton to the hydrogen peroxide leaving group.

1. Introduction

One of the most important factors of enzyme catalysis is pH. This can influence a number of parameters such as binding of substrates, turnover rate, and enzyme stability [1]. For instance, pH can affect the charge of an ionizable group either on the substrate or on a residue in the active site that interferes with substrate binding. Physiological pH can sometimes present a hurdle to enzyme catalysis where an ionizable group on a substrate needs to be (de)protonated in order for catalysis to occur, but the pK_a value of the ionizable group is significantly higher/lower than physiological pH [2-4]. Enzymes have the ability to compensate for this by altering the microenvironment and thus shifting the pK_a value of ionizable groups in the active site [2].

The FAD dependent L-Orn monooxygenase SidA from *Aspergillus fumigatus* faces this barrier to catalysis. SidA hydroxylates the N^5 of L-Orn through the generation of a C4a-hydroperoxyflavin intermediate [5, 6]. Hydroperoxyflavins perform electrophilic oxygenations on nucleophilic substrates (Scheme 4.1). Therefore, in order for SidA to be able to hydroxylate L-Orn, the N^5 must be in its deprotonated form. The pK_a value for the N^5 of L-Orn in free solution is 10.76 so at a physiological pH of 7.4, this group would primarily be in its protonated state [7]. SidA, however, efficiently converts L-Orn to N^5-hydroxy-L-Orn at physiological pH suggesting it

alters the microenvironment around the N^5 of L-Orn to lower the pK_a value so that it is in its deprotonated form in the active site.

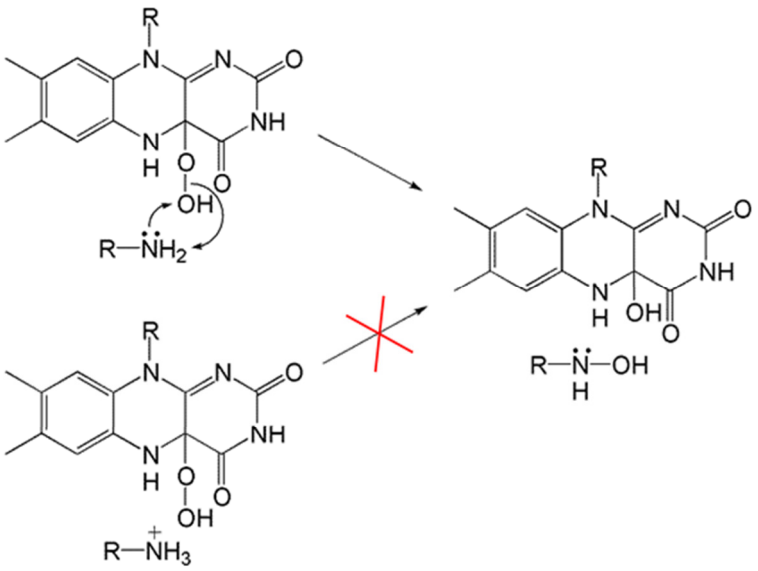

Scheme 4.1 Electrophilic hydroxylation of a primary amine by the C4a-hydroperoxyflavin. The substrate must be in its deprotonated form in order for hydroxylation to occur. Hydroxylation chemistry cannot occur when the substrate is in its deprotonated form.

Here, we examine the pH dependence of SidA under both steady-state and rapid reaction conditions with different substrates in order to determine the role of pH in the reaction of SidA. Also, we use D_2O to investigate the rate-limiting steps of flavin oxidation in the pL independent regions. Our findings show a high pK_a value for the N5 of the flavin when a substrate is not present. When L-Orn or L-Lys are bound, the observed pK_a values for flavin oxidation are significantly lower. This reflects the pK_a value for the terminal amines of L-Orn/L-Lys and suggests that SidA is able to modulate the microenvironment around this group. This allows for rapid deprotonation of L-Orn upon binding which ensures hydroxylation occurs. L-Lys however is not hydroxylated by SidA, but stimulates hydrogen peroxide elimination. We also show that the chemical steps of spontaneous hydrogen peroxide and water elimination in flavin oxidation

are rate-limiting/partially rate-limiting in flavin oxidation and the proton provided to the leaving group is mediated through the N5 of the flavin, consistent with previous studies [8, 9]. With L-Lys present, hydrogen peroxide elimination is not rate-limiting which could suggest that protrusion of the N^6 amine into the active site provides a proton to the hydrogen peroxide leaving group. These findings indicate a different chemical mechanism for L-Lys stimulated hydrogen peroxide elimination.

2. Materials and Methods

2.1 Materials. Buffers and media were obtained from Fisher Scientific (Pittsburgh, PA). BL21(DE3)-T1^R chemically competent cells were obtained from Sigma-Aldrich (St. Louis, MO). NADPH was obtained from EMD4 Biosciences (Billerica, MA). D_2O was obtained from Cambridge Isotope Laboratories (Tewksbury, MA). Chromatography columns were obtained from GE Healthcare.

2.2 Protein expression and purification. SidA was expressed in *E. coli* BL21(DE3)-T1^R competent cells and purified as previously described [10]. In general, ~25 mg of protein were obtained per liter of media. The purified proteins were stored in 100 mM sodium phosphate, 50 mM NaCl, pH 7.5, at -80 °C at a concentration of ~200 µM (based on flavin content) in 30 µL aliquots.

2.3 pH studies of oxygen consumption. The rate of oxygen consumption was measured using a Hansatech Oxygraph system (Norfolk, England). Reactions consisted of a 1 mL volume at 25 °C. Between pH values 6 – 8, 100 mM sodium phosphate was used, between pH values 8.5 – 9.0, 100 mM Tris-SO_4 was used, and at pH 9.5, 100 mM sodium carbonate/bicarbonate was used.

NADPH was kept constant at a concentration of 1 mM while L-Orn was varied between 0.1 − 10 mM. Reactions were initiated by addition of 2 μM SidA and monitored for 5 minutes with constant stirring.

2.4 pH studies of flavin oxidation. All rapid reaction experiments were carried out at 25 °C using an SX-20 stopped-flow spectrophotometer (Applied Photophysics, Leatherhead, UK) in an anaerobic glove box (Coy, Grass Lake, MI). Preparation of anaerobic buffer was carried out through five cycles of vacuum and flushing with O_2-free argon after 1 hr of continuous vacuum. This was repeated five times for a total of five hrs. The enzyme was made anaerobic through constant cycles of vacuum and flushing with O_2-free argon for 1 hr. The stopped-flow was made anaerobic by flushing with 1 mL of anaerobic 100 mM sodium acetate, pH 5.0, containing 100 mM D-glucose and 100 μg/mL glucose oxidase Type-X. Substrates were made anaerobic by dissolving in anaerobic buffer inside the glove box.

The rate of flavin oxidation was measured in double mixing mode. Anaerobic SidA (60 μM before mixing) was first mixed with an equal volume of NADPH (60 μM before mixing) in 20 mM Tris-Cl, 200 mM NaCl, pL 8.0. This mixture was allowed to incubate in an ageing loop for 60 seconds until the bound flavin was fully reduced. The reduced SidA–$NADP^+$ complex was then allowed to react with air saturated buffer (130 μM oxygen after mixing since at 1 atm and 25 °C $[O_2]$ = 260 μM). This air saturated solution contained 200 mM of buffer which rapidly jumped the pL to the desired value in the flow cell. Between pL values 6 − 8, sodium phosphate was used, between pL values 8.5 − 9.0 Tris-SO_4 was used, and between pL values 9.5 − 10.5, sodium carbonate/bicarbonate was used. In pL experiments with different amino acids present, 100 mM L-Orn, 15 mM L-Lys, and 15 mM L-Nva were used. For L-Orn dependency experiments

on flavin oxidation, L-Orn was varied between 2.5 − 100 mM at pH 6.0 and 0.1 − 15 mM at pH 9.0. For the reactions in D_2O, SidA was concentrated to ~400 µM (based on flavin content) and diluted to 60 µM in a 100% D_2O buffer of 20 mM Tris-Cl, 200 mM NaCl, pD 8.0. This gave a concentration of ~85% D_2O, and after two mixes in the stopped-flow with 100% D_2O buffer, a final D_2O concentration of ~96% was achieved. The proper pD of all D_2O buffers were calculated by adding 0.4 to the value on the pH meter, which is the variation from the change in the equilibrium on a hydrogen selective glass electrode [11]. All solutions were checked for their proper pL values with a Fisher Scientific Accumet AB15+ Basic pH meter. Spectra were taken on a logarithmic time scale until oxidation was complete.

2.5 Data analysis. All data were fit using KaleidaGraph (Synergy Software, Reading, PA). For flavin oxidation studies, the increase in absorbance at 372 nm which corresponds with formation of the C4a-hydroperoxyflavin intermediate was fit to eq. 1, which describes a single exponential rise. The subsequent increase in absorbance at 452 nm which corresponds with flavin oxidation was fit to eq. 2, which describes a double exponential rise. The first exponential rate of flavin oxidation calculated in eq. 2 is omitted in this study as it corresponds to the rate of formation of the C4a-hydroperoxyflavin calculated with eq. 1 at 372 nm.

$$v = c + a(1 - e^{-(k \times t)}) \tag{1}$$

$$v = c + a_1(1 - e^{-(k_1 \times t)}) + a_2(1 - e^{-(k_2 \times t)}) \tag{2}$$

For flavin oxidation studies with varying L-Orn at pH 6, the k_{obs} values obtained at 372 nm were fit to eq. 3 to determine k_{OOH}, K_D, and a substrate inhibition constant for L-Orn (K_I). The k_{obs} values obtained at 372 nm when L-Orn was varied at pH 9 were fit to eq. 4 as no substrate

inhibition was observed. The k_{obs} values obtained at 452 nm when L-Orn was varied at pH values 6 and 9 were fit to eq. 5 in order to determine k_{OX} and K_m values for L-Orn in regards to flavin oxidation.

$$k_{obs} = \frac{k_{OOH} \times [S]}{K_D + [S] + \frac{[S^2]}{K_I}} \quad (3)$$

$$k_{obs} = \frac{k_{OOH} \times [S]}{K_D + [S]} \quad (4)$$

$$k_{obs} = \frac{k_{OX} \times [S]}{K_m + [S]} \quad (5)$$

The pH dependence for formation of the C4a-hydroperoxyflavin intermediate at 372 nm was fit to eq. 6 which describes a bell-shaped curve with two pK_a values. The pL dependence of flavin oxidation at 452 nm and the pH dependences of k_{cat} and k_{cat}/K_m were fit to eq. 7 which describes a curve with a single pK_a value with increasing activity as the pL increases and plateau regions at high and low pL. The upper limits and lower limits for the pL profiles are denoted by *C* and *A*, respectively.

$$y = \frac{C}{1 + 10^{(pK_{a1} - pH)} + 10^{(pH - pK_{a2})}} \quad (6)$$

$$y = \frac{C + A(10^{(pK_a - pL)})}{1 + 10^{(pK_a - pL)}} \quad (7)$$

3. Results

3.1 pH profile for steady-state oxygen consumption with L-Orn. The steady-state pH profile of oxygen consumption with varying L-Orn was performed in order to determine the role of pH on

the activity of SidA and the protonation state of L-Orn upon binding to SidA. The data in Fig. 4.1A shows that as pH increases, the k_{cat} value of SidA increases with a single calculated pK_a value of 7.0 ± 0.2. The dependence of k_{cat}/K_m in Fig. 4.1B shows a similar trend as the k_{cat} pH profile with increasing values as pH increases and a single calculated pK_a value of 7.7 ± 0.1. The amplitude of the k_{cat}/K_m pH profile is greater than the k_{cat} pH profile because as pH increases, the apparent K_m for L-Orn decreases by ~10-fold across the pH range studied. This data suggests that L-Orn binds to SidA in the deprotonated state because as pH increases and the N^5 of L-Orn is deprotonated, the apparent affinity for L-Orn increases.

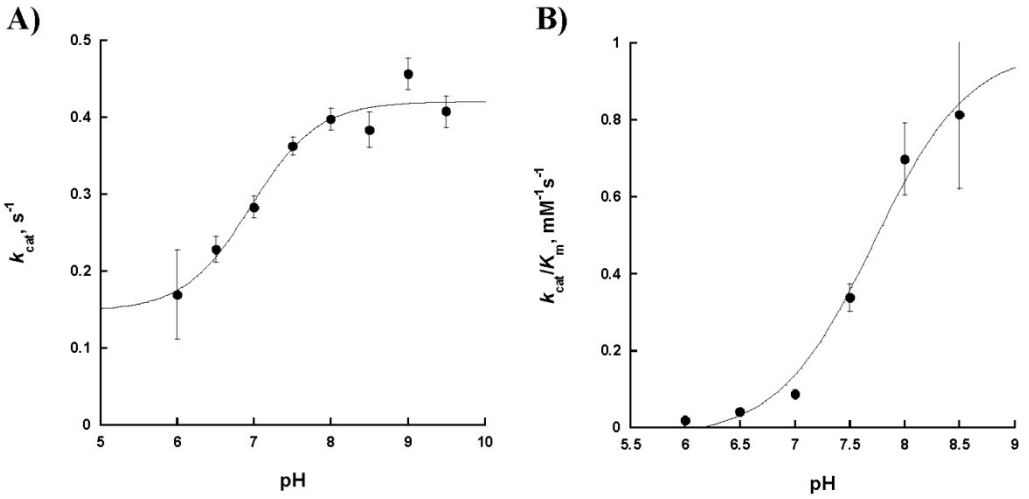

Figure 4.1 Effect of pH on the steady-state oxygen consumption activity of SidA. A) Effect of pH on the k_{cat} value for oxygen consumption of SidA. B) Effect of pH on the k_{cat}/K_m value for oxygen consumption of SidA.

3.2 pH profiles for formation of the C4a-hydroperoxyflavin. The pH profiles for formation of the C4a-hydroperoxyflavin intermediate were determined in both the presence and absence of L-Orn in order to determine if any ionizable groups contributed to oxygen reactivity in SidA. The data in Fig. 4.2 shows a bell-shaped pH profile for formation of the C4a-hydroperoxyflavin intermediate in both the presence and absence of L-Orn. At the extreme pH values, it appears

there is some decrease in oxygen reactivity, but this could possibly be due to denaturation of SidA. Accurate pK_a values were unable to be determined for formation of the C4a-hydroperoxyflavin, but if oxygen reactivity is dictated by ionizable groups in SidA, the pK_a values are well outside the physiological pH range (<6 and >10). This data also indicates that the solvent kinetic isotope effect (SKIE) experiments in our previous study reflect their true SKIE values as they were performed at pL 7.5 which appears to be in the pL independent region for formation of the C4a-hydroperoxyflavin [8].

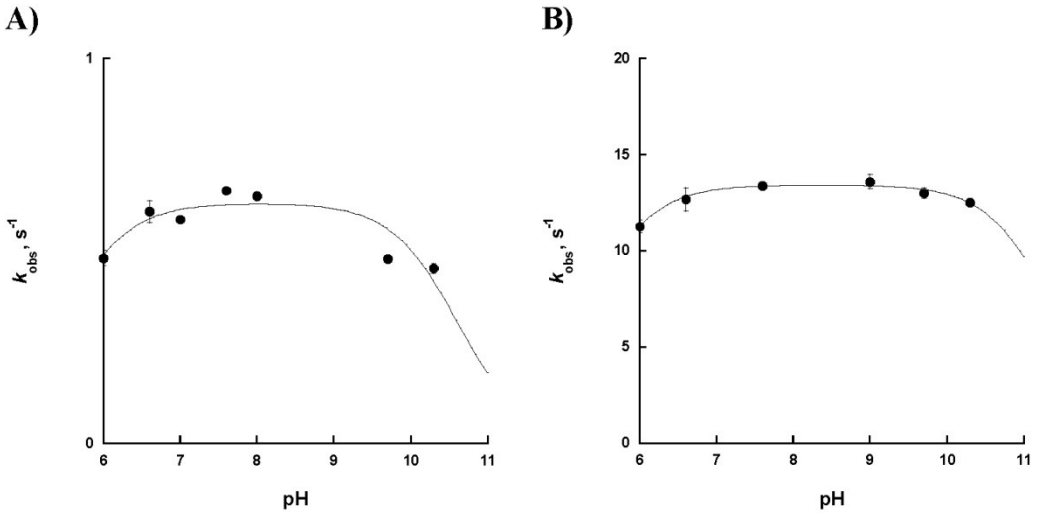

Figure 4.2 Effect of pH on formation of the C4a-hydroperoxyflavin for SidA determined at 372 nm on the stopped-flow spectrophotometer in the presence and absence of L-Orn. A) Effect of pH on formation of the C4a-hydroperoxyflavin in the absence of L-Orn. B) Effect of pH on formation of the C4a-hydroperoxyflavin in the presence of 100 mM L-Orn.

3.3 pL profile for flavin oxidation in the absence of a substrate. The pL profile for SidA flavin oxidation in the absence of a substrate was performed in order to calculate the pK_a value and SKIE of flavin oxidation in the pL independent region. It is essential to calculate SKIEs in their pL independent regions as the pK_a values of ionizable groups can change in D_2O. Therefore, a KIE in a pL dependent region would not be a true KIE as the pK_a change would have an effect

on the observed rates. The data in the absence of substrate in Fig. 4.3B and Table 4.1 indicates a single pK_a value for flavin oxidation >9 in H_2O and a pK_a value >10 in D_2O where the rate of flavin oxidation increases as pL increases. The pK_a values could not be accurately determined as SidA is unstable at pH ~10 and the upper rate limit of flavin oxidation could not be defined. This data is consistent with previous experiments with SidA where a high pK_a value was observed for flavin oxidation in the absence of a substrate [12, 13]. The kinetic traces at 452 nm in Fig. 4.3A show flavin oxidation occurs mainly in a single phase regardless of pH. Fig. 4.4 shows the spectra of oxidation do not change between the different pH values, but at high pH the stability of the C4a-hydroperoxyflavin is significantly lower where the peak at 372 nm is not as well resolved. A SKIE of 2.30 ± 0.07 was calculated at pL 7.0 which is consistent with our previous study at pL 7.5 [8]. Previously, in SidA and pyranose-2-oxidase, the N5 proton of the flavin has been shown to be involved in hydrogen peroxide elimination where it is in flight during a rate-limiting transition state [8, 9]. This data is consistent with the observed pK_a value for flavin oxidation in SidA in the absence of a substrate reflecting the pK_a value for the N5 of the flavin. Also, the high estimated pK_a value for the N5 of the flavin in SidA (>9) is consistent with NMR studies which estimate the pK_a value for the reduced form of the N5 to be ≥20 [14]. At lower pH values, the N5 proton of the C4a-hydroperoxyflavin is not readily available for extraction to the hydroperoxide leaving group leading to a slow rate of flavin oxidation. At higher pH values though, the N5 of the C4a-hydroperoxyflavin is rapidly deprotonated and transferred to the hydroperoxide leaving group, resulting in a less stable C4a-hydroperoxyflavin and a faster rate of flavin oxidation.

Table 4.1 Observed pK_a values and solvent kinetic isotope effect values for SidA oxidation.

Parameter	no substrate	L-Orn	L-Lys	L-Nva
pK_a, H_2O	>9	6.7 ± 0.1	7.73 ± 0.09	>9
pK_a, D_2O	>10	7.18 ± 0.05	8.42 ± 0.07	>10
SKIE	2.30 ± 0.07[a]	1.59 ± 0.01[b]	1.0 ± 0.1[b]	1.61 ± 0.01[a]

All pL experiments were performed at 25 °C. [a]The SKIE values for flavin oxidation with no substrate and L-Nva were calculated at pL 7.0. [b]The SKIE values for flavin oxidation with L-Orn and L-Lys were calculated using the upper limits obtained from the fits of the pL profiles.

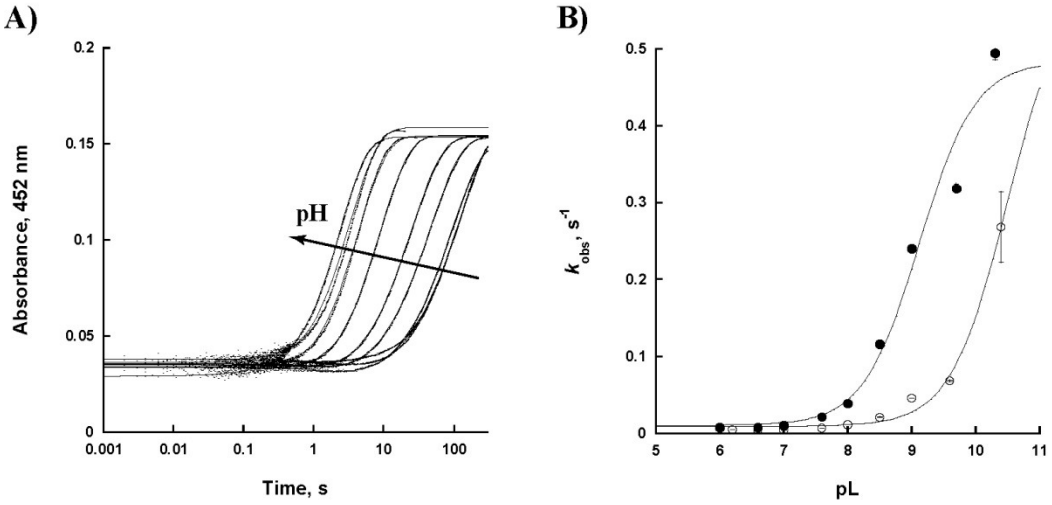

Figure 4.3 Effect of pL on flavin oxidation in the absence of a substrate for SidA determined at 452 nm on the stopped-flow spectrophotometer. A) Kinetic traces with fits of flavin oxidation at 452 nm for SidA in the absence of a substrate. B) Effect of pL on flavin oxidation in the absence of a substrate. Closed circles (●) denote pH studies in 100% H_2O and open circles (○) denote pD studies in ~96% D_2O.

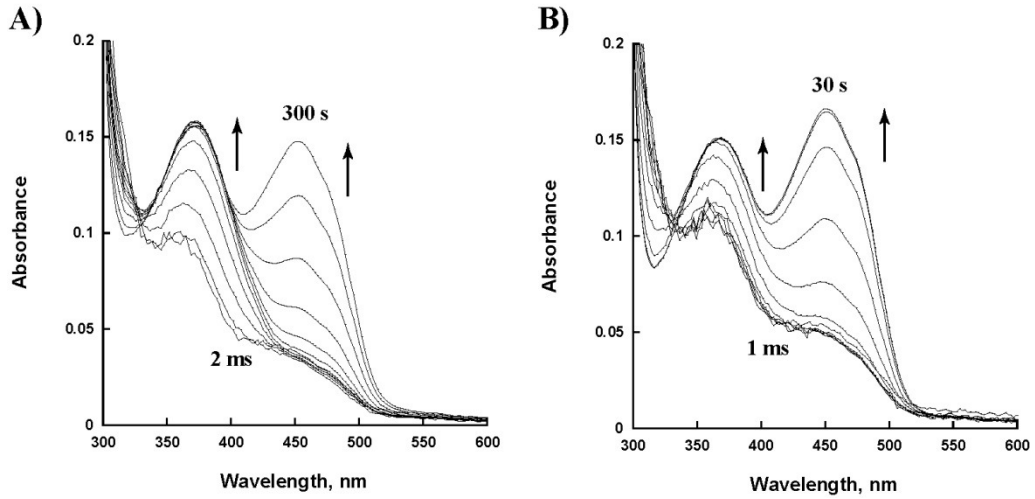

Figure 4.4 Flavin spectra of oxidation for SidA on the stopped-flow spectrophotometer in the absence of a substrate. A) Flavin spectra of oxidation at pH 6. B) Flavin spectra of oxidation at pH 9.

3.4 pL profile for flavin oxidation with L-Orn. The pL profile for flavin oxidation with L-Orn was performed in order to determine if the addition of a hydroxylatable substrate alters the pK_a value for flavin oxidation, and if the chemical steps of water elimination are rate-limiting in the pL independent region. The data in Fig. 4.5 shows a significant shift in the pL profile compared to in the absence of a substrate with single calculated pK_a values of 6.7 ± 0.1 in H_2O and 7.18 ± 0.05 in D_2O. The traces of flavin oxidation with L-Orn are consistent with the traces in the absence of a substrate where flavin oxidation occurs in a single phase throughout the pH values studied. One possibility for the shift in the observed pK_a value for flavin oxidation is that the N^5 of L-Orn is altering the pK_a value for the N5 of the flavin. This possibility can be ruled out as Fig. 4.6 shows that the N5 of the flavin and the N^5 of L-Orn are separated by a distance of 6.32 Å which is too far of a distance for any direct interaction to occur [15]. A more reasonable possibility is the observed pK_a value here is not for the N5 of the flavin, but rather the pK_a value for the N^5 of L-Orn in the active site. This would indicate the N^5 of L-Orn is deprotonated in the active site allowing for electrophilic hydroxylation by the C4a-hydroperoxyflavin [16]. A SKIE value of

1.59 ± 0.01 was calculated from the upper limit of the fits at high pL. This SKIE value is significantly lower than what was calculated in our previous study with L-Orn because the SKIE was not determined in the pL independent region [8]. Despite this, it appears that the chemical steps of water elimination after hydroxylation are partially rate-limiting to flavin oxidation.

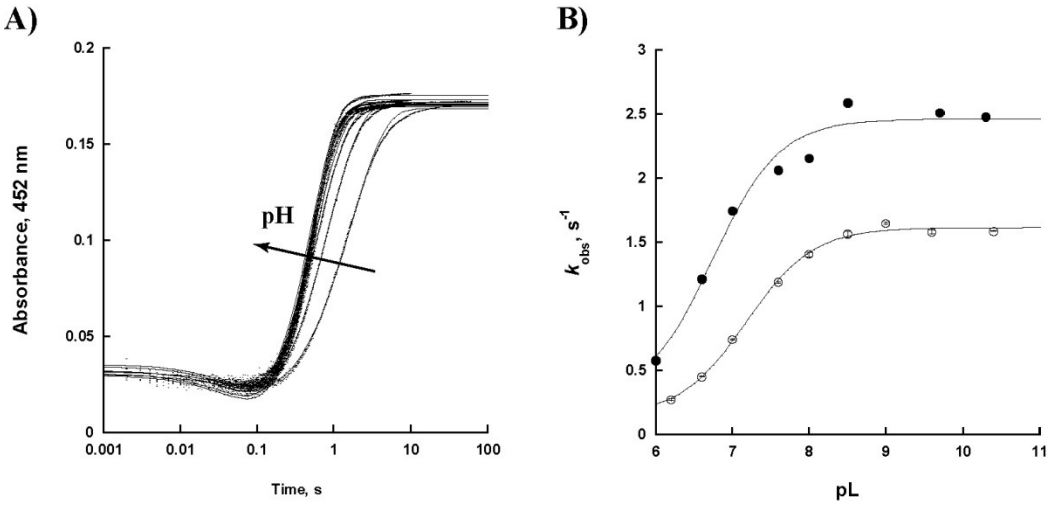

Figure 4.5 Effect of pL on flavin oxidation with L-Orn for SidA determined at 452 nm on the stopped-flow spectrophotometer. A) Kinetic traces with fits of flavin oxidation at 452 nm for SidA with 100 mM L-Orn present. B) Effect of pL on flavin oxidation in the presence of 100 mM L-Orn. Closed circles (●) denote pH studies in 100% H_2O and open circles (○) denote pD studies in ~96% D_2O.

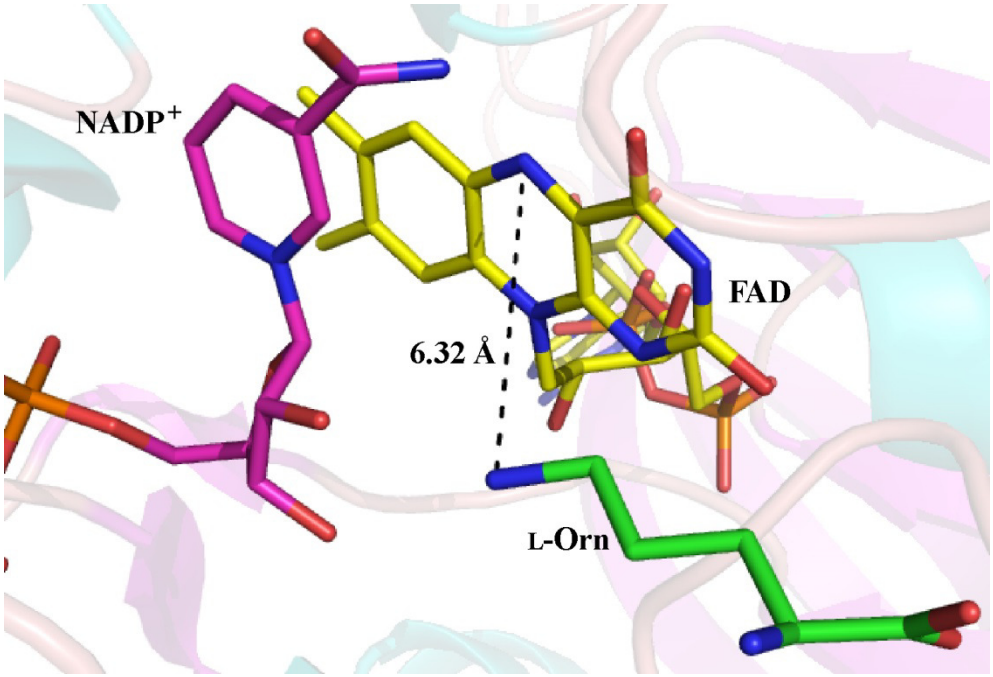

Figure 4.6 Active site of SidA with L-Orn bound (PDB code 4B63). The calculated distance between the N5 of the flavin and the N^5 of L-Orn of 6.32 Å suggests that L-Orn is not altering the pK_a value for the N5 for the flavin.

3.5 pL profile for flavin oxidation with L-Lys. SidA is selective for hydroxylation of L-Orn where L-Lys is a non-substrate effector that causes stimulation of hydrogen peroxide release [5, 6]. The pL profile of flavin oxidation with L-Lys present was performed in order to determine if its presence alters the pK_a value for flavin oxidation relative to in the absence of a substrate. The results show a pL profile with a single phase for flavin oxidation and single calculated pK_a values of 7.73 ± 0.09 in H_2O and 8.42 ± 0.07 in D_2O (Fig. 4.7). This data indicates that in the presence of L-Lys, the pK_a value for flavin oxidation is significantly lower than in the absence of a substrate. Similar to L-Orn, it appears the N^6 of L-Lys is not altering the pK_a value for the N5 of the flavin as they are separated by 4.75 Å (Fig. 4.8) [15]. This suggests that similar to flavin oxidation with L-Orn, the observed pK_a value is for the N^6 of L-Lys. The pK_a value for L-Lys is ~1 unit higher than the pK_a value for L-Orn, but this could be a function of the microenvironment around the terminal nitrogen atoms as L-Lys protrudes further into the active site (Figs. 4.6 and

4.8). A SKIE value of 1.0 ± 0.1 was also calculated from the upper limit of the fits at high pL (Table 4.1). The lowered SKIE in the presence of L-Lys compared to in the absence of a substrate suggests that the chemical steps of hydrogen peroxide release are less rate-limiting than in the absence of a substrate. This indicates that L-Lys lowers the transition state activation energy of a proton in flight to the hydroperoxide leaving group. This could be the result of the N^6 of L-Lys protruding near the C4a locus causing steric hindrance with the formed C4a-hydroperoxyflavin and/or protonation of the proximal oxygen of the C4a-hydroperoxyflavin by L-Lys, resulting in rapid hydrogen peroxide elimination and the lowered SKIE.

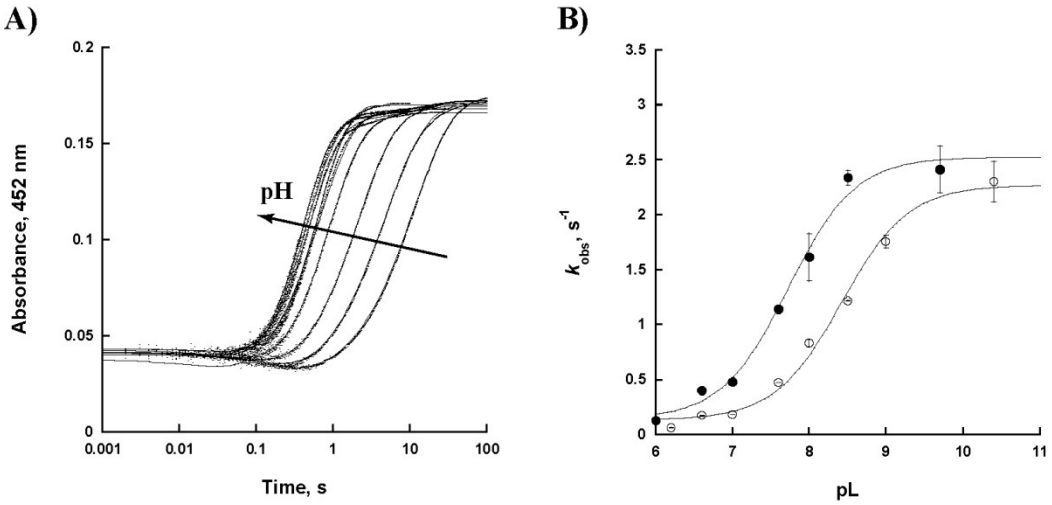

Figure 4.7 Effect of pL on flavin oxidation with L-Lys for SidA determined at 452 nm on the stopped-flow spectrophotometer. A) Kinetic traces with fits of flavin oxidation at 452 nm for SidA with 15 mM L-Lys present. B) Effect of pL on flavin oxidation in the presence of 15 mM L-Lys. Closed circles (●) denote pH studies in 100% H_2O and open circles (○) denote pD studies in ~96% D_2O.

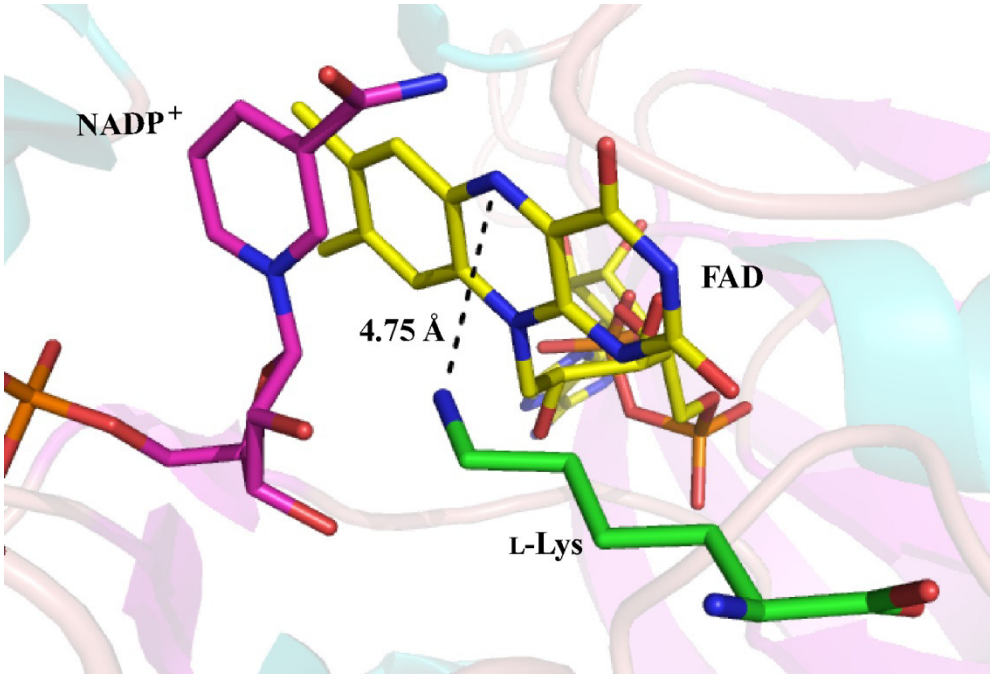

Figure 4.8 Active site of SidA with L-Lys bound (PDB code 4B64). The calculated distance between the N5 of the flavin and the N^5 of L-Lys of 4.75 Å suggests that L-Lys is not altering the pK_a value for the N5 of the flavin.

3.6 pL profile for flavin oxidation with L-Nva. The pL profile with L-Nva was performed in order to help determine if the observed pK_a value for flavin oxidation with L-Orn/L-Lys reflects the pK_a value for the terminal amine of these amino acids. L-Nva is structurally similar to L-Orn with the exception that L-Nva lacks a terminal amine group on its aliphatic side chain. The results in Fig. 4.9 and Table 4.1 indicate a single phase and pK_a values for flavin oxidation of >9 in H_2O and >10 in D_2O. This data indicates the pL profile for flavin oxidation with L-Nva is virtually identical to the pL profile for flavin oxidation in the absence of a substrate and further supports the hypothesis for the altered pK_a values with L-Orn/L-Lys reflecting the pK_a values for the N^5/N^6. A SKIE of 1.61 ± 0.01 was also calculated at pL 7.0 which is slightly lower than the SKIE in the absence of a substrate. This could suggest the chemical steps of hydrogen peroxide elimination are less rate-limiting in the presence of L-Nva, but is unlikely as the stability of the

C4a-hydroperoxyflavin is unchanged in either the presence or absence of L-Nva (data not shown).

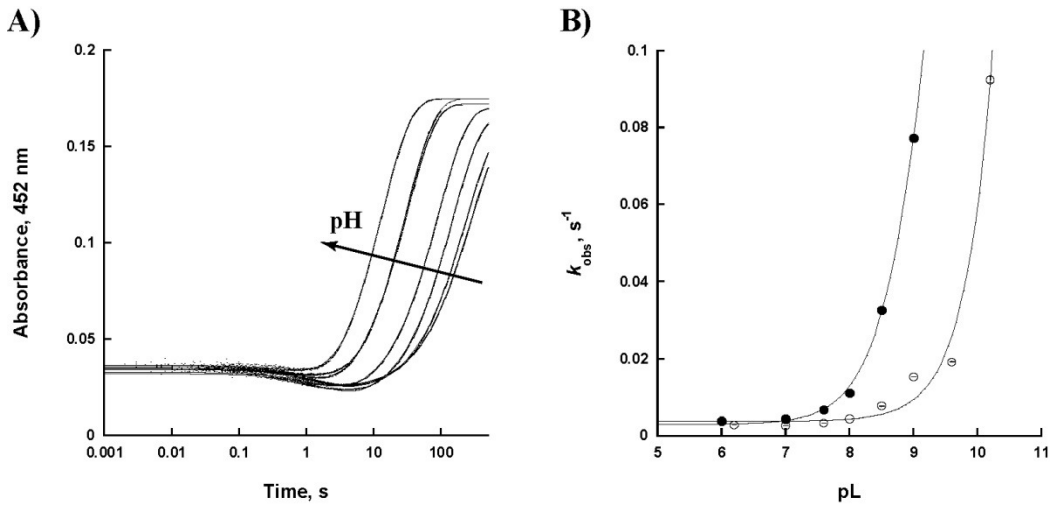

Figure 4.9 Effect of pL on flavin oxidation with L-Nva for SidA determined at 452 nm on the stopped-flow spectrophotometer. A) Kinetic traces with fits of flavin oxidation at 452 nm for SidA with 15 mM L-Nva present. B) Effect of pL on flavin oxidation in the presence of 15 mM L-Nva. Closed circles (●) denote pH studies in 100% H_2O and open circles (○) denote pD studies in ~96% D_2O.

3.7 Dependence of L-Orn on flavin oxidation at pH values 6 and 9. The dependence of L-Orn on flavin oxidation was performed at pH values 6 and 9 in order to determine the protonation state of the N^5 of L-Orn when it is bound to SidA. The data in Fig. 4.10 and Table 4.2 indicates that the rate of formation of the C4a-hydroperoxyflavin is not pH dependent which is consistent with the pH profiles for C4a-hydroperoxyflavin formation in Fig. 4.2. The K_D values calculated from the plots in Figs. 4.10A and 4.10C indicate that the binding of L-Orn is only slightly affected (~3-fold) by pH. This suggests that L-Orn can bind to the active site of SidA independent of its protonation state and stimulate oxygen reactivity. Slight substrate inhibition was observed for L-Orn at pH 6 for formation of the C4a-hydroperoxyflavin suggesting an unproductive binding mode for protonated L-Orn that reduces oxygen reactivity. The calculated k_{OX}/K_m values for

flavin oxidation show a ~200-fold increase at pH 9 compared to pH 6 (Table 4.2). This data suggests that at pH 6, L-Orn is mostly in the protonated form in the active site of SidA as the calculated pK_a value is 6.7 ± 0.1 (Table 4.1). The data indicates protonated L-Orn is capable of stimulating oxygen reactivity, but after the reaction with molecular oxygen at low pH, protonated L-Orn competitively inhibits catalysis until the N^5 of L-Orn is deprotonated. At pH 9 though, the population of L-Orn is almost entirely deprotonated upon binding, which leads to more efficient catalysis as indicated by the ~200-fold increased k_{OX}/K_m value. This data indicates that L-Orn can bind to SidA either in the protonated or deprotonated form, stimulate oxygen reactivity, but needs to be deprotonated in order for hydroxylation to occur.

Table 4.2 Parameters of L-Orn saturation of the oxidative half-reaction at pH 6 and 9.

	pH 6	**pH 9**
k_{OOH}, s^{-1}	13.1 ± 0.8	13.4 ± 0.4
$K_{D(L\text{-}orn)}$, mM	1.5 ± 0.4	0.55 ± 0.07
$k_{OOH}/K_{D(L\text{-}orn)}$, $M^{-1}s^{-1}$	8,700 ± 2,400	24,000 ± 3,000
$K_{I(L\text{-}orn)}$, mM	94 ± 18	-
k_{OX}, s^{-1}	1.20 ± 0.05	3.29 ± 0.06
$K_{m(L\text{-}orn)}$, mM	27 ± 3	0.35 ± 0.04
$k_{OX}/K_{m(L\text{-}orn)}$, $M^{-1}s^{-1}$	44 ± 5	9,400 ± 1,000

Conditions: All experiments were performed at 25°C. Reactions at pH 6 were performed in 100 mM sodium phosphate, 100 mM NaCl, pH 6. Reactions at pH 9 were performed in 100 mM Tris-SO_4, 100 mM NaCl, pH 9.

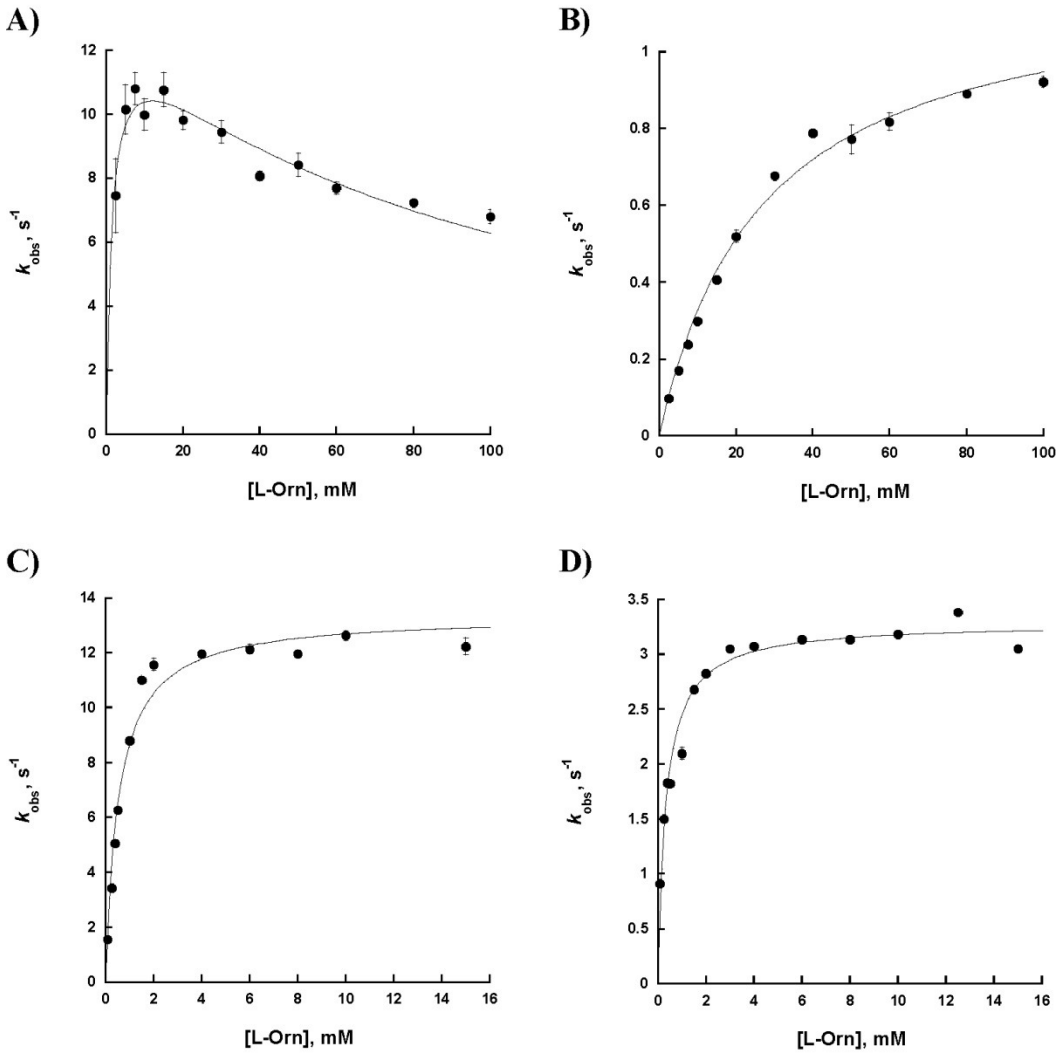

Figure 4.10 Effect of pH on the binding of L-Orn to SidA in the oxidative half-reaction. A) Dependency of L-Orn on k_{obs} at 372 nm for formation of the C4a-hydroperoxyflavin at pH 6. B) Dependency of L-Orn on k_{obs} at 452 nm for flavin oxidation at pH 6. C) Dependency of L-Orn on k_{obs} at 372 nm for formation of the C4a-hydroperoxyflavin at pH 9. D) Dependency of L-Orn on k_{obs} at 452 nm for flavin oxidation at pH 9.

4. Discussion

The active site of SidA is finely tuned where catalysis occurs efficiently at physiological pH [5, 6]. L-Orn must be in its deprotonated form when bound to SidA in order for hydroxylation to occur (Scheme 4.2). In the related L-Orn monooxygenase PvdA from *Pseudomonas aeruginosa*, it was first proposed that the protonated form of L-Orn transfers a proton to the C4a-

peroxyflavin to form the C4a-hydroperoxyflavin [17]. This yields the deprotonated form of L-Orn for hydroxylation chemistry to occur. Recent KIE and density functional theory (DFT) studies contrast from these conclusions by indicating the C4a-hydroperoxyflavin is formed in SidA through proton transfer from the 2'-OH of the nicotinamide ribose of $NADP^+$ [8]. This is consistent with the lack of a pH dependence for formation of the C4a-hydroperoxyflavin in the presence of L-Orn (Fig. 4.2B) where the protonation state of the N^5 of L-Orn is not affecting oxygen reactivity. Another recent study with SidA envoked a mechanism where L-Orn binds in the protonated state [13]. Our studies here show the pK_a value for L-Orn is altered to ~6.7 and at physiological pH it is primarily bound to SidA in the deprotonated form. L-Orn dependence studies at pH values 6 and 9 suggest though that the protonated and deprotonated forms of L-Orn bind to SidA with similar affinity (Table 4.2), but subsequent turnover is heavily dependent on the protonation state of L-Orn (Fig. 4.10). Past studies of the amino oxidase/monoamine oxidase family of enzymes set precedents for the alteration of pK_a values of amine groups so they can be in their deprotonated states at physiological pH. In tryptophan 2-monooxygenase, steady-state pH studies showed an ionizable group with a pK_a value of ~6.8 that must be deprotonated for activity which was attributed to deprotonation of the amine group of L-Ala which has an intrinsic pK_a value of 9.87 [18]. Also, in monoamine oxidase, the pK_a values of the substrates tested showed a decrease from their intrinsic values of 9.3 – 9.9 to 7.4 – 8.4 upon binding to the enzyme [19]. A decrease in the KIEs with increasing pH here allowed assignment of these observed pK_a values to the amine group which provides a hydride equivalent to the flavin. This is consistent with our data showing an altered pK_a value for flavin oxidation with L-Orn, and helps us to assign the altered pK_a values to the terminal amine of L-Orn.

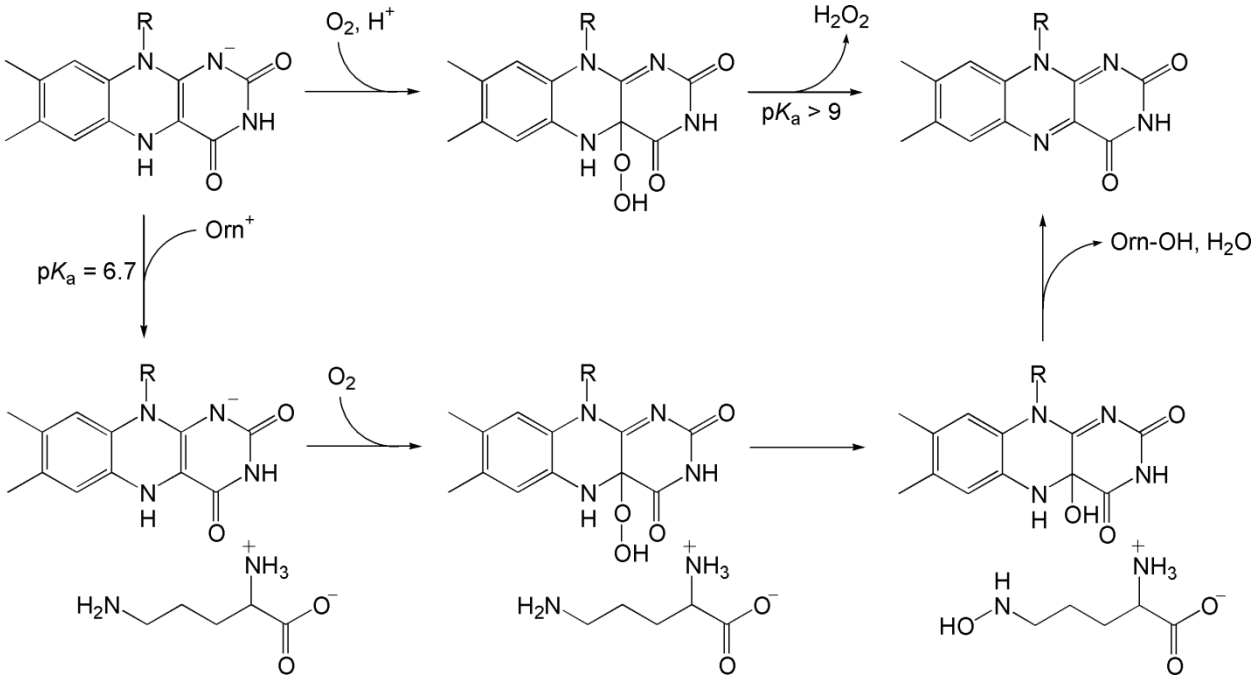

Scheme 4.2 The oxidative half-reaction of SidA in the absence and presence of L-Orn. In the absence of L-Orn, the C4a-hydroperoxyflavin intermediate decays to oxidized flavin and hydrogen peroxide with a pK_a value for oxidation of >9. In free solution at physiological pH, the N^5 of L-Orn is protonated (Orn^+), and upon binding to SidA, the N^5 of L-Orn obtains a pK_a value of 6.7. This altered pK_a value deprotonates the N^5 of L-Orn which is essential for efficient catalysis.

SidA is highly selective for L-Orn where L-Lys acts a non-substrate effector which enhances the decay of the C4a-hydroperoxyflavin to release hydrogen peroxide [5]. In a recent study where the pH dependence of SidA was examined with L-Lys present, it was proposed L-Lys accelerates hydrogen peroxide release through an acid–base mechanism [13]. Here, they propose the N^6 of L-Lys abstracts the proton from the N5 of the flavin, then donates this proton to the hydroperoxide motif of the C4a-hydroperoxyflavin which stimulates hydrogen peroxide release. This conclusion was primarily drawn from the large SKIE (6.6 ± 0.3) observed in the presence of L-Lys. This however was not performed in the pL independent region of the pL profile, hence an inflated SKIE is reasonable to expect since the data in Table 4.1 shows the pK_a value for flavin oxidation with L-Lys present shifts by ~0.7 units when in D_2O. Our data in the

pL independent region indicates hydrogen peroxide elimination with L-Lys present is not rate-limiting to flavin oxidation as a SKIE of 1.0 ± 0.1 was calculated. This is consistent with recent computational studies in SidA which show in the C4a-peroxyflavin–Lys complex, the hydrogen bonding interaction between the C4a-peroxyflavin and the 2'-OH of the nicotinamide ribose is interrupted by the protrusion of L-Lys [20]. This, along with the separation of the N^6 of L-Lys and the N5 of the flavin by 4.75 Å (Fig. 4.8) disfavors an acid–base mechanism with L-Lys in SidA. A recent study with phenylacetone monooxygenase showed that a C65D mutant effectively converted the enzyme into a NADPH oxidase [21]. In the crystal struture of C65D, the adjacent D66 was pointed inward towards the C4a locus of the flavin which was proposed to cause the high oxidase activity through a combination of steric hindrance with the C4a locus and protonation of the proximal oxygen of the C4a-peroxyflavin. Scheme 4.3 proposes a similar mechanism for L-Lys stimulated hydrogen peroxide elimination where the terminal side chain amine of L-Lys protonates the proximal oxygen of the C4a-hydroperoxyflavin leading to rapid oxidation. This is consistent with the observation that L-Lys is mostly in its protonated form in the active site of SidA at physiological pH (pK_a ~7.7), and the proximity of the N^6 amine to the C4a of the flavin.

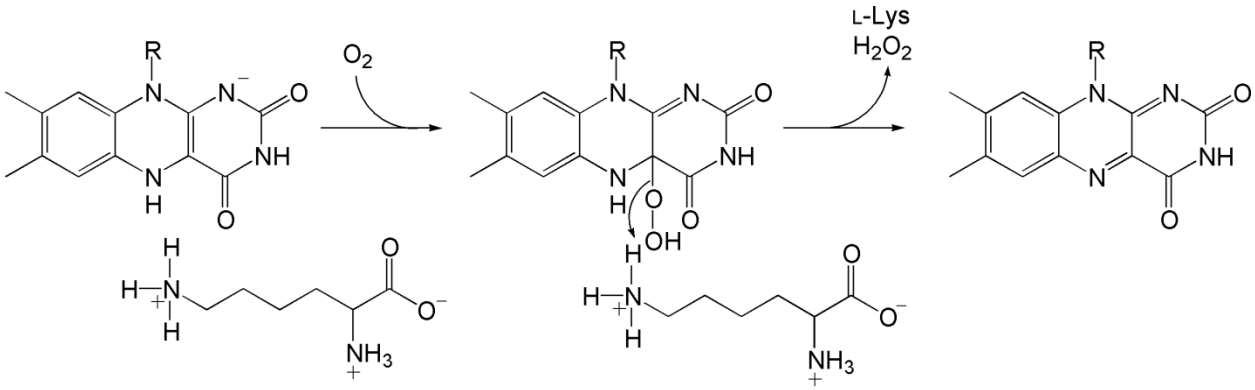

Scheme 4.3 Flavin oxidation stimulated by L-Lys. The pK_a value for the N^6 of L-Lys is ~7.7 which indicates that at physiological pH, a majority of bound L-Lys is in its protonated state. The lack of a SKIE on flavin oxidation with L-Lys present along with the protrusion of the terminal amine towards the C4a locus could indicate that protonated L-Lys transfers a proton to the proximal oxygen of the C4a-hydroperoxyflavin, resulting in rapid hydrogen peroxide release.

The data presented here indicates that SidA is able to overcome the high intrinisic pK_a value for the N^5 of L-Orn by altering its pK_a value in the active site. This allows SidA to bind L-Orn in the deprotonated form enabling rapid hydroxylation. The pK_a value for L-Lys is also altered in the active site of SidA, but the pK_a value for the N^6 is ~1 unit higher than the N^5 of L-Orn, likely due to differences in the microenvironments around the terminal nitrogens as L-Lys protrudes further into the active site. This results in a majority of bound L-Lys in its protonated form and protrusion by L-Lys appears to disrupt the interaction with $NADP^+$. Protonated L-Lys might transfer a proton to the proximal oxygen of the intermediate leading rapid hydrogen peroxide elimination. Further computational experiments could definitively answer questions raised by this study including the chemical mechanism of L-Lys stimulated hydrogen peroxide elimination.

5. Acknowledgements

This work was supported in part by a grant from the National Science Foundation MCB-1021384.

6. References

[1] K.F. Tipton, H.B. Dixon, Methods Enzymol 63 (1979) 183-234.
[2] T.K. Harris, G.J. Turner, IUBMB Life 53 (2002) 85-98.
[3] F.C. Kokesh, F.H. Westheimer, J Am Chem Soc 93 (1971) 7270-7274.
[4] P.A. Frey, F.C. Kokesh, F.H. Westheimer, J Am Chem Soc 93 (1971) 7266-7269.
[5] S.W. Chocklett, P. Sobrado, Biochemistry 49 (2010) 6777-6783.
[6] J.A. Mayfield, R.E. Frederick, B.R. Streit, T.A. Wencewicz, D.P. Ballou, J.L. DuBois, J Biol Chem 285 (2010) 30375-30388.
[7] R.M.C. Dawson, D.C. Elliot, W.H. Elliot, K.M. Jones, in: Data for Biochemical Research, 3rd ed., Oxford University Press, New York, NY, 1986, pp. 24-25.
[8] R. Robinson, S. Badieyan, P. Sobrado, Biochemistry 52 (2013) 9089-9091.
[9] J. Sucharitakul, T. Wongnate, P. Chaiyen, J Biol Chem 286 (2011) 16900-16909.
[10] S. Franceschini, M. Fedkenheuer, N.J. Vogelaar, H.H. Robinson, P. Sobrado, A. Mattevi, Biochemistry 51 (2012) 7043-7045.
[11] K.B. Schowen, R.L. Schowen, Methods Enzymol 87 (1982) 551-606.
[12] E. Romero, D. Ávila P. Sobrado, in: S. Miller, R. Hille, B. Palfey (Eds.), Flavins and Flavoproteins 2011, Lulu, Raleigh, NC, 2013, pp. 289-294.
[13] R.E. Frederick, S. Ojha, A. Lamb, J.L. Dubois, Biochemistry 53 (2014) 2007-2016.
[14] P. Macheroux, S. Ghisla, C. Sanner, H. Ruterjans, F. Muller, BMC Biochem 6 (2005) 26.
[15] T.E. Creighton, in: Proteins, 2nd ed., W.H. Freeman and Company, New York, NY, 1993, p. 140.
[16] V. Massey, J Biol Chem 269 (1994) 22459-22462.
[17] K.M. Meneely, E.W. Barr, J.M. Bollinger, Jr., A.L. Lamb, Biochemistry 48 (2009) 4371-4376.
[18] E.C. Ralph, M.A. Anderson, W.W. Cleland, P.F. Fitzpatrick, Biochemistry 45 (2006) 15844-15852.
[19] R.V. Dunn, K.R. Marshall, A.W. Munro, N.S. Scrutton, FEBS J 275 (2008) 3850-3858.
[20] S. Badieyan, R. Bach, P. Sobrado, J Org Chem (2015).
[21] P.B. Brondani, H.M. Dudek, C. Martinoli, A. Mattevi, M.W. Fraaije, J Am Chem Soc 136 (2014) 16966-16969.

CHAPTER 5

Arg279 is the key regulator of coenzyme selectivity in the flavin-dependent ornithine monooxygenase SidA

Reprinted with permission from Biochimica et Biophysica Acta, Robinson, R., Franceschini, S., Fedkenheuer, M., Rodriguez, P. J., Ellerbrock, J., Romero, E., Echandi, M. P., Martin del Campo, J. S., and Sobrado, P. "Arg279 is the key regulator of coenzyme selectivity in the flavin-dependent ornithine monooxygenase SidA" *Biochim Biophys Acta*. 2014 (ID 10.1016/j.bbapap.2014.02.005) Vol 1844: 778-784.

Author Contributions:
Reeder Robinson performed all the experiments with the exception of the ones listed below and helped write the article.

Stefano Franceschini solved the crystal structure of R279A.

Michael Fedkenheuer crystallized R279A and performed some of the steady-state experiments with R279A.

Pedro J. Rodriguez helped with some of the steady-state assays.

Jacob Ellerbrock helped with some steady-state assays with R279E.

Elvira Romero helped some of the stopped-flow experiments.

Maria Paulina Echandi helped with some of the steady-state assays.

Julia S. Martin del Campo helped with solving the structure of R279A.

Pablo Sobrado oversaw and directed the research, and helped write the article.

Abstract

Siderophore A (SidA) is a flavin-dependent monooxygenase that catalyzes the NAD(P)H- and oxygen-dependent hydroxylation of ornithine in the biosynthesis of siderophores in *Aspergillus fumigatus* and is essential for virulence. SidA can utilize both NADPH or NADH for activity; however, the enzyme is selective for NADPH. Structural analysis shows that R279

interacts with the 2'-phosphate of NADPH. To probe the role of electrostatic interactions in coenzyme selectivity, R279 was mutated to both an alanine and a glutamate. The mutant proteins were active but highly uncoupled, oxidizing NADPH and producing hydrogen peroxide instead of hydroxylated ornithine. For wtSidA, the catalytic efficiency was 6-fold higher with NADPH as compared to NADH. For the R279A mutant the catalytic efficiency was the same with both coenyzmes, while for the R279E mutant the catalytic efficiency was 5-fold higher with NADH. The effects are mainly due to an increase in the K_D values, as no major changes on the k_{cat} or flavin reduction values were observed. Thus, the absence of a positive charge leads to no coenzyme selectivity while introduction of a negative charge leads to preference for NADH. Flavin fluorescence studies suggest altered interaction between the flavin and $NADP^+$ in the mutant enzymes. The effects are caused by different binding modes of the coenzyme upon removal of the positive charge at position 279, as no major conformational changes were observed in the structure for R279A. The results indicate that the positive charge at position 279 is critical for tight binding of NADPH and efficient hydroxylation.

1. Introduction

Fungi from *Aspergillus spp.* are opportunistic human pathogens that cause bronchopulmonary infections in immunocompromised individuals and represent a significant health risk to individuals in intensive care units [1]. *Aspergillus fumigatus* is the most common human fungal pathogen and the mortality rate for *Aspergillus*-related infections is >50% [1, 2]. It has been shown that during infection, *A. fumigatus* synthesizes and secretes siderophores to scavange iron from the mammalian host. Since iron is required for growth, enzymes active in the biosynthesis of siderophores have been identified as potential drug targets [3, 4]. Ferricrocin and

triacetylfusarinine C are hydroxamate-containining siderophores that are required for virulence [5-7]. In the biosynthesis of these siderophores, N^5-hydroxyornithine is essential for the formation of the hydroxamate iron binding site.

The flavin-dependent monooxygenase siderophore A (SidA), catalyzes the hydroxylation of ornithine to N^5-hydroxyornithine. SidA utilizes NAD(P)H to reduce the flavin cofactor in order to react with molecular oxygen to form a C4a-hydroperoxyflavin intermediate, which is the hydroxylating species (Scheme 5.1) [8-10]. The formation and stabilization of the C4a-hydroperoxyflavin is critical for hydroxylation. In the absence of ornithine, this intermediate is very stable, eventually decaying to hydrogen peroxide and oxidized flavin (half-life of ~30 min) [8, 10, 11]. Rapid turnover only occurs when ornithine is present. Stabilization of the C4a-hydroperoxyflavin intermediate ensures that the enzyme couples NADPH oxidation and oxygen activation with ornithine hydroxylation [9, 10]. SidA is also able to use NADH, however, the K_M value is 10-fold higher than for NADPH. In addition, the enzyme is only ~50% coupled with NADH while with NADPH the coupling is ~95% [9]. This difference led us to explore the structural determinants of coenzyme selectivity in SidA. Here, we present biochemical and structural data which show that R279 is the key regulator of coenzyme selectivity in SidA.

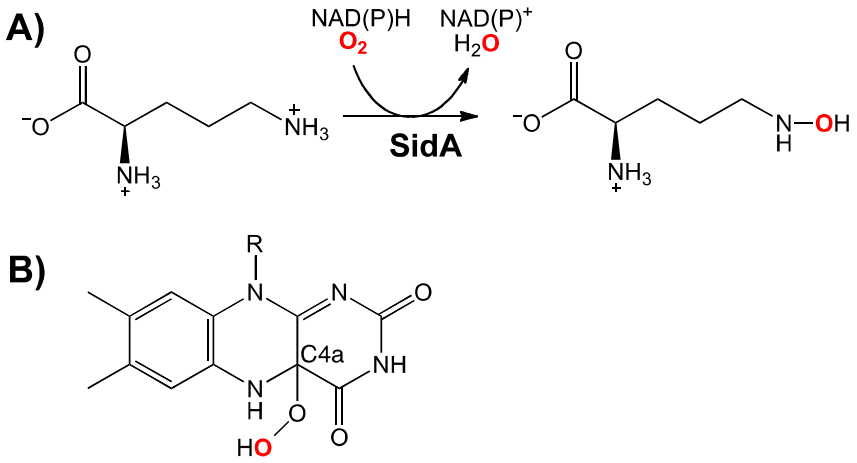

Scheme 5.1 A) Reaction catalyzed by SidA. B) Structure of the catalytic intermediate C4a-hydroperoxyflavin.

2. Materials and Methods

2.1 Materials. Buffers and media were obtained from Fisher Scientific (Pittsburg, PA). BL21(DE3)-T1^{R} chemically competent cells were obtained from Sigma-Aldrich (St. Louis, MO). NADH and NADPH were obtained from EMD4 Biosciences (Billerica, MA). DNA primers were synthesized by Integrated DNA Technologies (Coralville, IA). Plasmid preparation and gel purification kits were obtained from Qiagen (Valencia, CA). *Escherichia coli* TOP10 chemically competent cells were obtained from Invitrogen (Carlsbad, CA). Chromatography columns were obtained from GE Healthcare.

2.2 Site–directed mutagenesis. Mutagenesis of R279 to Ala or Glu was performed using the QuikChange (Agilent Technologies) method following the manufacturer's instructions. Wild-type SidA (wtSidA) gene, subcloned into the pET15b plasmid, was used as the template for mutagenesis reactions [12]. For the R279A mutation, the forward primer (5'-GCACCACCCTGATCATGGCCGACTCGGCTATGCGCCC-3') and reverse primer (5'-GGGCGCATAGCCGAGTCGGCCATGATCAGGGTGGTGC-3') were used. For the R279E

mutation, the forward primer (5'-CCCGCACCACCCTGATCATGGAAGACTCGGCTATGCGCCC-3') and reverse primer (5'-GGGCGCATAGCCGAGTCTTCCATGATCAGGGTGGTGCGGG-3') were used. The codon at position 279 is underlined.

2.3 Protein expression and purification. All mutant proteins were expressed in *E. coli* BL21(DE3)-T1^{R} cells and purified as previously described [12]. In general, ~25 mg of protein were obtained per liter of autoinduction media. The purified proteins were stored in 100 mM sodium phosphate, 50 mM NaCl, pH 7.5, at -80 °C at a concentration of ~200 µM (based on flavin content) in 30 µL aliquots.

2.4 Determination of flavin incorporation. Flavin incorporation was determined by measuring protein concentration via the Bradford assay (BioRad) and comparing it to the protein concentration based on the flavin spectra. SidA concentration based on flavin content was determined using an extinction coeficent of 13.7 $mM^{-1}cm^{-1}$ at 450 nm [9]. Flavin incorporation was generally close to 70% for wtSidA and mutant proteins.

2.5 Steady-state kinetics. The rate of oxygen consumption was measured using a Hansatech Oxygraph system (Norfolk, England). Reactions consisted of a 1 mL volume of 100 mM sodium phosphate, pH 7.5, at 25 °C. The concentration range of NADPH was 0.005 – 0.5 mM for wtSidA, 0.05 – 2 mM for R279A, and 0.1 – 5 mM for R279E. Similarly, the concentration range for NADH was 0.01 - 3 mM for wtSidA and R279A, and 0.05 - 5 mM for R279E. L-ornithine was held constant at 15 mM for all assays where NAD(P)H was varied. When L-ornithine was

varied, the coenzyme was kept constant at a concentration at least 5-times the K_M value. Reactions were initiated by addition of 2 μM of SidA and monitored for 5 min with constant stirring.

Hydroxylated ornithine was monitored using a variation of the Csaky iodine oxidation assay [13, 14]. The standard assay buffer contained 104 μL of 100 mM sodium phosphate (pH 7.5) with varying concentrations of L-ornithine (0 to 20 mM) and saturating concentrations of NAD(P)H (at least 5-times the K_M value). Reactions were initiated by addition of 2.0 μM SidA and incubated for 10 min at 25 °C with constant shaking at 750 rpm.

2.6 Pre-steady-state kinetics. All rapid reaction experiments were carried out at 15 °C using an SX-20 stopped-flow spectrophotometer (Applied Photophysics, Leatherhead, UK) in an anaerobic glove box (Coy, Grass Lake, MI). Anaerobic buffer was obtained through repeated cycles of vacuum (10 min) and flushing with O_2-free argon (1 min) for 1 hr. The same procedure was used to make the enzyme anaerobic. Substrates were made anaerobic by dissolving in anaerobic buffer inside the glove box. The rate of flavin reduction was measured by mixing anaerobic SidA (15 μM after mixing) with an equal volume of NADPH at final concentrations of 0.5 mM for wtSidA, 0.05 – 2 mM for R279A, and 0.5 – 5 mM for R279E. Reduction by NADH was performed at 0.05 – 1.5 mM for wtSidA, and 0.05 – 5 mM for both mutant enzymes. Spectra were taken on a logarithmic time scale until full reduction of the flavin was observed as determined by a decrease in absorbance at 452 nm. The rate constants at various coenzyme concentrations were determined by fitting the changes in absorbance at 452 nm to Eq. 1. In this double exponential equation, a is the change in absorbance, k is the rate, and c is the final absorbance. The resulting values were plotted as a function of reduced coenzyme concentration

and the data fit to Eq. 2 to obtain the maximum rate constant of flavin reduction (k_{red}) and the K_D value [15].

$$\upsilon = c + a_1 e^{-(k_1 * t)} + a_2 e^{-(k_2 * t)} \qquad (1)$$

$$k_{obs} = \frac{k_{red}[\text{NAD(P)H}]}{K_D + [\text{NAD(P)H}]} \qquad (2)$$

2.7 Flavin fluorescence. The effect of oxidized coenzyme on flavin fluorescence was determined on a SpectraMax M5e plate reader (Molecular Devices, Sunnyvale, CA). Excitation was performed at 450 nm, and the changes in flavin fluorescence were monitored from 500 to 625 nm. A 495 nm cutoff filter was used for each fluorescence experiment. The standard assay buffer contained 100 µL of 100 mM sodium phosphate, pH 7.5, with 15 µM SidA. For wtSidA, 0.9 mM $NADP^+$ or 4 mM NAD^+ were used. For R279A, 3 mM $NADP^+$ or 5 mM NAD^+ were used. For R279E, 15 mM $NADP^+$ or 5 mM NAD^+ were used.

2.8 Crystallization and structure determination. Crystals of *A. fumigatus* R279A SidA containing L-ornithine were obtained at 4 °C by the vapor diffusion method under the same conditions used for the wild-type protein (reservoir containing 1.6 M ammonium sulfate, 0.1 M HEPES, pH 6.6, 2% dioxane, and a protein solution of 8 mg/ml SidA in 25 mM HEPES, pH 7.5, 100 mM NaCl, 15 mM L-ornithine, 1 mM $NADP^+$ [12]. Data were collected at the European Synchrotron Radiation Facility (Grenoble, France). The structure was solved by molecular replacement starting from the structure of the wild-type enzyme (PDB entry 4B63). All crystallographic calculations were performed with programs of the CCP4 package [16]. Figures were generated using Pymol (www.pymol.org).

3. Results and Discussion

Class B flavin-dependent monooxygenases are highly selective for NADPH [17]. Some members of this family, such as phenylacetone monooxygenase (PAMO) and the ornithine hydroxylase from *Pseudomonas aeruginosa* (PvdA), are 100% selective for NADPH as these enzymes are reported to be unable to react with NADH [18, 19]. Similarly, the Baeyer-Villiger monooxygenases (BVMOs) cyclohexanone monooxygenase (CHMO) and 4-hydroxyacetophenone monooxygenase (HAPMO) have been shown to be highly selective for NADPH with a 700-fold preference over NADH (based on reported k_{cat}/K_M values) [20]. On the other hand, mammalian flavin-dependent monooxygenase (FMO) and SidA are less selective, with less than 20-fold preference for NADPH [9, 21, 22]. The x-ray crystal structure of SidA in complex with $NADP^+$ shows that the R279 ion pairs with the 2'-phosphate of $NADP^+$ and the guanidinium group is involved in stacking interactions with the adenine base (Fig. 5.1) [12]. We probed the role of this residue in coenzyme selectivity using site-directed mutagenesis and subsequent characterization of the resulting mutant enzymes.

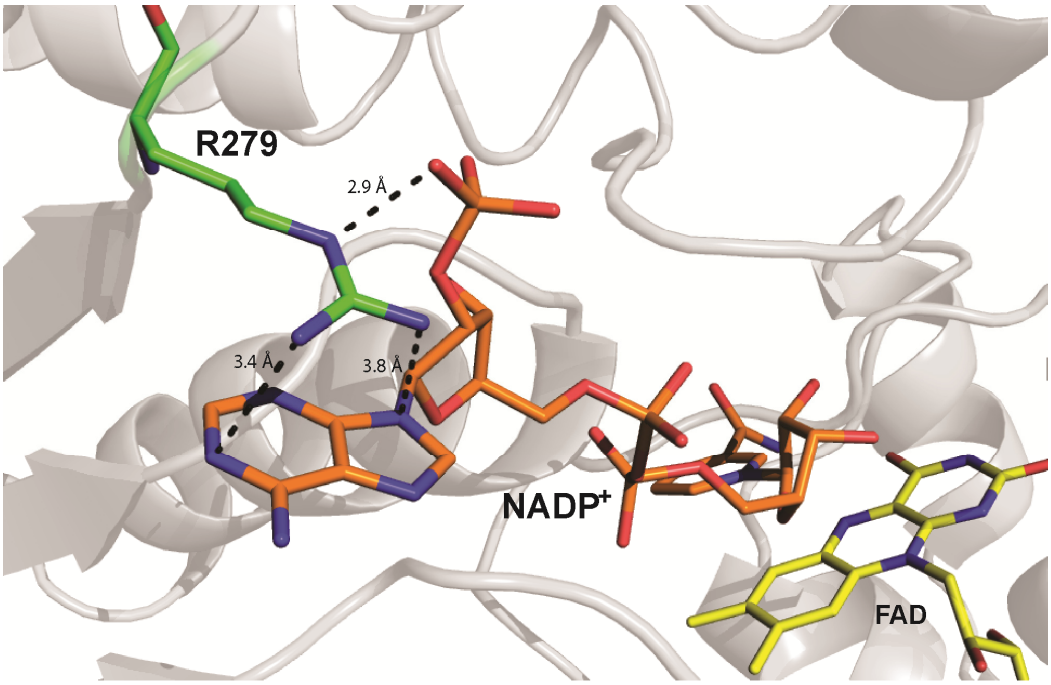

Figure 5.1 Interaction of R279 with $NADP^+$. The figure was made using Pymol with PDB entry 4B63.

The effect of removing the positive charge of R279 on coenzyme selectivity was probed by mutating this residue to alanine. The R279A enzyme was purified following the same procedures as wtSidA. The yield of the purified mutant enzyme was ~25 mg per liter of *E. coli* culture with a flavin content of ~70%. This data is consistent with previously reported values for wtSidA [8, 9]. Mutation of R279 to E was also performed in order to introduce a negative charge at this position, which would have a repulsion effect with the 2'-phosphate of NADPH, but not with NADH. The resulting R279E enzyme was purified as the R279A with similar yields. The flavin spectra for both mutants are identical to the flavin spectrum of the wtSidA (not shown).

The kinetic values determined by measuring the rate of oxygen consumption were calculated as a function of coenzyme concentration with ornithine saturating at 15 mM (Fig. 5.2). The data is summarized in Table 5.1. The catalytic efficiency with NADPH decreased ~40- and ~300-fold for the R279A and R279E enzymes, respectively. This decrease is mainly due to an

increase in the K_M values, since the k_{cat} value was unchanged for the R279A enzyme, while it decreased only by 30% for the R279E enzyme. With NADH, the catalytic efficiencies for R279A and R279E decreased only 7- and 11-fold, respectively. These relatively minor effects are also mainly due to changes in the K_M values. Interestingly, a slight increase in the k_{cat} value for NADH was observed for the R279E enzyme (~30%) (Table 5.1).

Table 5.1 Steady-state kinetic parameters determined by oxygen consumption.

Parameters/ variable substrate	**Wild-type**	**R279A**	**R279E**
NADPH			
k_{cat} (s^{-1})	0.45 ± 0.01	0.48 ± 0.01	0.30 ± 0.01
K_M (mM)	0.0070 ± 0.0001	0.31 ± 0.02	1.54 ± 0.20
k_{cat}/K_M ($M^{-1}s^{-1}$)	64000 ± 5000	1500 ± 100	200 ± 10
NADH			
k_{cat} (s^{-1})	0.75 ± 0.02	0.75 ± 0.03	1.00 ± 0.05
K_M (mM)	0.070 ± 0.007	0.51 ± 0.07	1.0 ± 0.1
k_{cat}/K_M ($M^{-1}s^{-1}$)	11000 ± 150	1500 ± 100	1000 ± 60

Conditions: 100 mM sodium phosphate, pH 7.5, and 25 ºC.

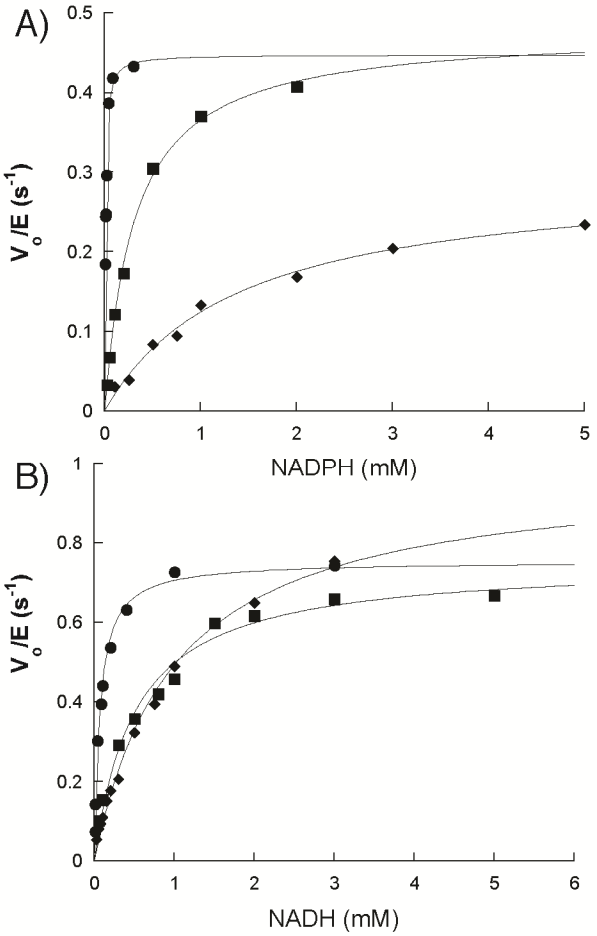

Figure 5.2 Initial rate of oxygen consumption as a function of NADPH (A) or NADH (B) for wtSidA (●), R279A (■), and R279E (♦). The assays were performed in 1 mL sodium phosphate, pH 7.5, at 25 °C. The lines are fit to the Michaelis-Menten equation.

Reduction of the flavin cofactor by NAD(P)H was monitored using a stopped-flow spectrophotometer under anaerobic conditions. We have previously determined that the hydride transfer step occurs in two phases and using stereospecifically labeled (4*R*)-4-^{2}H-NADPH the reaction was shown to be specific for the *pro*-R-hydrogen and a kinetic isotope effect value of ~5.5 was measured in both phases. This indicates that both phases of flavin reduction of wtSidA with NADPH correspond to hydride transfer. The affinity of wtSidA for NADPH is very high, which prevents accurate determination of the K_D value for this coenzyme in the stopped-flow spectrophotometer. Therefore, the K_D value for NADPH has been estimated to be ~1 μM [10].

The reaction of wtSidA with NADH also occurs in two phases. The first phase is fast, isotope sensitive, and increases as a function of NADH concentration, indicating that it corresponds to flavin reduction. The second phase has a much slower rate and is isotope and concentration independent. Therefore, this phase is believed to correspond to NAD^+ release [8]. With the R279 mutants, the reaction with NADPH also occurs in two phases. The first phase was fast and increased as a function of NADPH concentration, allowing determination of both the k_{red} and K_D values (Fig. 5.3 and Table 5.2). This relatively fast phase corresponds to flavin reduction. The second phase was slower (~0.07 s^{-1} for both mutant enzymes) and independent of NADPH concentration. We attribute this phase to $NADP^+$ release. The results indicate that alteration of the electrostatic environment at position 279 does not significantly affect the rate of flavin reduction. However, the affinity for NADPH is significantly affected (Table 5.2). Using the estimate of 1 μM for the K_D value of NADPH for wtSidA, it can be predicted that mutations of R279 changed the K_D for NADPH at least 270-fold for R279A and 1600-fold for R279E (Table 5.2).

Table 5.2 Rate constants for flavin reduction and dissociation constants with NAD(P)H.

	NADPH		**NADH**	
Enzyme	k_{red} (s^{-1})	K_D (mM)	k_{red} (s^{-1})	K_D (mM)
wtSidA	0.63 ± 0.01	~0.001	1.69 ± 0.01	0.070 ± 0.005
R279A	0.88 ± 0.01	0.27 ± 0.05	1.84 ± 0.04	0.37 ± 0.03
R279E	0.9 ± 0.1	1.6 ± 0.5	1.52 ± 0.02	0.26 ± 0.02

Conditions: 100 mM sodium phosphate, pH 7.5, and 25 ºC.

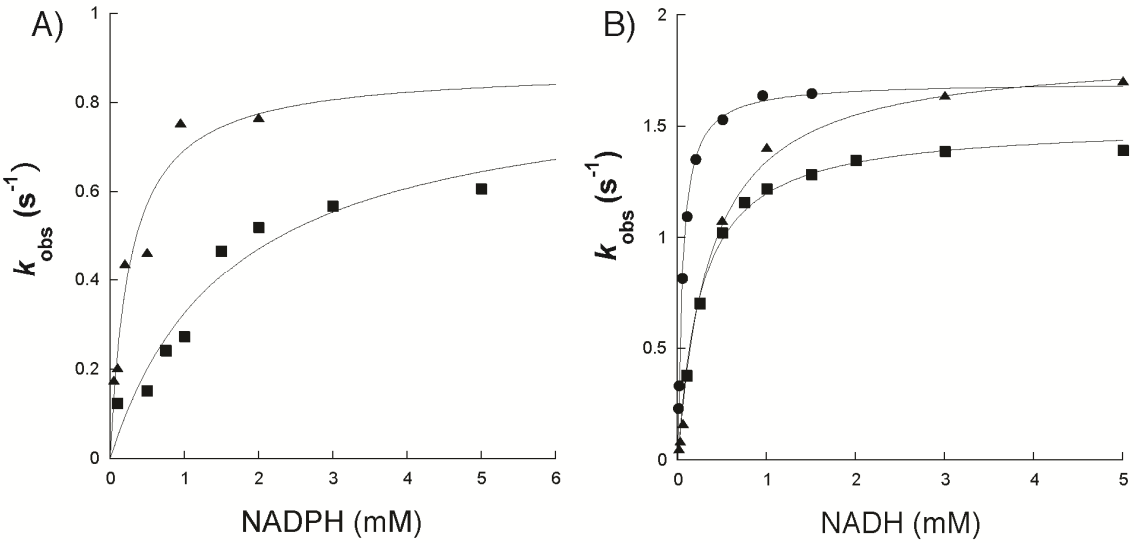

Figure 5.3 A) Flavin reduction as a function of NADPH for R279A (▲), and R279E (■). B) Flavin reduction as a function of NADH for wtSidA (●), R279A (▲), and R279E (■). The maximum rate constants for flavin reduction (k_{red}) and the K_D value were obtained by fitting the data to Eq. 2.

The lower affinity of wtSidA for NADH permits the accurate determination of both the k_{red} and K_D values (Fig. 5.3). Mutation of R279 resulted in a decrease in K_D values for NADH of only 3.7- to 5-fold. While no significant changes of the k_{red} values with either reduced dinucleotide were observed in the mutant enzymes. Clearly, the modification of R279 is less important for NADH binding. In summary, the steady-state and stopped-flow kinetic analyses of the R279A/E enzymes show that removal of the positive charge at position 279 significantly decreases the affinity for NADPH. Comparison of the catalytic efficiencies of the R279A enzyme with NADPH and NADH clearly shows no substrate selectivity. Furthermore, in the R279E enzyme, the coenzyme selectivity is reversed, favoring NADH by 5-fold.

The activity of wtSidA and the R279 mutants were also determined by following ornithine hydroxylation (Table 5.3). As expected, the K_M value for ornithine did not significantly change in the R279 mutants. However, the k_{cat} values for the R279A and R279E mutants decreased by ~2-6 fold (Table 5.3). The decrease in the k_{cat} values could originate from

uncoupling. If only some of the oxygen that is consumed in the reaction leads to hydroxylation of ornithine, and the rest is released as hydrogen peroxide, a lower rate of ornithine hydroxylation would be measured. Coupling of the enzymatic reaction was determined by dividing the turnover value from the oxygen consumption assay with the turnover value calculated in the hydroxylation assay. For wtSidA, coupling with NADPH is greater than 90%, but with NADH, coupling decreases to 50%. With the R279 mutants, the coupling is only between ~25-60% (Table 5.3). These results indicate that the positive charge is essential for efficient hydroxylation and for minimizing production of hydrogen peroxide. In SidA and other flavin-containing monooxygenases, NADPH remains bound throughout the catalytic cycle [9, 10, 23-25]. This is strictly required because NADP(H) plays a role in reducing the flavin, and stabilizing the C4a-hydroperoxyflavin. For wtSidA, the decrease in coupling with NADH can be attributed to a faster k_{off}, which in turn leads to fast decay of the C4a-hydroperoxyflavin. Similarly, in the mutant enzymes, since coenzyme binding affinity is lower, the decrease in coupling can be attributed at least in part to $NAD(P)^+$ being released prior to hydroxylation of ornithine.

Table 5.3 Steady-state kinetic parameters following ornithine hydroxylation.

Parameter/variable substrate	wtSidA	R279A	R279E
Ornithine[a]			
k_{cat} (s^{-1})	0.41 ± 0.01	0.25 ± 0.01	0.170 ± 0.003
K_M (mM)	0.65 ± 0.10	1.0 ± 0.2	0.72 ± 0.16
k_{cat}/K_M ($M^{-1}s^{-1}$)	700 ± 100	260 ± 40	220 ± 40
% coupling	91	52	56
Ornithine[b]			
k_{cat} (s^{-1})	0.40 ± 0.01	0.19 ± 0.01	0.070 ± 0.003
K_M (mM)	0.72 ± 0.11	1.0 ± 0.2	0.08 ± 0.01
k_{cat}/K_M ($M^{-1}s^{-1}$)	560 ± 70	200 ± 30	220 ± 20
% coupling	53	25	34

Conditions: 100 mM sodium phosphate, pH 7.5, and 25 ºC. Assays were performed at five times the K_M value for [a]NADPH or [b]NADH.

The structure of R279A was solved by x-ray crystallography at 2.0 Å resolution (Table 5.4). The enzyme was crystallized under the same conditions as wtSidA in the presence of ornithine and $NADP^+$. The structure of R279A is virtually identical to that of wtSidA with a root-mean-square deviation for the Cα atoms of 0.22 Å (with reference to PDB entry 4B63). The conformation of the alanine mutation is the same as for the Arg279 side chain of wtSidA (Fig. 5.4). The major difference between the crystal structures of wtSidA and R279A is the absence of electron density for $NADP^+$, which might be due to the lower binding affinity. We noticed minor differences on the side chain of some residues in the loop region that is close to the binding site of $NADP^+$, most notably Tyr324 (not shown). Clearly, no major conformational changes are observed in the structure of R279A. Thus, the decrease in binding is directly due to the lack of ionic interaction in the mutant protein.

Table 5.4 Crystallographic statistics

	R279A
PDB code	4NZH
unit cell axes (Å)[a]	77.9, 84.1, 144.9
resolution (Å)	2.0
R_{merge} (%)[b,c]	9.3 (61.9)
completeness (%)[c]	99.0 (97.1)
unique reflections	30,804
redundancy	15.5 (15.0)
$I/\sigma(I)$[c]	29.6 (3.7)
R_{cryst} (%)	20.7
R_{free} (%)	24.3
rmsd bond lengths (Å)	0.005
rmsd bond angles (°)	1

[a]Space group is I222.
[b]$R_{merge}=\Sigma|I_i-\langle I\rangle|/\Sigma I_i$, where I_i is the intensity of i^{th} observation and $\langle I\rangle$ is the mean intensity of the reflection.
[c]Values in parentheses are for reflections in the highest resolution shell.

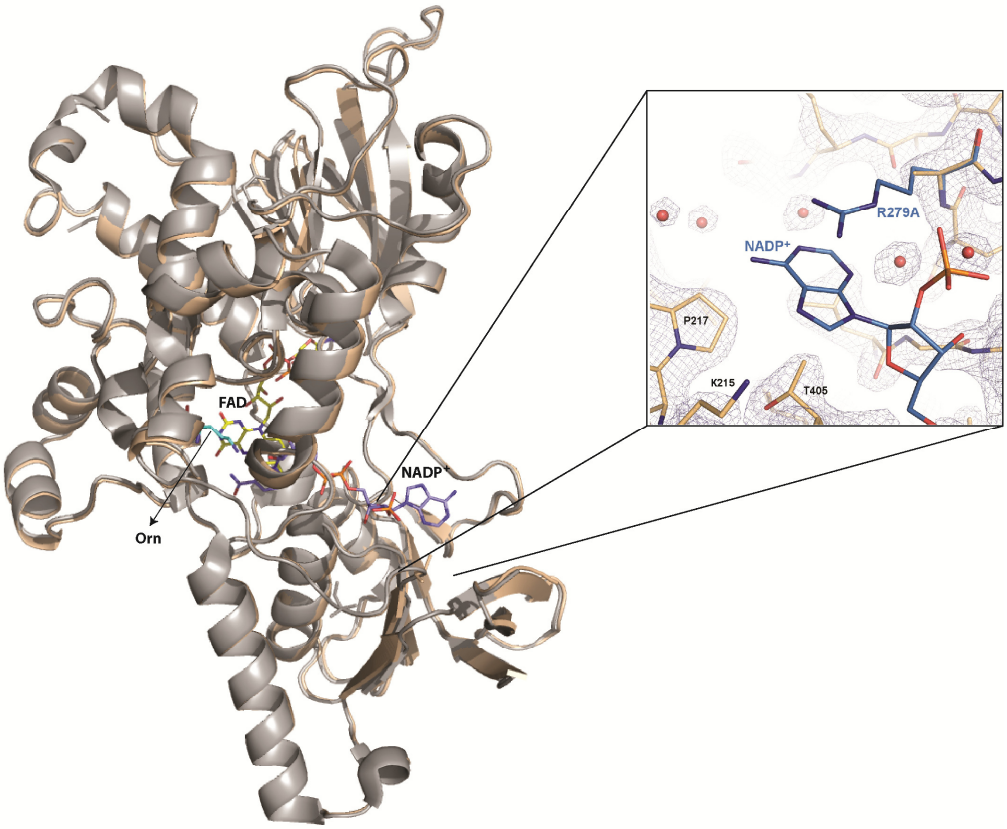

Figure 5.4 Superposition of the structure of wtSidA (gray) and R279A (gold). The FAD and Orn in R279A are those found in the structure of R279A. The $NADP^+$ is only observed in wtSidA (PDB entry 4B63). The insert shows the 2Fo-Fc weighted electron density map around the site of the R279A mutation contoured at the 1.4 σ level. The picture also shows the conformation of R279 and bound $NADP^+$ as observed in the wild-type enzyme (light blue carbons; PDB entry 4B63).

Intrinsic flavin fluorescence was used as a probe of the interaction between the nicotinamide ring and the isoalloxazine ring of FAD. With wtSidA, binding of $NADP^+$ causes a decrease in flavin fluorescence. In contrast, binding of NAD^+ causes an increase in flavin fluorescence (Fig. 5.5) [8]. Clearly, the interaction between the oxidized co-enzymes and the flavin is not the same, which results in differences in the flavin environment that can be detected by flavin fluorescence. As observed in the wtSidA structure in complex with $NADP^+$, the nicotinamide ring binds adjacent to the isoalloxazine ring. Thus, this interaction might be

responsible for the observed quenching of the flavin fluorescence. It is possible that with NAD^+, the nicotinamide ring is not binding so close to the flavin as to cause fluorescence quenching, but instead makes the active site more hydrophobic, which would enhance flavin fluorescence (Fig. 5.5). With the R279 mutants, NAD^+ binding causes a similar increase in the fluorescence, consistent with the results for wtSidA. In contrast, the binding of $NADP^+$ no longer quenches the fluorescence, but increases fluorescence in the mutant enzymes. These results suggest that interaction between R279 and the 2'-phosphate has an effect in the interaction of the nicotinamide ring and the flavin in the active site.

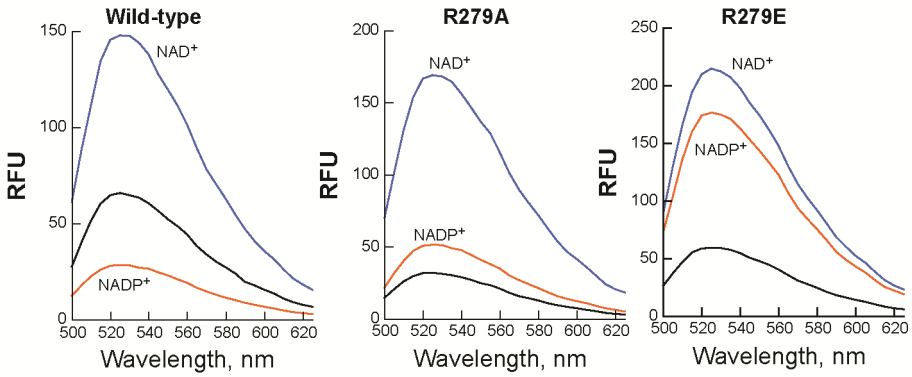

Figure 5.5 Changes in flavin fluorescence induced by oxidized coenzyme binding. The oxidized flavin fluorescence was excited at 450 nm. The emission of the free enzymes (black lines) or when bound to $NADP^+$ (orange) or NAD^+ (blue) were recorded from 500-630 nm.

A structurally homologous arginine is conserved in other Class B flavin-dependent monooxygenases such as FMO, CHMO, and PvdA [23, 26, 27]. As mentioned previously, PvdA has been reported to not recognize NADH as a substrate. This is surprising since the structure of PvdA and SidA are almost identical with an RMS of 1.049 Å. It is possible that protein dynamics important for NADPH binding are different between these two enzymes, however, this remains to be tested. In FMO, the role of the conserved Arg residue has not been determined. Based on

amino acid sequence alignment, several positively charged residues were targeted for mutagenesis in order to determine coenzyme selectivity in HAPMO from *Pseudomonas fluorescens* ACB [20]. Replacement of R339 with alanine (equivalent to R279 in SidA) resulted in a shift of the selectivity from NADPH to NADH. However, the selectivity originated from an almost complete loss of activity with NADPH. Thus, the interactions between an Arg residue and the 2'-phosphate of NADPH play different roles in HAPMO as compared to SidA. In addition, it was also shown that a lysine residue (K439) in HAPMO is also important for coenzyme selectivity. Mutagenesis of K439 to alanine decreased the selectivity for NADPH by ~100-fold. In CHMO from *Acinetobacter* sp. NCBI 9871, another BVMO, a lysine residue (K326) has also been shown to be involved in coenzyme selectivity. Characterization of the CHMO K326A mutant showed a decrease in the selectivity for NADPH of more than 50-fold [20]. The three-dimensional structure of CHMO was later solved and showed that K326 is in hydrogen bonding distance to the 2'-phosphate of $NADP^+$ [27]. The structure of SidA does not show the presence of another positive charged residue in close proximity to the 2'-phosphate of $NADP^+$. The large decrease in activity upon mutation of the R339 in HAPMO and the role of another positive residue indicates that the mechanism of coenzyme selectivity in BVMOs is more complex than in SidA.

In summary, the biochemical characterization of the R279 mutants clearly shows that this residue plays a key role in coenzyme selectivity. Removal of the positive charge at this position abolishes the ability to preferentially bind NADPH and the addition of a negative charge shifts the coenzyme selectivity to NADH. Even though this residue is not near the active site, the reaction becomes significantly uncoupled in the mutant enzymes. This can be attributed, in part, to the release of $NAD(P)^+$ from the active site due to the decrease in affinity. The changes in

flavin fluorescence indicate that the interaction between $NADP^+$ and the flavin is modified upon mutation. Therefore, it is possible that mutation of R279, in addition to affecting the binding affinity, also affects the positioning of $NADP^+$, which is required for optimal stabilization of the C4a-hydroperoxyflavin in SidA.

4. Acknowledgments

This work was supported by a grant from the National Science Foundation MCB-1021384.

5. References

[1] H. He, L. Ding, F. Li, Q. Zhan, Clinical features of invasive bronchial-pulmonary aspergillosis in critically ill patients with chronic obstructive respiratory diseases: a prospective study, Crit. Care 15 (2011) R5.

[2] A. Abad, J.V. Fernandez-Molina, J. Bikandi, A. Ramirez, J. Margareto, J. Sendino, F.L. Hernando, J. Ponton, J. Garaizar, A. Rementeria, What makes Aspergillus fumigatus a successful pathogen? Genes and molecules involved in invasive aspergillosis, Rev. Iberoam. Micol. 27 (2010) 155-182.

[3] H. Haas, Iron - A Key Nexus in the Virulence of Aspergillus fumigatus, Front. Microbiol. 3 (2012) 28.

[4] H. Haas, Eisendel, M.m Turgeon, B.G., Siderophores in fungal physiology and virulence. Annu. Rev. Phytopathol. 46 (2008) 149-87.

[5] A. Wallner, M. Blatzer, M. Schrettl, B. Sarg, H. Lindner, H. Haas, Ferricrocin, a siderophore involved in intra- and transcellular iron distribution in Aspergillus fumigatus, Appl. Environ. Microbiol. 75 (2009) 4194-4196.

[6] M. Eisendle, H. Oberegger, I. Zadra, H. Haas, The siderophore system is essential for viability of Aspergillus nidulans: functional analysis of two genes encoding l-ornithine N 5-monooxygenase (sidA) and a non-ribosomal peptide synthetase (sidC), Mol. Microbiol. 49 (2003) 359-375.

[7] A.H. Hissen, A.N. Wan, M.L. Warwas, L.J. Pinto, M.M. Moore, The Aspergillus fumigatus siderophore biosynthetic gene sidA, encoding L-ornithine N5-oxygenase, is required for virulence, Infect. Immun. 73 (2005) 5493-5503.

[8] E. Romero, M. Fedkenheuer, S.W. Chocklett, J. Qi, M. Oppenheimer, P. Sobrado, Dual role of NADP(H) in the reaction of a flavin dependent N-hydroxylating monooxygenase, Biochim. Biophys. Acta 1824 (2012) 850-857.

[9] S.W. Chocklett, P. Sobrado, Aspergillus fumigatus SidA is a highly specific ornithine hydroxylase with bound flavin cofactor, Biochemistry 49 (2010) 6777-6783.

[10] J.A. Mayfield, R.E. Frederick, B.R. Streit, T.A. Wencewicz, D.P. Ballou, J.L. DuBois, Comprehensive spectroscopic, steady state, and transient kinetic studies of a

representative siderophore-associated flavin monooxygenase, J. Biol. Chem. 285 (2010) 30375-30388.
[11] E. Romero, Avila, D, Sobrado, P, in, Effect of pH on the Reductive and Oxidative Half-reactions of Aspergillus fumigatus Siderophore A, *In Flavins and Flavoproteins* (Miller, S., Hille, R., Palfey, B., Eds). 289-294.Raleigh, NC: Lulu
[12] S. Franceschini, M. Fedkenheuer, N.J. Vogelaar, H.H. Robinson, P. Sobrado, A. Mattevi, Structural insight into the mechanism of oxygen activation and substrate selectivity of flavin-dependent N-hydroxylating monooxygenases, Biochemistry 51 (2012) 7043-7045.
[13] T. Csaky, On the Estimation of Bound Hydroxylamine in Biological Materials, Acta Chem. Scand. 2 (1948) 450-454.
[14] R. Robinson, Sobrado, P., Substrate binding modulates the activity of Mycobacterium smegmatis G (MbsG), a flavin-dependent monooxygenase involved in the biosynthesis of hydroxamate-containing siderophores Biochemistry 50 (2011) 8449-96.
[15] S. Strickland, G. Palmer, V. Massey, Determination of dissociation constants and specific rate constants of enzyme-substrate (or protein-ligand) interactions from rapid reaction kinetic data, J. Biol. Chem. 250 (1975) 4048-4052.
[16] M.D. Winn, C.C. Ballard, K.D. Cowtan, E.J. Dodson, P. Emsley, P.R. Evans, R.M. Keegan, E.B. Krissinel, A.G. Leslie, A. McCoy, S.J. McNicholas, G.N. Murshudov, N.S. Pannu, E.A. Potterton, H.R. Powell, R.J. Read, A. Vagin, K.S. Wilson, Overview of the CCP4 suite and current developments, Acta Crystallogr. D Biol. Crystallogr. 67 (2011) 235-242.
[17] W.J. van Berkel, N.M. Kamerbeek, M.W. Fraaije, Flavoprotein monooxygenases, a diverse class of oxidative biocatalysts, J. Biotechnol. 124 (2006) 670-689.
[18] K.M. Meneely, A.L. Lamb, Biochemical characterization of a flavin adenine dinucleotide-dependent monooxygenase, ornithine hydroxylase from Pseudomonas aeruginosa, suggests a novel reaction mechanism, Biochemistry 46 (2007) 11930-11937.
[19] M.W. Fraaije, J. Wu, D.P. Heuts, E.W. van Hellemond, J.H. Spelberg, D.B. Janssen, Discovery of a thermostable Baeyer-Villiger monooxygenase by genome mining, App. Microbiol. Biotechnol. 66 (2005) 393-400.
[20] N.M. Kamerbeek, M.W. Fraaije, D.B. Janssen, Identifying determinants of NADPH specificity in Baeyer-Villiger monooxygenases, Eur. J. Biochem. 271 (2004) 2107-2116.
[21] N.B. Beaty, D.P. Ballou, The reductive half-reaction of liver microsomal FAD-containing monooxygenase, J. Biol. Chem. 256 (1981) 4611-4618.
[22] N.B. Beaty, D.P. Ballou, Transient kinetic study of liver microsomal FAD-containing monooxygenase, J. Biol. Chem. 255 (1980) 3817-3819.
[23] A. Alfieri, E. Malito, R. Orru, M.W. Fraaije, A. Mattevi, Revealing the moonlighting role of NADP in the structure of a flavin-containing monooxygenase, Proc. Nat. Acad. Sci. U S A 105 (2008) 6572-6577.
[24] D.E. Torres Pazmino, B.J. Baas, D.B. Janssen, M.W. Fraaije, Kinetic mechanism of phenylacetone monooxygenase from Thermobifida fusca, Biochemistry 47 (2008) 4082-4093.
[25] L.L. Poulsen, D.M. Ziegler, The liver microsomal FAD-containing monooxygenase. Spectral characterization and kinetic studies, J. Biol. Chem. 254 (1979) 6449-6455.

[26] J. Olucha, K.M. Meneely, A.S. Chilton, A.L. Lamb, Two structures of an N-hydroxylating flavoprotein monooxgenase: the ornithine hydroxylase from Pseudomonas aeruginosa, J. Biol. Chem. 286 (2011) 31789-98.
[27] I.A. Mirza, B.J. Yachnin, S. Wang, S. Grosse, H. Bergeron, A. Imura, H. Iwaki, Y. Hasegawa, P.C. Lau, A.M. Berghuis, Crystal structures of cyclohexanone monooxygenase reveal complex domain movements and a sliding cofactor, J. Am. Chem. Soc. 131 (2009) 8848-8854.

CHAPTER 6

Lys107, Asn293, Asn323, and Ser469 coordinate binding of ornithine in SidA

Author Contributions:
Reeder Robinson performed all the research except the experiments mentioned below and wrote the chapter.

Catherine Klancher helped with some of the steady-state assays and pre-steady-state assays.

Pedro Rodriguez helped with some of the steady-state assays.

Jack Tanner solved the crystal structure of N323A.

Pablo Sobrado oversaw and directed the research.

Abstract

Siderophore A (SidA) from *Aspergillus fumigatus* is a flavin-containing monooxygenase that performs the NADPH dependent hydroxylation of the N^5 of Orn. This is the first step in siderophore biosynthesis in *Aspergillus spp.* and is essential for virulence. Here, we report the effect on the steady-state and pre-steady-state of four mutations; K107A, N293A, N323A, and S469A. Steady-state data shows these four residues all decrease the catalytic efficency for L-Orn in oxygen consumption and hydroxylation assays by >10-fold. Steady-state data for N293A and S469A indicates removal of one interaction around the α-carbon of Orn decreases the stereoselectivity of SidA. This data indicates K107, N293, N323, and S469 are important for proper L-Orn binding. Pre-steady-state data indicates all of the mutants react similarly with NADPH as wild-type, with the exception of N323A which showed a ~20-fold increase in the rate of flavin reduction and a higher observed KIE value. N323 hydrogen bonds with the 3'-hydroxyl of the nicotinamide ribose and the crystal structure of N323A shows a lack of electron density for both the nicotinamide ring and the nicotinamide ribose. This suggests NADPH is more

dynamic and “coenzyme sliding” is less rate-limiting where NADPH samples the flavin at a higher rate during the reductive half-reaction. The four mutants did not show any changes in the oxidative half-reaction indicating they are not important to the reaction with reduced flavin and oxygen, nor stabilization of the C4a-hydroperoxyflavin. This suggests the interaction provided by N323 to $NADP^+$ does not disrupt its interaction with the C4a-hydroperoxyflavin.

1. Introduction

Aspergillus fumigatus SidA is an N^5-Orn monooxygenase and a member of the microbial *N*-hydroxylating monooxygenases (NMOs) [1, 2]. SidA contains a bound flavin adenine dinucleotide (FAD) molecule, utilizes NADPH, and is selective for Orn. In the catalytic cycle, the flavin undergoes a redox reaction where NADPH first transfers a hydride equivalent to the N5 of the flavin, then molecular oxygen reacts with the reduced form of the flavin to form the C4a-hydroperoxyflavin, which is the hydroxylating species (Scheme 6.1). This intermediate is very stable in SidA with a half-life of ~30 minutes. After Orn binds to the active site, the distal oxygen of the C4a-hydroperoxyflavin is transferred to Orn to form N^5-hydroxy-Orn.

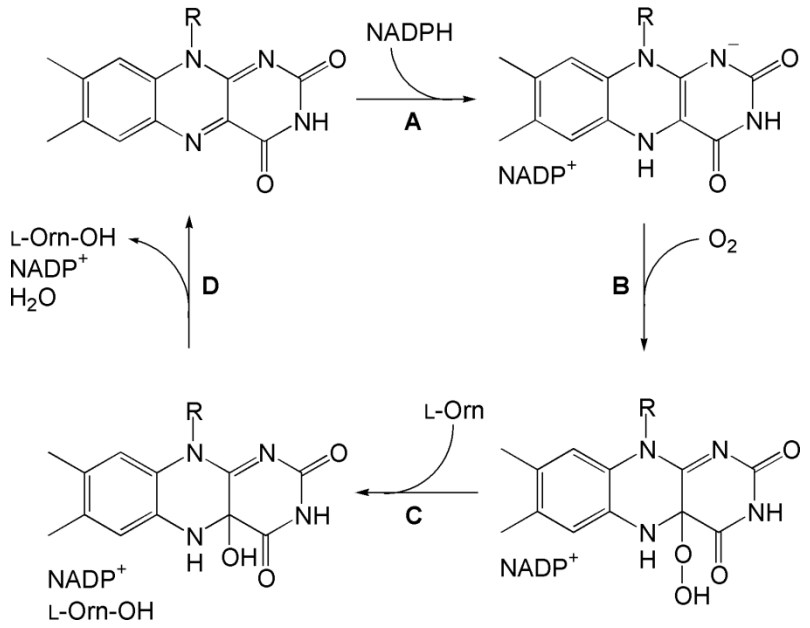

Scheme 6.1 Catalytic cycle of SidA. A) NADPH binds to the oxidized form of SidA and transfers a hydride equivalent to the N5 of the flavin. B) Molecular oxygen reacts with the reduced flavin to form a stable C4a-hydroperoxyflavin which is the hydroxylating species. C) The distal oxygen of the C4a-hydroperoxyflavin is transferred to the N^5 of L-Orn in the hydroxylation reaction. D) The hydroxyflavin is dehydrated and the products are released. $NADP^+$ remains bound throughout the catalytic cycle which provides a stabilizing interaction for the C4a-hydroperoxyflavin.

Perhaps the most interesting mechanistic aspect of the SidA reaction is that NADP(H) remains bound throughout the catalytic cycle [1]. This has a double-edged importance for achieving efficient catalysis and minimizing the release of reactive oxygen species. The first obvious role, is the transfer of a hydride equivalent to the N5 of the flavin. Next, the resulting $NADP^+$ swings into a conformation that promotes stabilization of the C4a-hydroperoxyflavin through interaction with the 2'-OH of the nicotinamide ribose [3]. This crucial role for NADP(H) in catalysis is a common mechanistic feature among NMOs as well as the broader family of Class B monooxygenases [4, 5].

SidA hydroxylates L-Orn with close to 100% efficiency where for every one molecule of oxygen consumed, a near stoichiometric amount of hydroxylated product is formed [1, 2, 6].

The three-dimensional crystal structure of SidA suggests this is at least partially achieved through several specific interactions with L-Orn that hold it in an optimal position for the N^5 to react with the distal oxygen of the C4a-hydroperoxyflavin (Fig. 6.1) [7]. The three residues K107, N293, and S469 appear to be oriented around the α-carbon of L-Orn forming a specific binding site that would only accept the L-stereoisomer of Orn. The fourth interaction provided by N323 appears to properly position the N^5 of Orn at an optimal distance for oxygen transfer with the C4a-hydroperoxyflavin. In this study, these four residues were mutated to Ala residues in order to determine their effect on Orn binding, stereospecificity, and roles in catalysis.

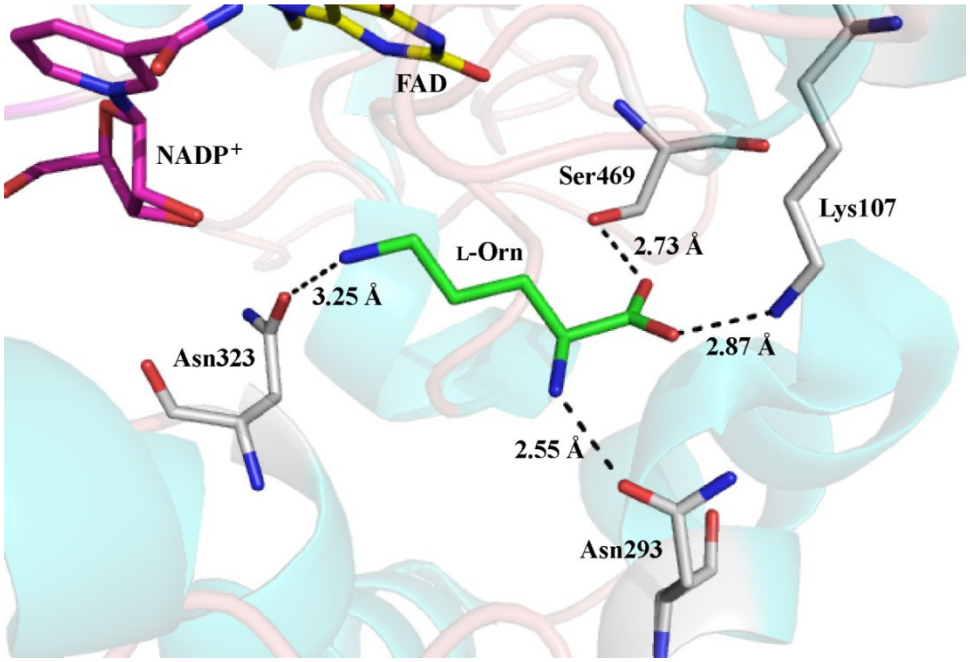

Figure 6.1 View of the Orn binding site in SidA (PDB code 4B63) and relative positions of residues Lys107, Asn293, Asn323, and Ser469.

2. Materials and Methods

2.1 Materials. Buffers and media were obtained from Fisher Scientific (Pittsburgh, PA). BL21(DE3)-T1^R chemically competent cells were obtained from Sigma-Aldrich (St. Louis, MO).

NADPH was obtained from EMD4 Biosciences (Billerica, MA). DNA primers were synthesized by Integrated DNA Technologies (Coralville, IA). Plasmid preparation and gel purification kits were obtained from Qiagen (Valencia, CA). *Escherichia coli* TOP-10 chemically competent cells were obtained from Invitrogen (Carlsbad, CA). Chromatography columns were obtained from GE Healthcare.

2.2 Site–directed mutagenesis. Mutagenesis of residues was performed using the QuikChange (Agilent Technologies) method following the manufacturer's instructions. The wild-type SidA gene, subcloned into the pET15b plasmid, was used as the template [7]. For K107A, the forward primer (5'-GCAGATCAGCTTCATCGCGGATCTCG-3') and reverse primer (5'-CGCGGAGGGTGGCGAGATCCGCGAT-3') were used. For N293A, the forward primer (5'-CTCGCCTTTCGTCGCGGAGATCTTCA-3') and reverse primer (5'-GGGTTGAAGATCTCCGCGACGAAAG-3') were used. For N323A, the forward primer (5'-GACAAGGCTACCGCGTACTCCGTCGT-3') and reverse primer (5'-CGGACGAC GGAGTACGCGGTAGCCT-3') were used. For S469A, the forward primer (5'-GA CTCCCTGCTGGCCGTCCTCGCCG-3') and reverse primer (5'-CGGCGAGGACGGCCAGC AGGGAGTC-3') were used. The codons for the mutated residues are underlined. The mutations were confirmed by DNA sequencing at Virginia Bioinformatics Core Sequencing Facility.

2.3 Protein expression and purification. All mutant proteins were expressed in *E. coli* BL21(DE3)-T1^{R} competent cells and purified as previously described [7]. In general, ~25 mg of protein were obtained per liter of media. The purified proteins were stored in 100 mM sodium phosphate, 50 mM NaCl, pH 7.5, at -80 °C at a concentration of ~200 μM (based on flavin

content) in 30 µL aliquots. The 6x-His tag was removed for the SidA N323A sample used for crystallization by incubation at 4 ºC with thrombin overnight as previously described [7].

2.4 Determination of flavin incorporation. There were no variations in the flavin spectra for any mutant enzyme (data not shown). Flavin incorporation was determined by measuring protein concentration via the Bradford assay (BioRad) and comparing it to the protein concentration based on the flavin spectra. SidA concentration based on flavin content was determined using an extinction coeficent of 13.7 $mM^{-1}cm^{-1}$ at 450 nm [1]. Flavin incorporation was generally close to ~70%.

2.5 Steady-state kinetics. The rate of oxygen consumption was measured using a Hansatech Oxygraph system (Norfolk, England). Reactions consisted of a 1 mL volume of 100 mM sodium phosphate, pH 7.5, at 25 °C. When NADPH was varied, L-Orn was held constant at 15 mM for wild-type, 200 mM for N293A, 30 mM for N323A, and 500 mM for S469A. When L-Orn was varied, NADPH was kept constant at a concentration of 1 mM for all tested mutants. For K107A, activity was tested for with 500 mM L-Orn and 1 mM NADPH. Reactions were initiated by addition of 2 µM SidA and monitored for 5 minutes with constant stirring.

Hydroxylated Orn was monitored using a variation of the Csaky iodine oxidation assay [8, 9]. The standard assay buffer contained 104 µL of 100 mM sodium phosphate (pH 7.5) with varying concentrations of L-Orn and NADPH held constant at 1 mM. Reactions were initiated by addition of 2.0 µM SidA and incubated for 10 min at 25 °C with constant shaking at 750 rpm.

2.6 Pre-steady-state kinetics. All rapid reaction experiments were carried out at 25 °C using an SX-20 stopped-flow spectrophotometer (Applied Photophysics, Leatherhead, UK) in an

anaerobic glove box (Coy, Grass Lake, MI). Preparation of anaerobic buffer was carried out through five cycles of vacuum and flushing with O_2-free argon after 1 hr of continuous vacuum. This was repeated five times for a total of five hrs. The enzyme was made anaerobic through constant cycles of vacuum and flushing with O_2-free argon for 1 hr. Substrates were made anaerobic by dissolving in anaerobic buffer inside the glove box. The stopped-flow was made anaerobic by flushing with 1 mL of anaerobic 100 mM sodium acetate, pH 5.0, containing 100 mM D-glucose and 100 µg/mL glucose oxidase Type-X. For all tested mutants, the rates of flavin reduction were measured in single mixing mode where anaerobic SidA (15 µM after mixing) was mixed with an equal volume of NADPH (100 µM after mixing).

The rates of flavin oxidation were measured in double mixing mode for all of the tested mutations. Anaerobic SidA (60 µM before mixing) was first mixed with an equal volume of NADPH (60 µM before mixing). This mixture was allowed to incubate in an ageing loop for 60 seconds until the bound flavin was fully reduced. The reduced SidA–$NADP^+$ complex was then allowed to react with molecular oxygen (300 µM after mixing). Spectra were taken on a logarithmic time scale until the half-reactions were complete.

2.7 Synthesis of 4-pro-R-4^{2}H-NADPH. 4-*pro-R*-4^{2}H-NADPH was synthesized by the method of Jeong with some minor modifications as described by Dhatwalia [10, 11]. Briefly, 25 mg of $NADP^+$ (5.6 mM final concentration), 480 µL 2-propanol-*d*8 (1 M final concentration), and 50 units of alcohol dehydrogenase from *Thermoanaerobium brockii* were added to 6 mL of 25 mM Tris-Cl pH 9.0. The reaction was allowed to proceed for 30 minutes at 40 ºC until the A_{260}/A_{340} reached ~2.5. The solution was then filtered with a 30 kDa molecular-weight cutoff filter and rotary evaporated to ~1.5 mL. The sample was then diluted up to 15 mL with 100% ethanol and

stored at -20 ºC for 30 minutes. The precipitated sample was then centrifuged for 10 minutes at 14,100 *g* at 4 ºC. The resulting pellets were then resuspended in 25 mM Tris-Cl pH 9.0 and stored at -20 ºC. NADPH was synthesized by the same method as a control to account for any differences with commercial samples.

2.8 Crystallization of SidA N323A. SidA N323A crystals were grown in similar conditions to wild-type [7]. In brief, crystals were obtained using the hanging drop vapor diffusion method and larger crystals for data collection were obtained from microseeding from smaller crystals. The reservoir solution contained 0.1 M HEPES pH 6.6, 1.86 M ammonium sulfate, and 1% (v/v) dioxane. This was mixed in a 1:1 ratio with 8 mg/mL SidA N323A which was pre-incubated with 1 mM $NADP^+$ and 100 mM L-Orn. The crystals were allowed to grow for one month and then flash frozen in the reservoir solution with 30% (v/v) glycerol as the cryoprotectant.

2.9 Structure determination. The structure of SidA N323A was determined to 1.9 Å resolution by the Tanner group by molecular replacement with the structure for wild-type SidA (PDB code 4B63).

2.10 Data analysis. All data were fit using KaleidaGraph (Synergy Software, Reading, PA). The rates of reduction were determined by fitting the decrease in absorbance at 452 nm to a double exponential decay equation (eq. 1).

$$v = c + a_1 e^{-(k_1 \times t)} + a_2 e^{-(k_2 \times t)} \quad (1)$$

For flavin oxidation studies, the increase in absorbance at 372 nm, which corresponds with formation of the C4a-hydroperoxyflavin intermediate, was fit to eq. 2, which describes a

single exponential rise. The subsequent increase in absorbance at 452 nm, which corresponds to flavin oxidation, was fit to eq. 3, which describes a double exponential rise. The first exponential rate of flavin oxidation calculated in eq. 3 is omitted in this study as it corresponds to formation of the C4a-hydroperoxyflavin calculated with eq. 2 at 372 nm.

$$v = c + a(1 - e^{-(k \times t)}) \tag{2}$$

$$v = c + a_1(1 - e^{-(k_1 \times t)}) + a_2(1 - e^{-(k_2 \times t)}) \tag{3}$$

3. Results

3.1 Steady-state oxygen consumption with L-Orn. The steady-state kinetic parameters for oxygen consumption for N293A, N323A, and S469A were determined using both NADPH and L-Orn as the variable substrates. K107A displayed no oxygen consumption with 1 mM NADPH and 500 mM L-Orn (data not shown). The data in Table 6.1 indicates for N293A and N323A, the k_{cat} values for oxygen consumption are ~50% and ~80% higher than wild-type, respectively. S469A however is ~4-fold less active than wild-type indicating that the mutation slightly affects the overall activity. N293A, N323A, and S469A most significantly affected the K_m value for L-Orn where ~16-fold, ~14-fold, and ~19-fold increases were observed, respectively.

Table 6.1 Steady-state kinetic parameters determined by oxygen consumption with L-Orn.

Parameter	Wild-type	K107A	N293A	N323A	S469A
k_{cat}, s^{-1}	0.59 ± 0.01	N/A	0.88 ± 0.08	1.06 ± 0.06	0.15 ± 0.01
$K_{m(L\text{-}Orn)}$, mM	1.1 ± 0.3	N/A	18 ± 2	15 ± 1	21 ± 2
$k_{cat}/K_{m(L\text{-}Orn)}$, $M^{-1}s^{-1}$	540 ± 20	N/A	50 ± 7	71 ± 6	7.1 ± 0.8
$K_{m(NADPH)}$, mM	0.0070 ± 0.0001	N/A	0.06 ± 0.01	0.010 ± 0.003	0.025 ± 0.009
$k_{cat}/K_{m(NADPH)}$, $M^{-1}s^{-1}$	84000 ± 2000	N/A	15000 ± 3000	110000 ± 32000	6000 ± 2000

Conditions: 100 mM sodium phosphate, pH 7.5, and 25 ºC.

3.2 Steady-state L-Orn hydroxylation. The steady-state L-Orn hydroxylation parameters for N293A, N323A, and S469A were calculated in order to determine the effect of these mutations on coupling. L-Orn hydroxylation data was not determined for K107A as it did not display any hydroxylation activity with 1 mM NADPH and 500 mM L-Orn (data not shown). The data indicates similar k_{cat} values for N293A and N323A as wild-type, whereas S469A displays ~5-fold less hydroxylation activity for L-Orn (Table 6.2). The K_m values for L-Orn for all three of the mutants displayed similar increases to their respective K_m values for oxygen consumption. The coupling percentages for all three mutants could be calculated by dividing the k_{cat} values for L-Orn hydroxylation and oxygen consumption. The results indicate that the coupling percentages for all three mutants are affected where they are less than wild-type (Table 6.2).

Table 6.2 Steady-state kinetic parameters determined by L-Orn hydroxylation.

Parameter	Wild-type	K107A	N293A	N323A	S469A
k_{cat}, s^{-1}	0.62 ± 0.02	N/A	0.53 ± 0.04	0.5 ± 0.1	0.107 ± 0.009
$K_{m(L\text{-}Orn)}$, mM	1.0 ± 0.2	N/A	16 ± 1	12 ± 2	18 ± 4
$k_{cat}/K_{m(L\text{-}Orn)}$, $M^{-1}s^{-1}$	600 ± 100	N/A	33 ± 3	42 ± 11	6 ± 1
Coupling, %	105 ± 4	N/A	60 ± 7	50 ± 10	71 ± 8

Conditions: 100 mM sodium phosphate, pH 7.5, and 25 ºC.

3.3 Steady-state oxygen consumption with D-Orn. The steady-state kinetic parameters for N293A and S469A were performed with D-Orn in order to determine if the removal of an interaction around the α-carbon of Orn introduces promiscuity between L- or D-Orn. The results for wild-type in Table 6.3 indicate a ~28-fold decrease in the k_{cat}/K_m value for oxygen consumption with D-Orn when compared to the k_{cat}/K_m value for oxygen consumption with L-Orn (Table 6.1). N293A however, displays only an 11-fold decrease in the k_{cat}/K_m value for oxygen consumption with D-Orn when compared to the k_{cat}/K_m value for oxygen consumption with L-Orn (Table 6.1). This indicates that N293A is slightly less selective between Orn stereoisomers when compared to wild-type. A K_m value for D-Orn could not be determined for S469A in the oxygen consumption assay because of the low observed k_{cat} value (data not shown).

Table 6.3 Steady-state kinetic parameters determined by oxygen consumption with D-Orn.

Parameter	Wild-type	N293A	S469A
k_{cat}, s^{-1}	0.085 ± 0.003	0.0367 ± 0.001	0.0185 ± 0.0002
$K_{m(D\text{-}Orn)}$, mM	4.4 ± 0.9	8 ± 1	N/A
$k_{cat}/K_{m(D\text{-}Orn)}$, $M^{-1}s^{-1}$	19 ± 4	4.6 ± 0.6	N/A
L-Orn specificity, fold	28 ± 6	11 ± 2	N/A

Conditions: 100 mM sodium phosphate, pH 7.5, and 25 ºC.

3.4 Steady-state D-Orn hydroxylation. The steady-state kinetic parameters with D-Orn were performed with N293A and S469A in order to determine if removal of one of these two interactions around the α-carbon of Orn affect the coupling with D-Orn. The results in Tables 6.2 and 6.4 indicate that wild-type has a ~100-fold higher specificity for hydroxylation of L-Orn over D-Orn. Here, the k_{cat}/K_m values indicate that N293A and S469A are specific for L-Orn hydroxylation by ~11-fold and ~26-fold, respectively. Also, the coupling for D-Orn hydroxylation in N293A and S469A are similar to wild-type. The data indicates that removal of one of the hydrogen bonds around the α-carbon of Orn slightly decreases selectivity between L- and D-Orn.

Table 6.4 Steady-state kinetic parameters determined by D-Orn hydroxylation.

Parameter	Wild-type	N293A	S469A
k_{cat}, s^{-1}	0.0405 ± 0.0006	0.0205 ± 0.0005	0.0079 ± 0.0003
$K_{m(D\text{-}Orn)}$, mM	9.2 ± 0.6	29 ± 2	35 ± 5
$k_{cat}/K_{m(D\text{-}Orn)}$, $M^{-1}s^{-1}$	4.7 ± 0.5	0.72 ± 0.06	0.23 ± 0.03
Coupling, %	48 ± 2	56 ± 2	42 ± 2
L-Orn specificity, fold	106 ± 24	11 ± 2	26 ± 6

Conditions: 100 mM sodium phosphate, pH 7.5, and 25 ºC.

3.5 Pre-steady-state kinetics of flavin reduction and oxidation. The pre-steady-state kinetic parameters of flavin reduction and oxidation were calculated in order to determine if any of the mutations had effects on either half-reaction. For the reductive half-reaction experiments in Table 6.5, 100 μM NADPH was used to determine the k_{red} values. Wild-type has a K_D value of ~1 μM and reduction of the mutants with a stoichiometric concentration (15 μM) of NADPH produced similar results as with 100 μM suggesting the mutations do not have a large effect towards the affinity for NADPH [2]. The results in Table 6.5 and Fig. 6.2A show the first phase

of reduction for N293A is ~2-fold higher than wild-type, while the reduction for K107A is ~2-fold slower than wild-type, while the reduction rate is similar for S469A. N323A, however, displayed a ~20-fold increase in the first phase reduction when compared to wild-type. This result prompted for the dependency of reduction on NAD(P)H concentration to be determined in order to calculate if this mutation affects coenzyme binding. Table 6.6 shows that for N323A, the binding affinities do not appear to be affected for NADPH while the K_D value for NADH is ~3-fold higher. The rates of reduction for the first phase with both coenzymes are ~15-20-fold faster than wild-type [12]. Figs. 6.2B-D show the spectra of flavin reduction for wild-type, K107A, and N323A and indicates the mutations do not perturb the spectra for flavin reduction. The spectra of flavin reduction for N293A and S469A are not shown, but are identical to wild-type and the other two mutants. For the oxidative half-reaction experiments, the reduced form of each enzyme was reacted with 300 μM O_2 in the absence of Orn in order to determine if the rate of formation of the C4a-hydroperoxyflavin or its stability were affected by any of the mutations. The results in Table 6.5 and Fig. 6.3A indicate the rate of formation of the C4a-hydroperoxyflavin for each mutation is not significantly different from wild-type with K107A showing the largest change at ~2-fold (Table 6.5). The results in Table 6.5 and Fig. 6.3B also indicate that the stability of the C4a-hydroperoxyflavin is unaffected by each mutation as the k_{ox} values are all similar to wild-type. Figs. 6.3C-D show that the spectra for oxidation of K107A and N323A are identical to wild-type [3]. The spectra of flavin oxidation for N293A and S469A are not shown, but are identical to wild-type and the other two mutants.

Table 6.5 Pre-steady-state kinetic parameters of flavin reduction and oxidation with NADPH.

Parameter	Wild-type	K107A	N293A	N323A	S469A
k_{red1}, s^{-1}	0.62 ± 0.01	0.30 ± 0.01	1.15 ± 0.03	11.24 ± 0.06	0.67 ± 0.03
k_{red2}, s^{-1}	0.220 ± 0.005	0.0788 ± 0.003	0.121 ± 0.006	0.46 ± 0.01	0.0569 ± 0.0008
k_{OOH}, s^{-1}	0.65 ± 0.07	1.4 ± 0.1	0.49 ± 0.06	0.95 ± 0.03	0.60 ± 0.07
k_{ox}, s^{-1}	0.0160 ± 0.0002	0.00704 ± 0.00002	0.0121 ± 0.0002	0.0116 ± 0.0002	0.0116 ± 0.0004

Conditions: 100 mM sodium phosphate, pH 7.5, and 25 ºC.

Table 6.6 Kinetic parameters of flavin reduction for wild-type and N323A.

	Wild-type		N323A	
	NADPH	NADH	NADPH	NADH
k_{red1}, s^{-1}	0.62 ± 0.01	1.55 ± 0.01	11.1 ± 0.1	22.2 ± 0.4
k_{red2}, s^{-1}	0.220 ± 0.005	0.090 ± 0.003	0.444 ± 0.007	8.3 ± 0.3
$K_{D(NAD(P)H)}$, μM	~1	56 ± 4	~1	143 ± 9

Conditions: 100 mM sodium phosphate, pH 7.5, and 25 ºC. The results for wild-type were obtained from a previous publication [12].

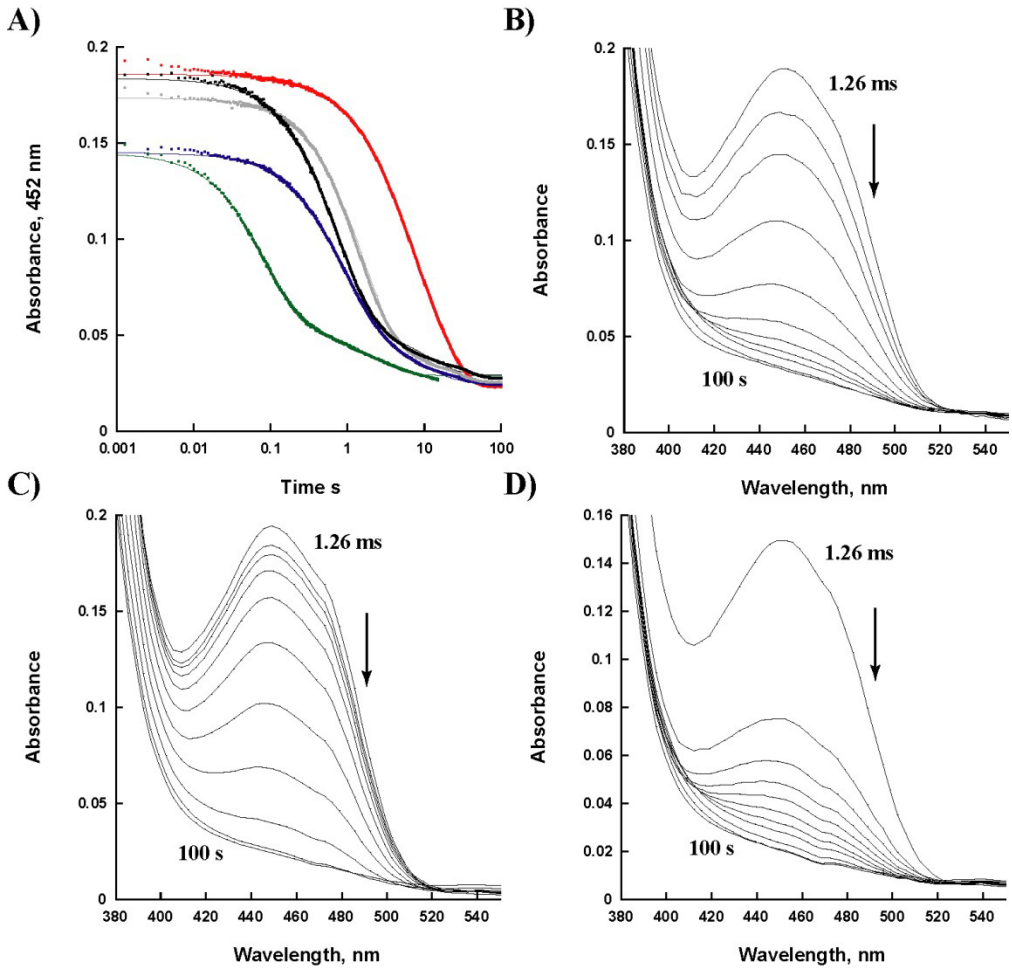

Figure 6.2 Rapid-reaction kinetics of flavin reduction. A) Traces of the absorbances at 452 nm of flavin reduction upon mixing with 100 µM NADPH in the stopped-flow spectrophotometer. The traces indicate flavin reduction for SidA wild-type (black), K107A (red), N293A (blue), N323A (green), and S469A (silver). B) Spectra of flavin reduction for SidA wild-type with 100 µM NADPH. C) Spectra of flavin reduction for SidA K107A with 100 µM NADPH. D) Spectra of flavin reduction for SidA N323A with 100 µM NADPH.

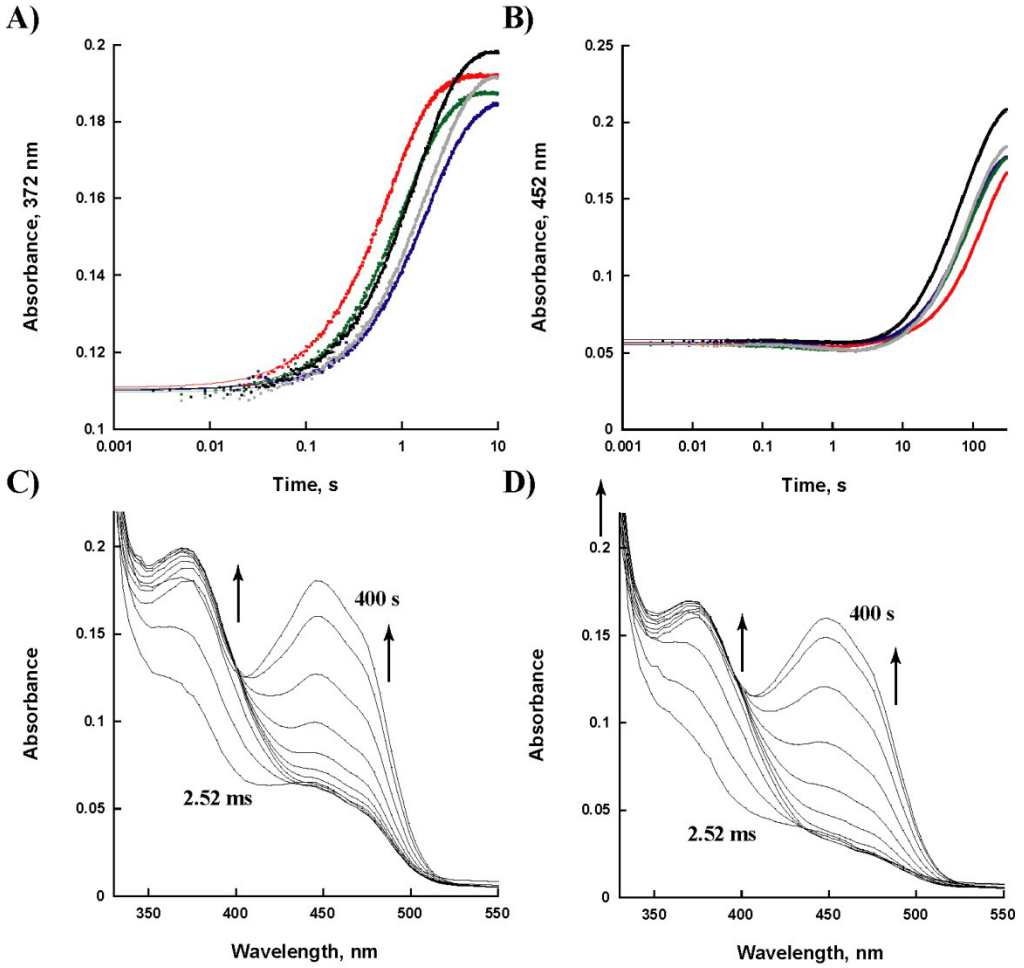

Figure 6.3 Rapid-reaction kinetics of flavin oxidation. A) Traces of the absorbances at 372 nm of C4a-hydroperoxyflavin formation upon mixing of 300 µM O_2 in the stopped-flow spectrophotometer with previously reduced SidA. The traces indicate reduction for SidA wild-type (black), K107A (red), N293A (blue), N323A (green), and S469A (silver). B) Traces of the absorbances at 452 nm of flavin oxidation upon mixing of 300 µM O_2 in the stopped-flow spectrophotometer with previously reduced SidA. The color scheme is the same as Fig. 6.2A. C) Spectra of flavin oxidation for SidA K107A with 300 µM O_2. D) Spectra of flavin oxidation for SidA N323A with 300 µM O_2.

3.6 Primary kinetic isotope effect (KIE) with N323A. The primary KIE for flavin reduction with N323A was determined to probe if the ~20-fold enhanced rate of reduction has an effect on the magnitude of hydride transfer. The results indicate a KIE using 4-*pro*-*R*-4^{2}H-NADPH on both phases of reduction for N323A while a KIE was only observed for the first phase of reduction with wild-type (Table 6.7). $^{D}k_{red}$ values of 3.9 ± 0.2 and 5.61 ± 0.05 were calculated for the first

phases of reduction for wild-type and N323A, respectively. For the second phases of reduction, $^{D}k_{red}$ values of 0.98 ± 0.03 and 2.05 ± 0.04 were calculated for wild-type and N323A, respectively. The calculated KIE values for wild-type differ from previously determined KIE values for SidA of ~5.5 which were determined for both phases of reduction [12]. This discrepancy will need to be resolved in future experiments.

Table 6.7 Primary KIE values of flavin reduction for wild-type and N323A.

	Wild-type	**N323A**
$^{D}k_{red1}$	3.9 ± 0.2	5.61 ± 0.05
$^{D}k_{red2}$	0.98 ± 0.03	2.05 ± 0.04

Conditions: 100 mM sodium phosphate, pH 7.5, and 15 ºC.

3.7 Three-dimensional structure analysis of N323A. The three-dimensional crystal structure of N323A was solved in order to possibly provide a structural explanation for the increased rate of flavin reduction. Preliminary results show the structure of N323A is virtually identical to wild-type (PDB code 4B63) with a calculated RMSD of 0.257 (Fig. 6.4A). This indicates the mutation of N323 to Ala does not affect any major folds in SidA. The active site of N323A is also very similar to wild-type with the flavin, L-Orn, and the adenine moiety of $NADP^+$ superimposable. The only notable difference with N323A is the lack of electron density for the nicotinamide ring and the nicotinamide ribose of $NADP^+$. In the wild-type structure, N323 appears to hydrogen bond with the 3'-OH of the nicotinamide ribose at a distance of 2.73 Å (Fig. 6.4B). Removal of this interaction is likely the reason for the lack of electron density for the nicotinamide ring and nicotinamide ribose as this portion of $NADP^+$ is now more disordered.

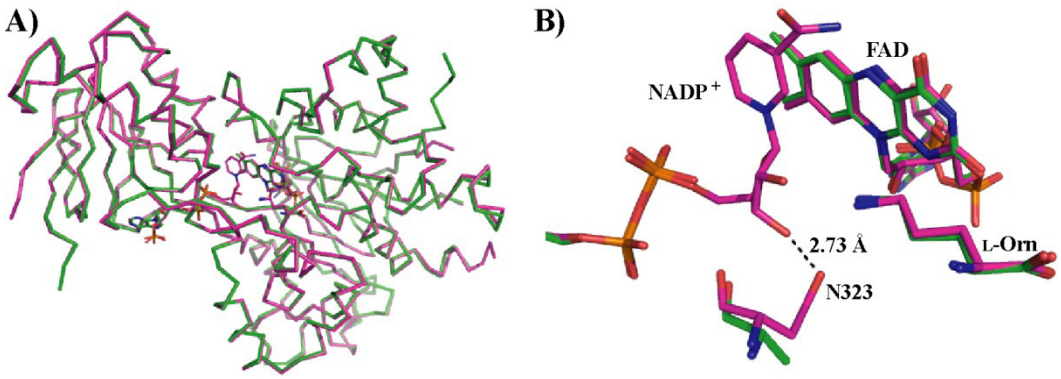

Figure 6.4 Comparison of the three-dimensional structures of SidA N323A with wild-type (PDB code 4B63). A) Ribbon diagrams of N323A (green) and wild-type (magenta). A RMSD of 0.257 was calculated between the two structures. B) Close-up view of the aligned active sites of N323A (green carbons) and wild-type (magenta carbons).

4. Discussion

The three-dimensional structure of SidA shows a very specific binding site for L-Orn. The geometry of this binding site is conserved among the other two Orn monooxygenases, PvdA and KtzI, whose structures have been elucidated [13, 14]. This allows for efficient binding of only one substrate, which is crucial in this family of enzymes as they are all involved in the biosynthesis of complex molecules. If another substrate such as Lys or D-Orn were to be non-specifically hydroxylated by these enzymes with a high catalytic efficiency, it would lead to the depletion of cellular resources, and potentially disrupt the function of the final product in their respective biosynthetic pathways. These enzymes have therefore evolved to become very specific in order to circumvent this problem.

The steady-state kinetic data for the studied mutants indicates they are all important in efficient L-Orn binding. While N293A and N323A decreased the catalytic efficiency for L-Orn by ~10−20 fold, S469A displayed a ~80−100 fold decrease (Tables 6.1 and 6.2). K107A on the other hand, showed no oxygen consumption activity or hydroxylation of L-Orn (data not shown). This suggests that K107 is perhaps the most important residue for L-Orn binding as deletion of

this one interaction completely abolishes activity. K107 is located on the surface of the L-Orn binding site and might coordinate entry of L-Orn into the active site (Fig. 6.5). This could explain the lack of activity in K107A where the protein is incapable of coordinating L-Orn binding. N293 is also located on the surface of the L-Orn binding site, but the modest decrease in activity suggests it has less of a role in guiding L-Orn into the active site than K107 (Fig. 6.5). These results are not dissimilar to the effect of mutation on R214 in *p*-hydroxybenzoate hydroxylase. Here, R214 interacts with the carboxylate group of *p*-hydroxybenzoate and mutation to Lys, Gln, or Ala all significantly increased the K_D value for *p*-hydroxybenzoate [15]. The Lys mutation also decreased the stability of the C4a-hydroperoxyflavin, leading to an increase in uncoupling. Similarly, N293A, N323A, and S469A all showed a decrease in coupling. This was not due however to the stability of the C4a-hydroperoxyflavin being affected, but likely due to increase in disorder of L-Orn in the active site causing hydrogen peroxide elimination rather than hydroxylation.

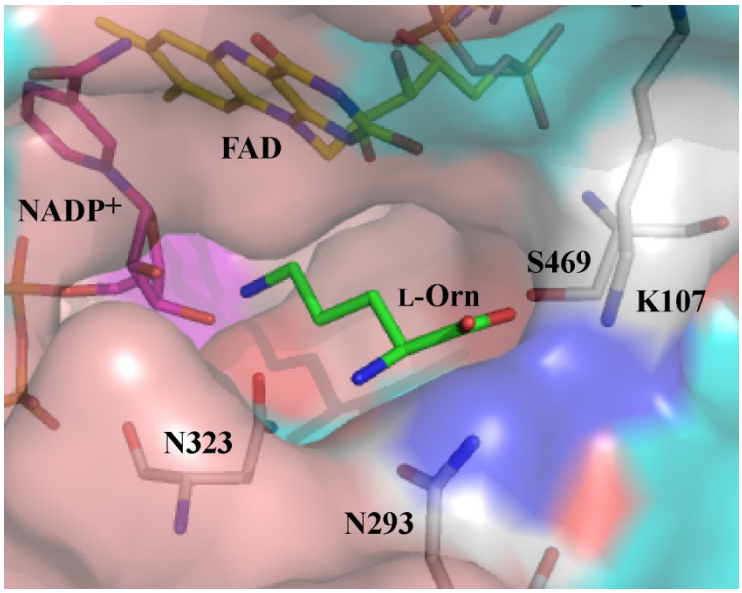

Figure 6.5 Accessibility of the L-Orn binding site in SidA (PDB code 4B63). The open cavity indicates that L-Orn binding can occur without any conformational changes. K107 and N293 are located on the surface and might coordinate L-Orn entry into the active site.

Wild-type is specific for L-Orn over D-Orn by ~100-fold when comparing k_{cat}/K_m values for hydroxylation (Tables 6.2 and 6.4). Both N293A and S469A are less stereoselective where they are ~11-fold and ~26 fold selective for L-Orn, respectively (Table 6.4). This is not the result of increased efficiency towards D-Orn induced through mutation, but rather the result of the mutants having less of a decrease in catalytic efficiency towards D-Orn relative to L-Orn. Also, it is worth noting that the coupling numbers for N293A and S469A do not change significantly over wild-type. This data indicates that the removal of one interaction around the α-carbon of Orn slightly loosens the stereoselectivity of SidA for Orn, but does not produce a more efficient D-Orn monooxygenase. Possibly, the contribution of all four interactions provides for the high stereoselectivity, and multiple simultaneous mutations would need to be performed to produce an efficient D-Orn monooxygenase.

Flavin reduction studies indicate that the rates are similar to wild-type for K107A, N293A, and S469A and the largest change among these mutants is a ~4-fold decrease with

K107A (Table 6.5). N323A however displayed a ~20-fold increase in the rate of reduction compared to wild-type indicating the replacement of this Asn to an Ala has a significant effect on the reductive half-reaction. This ~20-fold increase in reduction with N323A is not reflected in the steady-state k_{cat} value indicating that unlike wild-type, the rate-limiting step in N323A lies in the oxidative half-reaction since flavin reduction is significantly faster than the calculated k_{cat} value [12]. None of the mutations affect the formation or stability of the C4a-hydroperoxyflavin intermediate (Table 6.5) indicating that the observed decreases in coupling with the tested mutations are not a result of a more instable C4a-hydroperoxyflavin intermediate, but due to suboptimal binding of L-Orn in the active site causing elimination of hydrogen peroxide rather than hydroxylation. In wild-type, the presence of L-Lys during flavin oxidation causes rapid hydrogen peroxide elimination through disruption of the interaction between the 2'-OH of the nicotinamide ribose and the distal oxygen of the C4a-hydroperoxyflavin by protruding too far into the active site [7]. A similar mechanism here can be rationalized where the increased dynamics of L-Orn in the mutants cause disruption between $NADP^+$ and the C4a-hydroperoxyflavin. A recent computational study of SidA also shows that these four residues (K107, N293, N323, and S469) do not contribute significantly to the *N*-hydroxylation reaction providing further evidence these mutations do not affect the oxidative half-reaction in SidA [16]. This data also confirms the lack of observed activity in the steady-state for K107A is due to a stable C4a-hydroperoxyflavin and L-Orn does not bind properly to stimulate turnover.

The unexpected result of an increase in the rate of reduction for N323A prompted further studies. The crystal structure of wild-type indicates that N323 is providing an interaction with the 3'-hydroxyl of the nicotinamide ribose of NADP(H) (Fig. 6.4). Table 6.6 indicates this is not an important interaction for dinucleotide binding as the K_D value for NADH is ~3-fold higher when

compared to wild-type. This is a nominal effect when taking into account that a previously studied R279A mutation in SidA produced a ~250-fold higher K_D value for NADPH [17]. This suggests that while N323 appears to be providing an interaction to the 3'-OH group of the nicotinamide ribose of NADP(H), it is not an important interaction in coenzyme binding.

The primary KIE for flavin reduction was calculated using NADPD in order to determine if the ~20-fold higher rate of reduction in N323A is the result of an altered hydride transfer step. In SidA, and other Class B flavin monooxygenases, hydride transfer is typically the rate-limiting step with KIE values of ~6 observed with liver microsomal FMO, PAMO, and SidA wild-type [12, 18, 19]. In our experiments with N323A, the KIE was also determined for wild-type in order for an accurate comparison between enzymes with the same prepared NADPH/D samples. The results in Table 6.7 indicate a higher KIE in N323A than wild-type suggesting hydride transfer is more rate-limiting.

The structure of wild-type (PDB code 4B63) shows the carbonyl of the side chain of N323 is 2.73 Å from the 3'-hydroxyl of the nicotinamide ribose (Fig 6.7) [7]. This indicates the role for N323 is two-fold where it provides stabilizing interactions for both $NADP^+$ as well as L-Orn. It was noticed when the crystal structure of FMO was solved that the conformation adopted by $NADP^+$ suggests there would need to be a domain rotation where NADP(H) could adopt two modes to allow it to participate in both flavin reduction and oxidation [20]. This would in effect involve a "sliding" mechanism where the nicotinamide ring swings back and forth as depicted in Fig. 6.7. In the case of N323A, the "sliding" rate of NADPH might be higher as suggested by the increased disorder of the nicotinamide ring and the nicotinamide ribose in the crystal structure of N323A (Fig. 6.4B). The nicotinamide ring therefore likely "slides" at a higher rate leading to faster interaction between the C4 of the nicotinamide ring and the N5 of the flavin. In the FMN

dependent enzyme morphinone reductase, N189A was shown to enhance the rate of hydride transfer where there were less conformational restrictions on NADH which gave rise to multiple reactive configurations [21]. This is similar to SidA, where N323A allows NADPH more conformational freedom which in turn increases the observed rate of flavin reduction. The increase in the rate of flavin reduction in N323A is also similar to the previously studied S257A mutation in SidA. Here, deletion of the S257 interaction with the pyrophosphate group of NADPH increased the rate of "sliding" of the nicotinamide ring in flavin reduction leading to a ~5-fold increase in the rate of reduction [22].

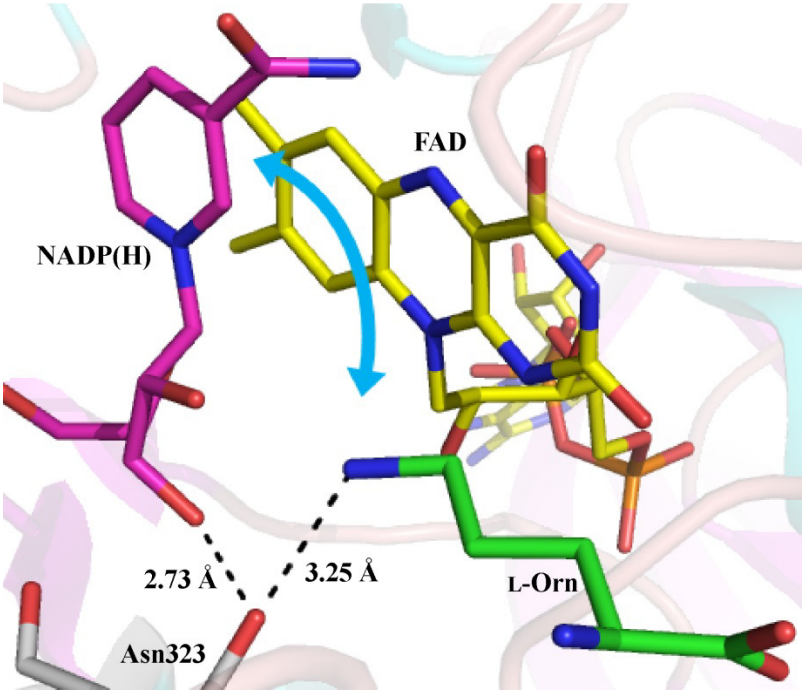

Figure 6.6 Movement of $NADP^+$ during the flavin redox reaction in SidA. The three-dimensional structure of SidA (PDB code 4B63) shows $NADP^+$ in a conformation that is favorable for C4a-hydroperoxyflavin formation. A "sliding" mechanism has been proposed where NADP(H) moves back and forth to reduce the flavin then subsequently stabilize the intermediate.

Currently, to our knowledge, there are no reports of a mutation in an enzyme increasing both the rate of reduction and the observed KIE; therefore we can only propose a number of hypotheses to these observations. The first possibility could be the geometry between the C4 of the nicotinamide ring of NADPH and the N5 of the flavin is different than wild-type, resulting in a higher KIE and a more rate-limiting hydride transfer step. Primary KIE values increase as the transition state forces become more symmetric [23]. Therefore, in order for there to be a higher KIE in N323A, the transitional state geometry between the C4 of the nicotinamide ring and the N5 of the flavin must be more symmetrical than wild-type. This is hard to envision where the nicotinamide ring is more disordered and the transition state forces are more symmetrical. Also, this event in N323A would produce a lower observed k_{red} value as the energy barrier to hydride transfer would be higher. A second possibility could be that the mutation is affecting hydrogen tunneling leading to a higher observed KIE. This has been observed in soybean lipoxygenase-1 and thermophilic alchohol dehydrogenase where mutations make the rate of hydride transfer via hydrogen tunneling less efficient leading to an increase in the observed KIEs [24, 25]. These mutations had a negative impact on hydride transfer leading to lower k_{cat} values which are opposite from our results. A third possibility could be that in wild-type, a conformational change is partially rate-limiting and masking the intrinsic KIE value, but in N323A this conformational change is less rate-limiting leading to a higher observed KIE (Scheme 6.2). This is a more reasonable explanation as the increase in disorder and mobility of the nicotinamide ring in N323A causes the "sliding" of NADPH to become less rate-limiting. This phenomenon has been described as "kinetic complexity" where an isotopically insensitive kinetic step is rate-limiting or partially rate-limiting and masks the intrinsic KIE value [26-28]. In a study of alcohol dehydrogenase from horse liver, mutants were made to crowd the active site and increase the rate

of product release which was partially rate-limiting to turnover [29]. The resulting mutants increased the rate of product release and "unmasked" the hydrogen tunneling in this enzyme. This proposal where NADPH "sliding" is less rate-limiting is consistent with our observed higher k_{red} and KIE values in N323A. Therefore, it appears in wild-type, that movement of NADP(H) prior to hydride transfer is at least partially rate-limiting in the reductive half-reaction of SidA. It is important to note that in our KIE experiments there are a lot of variable factors (differences in protein samples, convoluted reduction phases, impurities in synthesized NADPH/D) which results in high error. The differences in the observed KIE values here might not be significant especially when taking into account previously reported KIE values of ~5.5 for wild-type SidA [12]. If this is the case and the KIE values are unchanged, then the above analysis of a nonchemical step becoming less rate-limiting and enhancing the rate of reduction still applies. Further experiments are needed though in order to prove this hypothesis.

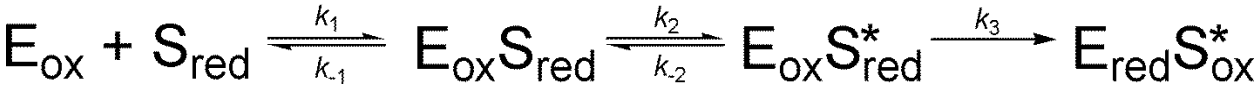

Scheme 6.2 Proposed mechanism of flavin reduction in SidA. First, SidA (E_{ox}) reversibly binds NADPH (S_{red}). Next, a conformational change occurs where NADPH "slides" to a conformation where hydride transfer can occur. Then, NADPH transfers a hydride equivalent irreversibly to the flavin of SidA. In wild-type, the equilibrium in the "sliding" step (k_2/k_{-2}) might have a lower ration than N323A where the ratio between k_2 and k_{-2} might be higher leading to a faster "slide." This suggests NADPH "sliding" is coupled to hydride transfer as indicated by the higher observed reduction rate in N323A.

Despite these drastic changes to reduction, removal of this N323 interaction does not appear to affect the oxidative half-reaction. In wild-type, the 2'-hydroxyl of the nicotinamide ribose of $NADP^+$ is critical for coupled catalysis. In addition to providing a proton for formation of the C4a-hydroperoxyflavin, it likely also provides a stabilizing interaction to the intermediate

[3]. The added mobility of NADP(H) in N323A does not appear to perturb this interaction as both formation and decay of the C4a-hydroperoxyflavin are unaffected. Previous computational studies where reduced FAD and $NADP^+$ in SidA were fully optimized produced a complex where $NADP^+$ is rotated up and the amide group of $NADP^+$ is H-bonded to the pyrimidine ring oxygen of the flavin allowing the nicotinamide ribose to shield the C4a-hydroperoxyflavin [30]. This orientation shows a conformation adopted by $NADP^+$ where the interaction between N323 and the 3'-hydroxyl of the nicotinamide ribose might not be essential for positioning of $NADP^+$ to properly stabilize the C4a-hydroperoxyflavin.

The effect on C4a-hydroperoxyflavin stability in N323A contrasts with S257A where the increase in movement of the nicotinamide ring decreased the stability of the C4a-hydroperoxyflavin to the point where it was only observed transiently [22]. S257 was hypothesized to be a "pivot point" for NADP(H) in SidA, and here, it appears that the positioning of the stabilizing interactions provided by S257 and N323 broadly affect intermediate stability. The differences between the stabilities of the C4a-hydroperoxyflavins in S257A and N323A might be due to the differences in the degrees of freedom introduced by the mutations. Fig. 6.7 shows that S257 interacts with the pyrophosphate group of NADP(H) whereas N323 interacts with the 3'-hydroxyl of the nicotinamide ribose. Deletion of the S257 interaction would allow for a larger portion of NADP(H) to have increased freedom relative to N323. This might explain the differences in the stabilities of the C4a-hydroperoxyflavin where $NADP^+$ is less dynamic than $NADP^+$ in S257A where $NADP^+$ can still adopt the necessary conformation to protect the C4a-hydroperoxyflavin from rapid decay.

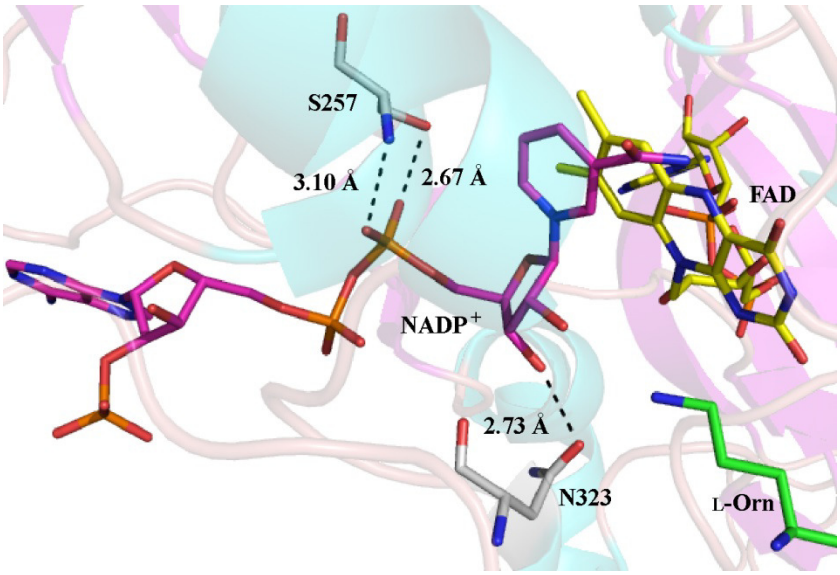

Figure 6.7 Interactions provided by S257 and N323 to $NADP^+$. S257A and N323A both increase the rate of reduction relative to wild-type which is potentially due to an increase in the rate of NADPH "sliding". However, their effects are opposite on flavin oxidation where N323A has no effect and S257A completely disrupts stabilization of the C4a-hydroperoxyflavin which is potentially due to the differences in positioning of the interactions. S257 interacts with the pyrophosphate group of $NADP^+$ and disruption of this interaction might lead to a larger range of freedom for $NADP^+$ in S257A compared to N323A.

In summary, the high specificity of SidA towards L-Orn is accomplished through four interactions by K107, N293, N323, and S469. These residues create a specific binding site for L-Orn and help, along with the inherent high stability of the C4a-hydroperoxyflavin, to ensure efficient coupling occurs to minimize oxygen reactive species. Alongside the role of L-Orn binding, N323 also provides a stabilizing interaction with NADP(H) which controls "sliding" in the active site. This data identifies these four residues as important for catalysis and proper positioning of L-Orn in the active site of SidA. These results will be important for future works of engineering different substrate specificities into SidA as well as developing novel inhibitors of SidA which target the L-Orn binding site.

5. Acknowledgements

This work was supported in part by a grant from the National Science Foundation MCB-1021384.

6. References

[1] S.W. Chocklett, P. Sobrado, Biochemistry 49 (2010) 6777-6783.
[2] J.A. Mayfield, R.E. Frederick, B.R. Streit, T.A. Wencewicz, D.P. Ballou, J.L. DuBois, J Biol Chem 285 (2010) 30375-30388.
[3] R. Robinson, S. Badieyan, P. Sobrado, Biochemistry 52 (2013) 9089-9091.
[4] A. Alfieri, E. Malito, R. Orru, M.W. Fraaije, A. Mattevi, Proc Natl Acad Sci U S A 105 (2008) 6572-6577.
[5] E. Malito, A. Alfieri, M.W. Fraaije, A. Mattevi, Proc Natl Acad Sci U S A 101 (2004) 13157-13162.
[6] R.E. Frederick, J.A. Mayfield, J.L. DuBois, J Am Chem Soc 133 (2011) 12338-12341.
[7] S. Franceschini, M. Fedkenheuer, N.J. Vogelaar, H.H. Robinson, P. Sobrado, A. Mattevi, Biochemistry 51 (2012) 7043-7045.
[8] T. Csaky, Acta Chem Scand (1948) 450-454.
[9] R. Robinson, P. Sobrado, Biochemistry 50 (2011) 8489-8496.
[10] S.S. Jeong, J.E. Gready, Anal Biochem 221 (1994) 273-277.
[11] R. Dhatwalia, H. Singh, M. Oppenheimer, D.B. Karr, J.C. Nix, P. Sobrado, J.J. Tanner, J Biol Chem 287 (2012) 9041-9051.
[12] E. Romero, M. Fedkenheuer, S.W. Chocklett, J. Qi, M. Oppenheimer, P. Sobrado, Biochim Biophys Acta (2012).
[13] J. Olucha, K.M. Meneely, A.S. Chilton, A.L. Lamb, J Biol Chem 286 (2011) 31789-31798.
[14] J.W. Setser, J.R. Heemstra, Jr., C.T. Walsh, C.L. Drennan, Biochemistry 53 (2014) 6063-6077.
[15] W. van Berkel, A. Westphal, K. Eschrich, M. Eppink, A. de Kok, Eur J Biochem 210 (1992) 411-419.
[16] S. Badieyan, R. Bach, P. Sobrado, J Org Chem (2015).
[17] R. Robinson, S. Franceschini, M. Fedkenheuer, P.J. Rodriguez, J. Ellerbrock, E. Romero, M.P. Echandi, J.S. Martin Del Campo, P. Sobrado, Biochim Biophys Acta 1844 (2014) 778-784.
[18] N.B. Beaty, D.P. Ballou, J Biol Chem 256 (1981) 4611-4618.
[19] D.E. Torres Pazmino, B.J. Baas, D.B. Janssen, M.W. Fraaije, Biochemistry 47 (2008) 4082-4093.
[20] A. Alfieri, E. Malito, R. Orru, M.W. Fraaije, A. Mattevi, Proc Natl Acad Sci USA 105 (2008) 6572-6577.
[21] C.R. Pudney, T. McGrory, P. Lafite, J. Pang, S. Hay, D. Leys, M.J. Sutcliffe, N.S. Scrutton, Chembiochem 10 (2009) 1379-1384.
[22] C. Shirey, S. Badieyan, P. Sobrado, J Biol Chem 288 (2013) 32440-32448.

[23] R.L. Fagan, B.A. Palfey, Biochemistry 48 (2009) 7169-7178.
[24] M.P. Meyer, D.R. Tomchick, J.P. Klinman, Proc Natl Acad Sci U S A 105 (2008) 1146-1151.
[25] Z.D. Nagel, C.W. Meadows, M. Dong, B.J. Bahnson, J.P. Klinman, Biochemistry 51 (2012) 4147-4156.
[26] D.B. Northrop, Biochemistry 20 (1981) 4056-4061.
[27] K. Francis, A. Kohen, Perspectives in Science 1 (2014) 110-120.
[28] D. Roston, Z. Islam, A. Kohen, Molecules 18 (2013) 5543-5567.
[29] B.J. Bahnson, D.H. Park, K. Kim, B.V. Plapp, J.P. Klinman, Biochemistry 32 (1993) 5503-5507.
[30] R.D. Bach, A. Mattevi, J Org Chem 78 (2013) 8585-8593.

CHAPTER 7

Met101, Gln102, and Arg144 are critical for efficient flavin oxidation in SidA

Author Contributions:
Reeder Robinson performed all the research except the experiments mentioned below and wrote the chapter.

Catherine Klancher performed the steady-state assays with M101A and R144A.

Jack Tanner solved the crystal structure of M101A.

Pablo Sobrado oversaw and directed the research.

Abstract

Siderophore A (SidA) from *Aspergillus fumigatus* is a flavin-containing monooxygenase that efficiently hydroxylates L-Orn through stabilization of a long-lived C4a-hydroperoxyflavin intermediate. This ensures for minimal release of oxygen reactive species during the catalytic cycle. In this study, we examined the effect of mutation on M101, Q102, and R144 to Ala in the catalytic cycle of SidA. The data indicates that all three of these mutants are important in the oxidative half-reaction of SidA. In M101A, flavin oxidation in the presence of L-Orn is slowed ~15-fold compared to wild-type. This effect is due to an altered conformation of the isoalloxazine ring of the flavin where it is flipped outwards from the reactive center and is unable to react with L-Orn. In Q102A, a high oxidase rate was observed which is consistent with the ~10-fold less stable C4a-hydroperoxyflavin. The side chain carbonyl of Q102 provides an H-bond network to the distal oxygen of the C4a-hydroperoxyflavin and removal of this interaction appears to disrupt this network and decrease intermediate stability. In R144A, a similar decrease in stability of the C4a-hydroperoxyflavin to Q102A was observed, but in the presence of L-Orn, flavin oxidation is slowed ~8-fold compared to in the absence of L-Orn. This is opposite to wild-

type where flavin oxidation is enhanced ~80-fold with L-Orn present. Also, an increase in the solvent kinetic isotope effect for flavin oxidation with L-Orn present of ~1.6 in wild-type to ~2.9 in R144A indicates that R144 plays a role in proton shuttling in flavin dehydration. The data presented here highlights unique roles of three residues in the oxidative half-reaction of SidA.

1. Introduction

The key feature of Class B flavin monooxygenases are their ability to stabilize long-lived C4a-(hydro)peroxyflavin intermediates [1-6]. This class includes the flavin-containing monooxygenases, Baeyer-Villiger monooxygenases, and the *N*-hydroxylating monooxygenases. Along with their distinguishing characteristic, they utilize flavin adenine dinucleotide (FAD) as a prosthetic group, bind and react with NADPH, and keep $NADP^+$ bound throughout catalysis [7]. In order for proper stabilization of the C4a-(hydro)peroxyflavin to occur in these systems, $NADP^+$ must be bound in a conformation that shields the C4a-(hydro)peroxyflavin from bulk solvent [1, 8, 9]. Fig. 7.1 shows the conformation of $NADP^+$ adopted in SidA to stabilize its C4a-hydroperoxyflavin. Here, $NADP^+$ is in a position that is not optimal for hydride transfer, but the 2'-OH of the nicotinamide ribose is positioned where it provides a proton to the C4a-peroxyflavin and a subsequent stabilizing interaction to the distal oxygen of the intermediate [10]. This multifunctional use of NADP(H) in not only providing a hydride equivalent, but also in flavin oxidation is unique for Class B monooxygenases.

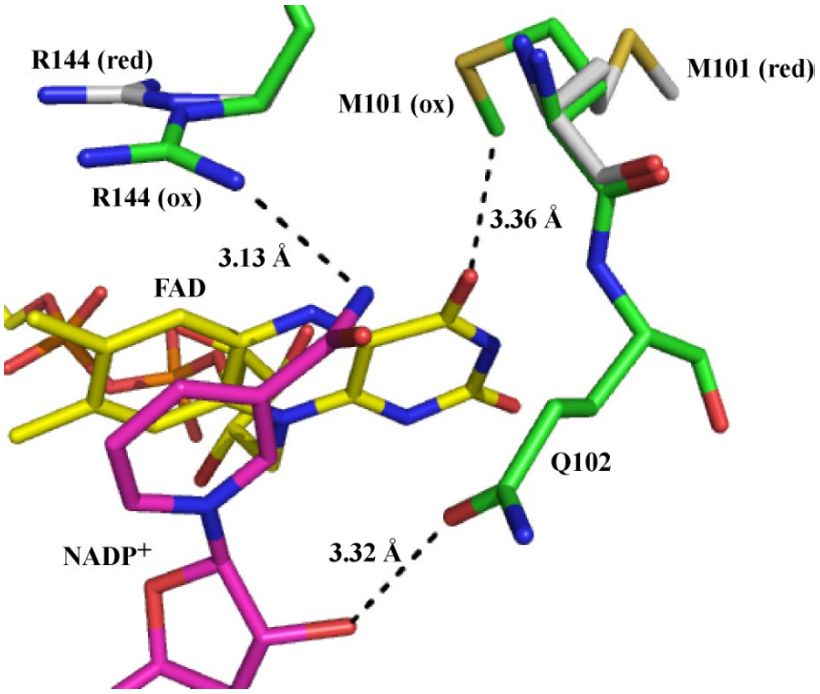

Figure 7.1 View of the active site of SidA in the oxidized (PDB code 4B63, green carbons) and reduced (PDB code 4B65, gray carbons) forms with the relative positions of M101, Q102, and R144. For the sake of clarity only the FAD (yellow carbons), $NADP^+$ (magenta carbons), and Q102 are shown from the oxidized structure as their conformations do not drastically change.

Until recently, flavin movement in catalysis of monooxygenases was only observed in the Class A aromatic hydroxylases [7, 11-13]. In the best studied enzyme in this class, *p*-hydroxybenzoate hydroxylase, the isoalloxazine ring swings like a pendulum from an "in" to an "out" conformation where it can react with NADPH. It then reacts with molecular oxygen, forming a C4a-hydroperoxyflavin, where it swings back to hydroxylate the bound substrate. In Class B monooxygenases, an opposite but analogous movement of NADP(H) in a "sliding" mechanism has been proposed to be involved in catalysis [1, 14-16]. This involves movement of NADP(H) between a conformation to transfer a hydride equivalent and a conformation that promotes stabilization of the C4a-(hydro)peroxyflavin. Recently, movement of the isoalloxazine ring of the flavin was observed in different crystal states of the Class B monooxygenase KtzI from *Kutzneria* sp. 744 [17]. Here, the isoalloxazine ring was observed in an "in" conformation

similar to the one observed in SidA (Fig. 7.1), and an "out" conformation that could not react with NADPH. This "out" conformation by FAD was proposed to be involved in $NADP^+$ release by acting as a "battering ram" to sterically clash with $NADP^+$. This is the first report of flavin movement in Class B monooxygenases and represents a previously unknown role for the flavin in catalysis.

Here, we examine the effect of mutation on three residues proximal to the isoalloxazine ring of the flavin in SidA; M101, Q102, and R144 (Fig. 7.1). Between the crystal structures of the oxidized and reduced forms of SidA, M101 and R144 were observed in different conformations. R144 is flipped inward towards the flavin in the oxidized form, and flipped outwards away from the flavin in the reduced form. M101 appears to be providing a van der Waals interaction with the O4 of the flavin and moves away where it is not interacting with the O4 in the reduced form. Q102 was not observed in different conformations between the oxidized and reduced structures (data not shown), but it is positioned in front of the flavin adjacent to the pocket where the C4a-(hydro)peroxyflavin has been proposed to form [9]. Here, we use a combination of steady-state, rapid reaction, and crystallographic techniques to show how these three residues participate in catalysis. The findings presented here define these residues as essential in flavin movement, stabilization of the C4a-hydroperoxyflavin, and dehydration of the flavin in SidA.

2. Materials and Methods

2.1 Materials. Buffers and media were obtained from Fisher Scientific (Pittsburgh, PA). BL21(DE3)-$T1^R$ chemically competent cells were obtained from Sigma-Aldrich (St. Louis, MO). NADPH was obtained from EMD4 Biosciences (Billerica, MA). DNA primers were synthesized

by Integrated DNA Technologies (Coralville, IA). Plasmid preparation and gel purification kits were obtained from Qiagen (Valencia, CA). *Escherichia coli* TOP-10 chemically competent cells were obtained from Invitrogen (Carlsbad, CA). Chromatography columns were obtained from GE Healthcare.

2.2 Site–directed mutagenesis. Mutagenesis of residues was performed using the QuikChange (Agilent Technologies) method following the manufacturer's instructions. The wild-type SidA gene, subcloned into the pET15b plasmid, was used as the template [9]. For M101A, the forward primer (5'-CGGTATGCTGGTCCCGGGCTCGAAGGCGCAGATCAGC TTCATCAAGGATCTC-3') and reverse primer (5'-GAGATCCTTGATGAAGCTGATCTGCG CCTTCGAGCCCGGGACCAGCATACCG -3') were used. For Q102A, the forward primer (5'-CCGGGCTCGAAGATGGCTATCAGCTTCATCAAG-3') and reverse primer (5'-CTTGATGAAGCTGATAGCCATCTTCGAGCCCGG -3') were used. For R144A, the forward primer (5'-CTGTCTACCTTCCTGCCCGCCGCGCTCGAGTTC GAGGACTACATGCGC-3') and reverse primer (5'-GCGCATGTAGTCCTCGAACTCGAGC GCGGCGGGCAGGAAGGTAGACAG -3') were used. The codons for the mutated residues are underlined. The mutations were confirmed by DNA sequencing at Virginia Bioinformatics Core Sequencing Facility.

2.3 Protein expression and purification. All mutant proteins were expressed in *E. coli* BL21(DE3)-T1^{R} competent cells and purified as previously described [9]. In general, ~25 mg of protein were obtained per liter of media. The purified proteins were stored in 100 mM sodium phosphate, 50 mM NaCl, pH 7.5, at -80 °C at a concentration of ~200 μM (based on flavin

content) in 30 µL aliquots. The 6x-His tag was removed for the SidA M101A sample used for crystallization by incubating the sample at 4 ºC overnight as previously described [9].

2.4 Determination of flavin extinction coefficient and incorporation. The spectra of purified M101A, Q102A, and R144A were determined in 100 mM sodium phosphate pH 7.5. The bound flavin molecules were removed by incubating each enzyme in 9% (w/v) SDS at 25 °C for 20 minutes, then the free flavin spectra were recorded. Extinction coefficients of 10,600 $M^{-1}cm^{-1}$ at 458 nm, 11,600 $M^{-1}cm^{-1}$ at 453 nm, and 11,000 $M^{-1}cm^{-1}$ at 450 nm were calculated for M101A, Q102A, and R144A, respectively, using an extinction coefficient at 450 nm for free FAD of 11,300 $M^{-1}cm^{-1}$ [18]. Flavin incorporation was determined by measuring protein concentration via the Bradford assay (BioRad) and comparing it to the protein concentration based on the flavin spectrum. Flavin incorporation was generally close to ~70% for M101A, ~40% for R144A, and ~40% for Q102A.

2.5 Steady-state kinetics. The rate of oxygen consumption was measured using a Hansatech Oxygraph system (Norfolk, England). Reactions consisted of a 1 mL volume of 100 mM sodium phosphate, pH 7.5, at 25 °C. NADPH was kept constant at a concentration of 1 mM for all tested mutants while L-Orn was varied between 0.1 − 15 mM. Reactions were initiated by addition of 2 µM SidA for wild-type and Q102A, and 5 µM SidA for M101A and R144A. Reactions were monitored for 5 minutes with constant stirring.

Hydroxylated Orn was monitored using a variation of the Csaky iodine oxidation assay [19, 20]. The standard assay buffer contained 104 µL of 100 mM sodium phosphate (pH 7.5) with varying concentrations of L-Orn and NADPH held constant at 1 mM. Reactions were

initiated by addition of 2 μM SidA for wild-type and Q102A, and 5 μM SidA for M101A and R144A. Reactions were incubated for 10 min at 25 °C with constant shaking at 750 rpm.

2.6 Pre-steady-state kinetics. All rapid reaction experiments were carried out at 25 °C using an SX-20 stopped-flow spectrophotometer (Applied Photophysics, Leatherhead, UK) in an anaerobic glove box (Coy, Grass Lake, MI). Preparation of anaerobic buffer was carried out through five cycles of vacuum and flushing with O_2-free argon after 1 hr of continuous vacuum. This was repeated five times for a total of five hrs. The enzyme was made anaerobic through constant cycles of vacuum and flushing with O_2-free argon for 1 hr. Substrates were made anaerobic by dissolving in anaerobic buffer inside the glove box. The stopped-flow was made anaerobic by flushing with 1 mL of anaerobic 100 mM sodium acetate, pH 5.0, containing 100 mM D-glucose and 100 μg/mL glucose oxidase Type-X. For all tested mutants, the rate of flavin reduction of SidA was measured in single mixing mode where anaerobic SidA (15 μM after mixing) was mixed with an equal volume of NADPH (15 − 1000 μM after mixing).

The rate of flavin oxidation was measured in double mixing mode for all of the tested mutations. Anaerobic SidA (60 μM before mixing) was first mixed with an equal volume of NADPH (60 μM before mixing). This mixture was allowed to incubate in an ageing loop for 60 seconds until the bound flavin was fully reduced. The reduced SidA−$NADP^+$ complex was then allowed to react with oxygen (300 μM after mixing). Oxidation of the mutant enzymes were all tested in both the presence and absence of 10 mM L-Orn. Spectra were taken on a logarithmic time scale until full reduction or oxidation, respectively, had occurred.

2.7 pH studies of flavin oxidation. The pH profile of flavin oxidation was measured in double mixing mode. Anaerobic SidA (60 μM before mixing) was first mixed with an equal volume of NADPH (60 μM before mixing) in 20 mM Tris-Cl, 200 mM NaCl, pL 8.0. This mixture was allowed to incubate in an ageing loop for 60 seconds until the bound flavin was fully reduced. The reduced SidA–$NADP^+$ complex was then allowed to react with air saturated buffer (130 μM oxygen after mixing since at 1 atm and 25 °C [O_2] = 260 μM). This air saturated solution contained 200 mM of buffer which rapidly jumped the pL to the desired value in the flow cell. Between pL values 6 – 8, sodium phosphate was used, between pL values 8.5 – 9.0, Tris-SO_4 was used, and between pL values 9.5 – 10.5, sodium carbonate/bicarbonate was used.

2.8 Solvent kinetic isotope effect studies of flavin oxidation. Solvent kinetic isotope effect (SKIE) experiments for wild-type, M101A, and R144A were performed in both the presence and absence of 15 mM L-Orn. For the reactions in D_2O, SidA was concentrated to ~400 μM (based on flavin content) and diluted to 60 μM in a 100% D_2O buffer of 20 mM Tris-Cl, 200 mM NaCl, pD 8.0. This gave a concentration of ~85% D_2O, and after two mixes in the stopped-flow with 100% D_2O buffer, a final D_2O concentration of ~96% was achieved. SKIEs in the absence and presence of L-Orn were determined at pL values 7.0 and 9.0, respectively. The proper pD of all D_2O buffers were calculated by adding 0.4 to the value on the pH meter, which is the variation from the change in the equilibrium on a hydrogen selective glass electrode [21]. All solutions were checked for their proper pL values with a Fisher Scientific Accumet AB15+ Basic pH meter. Spectra were taken on a logarithmic time scale until oxidation was complete.

2.9 Crystallization of SidA M101A. SidA M101A crystals were grown in similar conditions to wild-type [9]. In brief, crystals were obtained using the hanging drop vapor diffusion method and larger crystals for data collection were obtained from microseeding from smaller crystals. The reservoir solution contained 0.1 M HEPES pH 6.6, 2 M ammonium sulfate, and 1.5% (v/v) dioxane. The reservoir solution was mixed in a 1:1 ratio with 8 mg/mL SidA M101A which was pre-incubated with 1 mM $NADP^+$. The crystals were allowed to grow for one month and then flash frozen in the reservoir solution with 30% (v/v) glycerol as the cryoprotectant.

2.10 Structure determination. The structure of SidA M101A was determined to 1.9 Å resolution by the Tanner group by molecular replacement with the structure for wild-type SidA (PDB code 4B63).

2.11 Data analysis. All data were fit using KaleidaGraph (Synergy Software, Reading, PA). The rates of reduction were determined by fitting the decrease in absorbance at 452 nm to a double exponential decay equation (eq. 1).

$$v = c + a_1 e^{-(k_1 \times t)} + a_2 e^{-(k_2 \times t)} \quad (1)$$

For flavin oxidation studies, the increase in absorbance at 372 nm, which corresponds with formation of the C4a-hydroperoxyflavin intermediate, was fit to eq. 2, which describes a single exponential rise. The subsequent increase in absorbance at 452 nm, which corresponds with flavin oxidation, was fit to eq. 3, which describes a double exponential rise. The first exponential rate of flavin oxidation calculated in eq. 3 is omitted in this study as it corresponds to rate of formation of the C4a-hydroperoxyflavin calculated with eq. 2 at 372 nm. The pH dependences of flavin oxidation at 452 nm were fit to eq. 4, which describes a curve with a

single pK_a with increasing activity as the pH increases and plateau regions at high and low pH. The upper limits for the pH profiles are denoted by C.

$$v = c + a(1 - e^{-(k \times t)}) \tag{2}$$

$$v = c + a_1(1 - e^{-(k_1 \times t)}) + a_2(1 - e^{-(k_2 \times t)}) \tag{3}$$

$$y = \frac{C}{1 + 10^{(\mathrm{p}K_{a1} - \mathrm{pH})} + 10^{(\mathrm{pH} - \mathrm{p}K_{a2})}} \tag{4}$$

3. Results

3.1 UV-visible flavin spectra of M101A, Q102A, and R144A. The flavin spectra and extinction coefficients for M101A, Q102A, and R144A were determined as Fig. 7.1 indicates that each residue is proximal to the flavin and mutation of any of these three residues could perturb the spectrum. The extinction coefficient of wild-type has been previously calculated to be 13,700 $M^{-1}cm^{-1}$ at its λ_{max} of 450 nm [4]. The flavin spectra of the mutants show slightly altered peaks at 458 nm and 453 nm for M101A and Q102A, respectively, while R144A is consistent with wild-type at 450 nm (Fig. 7.2). Also, the extinction coefficients at these λ_{max} values are slightly altered at 10,600 $M^{-1}cm^{-1}$, 11,600 $M^{-1}cm^{-1}$, and 11,000 $M^{-1}cm^{-1}$ for M101A, Q102A, and R144A, respectively. Mutation of residues proximal to the isoalloxazine ring affecting the flavin spectrum are common among flavin-containing enzymes. In brief, W47F in flavin-containing monooxygenase (FMO), T37A in old yellow enzyme 1 (OYE1), and Y129F in glycolate oxidase all are in proximity to their respective oxidized flavins and alter the spectra [22-24]. These mutations had much greater effects on their respective flavin spectra than the mutations studied here as only relatively slight changes were observed.

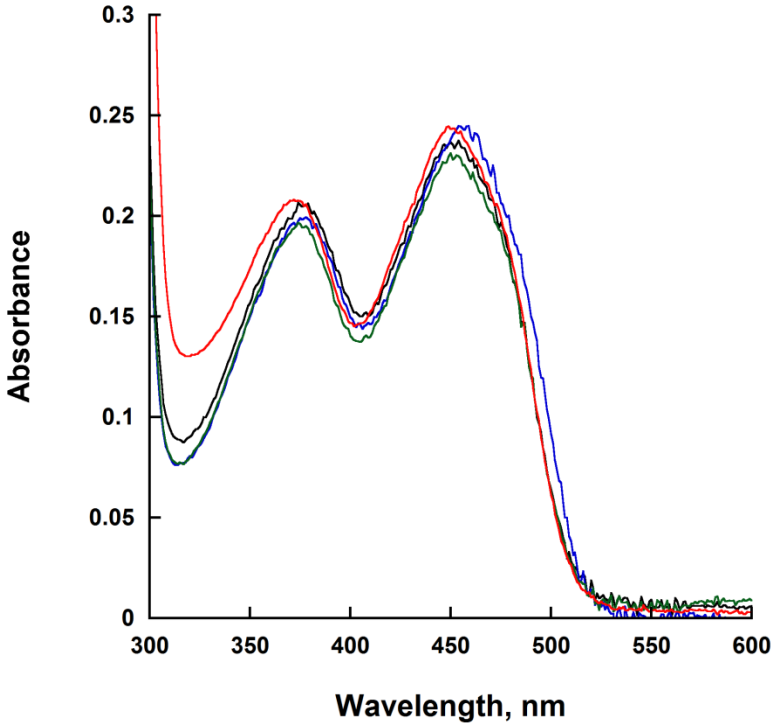

Figure 7.2 UV-visible spectra of the flavin bound to wild-type (black), M101A (blue), Q102A (green), and R144A (red).

3.2 Steady-state oxygen consumption. The steady-state kinetic parameters for oxygen consumption for M101A, Q102A, and R144A were determined using L-Orn as the variable substrate. M101A displayed very little activity towards oxygen consumption as the k_{cat} value was ~25-fold lower than wild-type (Table 7.1). The K_m value for L-Orn in M101A appears to be unaffected compared to wild-type indicating that mutation of M101 does not affect the binding of L-Orn, as predicted by the crystal structure (Fig. 7.1). The k_{cat} value for the rate of oxygen consumption in Q102A is comparable to wild-type, but a high rate of oxygen consumption (~0.5 s^{-1}) in the absence of L-Orn was observed suggesting significant oxidase activity (Fig. 7.3A). Similar to M101A, R144A displayed a very low rate of oxygen consumption at saturating concentrations of L-Orn (Fig. 7.3B). R144A displayed an unusual dependence on L-Orn for

oxygen consumption where the rate of oxygen consumption decreases as a function of L-Orn. This data indicates that all three mutations have relatively large effects on the activity of SidA. Q102A appears to simply increase the oxidase rate while M101A and R144A appear to almost completely abolish the activity of SidA. This, along with the unusual dependence of L-Orn on R144A oxygen consumption prompted further studies.

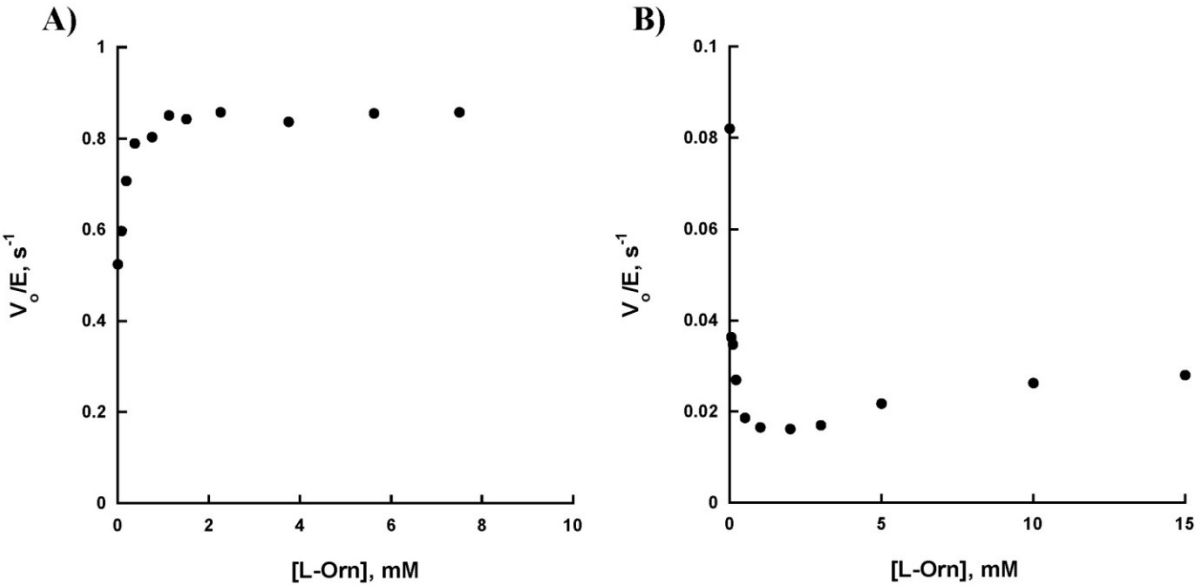

Figure 7.3 Steady-state oxygen consumption plots of A) Q102A and B) R144A. k_{cat} values for Q102A and R144A were estimated from the horizontal asymptote observed as saturating concentrations of L-Orn were approached. NADPH was kept constant at 1 mM in both assays.

Table 7.1 Steady-state kinetic parameters determined by oxygen consumption with L-Orn.

Parameter	Wild-type	M101A	Q102A	R144A
k_{cat}, s^{-1}	0.59 ± 0.01	0.023 ± 0.002	0.860 ± 0.004	0.028 ± 0.001
$K_{m\ (L\text{-}Orn)}$, mM	1.1 ± 0.3	0.7 ± 0.2	-	-
$k_{cat}/K_{m\ (L\text{-}Orn)}$, $M^{-1}s^{-1}$	500 ± 100	30 ± 10	-	-

Conditions: 100 mM sodium phosphate, pH 7.5, and 25 °C.

3.3 Steady-state L-Orn hydroxylation. The steady-state L-Orn hydroxylation parameters for M101A, Q102A, and R144A were calculated using L-Orn as the varied substrate under saturating concentrations of NADPH. The data indicates that M101A has very similar rates of L-Orn hydroxylation and oxygen consumption, thus the coupling percentage is ~100% and similar to wild-type (Table 7.2). As suggested by the high oxidase rate in the oxygen consumption assay with Q102A (~0.5 s^{-1}), the coupling percentage was lower at 37.7 ± 0.4% (Table 7.2). This data, along with the oxygen consumption data, indicates that Q102A could be affecting the stability of the C4a-hydroperoxyflavin. Despite the lowered rate of coupling in Q102A, the k_{cat}/K_m value for L-Orn is similar in Q102A to wild-type due to the slightly lower calculated K_m value (Table 7.2). The rate of L-Orn hydroxylation for R144A was barely detectable over background, but calculated at ~60-fold lower than wild-type (Table 7.2). From the estimated rate of oxygen consumption, the coupling percentage for R144A was calculated at 39 ± 3% (Table 7.2). This indicates that R144A affects the hydroxylation reaction and along with the oxygen consumption data, it appears that L-Orn inhibits the overall rate of R144A. Also in R144A, the K_m value for L-Orn is ~5-fold higher than wild-type, which along with the decreased k_{cat} value for L-Orn hydroxylation, indicates that R144A has a ~300-fold lower catalytic efficiency for L-Orn hydroxylation when compared to wild-type.

Table 7.2 Steady-state kinetic parameters determined by L-Orn hydroxylation.

Parameter	**Wild-type**	**M101A**	**Q102A**	**R144A**
k_{cat}, s^{-1}	0.62 ± 0.02	0.024 ± 0.001	0.324 ± 0.004	0.0108 ± 0.0008
$K_{m\ (L\text{-}Orn)}$, mM	1.0 ± 0.2	1.8 ± 0.3	0.64 ± 0.03	5.2 ± 0.9
$k_{cat}/K_{m\ (L\text{-}Orn)}$, $M^{-1}s^{-1}$	600 ± 100	14 ± 2	500 ± 30	2.1 ± 0.4
Coupling, %	105 ± 4	105 ± 9	37.7 ± 0.4	39 ± 3

Conditions: 100 mM sodium phosphate, pH 7.5, and 25 °C.

3.4 Pre-steady-state kinetics of flavin reduction and oxidation. The unusual characteristics observed for these three mutants in the steady-state required deconvolution of the mechanism by rapid reaction techniques. The reductive half-reaction was determined with M101A, Q102A, and R144A with varying concentrations of NADPH in order to determine if these mutations affected the affinity towards NADPH or the hydride transfer step. Fig. 7.4A indicates that all three mutants are reduced by NADPH in a double exponential manner similar to wild-type [5, 6]. M101A and Q102A are fully reduced by NADPH, but in R144A there appears to be a fraction of enzyme that does not react with NADPH suggesting a portion of the sample is not active. Q102A displayed the largest effect on the first exponential phase of reduction (k_{red1}) of a ~2-fold increase compared to wild-type whereas M101A and R144A displayed only slight changes (Table 7.3). For the second exponential phase of reduction (k_{red2}), M101A was unchanged while the rates for Q102A and R144A decreased ~2-fold and ~5-fold, respectively (Table 7.3). This ~5-fold decrease in k_{red2} for R144A might contribute to the observation of a population of R144A as inactive. Despite the slight variability, it appears that these mutants do not significantly affect the rate of reduction. Wild-type SidA has a very high affinity for NADPH and a precise K_D value is hard to calculate using a stopped-flow spectrophotometer [5, 6]. The data in Table 7.3 indicates that the three mutations likely do not significantly affect the affinity towards SidA with K_D values of ~1 − 2 μM observed for M101A and R144A. A K_D value of ~14 μM was observed for Q102A which is ~7-fold higher than wild-type. The structure of SidA in Fig. 7.1 suggests that Q102 forms a hydrogen bond with the 2'-OH of the nicotinamide ribose. This effect on K_D is nominal when compared to other NADPH-binding residues such as R279, which is a major residue in coenzyme binding [25]. In FMO, mutation of N78 to Lys and Asp, the homologous residue to Q102 in SidA, altered the K_D for NADPH by ~25-fold [26]. These mutations were

relatively more drastic as they introduced net charges at this position and possibly had repulsive effects on NADPH. Mutation of N78 to Ser however did not change the K_D for NADPH, and the crystal structure shows that this mutation does not interact with $NADP^+$. This data suggests that Q102 could play a slight role in binding of NADPH, but is not a major determinant.

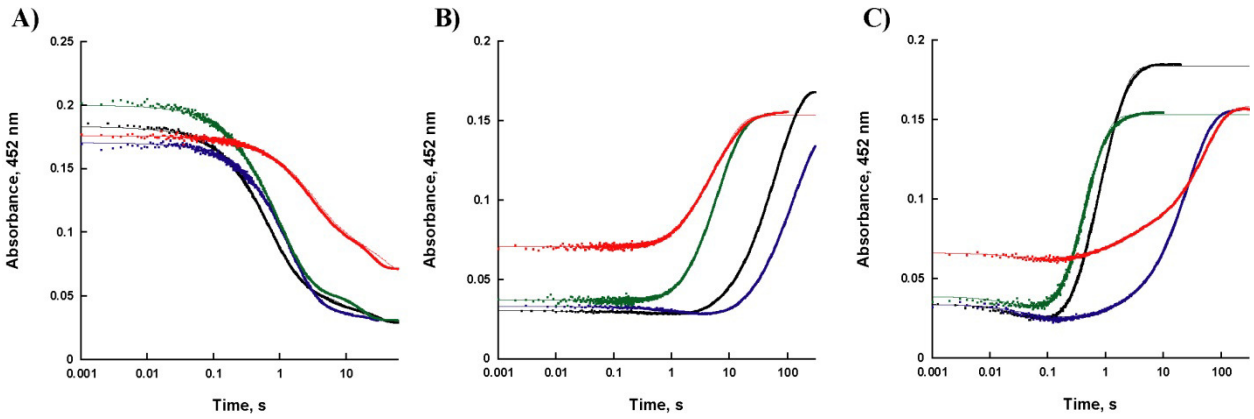

Figure 7.4 Rapid-reaction kinetics of flavin reduction and oxidation. A) Traces of the absorbances at 452 nm of flavin reduction upon mixing with 500 µM NADPH in the stopped-flow spectrophotometer. The traces were fit to eq. 1. B) Traces of the absorbances at 452 nm of flavin oxidation. C) Traces of the absorbances at 452 nm of flavin oxidation in the presence of 10 mM L-Orn. The traces in panels B and C were fit to eq. 2. The traces indicate reduction/oxidation for SidA wild-type (black), M101A (blue), Q102A (green), and R144A (red).

Table 7.3 Pre-steady-state kinetic parameters of flavin reduction with NADPH.

	Wild-type	**M101A**	**Q102A**	**R144A**
k_{red1}, s^{-1}	0.62 ± 0.01	0.87 ± 0.01	1.17 ± 0.03	0.401 ± 0.005
k_{red2}, s^{-1}	0.220 ± 0.005	0.25 ± 0.04	0.093 ± 0.006	0.057 ± 0.003
$K_{D(NADPH)}$, µM	~1	~2	~14	~1

Conditions: 100 mM sodium phosphate, pH 7.5, and 25 °C.

Since the flavin reduction data for M101A, Q102A, and R144A indicates that this half-reaction is relatively unaffected by these mutations, the oxidative half-reaction in both the presence and absence of L-Orn was performed to determine if the reaction with molecular

oxygen, stabilization of the C4a-hydroperoxyflavin intermediate, or flavin dehydration step was affected by any of the mutations. The data in Table 7.4 shows the calculated rate constants for reaction with molecular oxygen (k_{OOH}). In all three cases, the reaction with molecular oxygen is enhanced similar to wild-type when L-Orn is present. The rate for M101A in the absence of L-Orn is unchanged whereas Q102A and R144A are ~2-fold faster (Table 7.4). There is some variability in the reaction with molecular oxygen in the presence of L-Orn. The largest effects are for M101A and Q102A which show a ~40% increase and decrease, respectively, in the rate of reaction with molecular oxygen whereas the rate for R144A is unchanged. These changes are minor however, and suggest that none of these mutations significantly affect the reaction with molecular oxygen. In flavin-containing enzymes that react with oxygen, it has been hypothesized that a positive charge is necessary for acceleration of the reaction with molecular oxygen to stabilize a caged radical pair [27, 28]. Simulations with pyranose-2-oxidase show that a positive charge of a His residue are important for a proton-coupled electron transfer to accelerate oxygen reactivity [29]. This, along with the data presented here for R144A, indicates that the positive charge provided by R144 near the N5 of the flavin is not involved in formation of the C4a-hydroperoxyflavin intermediate in SidA. This is consistent with solvent kinetic isotope effects and computational studies in SidA which show that the 2'-OH of the nicotinamide ribose of $NADP^+$ is important for C4a-hydroperoxyflavin formation [10].

Table 7.4 Pre-steady-state kinetic parameters of flavin oxidation.

	(-) L-Orn		(+) L-Orn	
	k_{OOH}, s^{-1}	k_{H2O2}, s^{-1}	k_{OOH}, s^{-1}	k_{H2O}, s^{-1}
Wild-type	0.65 ± 0.06	0.0149 ± 0.0005	18 ± 2	1.20 ± 0.03
M101A	0.73 ± 0.08	0.0080 ± 0.0001	25 ± 2	0.084 ± 0.007
Q102A	1.29 ± 0.05	0.152 ± 0.005	13.1 ± 0.8	2.48 ± 0.08
R144A	1.29 ± 0.07	0.165 ± 0.001	18 ± 1	0.020 ± 0.001

Conditions: 100 mM sodium phosphate, pH 7.5, and 25 °C.

Flavin oxidation experiments with these mutants indicate that the rates of hydrogen peroxide elimination (k_{H2O2}) and flavin dehydration (k_{H2O}) are the most significantly affected parameters (Table 7.4). M101A does not appear to have a significant effect on the rate of flavin oxidation in the absence of L-Orn as it is only ~2-fold slower than wild-type. In the presence of L-Orn however, the rate of flavin oxidation is ~15-fold slower than in wild-type. This data could indicate two possibilities; mutation of M101 to Ala affects the flavin dehydration process where the chemical steps of flavin dehydration are now more rate-limiting, or the isoalloxazine ring of the flavin has moved where L-Orn doesn't stimulate oxidation as efficiently as in wild-type. Flavin oxidation studies with Q102A indicate that the C4a-hydroperoxyflavin is less stable as the rate of flavin oxidation is ~10-fold faster in the absence of L-Orn (Table 7.4). This is consistent with the high oxidase rate observed in the oxygen consumption assay (Fig. 7.4A) and suggests that along with the 2'-OH of the nicotinamide ribose, Q102 is important for C4a-hydroperoxyflavin stabilization. Q102A also does not appear to have a significant effect on flavin oxidation with L-Orn present as it is only ~2-fold faster than wild-type (Table 7.4). The flavin oxidation process in the absence of L-Orn with R144A indicates that this mutation has a similar effect on the stability of the C4a-hydroperoxyflavin as Q102A where it is ~10-fold less stable than wild-type. This residue interacts with the amide nitrogen of $NADP^+$ (Fig. 7.1) and

mutation of this residue might affect the orientation of $NADP^+$ where it now is not as effective at shielding the C4a-hydroperoxyflavin from bulk solvent. In the presence of L-Orn, the rate of flavin oxidation for R144A is ~8-fold slower than in the absence of L-Orn and ~60-fold slower than wild-type. This is consistent with the oxygen consumption data where the rate of oxygen consumption decreases with increasing concentrations of L-Orn (Fig. 7.4B). This data could indicate that mutation of R144 to Ala alters the chemical steps of flavin dehydration where flavin dehydration is now more rate-limiting.

3.5 pH profile for flavin oxidation in the presence and absence of L-Orn. The pH profiles of flavin oxidation for M101A, Q102A, and R144A were performed in order to determine if any of these mutations affect the pK_a for the N5 of the flavin, which in the absence of L-Orn could contribute to the higher oxidase rates in Q102A and R144A. In Chapter 3 of this dissertation, the pK_a values for flavin oxidation with L-Orn absent and present were proposed to reflect the pK_a values for the N5 of the flavin and for the N^5 of L-Orn in the active site, respectively. None of these mutations here should affect the pK_a value in the presence of L-Orn, as these residues do not interact with L-Orn, but nonetheless the pH profiles were determined as controls. The results in Table 7.5 and Fig. 7.5 show the results for the pH profiles in the absence and presence of L-Orn. The pK_a values in the absence of L-Orn are hard to estimate here since they are at least towards the upper end of the pH range tested (see Chapter 3). The data in Table 7.5 and the traces in Fig. 7.5A suggest that Q102A and R144A slightly alter the pK_a for flavin oxidation. In Q102A, this might have an effect on C4a-hydroperoxyflavin stability as the apparent decrease in the pK_a value for flavin oxidation provides a faster rate of oxidation at physiological pH. Previous estimations on free flavin assigned a pK_a value of 20 to the N5, so it is currently unclear

how Q102 influences the pH profile for flavin oxidation in the absence of L-Orn [30]. In the presence of L-Orn, only the pK_a value for flavin oxidation appears to be affected for R144A (Table 7.5 and Fig. 7.5B). In Chapter 3, this pK_a value in the presence of L-Orn was attributed to an altered pK_a value for the N^5 of L-Orn. R144 does not interact with L-Orn, so at this point it is unclear how removal of R144 alters the pK_a value for flavin oxidation in the presence of L-Orn.

Table 7.5 Observed pK_a values for SidA oxidation.

	pK_a, no substrate	**pK_a, L-Orn**
Wild-type	>9	6.7 ± 0.1
M101A	>9	6.9 ± 0.1
Q102A	>8	6.4 ± 0.2
R144A	>10	7.26 ± 0.09

All pH experiments were performed at 25 °C. 100 mM L-Orn was used in pH experiments with L-Orn present.

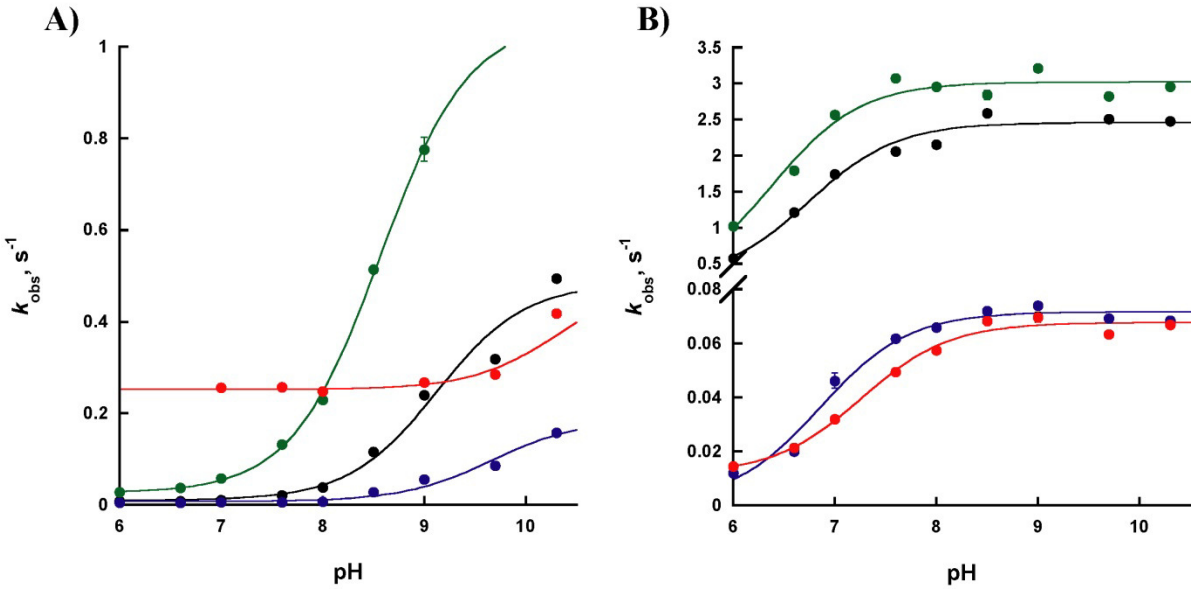

Figure 7.5 pH profiles of flavin oxidation for wild-type SidA (black), M101A (blue), Q102A (green), and R144A (red) in the A) absence and B) presence of 100 mM L-Orn. The traces were fit to eq. 4.

3.6 Solvent kinetic isotope effect of flavin oxidation with M101A and R144A. The SKIEs of flavin oxidation were determined in the pL independent regions for M101A and R144A in order to determine if their unusual oxidation features are due to a chemical step becoming more rate-limiting from the introduced mutations. A recent study showed SKIEs for flavin oxidation in SidA for both hydrogen peroxide and water elimination that occur through a proton in flight originating from the N5 of the flavin [10]. The data in Table 7.6 indicates that in both the absence and presence of L-Orn, the SKIEs are lower for M101A and higher for R144A. This data indicates that for M101A, the lack flavin oxidation acceleration when L-Orn is present is not due to the chemical steps of water elimination becoming more rate-limiting. The significantly higher SKIEs for R144A indicate that the chemical steps of hydrogen peroxide/water elimination are more rate-limiting. A recent computational study showed there is a high energy barrier for spontaneous hydrogen peroxide elimination from the C4a-hydroperoxyflavin and that proton shuttle mediators are necessary to lower the energy barrier [31]. Another recent computational study of SidA also showed a high energy barrier for dehydration of the C4a-hydroxyflavin and proposed that R144 could be involved as a proton shuttle mediator to lower the activation energy barrier [32]. These computational studies along with the SKIE data for R144A here indicate that R144 likely participates in the process of proton shuttling for both hydrogen peroxide and water elimination.

Table 7.6 Observed solvent kinetic isotope effect values for SidA oxidation.

	SKIE, no substrate[a]	**SKIE, L-Orn**[b]
Wild-type	2.30 ± 0.07	1.59 ± 0.01
M101A	1.59 ± 0.09	1.35 ± 0.08
R144A	3.6 ± 0.2	2.9 ± 0.3

[a]The SKIE values for flavin oxidation with no substrate were calculated at pL 7.0. [b]The SKIE values for flavin oxidation with L-Orn were calculated at pL 9.0.

3.7 Three-dimensional structure analysis of M101A. Since the SKIE studies did not indicate flavin dehydration is more rate-limiting in M101A, the three-dimensional crystal structure of M101A was solved in order to possibly provide a structural explanation for the lack of acceleration of flavin oxidation with L-Orn present. The preliminary structure of M101A is virtually identical to wild-type (PDB code 4B63) with a calculated RMSD of 0.208 (Fig. 7.6A) [9]. This indicates the mutation of M101 to Ala does not affect any major folds in SidA. The primary difference between the wild-type and M101A structures are the orientations of the isoalloxazine rings of the flavins (Fig. 7.6B). In M101A, the isoalloxazine ring is rotated ~90 ° counterclockwise and flipped "out" relative to the re face of the isoalloxazine ring of the flavin in wild-type. This conformation of the isoalloxazine ring is identical to the observed "out" position of the isoalloxazine ring in the L-Orn monooxygenase KtzI (Fig. 7.6B) [17]. It was proposed that the oxidized flavin states of the L-Orn monooxygenases exist in an equilibrium between the "in" and "out" positions, and the "out" position acts as a "battering ram" to eject $NADP^+$. Fig. 7.6B shows that M101A in SidA interacts with the O4 atom of the flavin. It appears that this interaction might help to position the flavin properly during catalysis where the distal oxygen of the C4a-hydroperoxyflavin can be efficiently transferred to L-Orn. In M101A, the crystal structure could suggest that deletion of the M101 interaction shifts the equilibrium of the flavin position to the "out" position. The mechanistic data from M101A also suggests that the C4a-hydroperoxyflavin is as equally as stable in the "out" position as the "in" position which would rationalize the lack of steady-state turnover with L-Orn present in M101A. If the flavin of M101A exists primarily in the "out" position, then the distal oxygen of the C4a-hydroperoxyflavin and the N^5 of L-Orn would not be able to react and the enzyme would remain in a "dead-end state" until the flavin swung back to the "in" position. This conformation of the

isoalloxazine ring does not appear to affect flavin reduction in M101A as the rates of flavin reduction are similar to wild-type (Table 7.3). In KtzI, this "out" conformation could not react with NADPH, so in M101A it is possible that prior to reduction, the flavin is more mobile where it can adopt the proper conformation to accept a hydride equivalent. This data does not rationalize the movement observed for M101 between the oxidized and reduced structures (Fig. 7.1) and further experiments are required to elucidate if this movement is catalytically important.

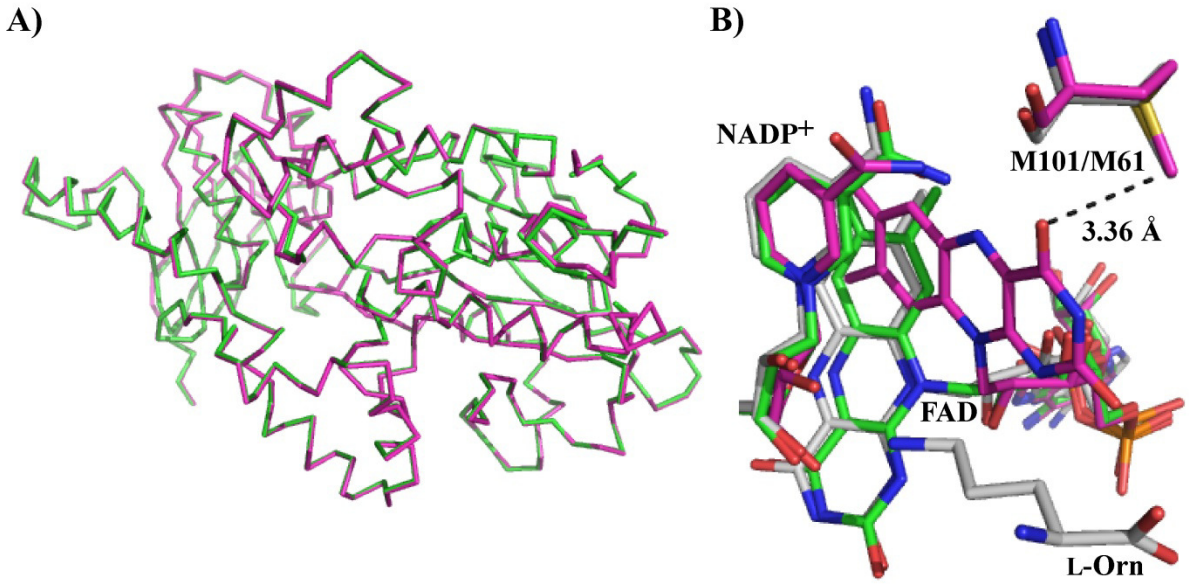

Figure 7.6 Comparison of the three-dimensional structures of SidA M101A with wild-type (PDB code 4B63) and the "out" structure of KtzI (PDB code 4TLZ). A) Ribbon diagrams of M101A (green) and wild-type (magenta). A RMSD of 0.208 was calculated between the two structures. B) Close-up view of the aligned active sites of M101A (green carbons), wild-type (magenta carbons) and KtzI (gray carbons). M61 is the homologous residue to M101A in KtzI.

4. Discussion

The data presented here provides mechanistic and structural characterization of three residues in the active site of SidA that are critical for efficient catalysis. Analysis shows that M101, Q102, and R144 are all very important in different processes of the SidA reaction. Mechanistic analysis of M101A indicates that L-Orn stimulates turnover ~15-fold slower than

wild-type (Table 7.4). The M101A structure shows the isoalloxazine ring is in an "out" position, similar to a structure of KtzI (PDB code 4TLZ) [17]. This might indicate that M101 provides a van der Waals interaction with the O4 of the flavin to hold it in the "in" position (Fig. 7.1). Removal of this interaction could shift the equilibrium of the flavin position to the "out" position where mechanistic data suggests that the C4a-hydroperoxyflavin is as equally as stable, but not in a suitable position to hydroxylate L-Orn. There is a similar space in the M101A structure between the FAD and $NADP^+$ which might provide for proper interaction of the distal oxygen of the C4a-hydroperoxyflavin with $NADP^+$ to contribute to its stability (Fig. 7.7). In wild-type, this interaction is provided by the 2'-OH of the nicotinamide ribose, but in M101A, this interaction would be provided by the 3'-OH of the nicotinamide ribose. Future modeling of the C4a-hydroperoxyflavin by computational studies would provide evidence if this is true where the intermediate is equally as stable in the "in" position as the "out" position and indicate how the C4a-hydroperoxyflavin maintains its stability as the flavin moves.

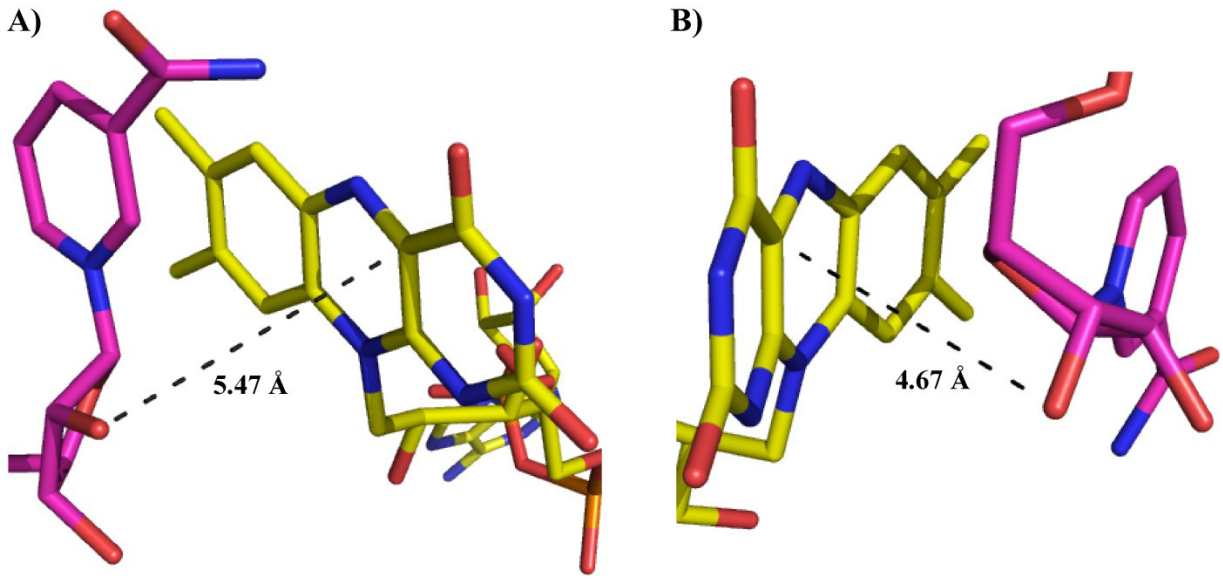

Figure 7.7 Distances from the C4a of the flavin in the wild-type and M101A structures to $NADP^+$. A) Distance between the C4a of the flavin and the 2'-OH of the nicotinamide ribose in the wild-type structure (PDB code 4B63). B) Distance between the C4a of the flavin and the 3'-OH of the nicotinamide ribose in the M101A structure. Since the distances between the respective hydroxyl groups are similar, this interaction in M101A might contribute to the stability of the C4a-hydroperoxyflavin when the flavin is flipped in this conformation. FAD molecules are shown with yellow carbons and $NADP^+$ molecules are shown with magenta carbons.

A van der Waals interaction on the si face of the flavin, similar to the one provided by M101 in SidA, is conserved among Class B monooxygenases (Fig. 7.8). In KtzI, a Met residue is interacting with the O4 of the flavin similar to SidA (Fig. 7.8A). In PvdA and phenylacetone monooxygenase (PAMO), Leu and Cys residues are present, respectively, and they appear to be interacting in a similar manner as M101 in SidA (Figs. 7.8B and 7.8D). There is not a conserved residue interacting with the O4 of the flavin in flavin-containing monooxygenase from *Methylophaga* sp. strain SK1 (FMO), but there is a Met that appears to provide a van der Waals interaction with the C5a, possibly providing the same role as M101 in SidA, but in a different position. In PAMO, the homologous Cys residue to M101, C65, was mutated to Asp which resulted in high oxidase activity. This mutation differs from M101A as C65D in PAMO is

isosteric and introduction of the negative charge induced rotation of the adjacent D66 which was proposed to cause high oxidase activity through either steric hindrance with the C4a or by rapidly protonating the proximal oxygen of the C4a-peroxyflavin and triggering rapid hydrogen peroxide release [33]. This mutation however did not produce the same effect as M101A in SidA presented here, where the flavin in PAMO was observed in the same conformation as wild-type.

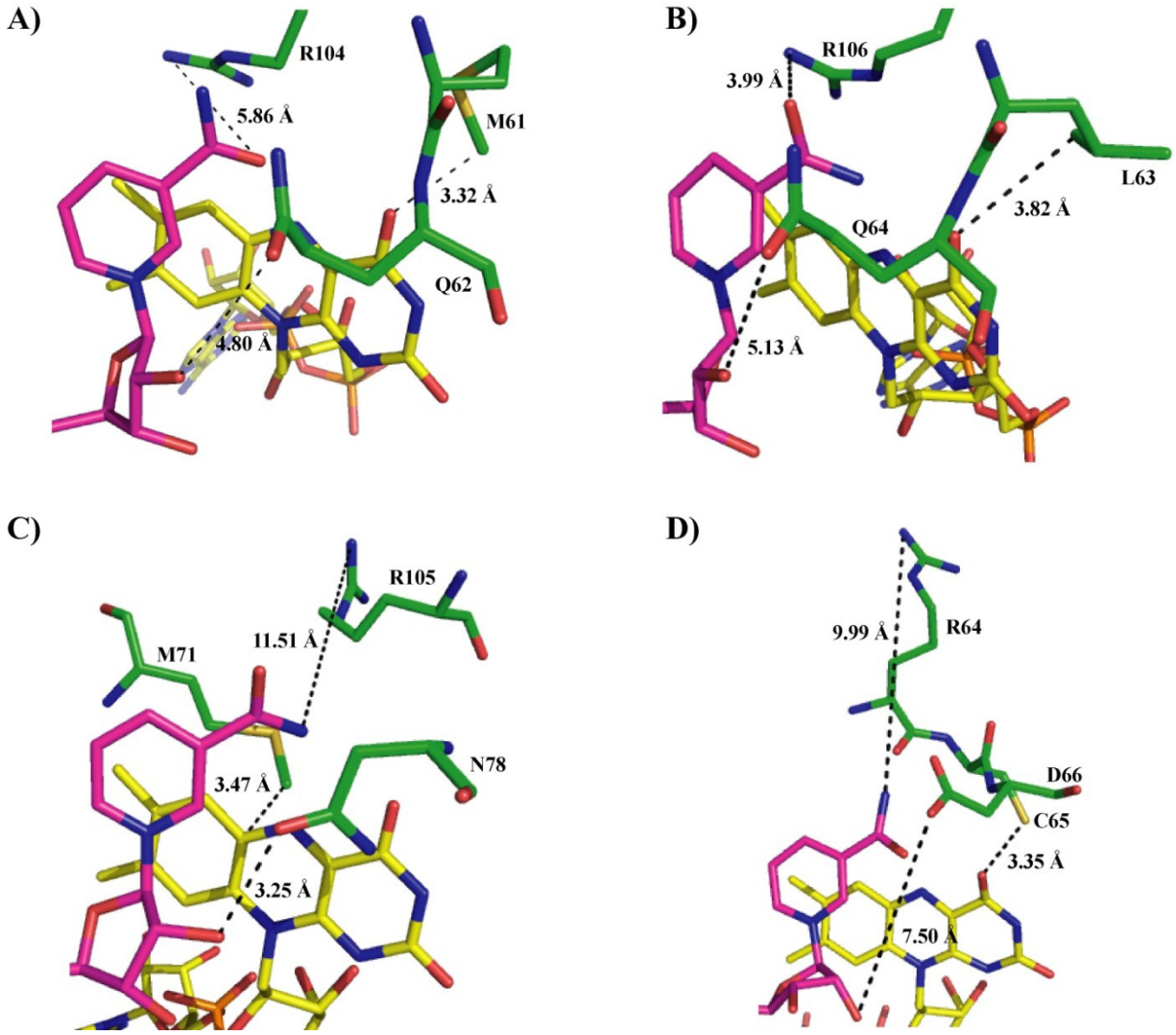

Figure 7.8 Active sites of A) KtzI (PDB code 4TLX) [17], B) PvdA (PDB code 3S61) [34], C) FMO (PDB code 2VQ7) [1], and D) PAMO (PDB code 2YLR) [35]. The FAD molecules (yellow carbons), $NADP^+$ molecules (magenta carbons), and residues in similar positions to M101, Q102, and R144 in SidA (green carbons) are shown.

Steady-state and pre-steady-state mechanistic analysis of Q102A indicates it shares similar properties to wild-type, with the exception that the coupling and stability of the C4a-hydroperoxyflavin are decreased (Tables 7.2 and 7.4). The steady-state data indicates a high oxidase rate (Table 7.1) which results in lower coupling for Q102A (Table 7.2). The data in Table 7.4 indicates that the C4a-hydroperoxyflavin is ~10-fold less stable in Q102A as wild-type which is consistent with the lower coupling. When the structure of SidA was solved, a water molecule was observed in the active site which appeared to mimic the proper position of the distal oxygen of the C4a-hydroperoxyflavin [9]. Fig. 7.9 shows that along with the 2'-OH of the nicotinamide ribose, which has been proposed to transfer the proton to the C4a-peroxyflavin, the side chain carbonyl of Q102 acts as an H-bond acceptor to this water molecule [10]. Along with our mechanistic data which shows a decrease in C4a-hydroperoxyflavin stability for Q102A, it appears that Q102 is essential for an H-bond network in the active site that coordinates stabilization of the C4a-hydroperoxyflavin.

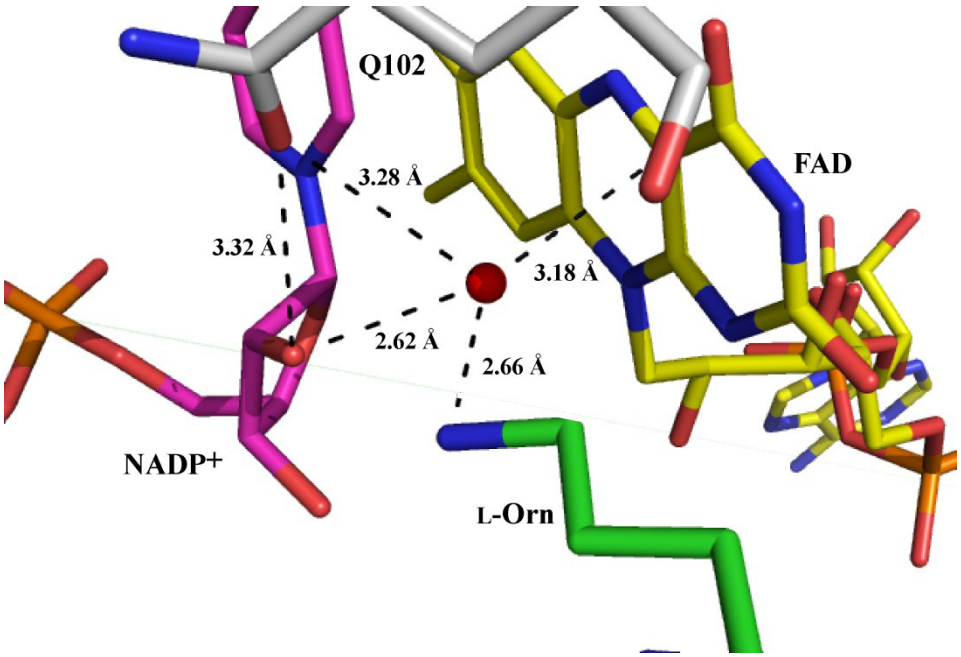

Figure 7.9 Hydrogen bonding network provided by Q102 in wild-type SidA (PDB code 4B63) [9]. Q102 provides interaction to the 2'-OH of the nicotinamide ribose and a water molecule (red sphere) in the active site that has been proposed to mimic the position of the distal oxygen of the C4a-hydroperoxyflavin. FAD (yellow carbons), $NADP^+$ (magenta carbons), L-Orn (green carbons), and Q102 (gray carbons) are shown.

In a recent computational study of SidA, the relative energy contribution of Q102 in the hydroxylation process of L-Orn was calculated [32]. Here, they showed that because this residue has a long and flexible side chain, it contributes differently to the hydroxylation process at each step where in the Orn hydroxylation reaction, it contributes most in the Orn oxidation step (~1.5 kcal/mol). The data presented here for Q102A does not suggest that the hydroxylation step is being affected, other than the lower coupling number consistent with the decreased stability of the C4a-hydroperoxyflavin, but further experiments are needed in order to confirm this. Fig. 7.8 shows a carbonyl near the C4a of the flavin is conserved in the Class B monooxygenases KtzI, PvdA, FMO, and PAMO [1, 17, 34, 35]. In the L-Orn monooxygenases KtzI and PvdA, a Gln residue is positioned in a similar orientation around the C4a locus (Figs 7.6A-B). In FMO and PAMO, an Asn and Asp, respectively, are present in proximity to the C4a locus (Figs. 7.8C-D).

These similarities around the C4a reactive center suggest that interaction of a carbonyl with the distal oxygen of the C4a-hydroperoxyflavin in Class B monooxygenases is important for stabilization of the intermediate.

The positive charge of R144 above the N5 of the flavin appears to be important for stabilization of the C4a-hydroperoxyflavin, as similar to Q102A, it is ~10-fold less stable than wild-type (Table 7.4). While R144 does not directly interact with the N5 of the flavin, in the oxidized structure of SidA, it appears to interact with the nitrogen of the amide group on $NADP^+$ (Fig. 7.1). Then, in the reduced structure, R144 swings away and the amide group rotates so the carbonyl is acting as a hydrogen-bond acceptor to the N5-H of the flavin [9]. Bach and Mattevi recently performed computational studies where they modeled a C4a-hydroperoxyflavin in the active site of SidA and showed that with the intermediate formed, the nitrogen of the amide group on $NADP^+$ is interacting with the N5-H and O4 of the flavin which stabilizes the intermediate so that the N5-H is unavailable for hydrogen peroxide elimination [31]. In this conformation, it is conceivable that R144 is flipped in a similar orientation as the oxidized structure to properly position the amide group of $NADP^+$ (Scheme 7.1A). In R144A, removal of this interaction might disrupt the positioning of the amide group resulting in the lower observed stability of the C4a-hydroperoxyflavin where the N5-H is more readily transferred to the hydrogen peroxide leaving group (Scheme 7.1B).

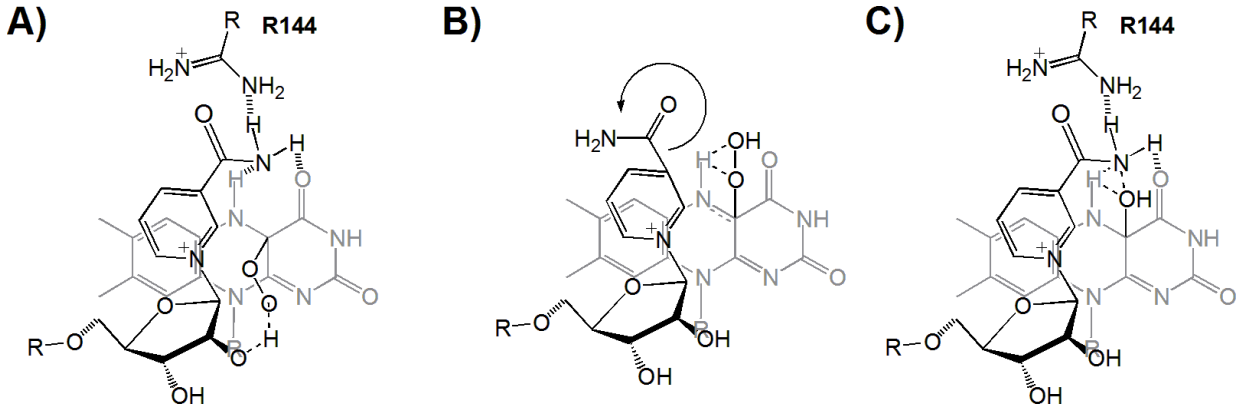

Scheme 7.1 Role of R144 in flavin oxidation. A) R144 interacts with the amide group of $NADP^+$, positioning the amide nitrogen so that it interacts with the N5 and O4 of the flavin to favor stability of the C4a-hydroperoxyflavin. B) Removal of R144 alters the positioning of the amide group, leading to transfer of the N5-H to the hydroperoxide leaving group. C) R144 might help position the amide nitrogen so that it acts as a proton shuttle mediator in flavin dehydration after hydroxylation.

R144A also displayed a decrease in the rate of flavin oxidation upon the addition of L-Orn (Table 7.4). Here, the chemical steps of flavin dehydration appear to be more rate-limiting as supported by the SKIE data in Table 7.6. Proton shuttle facilitators have been shown recently in computational studies to lower the activation energy for hydrogen peroxide elimination as the N5-H is transferred to the hydrogen peroxide leaving group [31]. Also, it was suggested that this might be necessary to lower the energy barrier for flavin dehydration in SidA and that R144 might facilitate this proton shuttling [32]. The oxidized structure of SidA indicates the N5 and R144 are separated by a distance of ~5 Å which is too far for R144 to act as a proton shuttle mediator (data not shown). While the side chain of R144 appears to be dynamic, it might help in facilitating flavin dehydration by positioning the amide nitrogen of $NADP^+$ to transfer a proton transfer between the N5 and C4a-OH (Scheme 7.1C). Fig. 7.8 shows that among Class B monooxygenases, a conserved Arg residue is present above the N5 of the respective flavins. These Arg residues are present in different conformations where in FMO and PAMO in particular, they are flipped away from the flavin (Figs. 7.8C-D). Since this Arg is observed in

multiple conformations in SidA, it is reasonable to propose that this side chain is dynamic where it might move to similar orientations along the catalytic cycle in other Class B monooxygenases help facilitate flavin dehydration after hydroxylation.

These findings highlight the importance of three residues in catalysis of SidA. Each is important for efficient, coupled oxidation to occur. Class B monooxygenases have appeared to evolve these interactions to facilitate stabilization of the C4a-(hydro)peroxyflavin, dehydration of the C4a-hydroxyflavin, and positioning of the flavin during catalysis. Further computational and crystallographic experiments involving these three residues would help answer a number of questions raised by this study such as the exact role of the isoalloxazine ring movement in catalysis, lowering of the energy barrier of flavin dehydration and positioning of the amide group of $NADP^+$ by R144, and contribution to the activation energy by Q102 in preventing breakdown of the C4a-hydroperoxyflavin.

5. Acknowledgements

This work was supported in part by a grant from the National Science Foundation MCB-1021384.

6. References

[1] A. Alfieri, E. Malito, R. Orru, M.W. Fraaije, A. Mattevi, Proc Natl Acad Sci U S A 105 (2008) 6572-6577.
[2] D.E. Torres Pazmino, B.J. Baas, D.B. Janssen, M.W. Fraaije, Biochemistry 47 (2008) 4082-4093.
[3] K.M. Meneely, E.W. Barr, J.M. Bollinger, Jr., A.L. Lamb, Biochemistry 48 (2009) 4371-4376.
[4] S.W. Chocklett, P. Sobrado, Biochemistry 49 (2010) 6777-6783.
[5] E. Romero, M. Fedkenheuer, S.W. Chocklett, J. Qi, M. Oppenheimer, P. Sobrado, Biochim Biophys Acta (2012).

[6] J.A. Mayfield, R.E. Frederick, B.R. Streit, T.A. Wencewicz, D.P. Ballou, J.L. DuBois, J Biol Chem 285 (2010) 30375-30388.
[7] W.J. van Berkel, N.M. Kamerbeek, M.W. Fraaije, J Biotechnol 124 (2006) 670-689.
[8] E. Malito, A. Alfieri, M.W. Fraaije, A. Mattevi, Proc Natl Acad Sci USA 101 (2004) 13157-13162.
[9] S. Franceschini, M. Fedkenheuer, N.J. Vogelaar, H.H. Robinson, P. Sobrado, A. Mattevi, Biochemistry 51 (2012) 7043-7045.
[10] R. Robinson, S. Badieyan, P. Sobrado, Biochemistry 52 (2013) 9089-9091.
[11] B.A. Palfey, C.A. McDonald, Arch Biochem Biophys 493 (2010) 26-36.
[12] B. Entsch, L.J. Cole, D.P. Ballou, Arch Biochem Biophys 433 (2005) 297-311.
[13] P.J. Goldman, K.S. Ryan, M.J. Hamill, A.R. Howard-Jones, C.T. Walsh, S.J. Elliott, C.L. Drennan, Chem Biol 19 (2012) 855-865.
[14] I.A. Mirza, B.J. Yachnin, S. Wang, S. Grosse, H. Bergeron, A. Imura, H. Iwaki, Y. Hasegawa, P.C. Lau, A.M. Berghuis, J Am Chem Soc 131 (2009) 8848-8854.
[15] B.J. Yachnin, T. Sprules, M.B. McEvoy, P.C. Lau, A.M. Berghuis, J Am Chem Soc 134 (2012) 7788-7795.
[16] C. Shirey, S. Badieyan, P. Sobrado, J Biol Chem 288 (2013) 32440-32448.
[17] J.W. Setser, J.R. Heemstra, Jr., C.T. Walsh, C.L. Drennan, Biochemistry 53 (2014) 6063-6077.
[18] P. Macheroux, in: S.K. Chapman, G.A. Reid (Eds.), Flavoprotein Protocols, Humana Press, Totowa, NJ, 1999, pp. 1-7.
[19] T. Csaky, Acta Chem Scand (1948) 450-454.
[20] R. Robinson, P. Sobrado, Biochemistry 50 (2011) 8489-8496.
[21] K.B. Schowen, R.L. Schowen, Methods Enzymol 87 (1982) 551-606.
[22] A. Han, R.M. Robinson, S. Badieyan, J. Ellerbrock, P. Sobrado, Arch Biochem Biophys 532 (2013) 46-53.
[23] D. Xu, R.M. Kohli, V. Massey, Proc Natl Acad Sci U S A 96 (1999) 3556-3561.
[24] P. Macheroux, V. Kieweg, V. Massey, E. Soderlind, K. Stenberg, Y. Lindqvist, Eur J Biochem 213 (1993) 1047-1054.
[25] R. Robinson, S. Franceschini, M. Fedkenheuer, P.J. Rodriguez, J. Ellerbrock, E. Romero, M.P. Echandi, J.S. Martin Del Campo, P. Sobrado, Biochim Biophys Acta 1844 (2014) 778-784.
[26] R. Orru, D.E. Pazmino, M.W. Fraaije, A. Mattevi, J Biol Chem 285 (2010) 35021-35028.
[27] G. Gadda, Biochemistry 51 (2012) 2662-2669.
[28] C.A. McDonald, R.L. Fagan, F. Collard, V.M. Monnier, B.A. Palfey, J Am Chem Soc 133 (2011) 16809-16811.
[29] T. Wongnate, P. Surawatanawong, S. Visitsatthawong, J. Sucharitakul, N.S. Scrutton, P. Chaiyen, J Am Chem Soc 136 (2014) 241-253.
[30] U.V. Venkataram, T.C. Bruice, Journal of the American Chemical Society 106 (1984) 5703-5709.
[31] R.D. Bach, A. Mattevi, J Org Chem 78 (2013) 8585-8593.
[32] S. Badieyan, R.D. Bach, P. Sobrado, J Org Chem 80 (2015) 2139-2147.
[33] P.B. Brondani, H.M. Dudek, C. Martinoli, A. Mattevi, M.W. Fraaije, J Am Chem Soc 136 (2014) 16966-16969.
[34] J. Olucha, K.M. Meneely, A.S. Chilton, A.L. Lamb, J Biol Chem 286 (2011) 31789-31798.

[35] E. Malito, A. Alfieri, M.W. Fraaije, A. Mattevi, Proc Natl Acad Sci U S A 101 (2004) 13157-13162.

CHAPTER 8

Substrate binding modulates the activity of *Mycobacterium smegmatis* G (MbsG), a flavin-dependent monooxygenase involved in the biosynthesis of hydroxamate-containing siderophores

Reprinted with permission from Biochemistry, Robinson, R., and Sobrado, P. "Substrate binding modulates the activity of *Mycobacterium smegmatis* G (MbsG), a flavin-dependent monooxygenase involved in the biosynthesis of hydroxamate-containing siderophores" *Biochemistry*. 2011 (ID 10.1021/bi200933h) Vol 50: 8489-8496.

Author Contributions:
Reeder Robinson performed all the research and helped write the article.

Pablo Sobrado oversaw and directed the research and helped write the article.

Abstract

Mycobacterium smegmatis G (MbsG) is a flavin-dependent monooxygenase that catalyzes the NAD(P)H- and oxygen-dependent hydroxylation of the terminal amino group on the side chain of L-lysine in the biosynthetic pathway of the siderophore mycobactin. Mycobactins are essential for mycobacterium growth under iron limiting conditions encountered during infection in mammals. Thus, enzymes involved in the biosynthesis of mycobactin represent potential drug targets. MbsG was expressed in *E. coli* and purified using metal affinity and ionic exchange chromatographies. Recombinant MbsG represents the first member of this class of enzymes isolated in the active form, with a tightly bound FAD cofactor. The k_{cat} value for formation of hydroxylated L-lysine under steady-state conditions was 5.0 min^{-1}, and K_m values of 0.21 mM for L-lysine, 1.1 mM for NADH, and 2.4 mM for NADPH were calculated. The enzyme functioned as an oxidase when the activity of MbsG was measured by monitoring

oxygen consumption in the absence of L-lysine, oxidizing NADH and NADPH with k_{cat} values of 59 min^{-1} and 49 min^{-1}, respectively. Under these conditions, MbsG produced both hydrogen peroxide and superoxide. In contrast, when L-lysine was present, the reaction became more coupled, producing hydroxylated L-lysine and decreasing the oxidase activity. These results suggest that substrate binding modulates the function of MbsG from an oxidase to a monooxygenase.

1. Introduction

Iron is an essential nutrient and is typically present in concentrations too low to support proliferation of microbial pathogens in mammalian hosts [1]. The low concentration of iron is partly due to the fact that it is present as insoluble ferric hydroxides and is sequestered by mammalian iron-binding proteins such as ferritin and lactoferrin, which further reduce iron availability [1, 2]. To overcome this iron deficiency, many invasive pathogens such as *Mycobacterium tuberculosis* and *Aspergillus fumigatus* obtain iron via siderophores. These compounds are low molecular weight metal chelators that are involved in iron uptake [3].

Siderophores vary among species and are diverse in many respects, particularly in the presence of catechol, carboxylate, or hydroxamate functional groups at the iron-binding site [4]. *Mycobacteria* spp., including *M. tuberculosis*, synthesize and secrete the hydroxamate-containing siderophore mycobactin. Biosynthesis of hydroxamate-containing siderophores involves the action of novel flavin-containing *N*-hydroxylating monooxygenases (NMO). The gene coding for NMOs in *M. tuberculosis* and *M. smegmatis* have been identified as MbtG and MbsG, respectively. These enzymes catalyze the NAD(P)H- and oxygen-dependent hydroxylation of the side chain amino group of L-lysine which is incorporated into the

siderophore mycobactin (Scheme 8.1). Mycobactins have been shown to be essential for growth in iron-limiting conditions [5, 6]. The importance of this enzyme in mycobactin biosynthesis and the lack of homologous enzymes in humans, suggests that MbtG is an attractive drug target against tuberculosis.

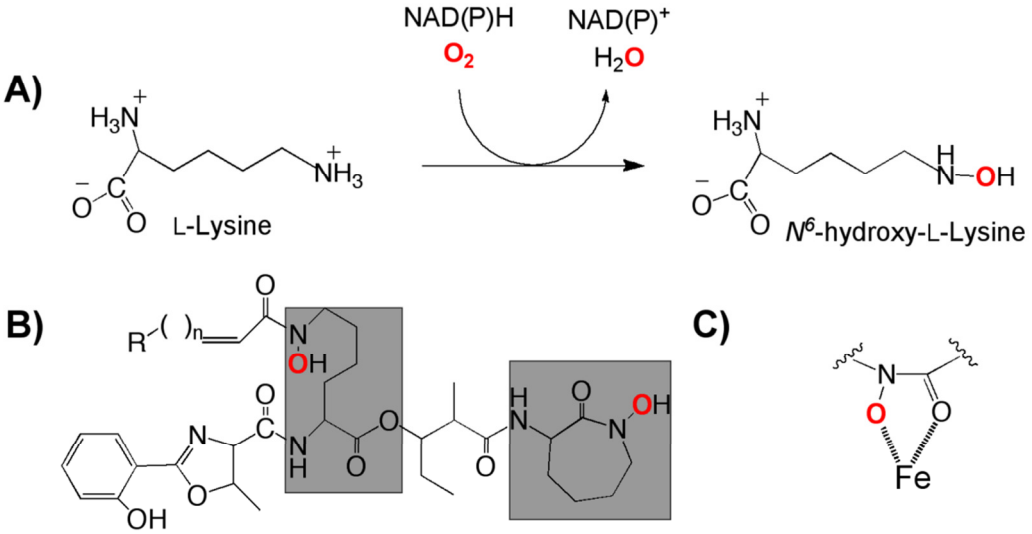

Scheme 8.1 A) Reaction catalyzed by MbsG. B) Structure of the siderophore mycobactin. Hydroxylated L-lysines are shown in gray boxes. C) Role of the hydroxamate residues in metal binding.

Here, we present the recombinant expression and characterization of the N^6-lysine hydroxylase from *M. smegmatis*, a homolog of MbtG that shares 75% identity. This enzyme was isolated in the active form with a bound FAD cofactor and represents the first member of the bacterial NMO that acts on L-lysine to be isolated in its functional form. Kinetic characterization shows that in the absence of L-lysine, MbsG functions as an oxidase and the addition of the amino acid substrate, converts the activity to a monooxygenase. This represents a novel mechanism of regulation for flavin-dependent monooxygenases.

2. Materials and Methods

*2.1 Materials. Pme*I and *Sgf*I restriction endonucleases were from Promega Corporation (Madison, WI). *E. coli* TOP10 and BL21-T1^{R} chemically competent cells were from Invitrogen. The plasmids pVP55A and pVP56K were obtained from the Center for Eukaryotic Structural Genomics (University of Wisconsin-Madison). DNA sequencing was performed at the Virginia Bioinformatics Institute DNA sequencing facility. Isopropyl-β-D-1-thiogalactopyranoside (IPTG) was from Gold Biotechnology, St. Louis, MO, and protein purification was performed on an ÄKTA Prime FPLC system (GE Healthcare). L-Lysine, substrates, NADPH, NADH, as well as buffers and salts, were purchased from Thermo Fisher Scientific and used without further purification.

2.2 Cloning. M. smegmatis mbsG gene was amplified directly from genomic DNA using the oligos 5'-ggttgcgatcgccatgagcgagacgaccccacggctg-3' (*Sgf*I site underlined) and 5'-gggggtttaaactcgaacggattggtgctcatcgg -3' (*Pme*I site underlined). The PCR product was digested with *Sgf*I and *Pme*I endonucleases for 20 min at 37 ^{o}C. The digestion reaction was terminated by incubation at 65 ^{o}C for 30 minutes. The digested mbsG gene was ligated into the pVP55A or pVP56K plasmid, both previously digested with *Sgf*I and *Pme*I enzymes. Plasmid pVP55A carries an ampicillin resistant gene while pVP56K carries a kanamycin resistant gene. Ligation reactions were transformed into *E. coli* TOP10 cells and plated on LB-agar plates with the appropriate antibiotic. Positive clones were identified by DNA sequencing.

2.3 Protein expression and purification. Initial expression tests with the pVP55A plasmid, which produced an MbsG with an N-terminal fusion to a His_8-tag yielded insoluble protein. Therefore,

protein expression was done using the pVP56K plasmid. This plasmid expressed MbsG as a fusion to maltose binding protein (MBP). An overnight culture of *E. coli* BL21-T1^{R} cells containing the *pVP56K:mbsG* plasmid was used to inoculate six 1.5-L flasks of LB broth containing kanamycin (50 µg/ml). Cultures were grown at 37 ^{o}C with agitation, set at 250 rpm, to an optical density at 600 nm (OD_{600}) of ~ 0.6. Protein expression was initiated by addition of 300 µM IPTG. Cells were harvested after four hours of induction at 20 ^{o}C by centrifugation and stored at -80 ^{o}C. For protein isolation, all of the steps were performed at 4 ^{o}C. 30 g of cell pellet was resuspended in 90 mL buffer A (25 mM HEPES, 300 mM NaCl, 25mM imidazole, 5% glycerol, pH 7.5) and the cell suspension was incubated with constant stirring for 30 minutes in the presence of 1 mM phenylmethylsulfonyl fluoride and 25 µg/mL each of DNAse I, RNAse, and lysozyme. Cells were then lysed by sonication and the cellular debris and insoluble material were precipitated by centrifugation at 35,000 *g* for 45 minutes. The resulting supernatant was loaded onto two-in-tandem 5 mL HisTrap columns (GE Healthcare) previously equilibrated with buffer A. The columns were washed with buffer A and MbsG was eluted with a 150 mL imidazole gradient (25 – 300 mM) at a flow rate of 5 mL/minute. Fractions were analyzed by SDS-PAGE and those containing His_8-MBP-MbsG were pooled and dialyzed in 2 L of buffer A overnight. MbsG was liberated from the His_8-MBP tag by the addition of tobacco etch virus (TEV) protease (approx. 0.5 mg TEV/mg MbsG based on flavin content) during dialysis. After overnight cleavage, the protein solution was centrifuged at 35,000 *g* for 45 minutes to remove traces of precipitate and the sample was loaded onto two-in-tandem 5 mL HisTrap columns equilibrated with buffer A. In this step, His_8-MBP and His_8-TEV remained bound to the column but MbsG did not. The yellow flow through containing MbsG was pooled and dialyzed for 2 hours in 2 L of buffer B (25 mM HEPES, 5% glycerol, pH 7.5). The sample was then loaded

onto two-in-tandem 5 mL DEAE columns (GE Healthcare) equilibrated with buffer B. MbsG was eluted with a 200 mL NaCl gradient (10 – 400 mM) at a flow rate of 3 mL/minute. Fractions containing MbsG were pooled and concentrated to a 2 mL volume. Aliquots were frozen in liquid nitrogen prior to storage at -80 ^{o}C.

2.4 Determination of bound flavin extinction coefficient. The spectrum of purified MbsG (40 μM) in 100 mM sodium phosphate, pH 7.5, was recorded. The flavin was extracted by addition of 10% SDS and incubated at 95 ^{o}C for one minute, and the spectrum of the liberated FAD was recorded. An extinction coefficient at 450 nm of 12,800 M^{-1} cm^{-1} was calculated for the FAD bound to MbsG from the extinction coefficient at 450 nm for free FAD, 11,300 M^{-1} cm^{-1} [7].

2.5 Identification of the bound FAD cofactor by mass spectrometry. MbsG was incubated at 95 ºC for five minutes. Denatured protein was precipitated by centrifugation at 9,300 *g* for five minutes. The supernatant was removed and a 1 μL aliquot was spotted onto a MALDI target plate and allowed to air-dry. Then, 1 μL of matrix solution (4 mg/mL α-cyano-4-hydroxycinnamic acid in 50:50 water:acetonitrile supplemented with 0.1% trifluroacetic acid) was added to the spot and allowed to air dry. The sample was analyzed using an AB Sciex 4800 MALDI TOF/TOF operating in reflector negative ion mode following tuning and calibration utilizing commercial FAD. Both MS and MS/MS spectra were compared to that of commercial FAD to validate the identification of the bound FAD cofactor.

2.6 Iodine oxidation assay. The amount of hydroxylated product formed by MbsG was assayed by a variation of the Csaky iodine oxidation reaction [8]. The standard assay buffer contained

104 µL of 100 mM sodium phosphate, pH 7.5, and concentrations of L-lysine and NAD(P)H ranging from 0-20 mM and 0-15 mM, respectively. In assays that were performed with varying amounts of L-lysine, NADH and NADPH concentrations were kept constant at 3 mM and 5 mM, respectively. In assays that were performed with varying amounts of NADH and NADPH, L-lysine concentrations were kept constant at 3 mM. The reaction was initiated by addition of MbsG (2.0 µM) and the reaction was allowed to proceed for 10 min at 25 ^{o}C with shaking at 750 rpm. The reaction was quenched by the addition of 52.5 µL of 2 N perchloric acid. Aliquots (47.5 µL each) of the terminated reaction mixture were transferred into a 96-well plate for color development. The pH of the reaction mixtures were neutralized by the addition of 47.5 µL of 10% (w/v) sodium acetate solution, followed by the addition of 47.5 µL of 1% (w/v) sulfanilic acid in 25% (v/v) acetic acid. Then, 19 µL of 0.5% (w/v) iodine in glacial acetic acid were added and the reaction was incubated with orbital shaking at 25 ^{o}C for 15 minutes. Excess iodine was removed by the addition of 19 µL of 0.1 N sodium thiosulfate and the color was then developed by adding 19 µL of 0.6% (w/v) α-naphthylamine in 30% (v/v) acetic acid. The absorbance at 562 nm was measured after 45 minutes of incubation on a SpectraMax M5e plate reader (Molecular Devices). A standard curve of hydroxylamine hydrochloride was used to calculate the amount of hydroxylated product produced.

2.7 Oxygen consumption assay. The amount of molecular oxygen consumed by MbsG was monitored using a Hansatech Oxygraph (Norfolk, UK). The standard assay contained 1 mL of 100 mM sodium phosphate, pH 7.5, with concentrations of NAD(P)H ranging from 0-20 mM and L-lysine concentrations of either 0 or 3 mM. The reaction was initiated by addition of MbsG (2.0 µM) and the reaction was allowed to proceed for one minute at 25 ^{o}C with constant stirring.

2.8 Hydrogen peroxide formation assay. The amount of hydrogen peroxide formed from MbsG was measured using the Pierce Hydrogen Peroxide Detection Kit. The standard assay buffer contained 150 µL of 100 mM sodium phosphate, pH 7.5, and concentrations of L-lysine and NAD(P)H both ranging from 0-10 mM. In assays that were performed with varying amounts of L-lysine, NADH and NADPH concentrations were kept constant at 3 mM and 5 mM respectively. In assays that were performed with varying amounts of NADH and NADPH, L-lysine concentrations were kept constant at either 0 or 3 mM. The reaction was initiated by MbsG (2.0 µM) and incubated at 25 ^{o}C with shaking at 750 rpm for 10 minutes. The assay mixture was terminated by the addition of 52.5 µL 2 N perchloric acid. Aliquots of 20 µL of the assay mixture were then added to 200 µL of working reagent (100 mM sorbitol, 125 µM xylenol orange, 250 µM ammonium ferrous (II) sulfate in water and 25 mM H_2SO_4) in a 96-well plate. The mixture was incubated for 20 min at 25 ^{o}C with orbital shaking, at which time the absorbance at 595 nm was measured. A standard curve of hydrogen peroxide was used to calculate the amount of hydrogen peroxide produced by MbsG.

2.9 Superoxide formation assay. The amount of superoxide formed by MbsG was measured by coupling the assay mixture with WST-1 (Dojindo Molecular Technologies, Inc.). WST-1 was added directly into the reaction mixture in a 96-well plate at a concentration of 200 µM. The standard assay buffer contained 200 µL of 100 mM sodium phosphate, pH 7.5, and concentrations of L-lysine and NAD(P)H both ranging from 0-10 mM. In assays that were performed with varying amounts of L-lysine, NADH and NADPH concentrations were kept constant at 3 mM and 5 mM respectively. In assays that were performed with varying amounts of NADH and NADPH, L-lysine concentrations were kept constant at either 0 or 3 mM. The

reaction (200 µL) was initiated by MbsG (2.0 µM) and incubated at 25 ^{o}C with orbital shaking at 750 rpm. After 10 minutes, the absorbance of the assay mixture was measured at 438 nm. The extinction coefficient of the formed WST-1 formazan (ε_{438} = 37,000 M^{-1} cm^{-1}) was used to calculate the amount of superoxide produced by MbsG.

2.10 Data analysis. Kinetic data were analyzed using the programs KaleidaGraph (Synergy, Reading, PA). Initial rate data were fit to the Michaelis-Menten equation to obtain k_{cat} and K_m values. The substrate inhibition constant for reduced nicotinamide dinucleotide and L-lysine (K_{is}) was determined by fitting the data to Equation 1.

$$v = \frac{k_{cat} S}{K_m + S + S^2 / K_{is}} \quad (1)$$

3. Results

3.1 Expression and Purification of MbsG. Expression of MbsG in pVP55A, which expressed the protein as a fusion to a His_8-tag, resulted in high amounts of recombinant protein that was completely insoluble (data not shown). To increase protein solubility, MbsG was expressed as a fusion to His_8-MBP in the pVP56K plasmid (Fig. 8.1A). This fusion protein remained in the supernatant after centrifugation. The fusion protein contained a His_8-tag at the N-terminus of MBP, which permitted the use of an IMAC column. The partially purified fusion protein was treated with His_8-TEV protease, which cleaves at the recognition sequence engineered between the C-terminus of MBP and the N-terminus of MbsG. In order to isolate MbsG from His_8-MBP and the His_8-TEV protease, the sample was loaded back onto the IMAC and the flow-through was collected. Since MbsG does not have affinity for the column, the His_8-MBP and His_8-TEV remained bound while MbsG eluted in the mobile phase. This protein was further purified using

a DEAE anion exchange chromatographic step (Fig. 8.1A). Upon purification of MbsG, a 36-fold increase in the specific activity was obtained. In general, a yield of 32 mg of homogeneous protein was obtained from 33 g of cell paste (Table 8.1). The purified MbsG was found to have a specific activity of 124.5 μmol min^{-1} mg^{-1}. The optical spectrum in Fig. 8.1B shows the presence of an FAD cofactor bound to the purified enzyme. Absorbance maxima can be seen at 380 nm and 450 nm with a "shoulder" occurring at wavelengths above 450 nm as the absorbance diminishes. The percent of flavin incorporation in MbsG was calculated to be 45% by comparing the concentration of purified MbsG based on the extinction coefficient of the FAD cofactor at 450 nm (12,800 M^{-1} cm^{-1}) and total protein concentration was determined using the Bradford dye-binding assay. High resolution MALDI-TOF mass spectra analysis in negative ion mode of the isolated flavin cofactor indicated a mass of 784.14 m/z, consistent with the mass of a deprotonated flavin adenine dinucleotide (data not shown). It is worth noting that MbsG is the first reported flavin-dependent N^6-lysine hydroxylase to be isolated in its active form with bound flavin [9-11].

Table 8.1 Summary of the purification of MbsG.

Sample	Total (mg)	Total (mL)	Activity (μmol min^{-1})	Specific activity (μmol min^{-1} mg^{-1})	Recovery (%)	Fold
Complete Lysate	3800	110	13200	3.5	100	1
Supernatant	2500	108	16800	6.7	127.3	1.9
Ni^{++}	100	75	7230	72.3	54.8	20.5
DEAE	32	35	3940	123.1	29.9	35.8

Rate values were calculated using the iodine oxidation assay at 25 ˚C with 100 mM sodium phosphate, pH 7.5, 3 mM NADH, and 3 mM L-lysine.
Protein quantities were calculated using the Bradford dye-binding assay (Bio-Rad) using Bovine Serum Albumin as a standard.

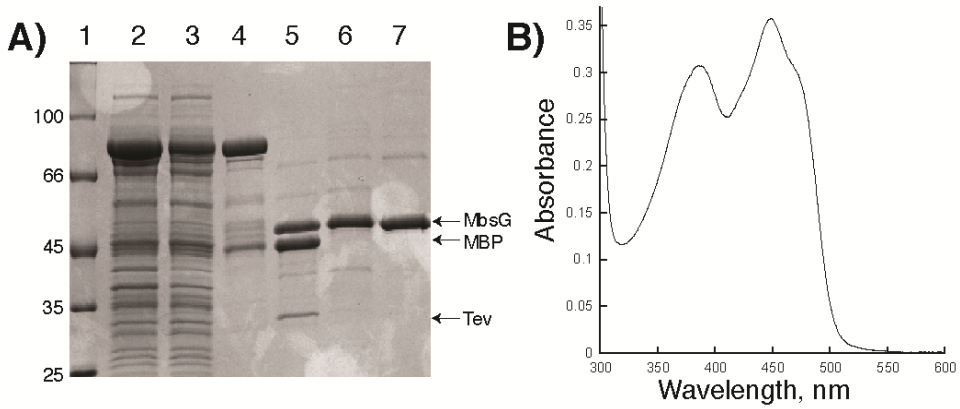

Figure 8.1 Summary of the purification of MbsG. A) 10% SDS-PAGE gel summarizing the purification of MbsG. 1. molecular weight markers. 2. complete lysate. 3. lysate supernatant. 4. IMAC. 5. sample after treatment with TEV protease. 6. second IMAC. 7. sample from DEAE chromatography. B) UV-visible spectrum of purified MbsG.

3.2 Kinetic parameters measuring N^6-hydroxylated lysine. The steady-state kinetic parameters of MbsG with respect to product formation are given in Table 8.2. MbsG was shown to utilize NADH and NADPH promiscuously as dinucleotides. k_{cat} values of 4.5 ± 0.1 min^{-1} and 4.2 ± 0.1 min^{-1} were determined with NADH and NADPH, respectively. K_m values of 0.260 ± 0.023 mM, 1.1 ± 0.2 mM, and 2.4 ± 0.4 mM were calculated for L-lysine, NADH, and NADPH, respectively (Table 8.2 and Fig. 8.2). These results suggest similarities in the first-order kinetic steps with these two reduced dinucleotides.

Table 8.2 Steady-state kinetic parameters of MbsG measuring product formation.

Parameter	**NADH**	**NADPH**
k_{cat} (min^{-1})	4.5 ± 0.1	4.2 ± 0.1
$K_{m,\ L\text{-}lys}$ (mM)	0.260 ± 0.023	0.209 ± 0.020
$K_{I,\ L\text{-}lys}$ (mM)	32 ± 4	42 ± 6
$k_{cat}/K_{m,\ L\text{-}lys}$ (min^{-1} mM^{-1})	26 ± 5	27 ± 5
$K_{m,\ dinucleotide}$ (mM)	1.1 ± 0.2	2.4 ± 0.4
$K_{I,\ dinucleotide}$ (mM)	9 ± 2	11 ± 2
$k_{cat}/K_{m,\ dinucleotide}$ (min^{-1} mM^{-1})	13 ± 4	4 ± 1

Conditions: 100 mM sodium phosphate at pH 7.5 and 25 ˚C.

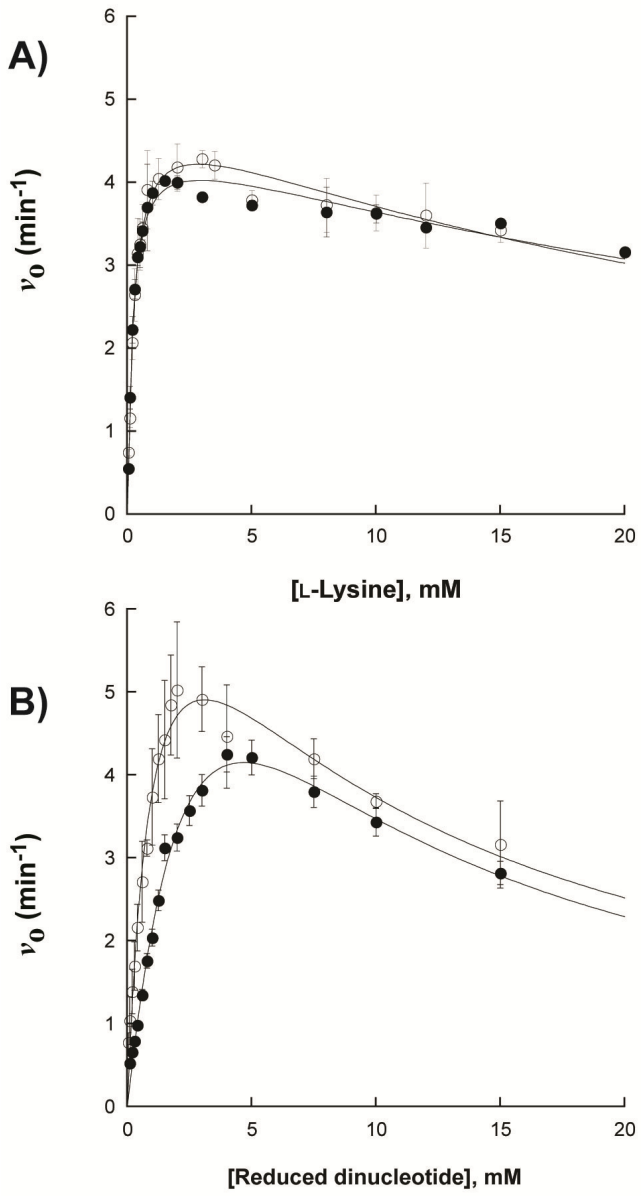

Figure 8.2 Steady state kinetics of MbsG measuring the formation of N^6-hydroxy-L-lysine. (A) N^6-hydroxy-L-lysine formation as a function of L-lysine in the presence of 3 mM NADH (○) or 5 mM NADPH (●). (B) N^6-hydroxy-L-lysine formation as a function of NADH (○) or NADPH (●) in the presence of 3 mM L-lysine.

The difference in the K_m values for reduced dinucleotides resulted in over a 3-fold higher catalytic efficiency (k_{cat}/K_m) with NADH compared to NADPH. A decrease in activity was observed at high concentrations of L-lysine and reduced nucleotide, suggesting substrate inhibition. The K_I value for L-lysine was determined to be 32 ± 4 mM, 9 ± 2 mM for NADH, and

11 ± 2 mM for NADPH. Intracellular concentrations of 410 μM for L-lysine, 83 μM for NADH, and 120 μM for NADPH have been reported in *E. coli* [12]. If we assume that similar values are present in *M. smegmatis,* then the inhibitory effects of both coenzyme and L-lysine are not physiologically relevant.

3.3 Kinetic parameters measuring oxygen consumption. Since the hydroxylation of L-lysine requires the utilization of a molecule of oxygen, MbsG activity can be monitored by measuring the changes in the concentration of oxygen over time. Steady-state kinetic traces of the rate of oxygen consumption are shown in Fig. 8.3 and the parameters are summarized in Table 8.3. With L-lysine at saturating (3 mM) concentrations, a k_{cat} value of 26 ± 0.4 min^{-1} was obtained when NADH was varied. Under the same conditions, when NADPH was the variable substrate, a k_{cat} value of 33 ± 2 min^{-1} was obtained. The k_{cat}/K_m value for NADH is four fold higher than for NADPH. This results from a much higher K_m value for NADPH. The relative promiscuity of either reduced dinucleotide with MbsG is a unique feature as in general, flavin-dependent monooxygenases are specific to, or prefer NADPH [13].

Table 8.3 Steady-state kinetic parameters of MbsG measured by oxygen consumption.

	NADH		**NADPH**	
	(-) L-lysine	(+) L-lysine, 3 mM	(-) L-lysine	(+) L-lysine, 3 mM
k_{cat}, min^{-1}	54 ± 1	26 ± 0.4	44 ± 4	33 ± 1
$K_{m,\ dinucleotide}$ mM	7 ± 0.2	2.4 ± 0.1	12 ± 1	12 ± 1
k_{cat}/K_m, min^{-1} mM	7.7 ± 0.1	11 ± 0.3	4 ± 0.3	2.8 ± 0.1

Conditions: 100 mM sodium phosphate at pH 7.5 and 25 ˚C.

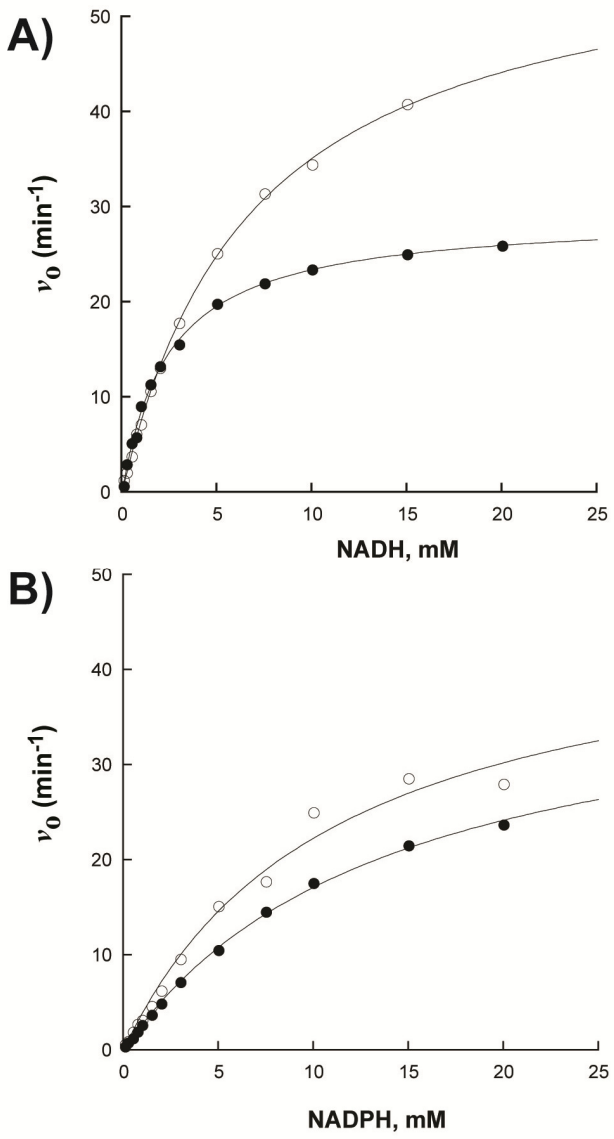

Figure 8.3 Steady state kinetics of MbsG measuring the consumption of oxygen. (A) Oxygen consumption as a function of NADH in the absence (○) or presence (●) of 3 mM L-lysine. (B) Oxygen consumption as a function of NADPH in the absence (○) or presence (●) of 3 mM L-lysine.

In the absence of L-lysine, MbsG displays a higher k_{cat} value, reacting with reduced dinucleotide and molecular oxygen. Under these conditions MbsG functions as a flavin oxidase. Upon the addition of 3 mM L-lysine, a slower k_{cat} value is measured. This shows that in the absence of substrate, MbsG reacts with reduced dinucleotide and is highly uncoupled, but in the

presence of substrate the reaction becomes more coupled and is driven towards product formation (N^6-hydroxy L-lysine).

3.4 Regulation by ligands. As previously mentioned, the oxidase activity of MbsG is regulated by the addition of L-lysine. Analogs of L-lysine were tested to determine if they also regulated the oxidase activity of MbsG. L-Lysine was found to regulate the activity most significantly, but 6-amino-1-hexanol was found to have similar effects (Fig. 8.4B). L-Arginine and L-ornithine were determined to affect the oxidase activity of MbsG as well, but to a lesser extent. One possible explanation for the observed decrease in the oxidase activity by these ligands is that they interact with the active site of MbsG and help stabilize the C4a-hydroperoxyflavin intermediate; however, hydroxylation was detected only with L-lysine.

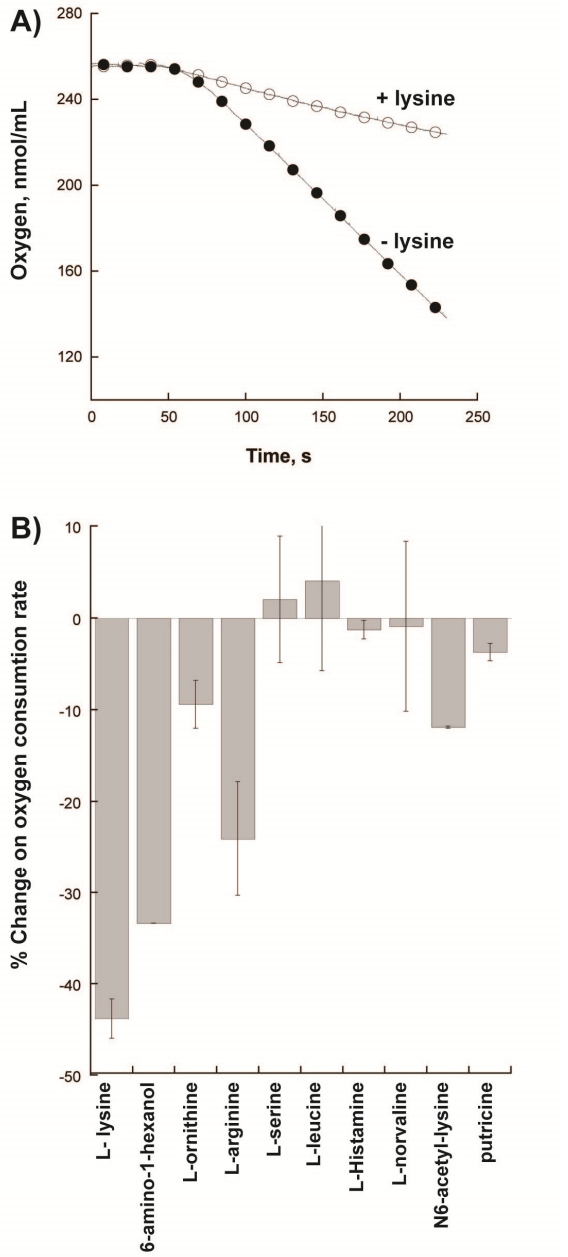

Figure 8.4 Effects of substrate or ligands on MbsG. A) Oxygen consumption assay traces in the absence (●) or presence of L-lysine (○). B) Regulation of MbsG oxidase activity by various ligands.

3.5 Hydrogen peroxide formation. The concentrations of hydrogen peroxide produced over a 10 minute time interval with varying concentrations of NAD(P)H or substrate are shown in Fig. 8.5. These graphs indicate that the enzymatic reaction of MbsG is significantly uncoupled as it

produces large amounts of hydrogen peroxide. In Fig. 8.5A, it can be seen that as the concentration of L-lysine is increased, the amount of hydrogen peroxide produced decreases, suggesting that the reaction becomes more coupled. This is consistent with the oxygen consumption assay results where, in the absence of L-lysine, MbsG rapidly consumes oxygen, but in the presence of L-lysine the oxidase activity is significantly decreased. In Figs. 8.5B and 8.5C, it can be seen that as the concentration of either reduced dinucleotide is increased, greater amounts of hydrogen peroxide are produced. The amount of hydrogen peroxide produced in the presence of NADPH is ~3-fold lower than the amount of hydrogen peroxide produced in the presence of NADH. Thus, with NADH, the formation of the hydro-peroxyflavin intermediate is much less stable. This is consistent with the higher oxidase activity of MbsG with NADH compared to NADPH in the absence of L-lysine (Table 8.3).

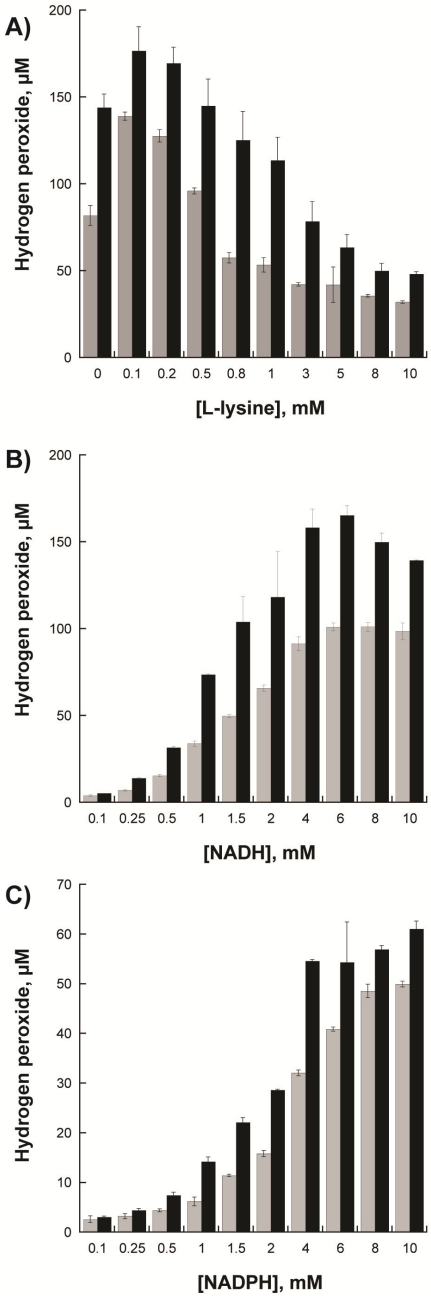

Figure 8.5 Hydrogen peroxide formation of MbsG. A) Hydrogen peroxide formation as a function of L-lysine in the presence of 3 mM NADH (solid bars) or 5 mM NADPH (gray bars). B) Hydrogen peroxide formation as a function of NADH in the presence (gray bar) or absence of 3 mM L-lysine (solid bars). C) Same as B but with NADPH.

3.6 Superoxide formation. The differences in the k_{cat} values obtained by directly measuring the formation of hydroxylated lysine (~5 min^{-1}) and the values measured by monitoring oxygen

concentration (~30 min^{-1}) show extensive uncoupling in this enzyme. Since a possible product of the reaction between reduced flavin and molecular oxygen is superoxide, we tested to see if this oxygen reactive species was also being produced by MbsG [13, 14]. Superoxide production was measured at saturating concentrations of either NADH (3 mM) or NADPH (5 mM). In the absence of L-lysine, ~100 μM of superoxide was detected. Varying the concentration of L-lysine reduced the amount of superoxide produced 2-fold (Fig. 8.6). Superoxide formation increased as the concentration of reduced dinucleotides were increased, while the presence of saturating amounts of L-lysine (3 mM) reduced the levels of superoxide produced. Similarly, as observed with the production of hydrogen peroxide, more superoxide was produced with NADH compared to NADPH in the absence of L-lysine (Fig. 8.6). However, using L-lysine and NADH concentration found in *E. coli* (400 μM L-lysine and 100 μM NADH), we determined that for every 20 ± 3 nmols of NADH oxidized, 15 ± 1 nmol superoxide, 6.8 ± 1 nmol hydrogen peroxide, and 1.8 ± 1 nmol N^6-hydroxy L-lysine were measured (data not shown)[12]. When 12 ± 1 nmol NADPH were consumed, 9.0 ± 0.2 nmol superoxide, 3 ± 0.5 nmol hydrogen peroxide, and 0.9 ± 0.3 nmol N^6-hydroxy L-lysine were formed. These data give a ~12% and ~7% coupling of under "physiological conditions" with NADH and NADPH, respectively.

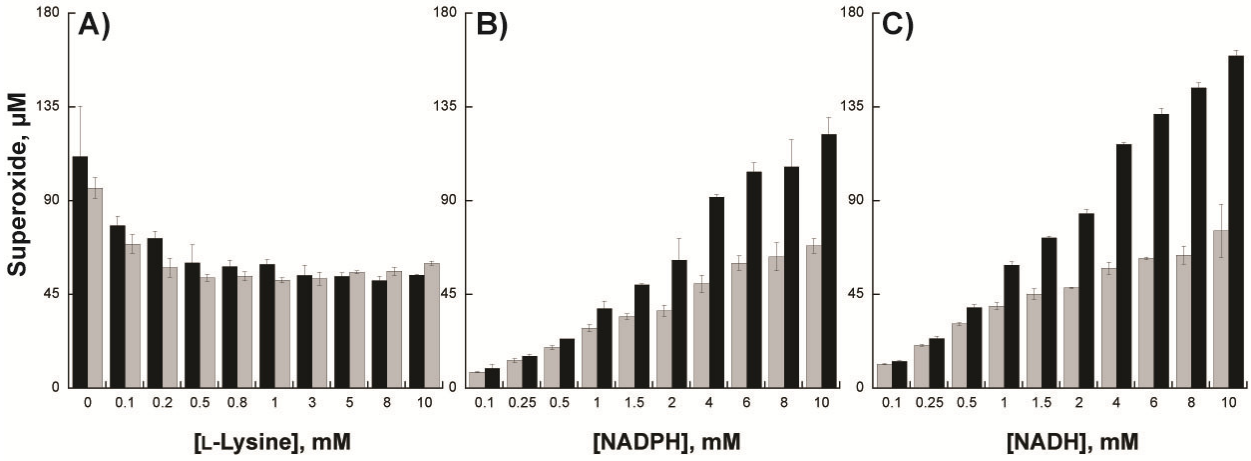

Figure 8.6 Quantification of superoxide produced by MbsG. The conditions are the same as those described in the legend of Fig. 8.5.

4. Discussion

Iron is an essential element for most living organisms. The availability of iron in mammals is too low for pathogenic bacteria, such as *Mycobacteria* spp., to establish an infection. To overcome this barrier, pathogens have developed strategies to acquire iron for their metabolic processes through the biosynthesis of low molecular weight (<1500 Da) metabolites with high iron affinity, termed siderophores. These molecules can scavenge for iron in hosts and support virulence.

MbsG is an N^6-lysine hydroxylase that operates through the use of a bound FAD cofactor. This enzyme is responsible for the formation of the hydroxamate functional group found on siderophores that gives these molecules their high affinity for iron. Studies of flavin-dependent *N*-hydroxylating enzymes have been limited, in part, to the fact that recombinant enzymes were isolated in the inactive form without the flavin cofactor [10, 11]. We show the expression and isolation of the recombinant form of this enzyme with a tightly bound FAD cofactor.

High levels of stable and active enzyme were isolated and detailed characterization was performed. MbsG, though, was found to express in lower amounts than a related enzyme, N^5-ornithine hydroxylase from *A. fumigatus* (SidA). The yield of soluble and active MbsG was ~3.5 mg/L of culture while the yield of SidA was 15 mg/L of culture [15]. MbsG was shown to be specific to L-lysine, as no other amino acids or L-lysine analogs were hydroxylated. The enzyme can effectively use NADPH or NADH as the reduced dinucleotide and, in the absence of L-lysine, this monooxygenase has chemistry similar to an oxidase, producing hydrogen peroxide and superoxide. This oxidase activity can be compared to another FAD-containing enzyme, xanthine oxidase, which produces large amounts of superoxide and hydrogen peroxide [16].

Interestingly, the activity of MbsG for product formation was determined to be slightly lower than that of SidA, to an extent of 6-fold. MbsG also exhibits a small preference to NADH as the dinucleotide while SidA prefers NADPH. These results suggest differences in the rate limiting step and a unique reduced dinucleotide preference among flavin monooxygenases. It is possible that since *Mycobacteria* spp. are slow growing organisms the low activity of this NMO suffices the bacterial siderophore biosynthesis.

The byproducts of the MbsG reaction, superoxide and hydrogen peroxide, would be expected to be deleterious to the bacteria *in vivo*. However, it is well established that *Mycobacteria* spp. contain a number of enzymes to reduce the amount of oxygen reactive species including, the Fe, Mn superoxide dismutase, SodA, the Cu, Zn superoxide dismutase, SodC, and catalase-peroxidase, KatG [19, 20]. The function of these enzymes is expected to minimize any cellular damage produced by the uncoupling reaction of MbsG.

The catalytic cycle of flavin monooxygenases includes the reaction with NAD(P)H to reduce the flavin cofactor. Subsequent reaction with molecular oxygen leads to the formation of

a C4a-hydroperoxyflavin, which is required for hydroxylation [13, 14]. Stabilization of this intermediate is key to ensure coupling of the reaction. The mechanism of stabilization of oxygenated flavin intermediates in SidA is shown to involve interaction of $NADP^+$. In the absence of L-ornithine, $NADP^+$ stabilizes the flavin intermediate preventing the formation of hydrogen peroxide. Rapid turnover is observed only when L-ornithine is present [15]. This is markedly different in MbsG where rapid oxidase turnover occurs in the absence of L-lysine, but is decreased when L-lysine is introduced to the system. SidA is capable of reacting with NADPH in the absence of L-ornithine which reduces the oxidized flavin cofactor [17]. This shows that L-ornithine is needed for oxygen reactivity in SidA, but is not necessary in the reductive half-reaction. This is distinct from MbsG where L-lysine does not control oxygen reactivity. Similar mechanisms have also been shown for other flavin monooxygenases such as the flavin-monooxygenase from *Methylophaga* sp. strain SK1, and the phenylacetone monooxygenase from *Thermobifida fusca* [21, 22].

MbsG is shown to operate quite differently from another FAD containing hydroxylase, *p*-hydroxybenzoate hydroxylase (PHBH). PHBH forms a ternary complex with its substrate, *p*-hydroxybenzoate, and NADPH [18]. This complex then proceeds to react with molecular oxygen and form product, 3,4-dihydroxybenzoate. Binding of *p*-hydroxybenzoate enhances the rate of flavin reduction in PHBH by 1.4×10^5 fold. This is in contrast to MbsG where the rate of oxidation NAD(P)H is increased in the absence of its corresponding substrate, L-lysine.

The mechanism of stabilization of the C4a-hydroperoxyflavin in MbsG does not only depend on interactions with $NADP^+$ or NAD^+, since high levels of oxidase activity are observed when the enzyme reacts with reduced dinucleotides alone. The results presented suggest that the C4a-hydroperoxyflavin in MbsG that is regulated by the binding of the substrate, L-lysine. This

binding modulates the activity of the enzyme converting it from an oxidase to a monooxygenase (Scheme 8.2). This mechanism represents a novel mechanism of regulation of activity among flavin monooxygenases.

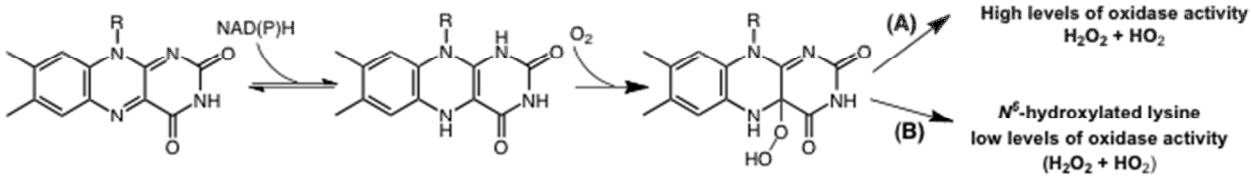

Scheme 8.2 Substrate regulation mechanism of MbsG. A) High levels of oxidase activity observed in the absence of L-lysine. B) In the presence of L-lysine the oxidase activity of MbsG decrease and the monooxygenase activity increased.

5. Acknowledgements

We thank Drs. Rich Helm and Keith Ray for the MS analysis. We would also like to thank Wyatt Chocklett for help in the purification of *Ms* MbsG. This work was supported, in part, by a grant from the National Science Foundation MCB-1021384, the Allan T. Gwathmey Chemistry award from the Virginia Academy of Sciences, and the Ralph Powe Junior Faculty Enhancement award from the Oak Ridge Associated Universities.

6. References

1. Fischbach, M.A., et al., *How pathogenic bacteria evade mammalian sabotage in the battle for iron.* Nat Chem Biol, 2006. **2**(3): p. 132-8.
2. Frederick, R.E., J.A. Mayfield, and J.L. DuBois, *Iron trafficking as an antimicrobial target.* Biometals, 2009. **22**(4): p. 583-93.
3. Wandersman, C. and P. Delepelaire, *Bacterial iron sources: from siderophores to hemophores.* Annu Rev Microbiol, 2004. **58**: p. 611-47.
4. Hider, R.C. and X. Kong, *Chemistry and biology of siderophores.* Nat Prod Rep, 2010. **27**(5): p. 637-57.
5. Sassetti, C.M., D.H. Boyd, and E.J. Rubin, *Genes required for mycobacterial growth defined by high density mutagenesis.* Mol Microbiol, 2003. **48**(1): p. 77-84.

6. Quadri, L.E., et al., *Identification of a Mycobacterium tuberculosis gene cluster encoding the biosynthetic enzymes for assembly of the virulence-conferring siderophore mycobactin.* Chem Biol, 1998. **5**(11): p. 631-45.
7. Chapman, S.K. and G.A. Reid, *Flavoprotein protocols*. Methods in molecular biology. 1999, Totowa, N.J.: Humana Press. xii, 256 p.
8. Csaky, T., *On the Estimation of Bound Hydroxylamine in Biological Materials.* Acta Chem Scand, 1948(2): p. 450-454.
9. Dick, S., et al., *Lysine: N6-hydroxylase: stability and interaction with ligands.* J Protein Chem, 1999. **18**(8): p. 893-903.
10. Thariath, A.M., et al., *Physico-chemical characterization of a recombinant cytoplasmic form of lysine: N6-hydroxylase.* Biochim Biophys Acta, 1993. **1203**(1): p. 27-35.
11. Stehr, M., et al., *Studies with lysine N6-hydroxylase. Effect of a mutation in the assumed FAD binding site on coenzyme affinities and on lysine hydroxylating activity.* Biol Chem, 1999. **380**(1): p. 47-54.
12. Bennett, B.D., et al., *Absolute metabolite concentrations and implied enzyme active site occupancy in Escherichia coli.* Nat Chem Biol, 2009. **5**(8): p. 593-9.
13. van Berkel, W.J., N.M. Kamerbeek, and M.W. Fraaije, *Flavoprotein monooxygenases, a diverse class of oxidative biocatalysts.* J Biotechnol, 2006. **124**(4): p. 670-89.
14. Massey, V., *Activation of molecular oxygen by flavins and flavoproteins.* J Biol Chem, 1994. **269**(36): p. 22459-62.
15. Chocklett, S.W. and P. Sobrado, *Aspergillus fumigatus SidA is a highly specific ornithine hydroxylase with bound flavin cofactor.* Biochemistry, 2010. **49**(31): p. 6777-83.
16. McCord, J.M. and I. Fridovich, *The reduction of cytochrome c by milk xanthine oxidase.* J Biol Chem, 1968. **243**(21): p. 5753-60.
17. Mayfield, J.A., et al., *Comprehensive spectroscopic, steady state, and transient kinetic studies of a representative siderophore-associated flavin monooxygenase.* J Biol Chem, 2010. **285**(40): p. 30375-88.
18. Husain, M. and V. Massey, *Kinetic studies on the reaction of p-hydroxybenzoate hydroxylase. Agreement of steady state and rapid reaction data.* J Biol Chem, 1979. **254**(14): p. 6657-66.
19. Harth, G. and M.A. Horwitz, *Export of recombinant Mycobacterium tuberculosis superoxide dismutase is dependent upon both information in the protein and mycobacterial export machinery. A model for studying export of leaderless proteins by pathogenic mycobacteria.* J Biol Chem, 1999. **274**(7): p. 4281-92.
20. Piddington, D.L., et al., *Cu,Zn superoxide dismutase of Mycobacterium tuberculosis contributes to survival in activated macrophages that are generating an oxidative burst.* Infect Immun, 2001. **69**(8): p. 4980-7.
21. Malito, E., et al., *Crystal structure of a Baeyer-Villiger monooxygenase.* Proc Natl Acad Sci U S A, 2004. **101**(36): p. 13157-62.
22. Alfieri, A., et al., *Revealing the moonlighting role of NADP in the structure of a flavin-containing monooxygenase.* Proc Natl Acad Sci U S A, 2008. **105**(18): p. 6572-7.

CHAPTER 9

Mechanistic studies on the flavin-dependent N^6-lysine monooxygenase MbsG reveal an unusual control for catalysis

Reprinted with permission from Archives of Biochemistry and Biophysics, Robinson, R. M., Rodriguez, P. J., and Sobrado, P. "Mechanistic studies on the flavin-dependent N^6-lysine monooxygenase MbsG reveal an unusual control for catalysis" *Archives of Biochemistry and Biophysics*. 2014 (ID 10.1016/j.abb.2014.04.006) Vols 550-551: 58-66.

Author Contributions:
Reeder M. Robinson performed all the research except the experiments mentioned below, and helped write the article.

Pedro J. Rodriguez helped with some of the steady-state assays.

Pablo Sobrado oversaw and directed the research, and helped write the article.

Abstract

The mechanism of *Mycobacterium smegmatis* G (MbsG), a flavin-dependent L-lysine monooxygenase, was investigated under steady-state and rapid reaction conditions using primary and solvent kinetic isotope effects, substrate analogs, pH and solvent viscosity effects as mechanistic probes. The results suggest that L-lysine binds before NAD(P)H, which leads to a decrease in the rate constant for flavin reduction. L-lysine binding has no effect on the rate of flavin oxidation, which occurs in a one-step process without the observation of a C4a-hydroperoxyflavin intermediate. Similar effects were determined with several substrate analogs. Flavin oxidation is pH independent while the k_{cat}/K_m and k_{red}/K_D pH profiles for NAD(P)H exhibit single pK_a value of ~6.0, with increasing activity as the pH decrease. At lower pH, the enzyme becomes more uncoupled, producing more hydrogen peroxide and superoxide. Hydride transfer is partially rate-limiting at neutral pH and becomes more rate-limiting at low pH. An inverse

solvent viscosity effect on k_{cat}/K_m for NAD(P)H was observed at neutral pH whereas a normal solvent viscosity effect was observed at lower pH. Together, the results indicate a unique mechanism where a rate-limiting and pH-sensitive conformational change occurs in the reductive half-reaction, which affects the efficiency of lysine hydroxylation.

1. Introduction

Iron is an essential nutrient required by most living organisms [1]. However, Fe^{III} is very insoluble, forming iron-hydroxide complexes [2]. This, along with iron sequestration by iron-binding proteins in human serum, presents a barrier that invading microbes must overcome in order to establish infection [3, 4]. Many microbes have developed an elegant solution to this problem through the synthesis and secretion of low molecular-weight compounds called siderophores. Siderophores are structurally diverse and contain a number of functional groups, including catechols, phenols, hydroxamates, and carboxylates, which coordinate to chelate Fe^{III} [5, 6]. Siderophores have been shown to be essential for virulence in a number of human pathogens including *Aspergillus fumigatus*, *Pseudomonas aeruginosa*, and *Mycobacterium tuberculosis* [7-10]. Because of their important role in pathogenesis and the absence of human homologs, enzymes involved in the biosynthesis of siderophores are promising drug targets.

One group of enzymes critical for hydroxamate-containing siderophore biosynthesis is the microbial *N*-hydroxylating monooxygenases (NMOs). These are flavin adenine dinucleotide (FAD) dependent enzymes that selectively catalyze the hydroxylation of the soft nucleophilic terminal amine groups of L-ornithine, L-lysine, or several aliphatic diamines [11-16]. NMOs are typically highly coupled, selective for NADPH, and stabilize long-lived C4a-hydroperoxyflavin intermediates [17-20]. *Mycobacterium smegmatis* G (MbsG) is an L-lysine monooxygenase involved in the biosynthesis of the siderophore mycobactin (Scheme 9.1). This enzyme is a

homolog of the L-lysine monooxygenase from *Mycobacterium tuberculosis* MbtG (~75% identity), which is essential for virulence [9, 10]. Previous biochemical characterization has shown that MbsG does not share the same characteristics as other NMOs [21]. MbsG is non-specific for reduced pyridine dinucleotide, as it can utilize both NADH and NADPH with similar catalytic efficiency. While this enzyme hydroxylates L-lysine, it is highly uncoupled, producing unusually high levels of superoxide and hydrogen peroxide. To gain insight into the mechanism of action of this unique flavin monooxygenase, we investigated the reaction with both NAD(P)H and molecular oxygen in the stopped-flow spectrophotometer. Furthermore, the mechanism of MbsG was probed using primary and solvent kinetic isotope effects, substrate analogs, pH, and viscosity effects. Together, the results suggest the presence of a rate-limiting conformational change that is sensitive to pH and solvent viscosity. This conformational change, which is coupled to flavin reduction, is modulated by L-lysine binding. We propose that this represents an unusual mechanism of regulation among flavin monooxygenases.

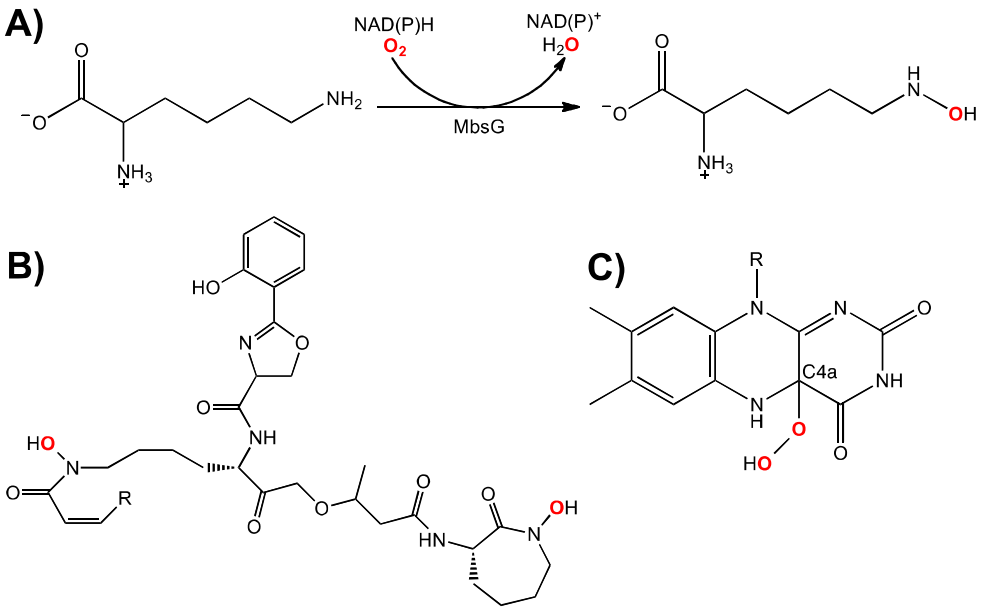

Scheme 9.1 (A) NAD(P)H- and oxygen-dependent reaction catalyzed by MbsG. (B) Structure of the siderophore mycobactin. C) Structure of the C4a-hydroperoxyflavin. This intermediate is the hydroxylating species that is commonly stabilized by Class B flavin-monooxygenases.

2. Materials and Methods

2.1 Materials. L-Lysine, L-ornithine, 6-amino-1-hexanol, L-arginine, putrescine, cadaverine, NADH, NADPH, NAD^+, $NADP^+$, glycerol, buffers, and salts were purchased from Fisher Scientific (Pittsburgh, PA). WST-1 was purchased from Dojindo Molecular Technologies, Inc. (Rockville, MD). Glucose oxidase was purchased from MP Biomedical (Solon, OH). MbsG was expressed and purified as described previously [21].

2.2 Steady-state activity assays. The steady-state reaction catalyzed by MbsG was monitored either by measuring the concentration of oxygen consumed in the reactions or by measuring the concentration of L-N^6-hydroxy-lysine produced. In addition, hydrogen peroxide and superoxide, produced as a result of the uncoupling of the reaction, were also quantified as previously described [21]. Oxygen consumption was monitored using a Hansatech Oxygraph (Norfolk,

U.K.) and hydroxylated lysine was quantified by a variation of the Csaky iodine oxidation assay following procedures previously reported [21, 22]. These assays were performed in 100 mM sodium phosphate, pH 7.5, at 25 °C.

2.3 Monitoring flavin reduction. Flavin reduction by NAD(P)H was performed under anaerobic conditions on an Applied Photophysics SX20 stopped-flow spectrophotometer (Leatherhead, UK) housed in a Coy glove box (Grass Lake, MI). Reactions were performed at 25 ºC in 100 mM sodium phosphate, pH 7.5. Buffer was made anaerobic by 5 cycles of vacuum and argon flushing in 20 min intervals with constant stirring. Oxygen was removed from the stopped-flow by flushing with 1 mL of anaerobic 100 mM sodium acetate, pH 5.0, containing 100 mM glucose and 100 µg/mL glucose oxidase Type-X. This solution remained in the stopped-flow overnight to completely remove any residual oxygen. MbsG was made anaerobic by degassing with five, 20 min cycles of vacuum and argon flushing. Oxidized MbsG (15 µM after mixing) was mixed with various concentrations of NAD(P)H (0.25 – 7.5 mM after mixing) and monitored with a photodiode array spectrophotometer until the enzyme was fully reduced. This experiment was repeated in the presence of L-lysine at a final concentration of 3 mM after mixing.

2.4 Monitoring flavin oxidation. Flavin oxidation of MbsG was studied by first reducing the enzyme with near stoichiometric concentrations of NADH by mixing 30 µM of MbsG with 1.5-fold (45 µM) NADH. This was allowed to reduce in the glove box for 45 minutes under anaerobic conditions. Double mixing on the stopped-flow spectrophotometer was unable to be utilized for this experiment due to the slow reduction of MbsG with NADH at stoichiometric concentrations. Oxidation reactions were performed at 25 ºC in 100 mM sodium phosphate, pH

7.5. Oxygen saturated buffer (1.2 mM) was obtained by bubbling 100% oxygen gas into a closed vial for 30 minutes at 25 ºC [23]. Various concentrations of oxygen were obtained by mixing 100% oxygen saturated buffer with anaerobic buffer. Reduced MbsG (15 µM after mixing) was mixed with various concentrations of oxygenated buffer (100 – 600 µM after mixing). The reaction was monitored with a photodiode array spectrophotometer until the enzyme was fully oxidized. This experiment was repeated with L-lysine present at a final concentration of 3 mM after mixing.

2.5 Synthesis of deuterated coenzymes. 4-pro-R-4^{2}H-NADPH was synthesized by the method of Jeong and *4-pro-R*-4^{2}H-NADH was synthesized by the method of Sucharitakul [24, 25]. *4-pro-S*-4^{2}H-NADH and *4-pro-S*-4^{2}H-NADPH were synthesized by the method of Viola *et al* [26], with minor modifications as previously described [27]. NADH and NADPH were synthesized by the same methods as controls.

2.6 pL profile and solvent kinetic isotope effects. The effect of pH on the activity of MbsG was determined under steady-state conditions following oxygen consumption, lysine hydroxylation, and hydrogen peroxide and superoxide formation. MbsG was used at a concentration of 2 µM for all steady-state assays. The effects on enzymatic activity were monitored between pH values 5.4 and 9.0 as MbsG was found to be stable in this pH range. For experiments at pH 5.4 - 7.4, a citrate/phosphate buffering system was used and prepared by mixing different ratios of 100 mM citric acid and 200 mM sodium phosphate [28]. At pH 7.5 - 8.0, 100 mM sodium phosphate was used, and between pH values 8.5 and 9.0, 100 mM sodium pyrophosphate was used. Tests were performed to ensure that the activity of MbsG did not change between the different buffers. For

pH studies using the stopped-flow spectrophotometer, MbsG was stored in 10 mM sodium phosphate, pH 7.5, and mixed in the stopped-flow spectrophotometer with the appropriate buffer to rapidly equilibrate to the desired pH value. To measure the solvent kinetic isotope effect in the pL-independent region, the pD profile was also determined in the same buffer solutions made in 99% D_2O (all pD values were calculated by adding 0.4 to the value on the pH meter, which is the variation from the change in the equilibrium on a hydrogen-selective glass electrode) [29]. All solutions were checked for their proper pL values with a Fisher Scientific Accumet AB15+ Basic pH meter.

2.7 Effects of ligand binding. The effect of different ligands on activity was monitored by following the rate of oxygen consumption. 10 mM each of L-lysine, L-ornithine, L-arginine, 6-amino-1-hexanol, putrescine, or cadaverine were present with 5 mM NADH in 100 mM sodium phosphate pH 7.5. The reaction was initiated by addition of MbsG at a final concentration of 2 µM. Formation of hydroxylated products were also tested for all of these ligands using the Csaky assay in the presence of 5 mM NADH and 10 mM ligand with 2 µM MbsG incubated for 10 minutes. To determine if the presence of the these ligands influenced the rate constant for flavin reduction, oxidized MbsG (15 µM after mixing) was mixed in the stopped-flow spectrophotometer with various concentrations of NADH (1 – 5 mM after mixing) and either no ligand, or 10 mM (after mixing) of the tested ligands. The characteristic decrease at 452 nm for flavin reduction was recorded in the stopped-flow spectrophotometer. Effects of pre-incubating L-lysine with MbsG before mixing with NADH were also performed by incubating 10 mM L-lysine with oxidized MbsG for ~5 minutes before determining the reduction rates at various concentrations of NADH containing 10 mM L-lysine present, to keep the concentration of L-

lysine constant after mixing. The effect of L-lysine and analog binding on the rate of flavin oxidation was also investigated in the stopped-flow spectrophotometer. In these experiments, reduced MbsG (15 μM after mixing) was mixed with oxygenated buffer (300 μM after mixing) with either no ligand or 10 mM of the tested ligands. When L-lysine was pre-equilibrated with MbsG, 10 mM L-lysine was incubated with 30 μM reduced MbsG for ~5 minutes (concentrations before mixing) and the MbsG: L-lysine solution was mixed with oxygen and L-lysine, present at 300 μM and 10 mM after mixing, respectively.

2.8 Solvent viscosity effects. The effects of solvent viscosity on the rate of oxygen consumption were determined in either 100 mM sodium phosphate, pH 7.5, or in citrate/phosphate, pH 5.6, at 25 ºC using glycerol as the viscosigen. The values for the relative glycerol viscosities (η_{rel}) were obtained from Weast [30].

2.9 Data analysis. All data were fit using KaleidaGraph (Synergy Software, Reading, PA). The rates of reduction at different concentrations of NAD(P)H were determined by fitting the decrease in absorbance at 452 nm to Eq. (1) which describes a single exponential decay equation. The resulting k_{obs} values were plotted as a function of NAD(P)H concentration. These data were fit using Eq. (2) in order to determine k_{red} and K_D values.

$$v = c + ae^{-(k \times t)} \quad (1)$$

$$k_{obs} = \frac{k_{red} \times [S]}{K_D + [S]} \quad (2)$$

For flavin oxidation studies, the increase in absorbance at 452 nm was fit to Eq. (3), which describes a single exponential rise equation. The resulting k_{obs} values were plotted as a

function of oxygen concentration. These data were fit to a linear equation to determine the bimolecular rate constant of flavin oxidation (k_{ox}).

$$v = c + a(1 - e^{-(k \times t)}) \quad (3)$$

The k_{cat}/K_m and k_{red}/K_D pL profiles were fit to Eq. (4), which describes a curve with a slope of 1 at low pL (pH or pD) and an independent region at high pL values.

$$\log(k) = \log[k(\text{lim}) \times (1 + 10^{pK_a - pL})] \quad (4)$$

3. Results

3.1 Flavin reduction. The rate constants for flavin reduction (k_{red}) were determined by mixing oxidized MbsG with varying amounts of NAD(P)H in both the presence and absence of 3 mM L-lysine in the stopped-flow spectrophotometer under anaerobic conditions at pH 7.5. The decrease in absorbance at 452 nm best fit to Eq. (1), which describes a single exponential decay (Figs. 9.1A and 9.1B). Fig. 9.1C shows the dependence of flavin reduction as a function of increasing concentrations of NADH, in both the absence and presence of 3 mM L-lysine (the data for NADPH is shown in Fig. 9.2). The results are summarized in Table 9.1. The k_{red} value for NADH is slightly higher than for NADPH in the absence of L-lysine. In the presence of L-lysine, the k_{red} value decreases to ~0.4 s^{-1} for both coenzymes. The K_D value does not change for NADPH in the presence of L-lysine; however, it decreases 2-fold for NADH. The decrease in the k_{red} value in the presence of L-lysine is similar to the decrease in steady-state k_{cat} values determined by measuring rates of oxygen consumption (Table 9.1) [21].

Table 9.1 Pre-steady state and steady-state kinetic parameters for MbsG.

	NADH		NADPH	
	no L-lysine	3 mM L-lysine	no L-lysine	3 mM L-lysine
$^{a}k_{red}$ (s^{-1})	0.82 ± 0.08	0.46 ± 0.02	0.54 ± 0.07	0.44 ± 0.04
$^{a}K_D$ (mM)	6.3 ± 0.9	3.7 ± 0.4	6.0 ± 1.4	6.2 ± 1.1
$^{a}k_{red}/K_D$ (M^{-1} s^{-1})	131 ± 23	125 ± 6	90 ± 10	71 ± 6
$^{b}k_{cat}$ (s^{-1})	0.90 ± 0.02	0.43 ± 0.01	0.73 ± 0.07	0.55 ± 0.02
$^{b}K_m$ (mM)	7.0 ± 0.2	2.4 ± 0.1	12 ± 1	12 ± 1
$^{b}k_{cat}/K_m$ ($M^{-1}s^{-1}$)	128 ± 2	183 ± 5	67 ± 5	47 ± 2

Conditions: Reactions were performed in 100 mM sodium phosphate at pH 7.5 and 25 ºC. [a]Kinetic parameters of flavin reduction. [b]Steady-state kinetic parameters determined by monitoring oxygen consumption [21].

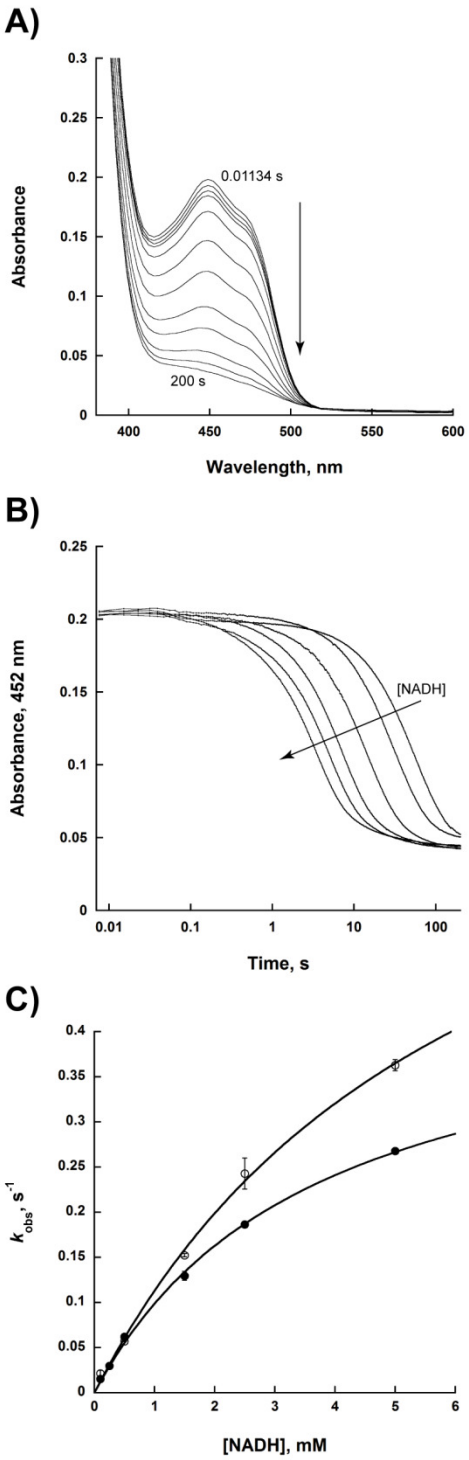

Figure 9.1 Reaction of oxidized MbsG with NADH. (A) Time resolved flavin reduction spectra with 500 µM NADH and 3 mM L-lysine collected over 200 seconds. (B) Traces of flavin reduction at 452 nm with 0.1 – 5 mM NADH and 3 mM L-lysine. The absorbance changes at 452 nm were fit to Eq. 1. (C) k_{obs} values of flavin reduction as a function of NADH in the absence (○) or presence (●) of 3 mM L-lysine. The data was fit to Eq. 2.

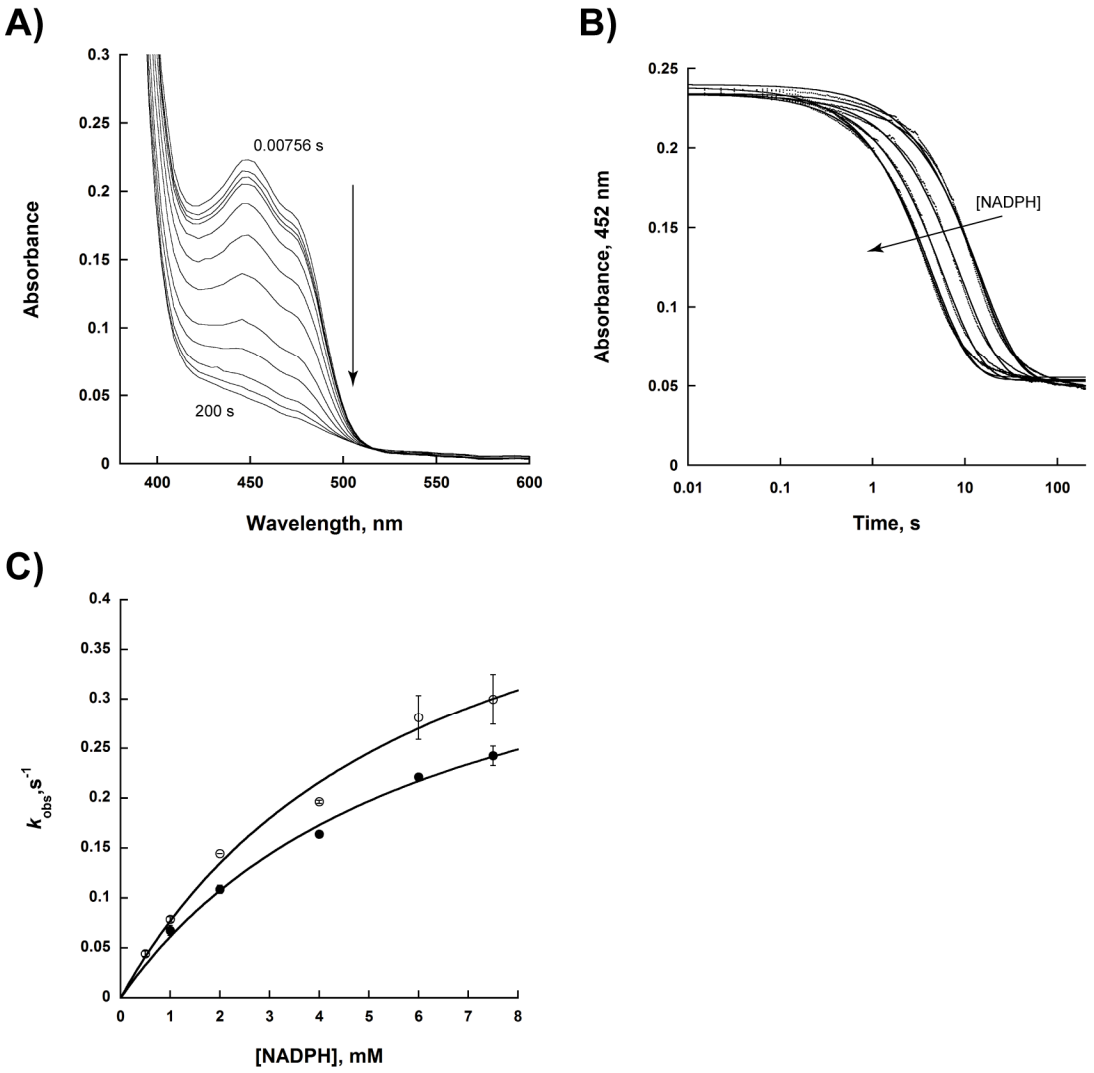

Figure 9.2 Reaction of oxidized MbsG with NADPH. (A) Time resolved flavin reduction spectra with 500 μM NADPH and 3 mM L-lysine collected over 200 seconds. (B) Traces of flavin reduction at 452 nm with 0.5 – 7.5 mM NADPH and 3 mM L-lysine. The absorbance changes at 452 nm were fit to a single exponential decay equation (Eq. 1). (C) k_{obs} values of flavin reduction as a function of NADPH in the absence (○) or presence (●) of 3 mM L-lysine.

3.2 Flavin oxidation. The rates of flavin oxidation were determined by mixing varying concentrations of oxygen with reduced MbsG in both the presence and absence of L-lysine. The reaction of reduced MbsG with oxygen occurs in a one-step process, with no detectable intermediates (Figs. 9.3A and 9.3B). In Fig. 9.3B, the increase in absorbance at 452 nm best fit to Eq. (3), which describes a single exponential rise. The observed rates of flavin oxidation were

plotted as a function of molecular oxygen concentration (Fig. 9.3C). The bimolecular rate constant of flavin oxidation is $3.64 \times 10^3 \pm 0.06$ $M^{-1}s^{-1}$ in the absence of L-lysine and $3.1 \times 10^3 \pm 0.2$ $M^{-1}s^{-1}$ in presence of 3 mM L-lysine.

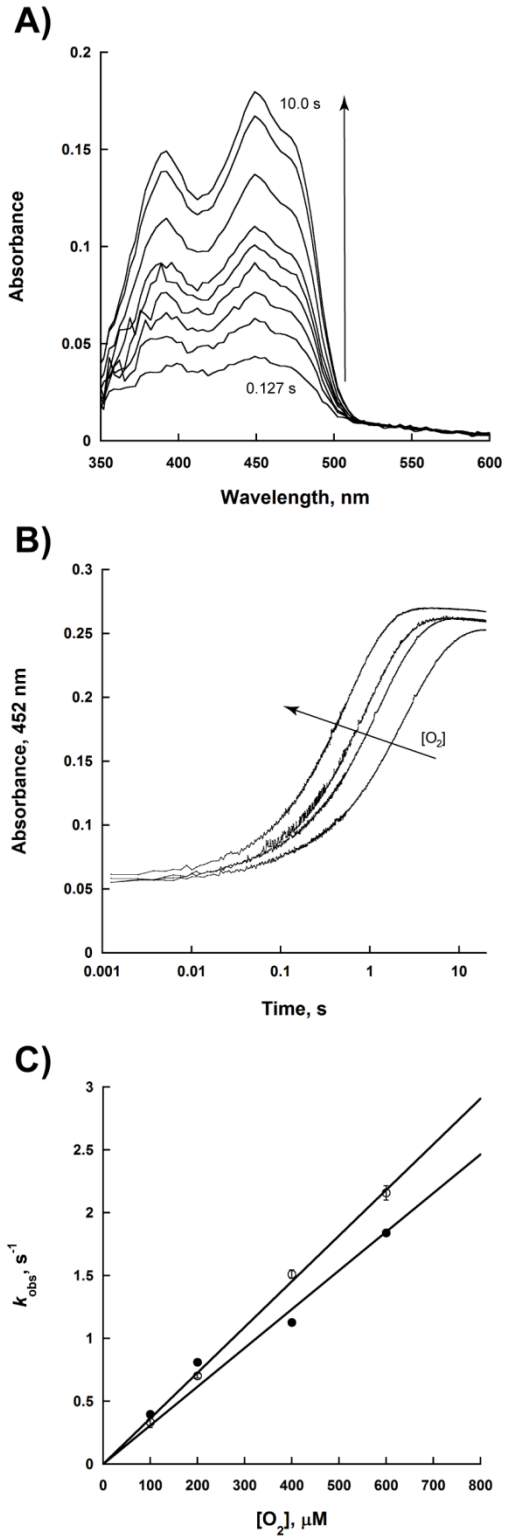

Figure 9.3 Reaction of reduced MbsG with O_2. (A) Time resolved flavin oxidation spectra with 300 µM O_2 over 10 seconds. (B) Traces of flavin oxidation at 452 nm with 100 – 600 µM O_2 and 3 mM L-lysine. The absorbance changes at 452 nm were fit to Eq. 3. (C) k_{obs} values of flavin oxidation as a function of molecular oxygen in the absence (○) or presence (●) of 3 mM L-lysine.

3.3 Primary kinetic isotope effects. The steady-state primary kinetic isotope effect (KIE) was measured to determine if hydride transfer is rate-limiting using both *4-pro-R*-4^{2}H-NADH and *4-pro-R*-4^{2}H-NADPH (Fig. 9.4) at saturating concentrations of L-lysine (3 mM). $^{D}k_{cat}$ values of 1.6 ± 0.1 for *4-pro-R*-4^{2}H-NADH and 1.3 ± 0.2 for *4-pro-R*-4^{2}H-NADPH were determined at pH 7.5. $^{D}(k_{cat}/K_m)$ values at pH 7.5 of 1.4 ± 0.1 and 1.7 ± 0.1 were also obtained for *4-pro-R*-4^{2}H-NADH and *4-pro-R*-4^{2}H-NADPH, respectively. At pH 5.6, the K_M value for NADH is very high and saturation was not achieved at the highest concentration tested (7.5 mM). Thus, the k_{cat} value could not be accurately determined, which prevented analysis of the KIE on this kinetic constant (Fig. 9.4C). However, the k_{cat}/K_m could be accurately determined allowing the determination of a higher $^{D}(k_{cat}/K_m)$ value for *4-pro-R*-4^{2}H-NADH at pH 5.6 of 2.0 ± 0.1. Assays with *4-pro-S*-4^{2}H-NADH and *4-pro-S*-4^{2}H-NADPH resulted in KIE values not different from unity at pH 7.5 (data not shown).

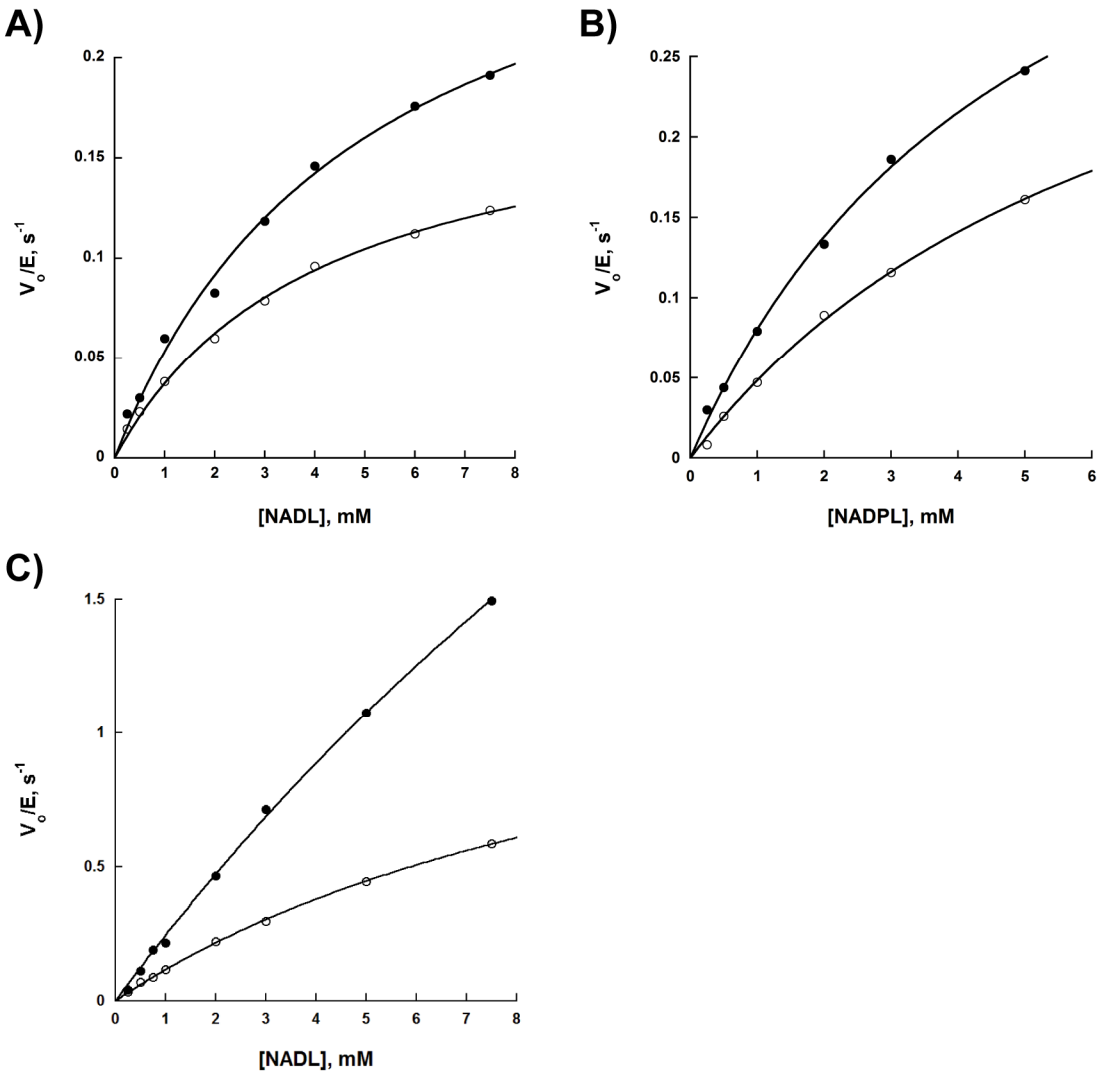

Figure 9.4 Primary kinetic isotope effects of MbsG. (A) Oxygen consumption as a function of NADH (●) or *pro-R*-4^{2}H-NADH (○) in the presence of 3 mM L-lysine at pH 7.5. (B) Oxygen consumption as a function of NADPH (●) or *pro-R*-4^{2}H-NADPH (○) in the presence of 3 mM L-lysine at pH 7.5. (C) Oxygen consumption as a function of NADH (●) or *pro-R*-4^{2}H-NADH (○) in the presence of 3 mM L-lysine at pH 5.6.

3.4 pH profile. The effect of pH on the activity of MbG was determined by following the rate of oxygen consumption. At lower pH values, the rate of oxygen consumption is linear as a function of NADH concentration (data not shown). Coenzyme saturation was not achieved even at 10 mM coenzyme. Thus, the k_{cat} values could not be accurately determined (data not shown). k_{cat}/K_m for NAD(P)H increases at low pH and is relatively unchanged at pH values greater than 7.5. A

pK_a value of 5.9 ± 0.1 was calculated from the k_{cat}/K_m pH profile (Fig. 9.5A closed circles). The pH dependence of k_{red} with NADH was also determined. Here, a single ionizable group with a pK_a value of 6.1 ± 0.1 was determined for the k_{red}/K_D pH profile. This pK_a value is very similar to the pK_a value determined in the oxygen consumption assay under steady-state conditions (Fig. 9.6A). Similar pH experiments with NADPH yielded consistent results (data not shown). The bimolecular rate constant for flavin oxidation did not significantly change as a function of pH, indicating that flavin oxidation is independent of pH (Fig. 9.6B). Similarly, formation of hydroxylated lysine showed very little change as a function of pH (Fig. 9.7A). In contrast, the rates of superoxide and hydrogen peroxide formation increased with decreasing pH (Fig. 9.7B).

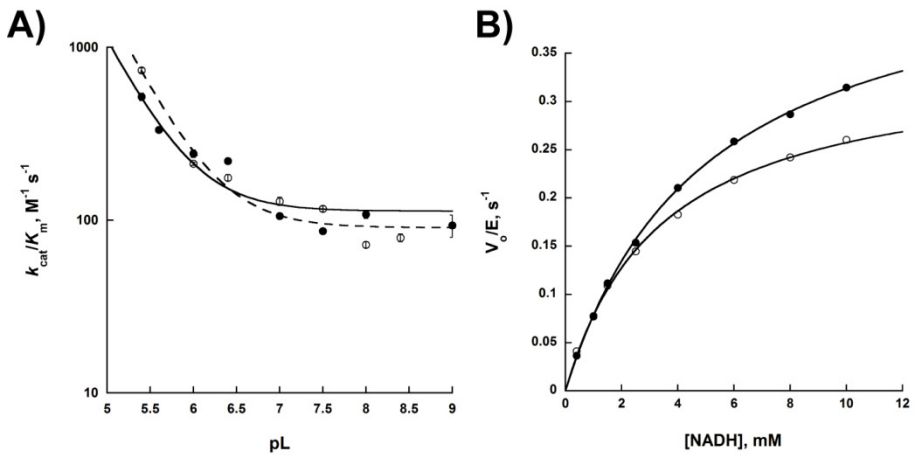

Figure 9.5 (A) Effects of pH (● solid line) on the k_{cat}/K_m values for NADH following oxygen consumption. The same experiment was performed in D_2O (○ dashed line). Experiments at each pL value were performed as a function of NADH with 3 mM L-lysine present. (B) Steady-state oxygen consumption of MbsG in H_2O (●) and D_2O (○) as a function of NADH in the presence of 3 mM L-lysine at pL 7.5.

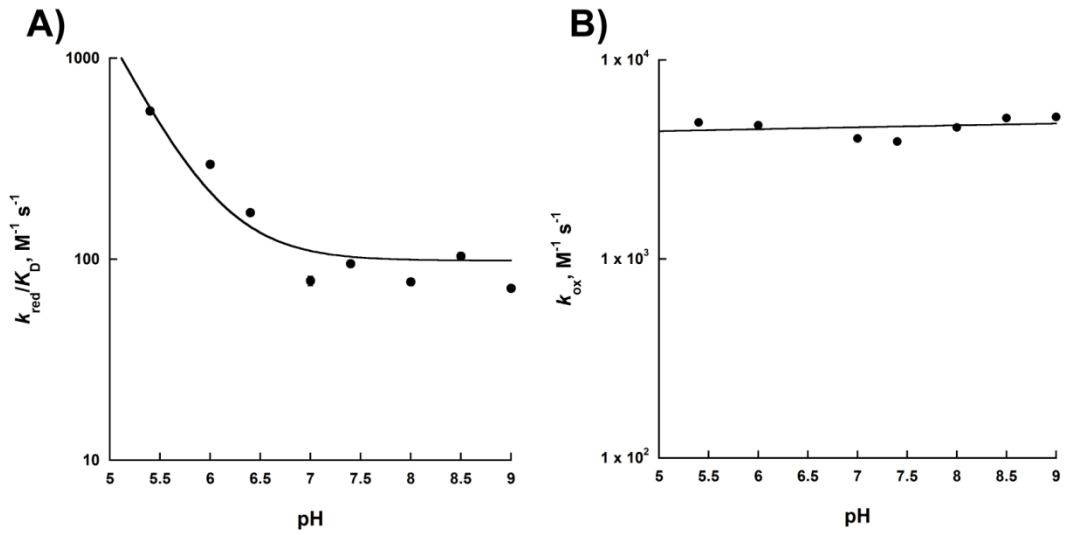

Figure 9.6 pH dependence of flavin reduction and oxidation. (A) pH profile of k_{red}/K_D for NADH in the presence of 3 mM L-lysine (B) pH profile of flavin oxidation in the presence of 3 mM L-lysine.

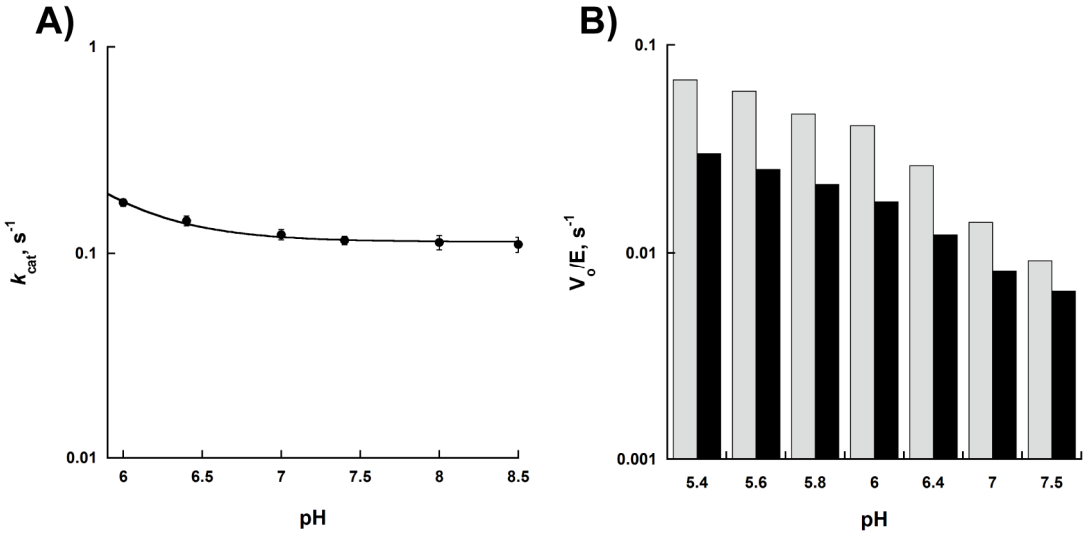

Figure 9.7 pH dependence of L-lysine hydroxylation and reactive oxygen species formation. (A) pH profile of L-lysine hydroxylation. Experiments at each pH value were performed as a function of NADH in the presence of 3 mM L-lysine. (B) Effect of pH on hydrogen peroxide (gray bars) and superoxide (black bars) formation with 3 mM NADPH and 3 mM L-lysine.

3.5 Effect of ligand binding. We previously showed that the presence of L-lysine and several substrate analogs slow the rate of oxygen consumption of MbsG [21]. To determine what step of the reaction is affected, both flavin reduction and oxidation were monitored in the presence of 10

mM each of L-ornithine, 6-amino-1-hexanol, L-arginine, L-lysine, putrescine, and cadaverine. The rate constants obtained in the presence of the second substrate (or analog) were compared to the values obtained in the absence of a ligand (with only NADH) (Fig. 9.8). Oxygen consumption and amine hydroxylation with these ligands were tested to determine the extent to which the rate of oxygen consumption was decreased and to measure whether hydroxylation occurred. The results indicate that all ligands tested decreased the rate of oxygen consumption, while only L-lysine is hydroxylated by MbsG (Figs. 9.8A and 9.8B). Addition of L-lysine results in a decrease of ~50% in the rate of oxygen consumption. Similarly, a decrease of ~40% is observed in the k_{red}/K_D value. Thus, L-lysine binding is controlling the reaction of oxidized MbsG and NADH. With the exception of L-ornithine, all other ligands decreased the oxygen consumption rate by >30% and k_{red}/K_D by >15%, with putrescine and cadaverine showing the highest decrease (down to ~40% in the rate of oxygen consumption and >50% in k_{red}/K_D). Incubation of L-lysine with MbsG before reacting with NADH had an equal effect on reduction, suggesting that L-lysine binding occurs more rapidly than with NADH. All tested ligands did not have a significant effect on the rate constant for flavin oxidation (Fig. 9.8D). The data indicates that L-lysine/ligand binding modulates the reactivity of MbsG with NAD(P)H leading to a decrease in the rate of hydride transfer.

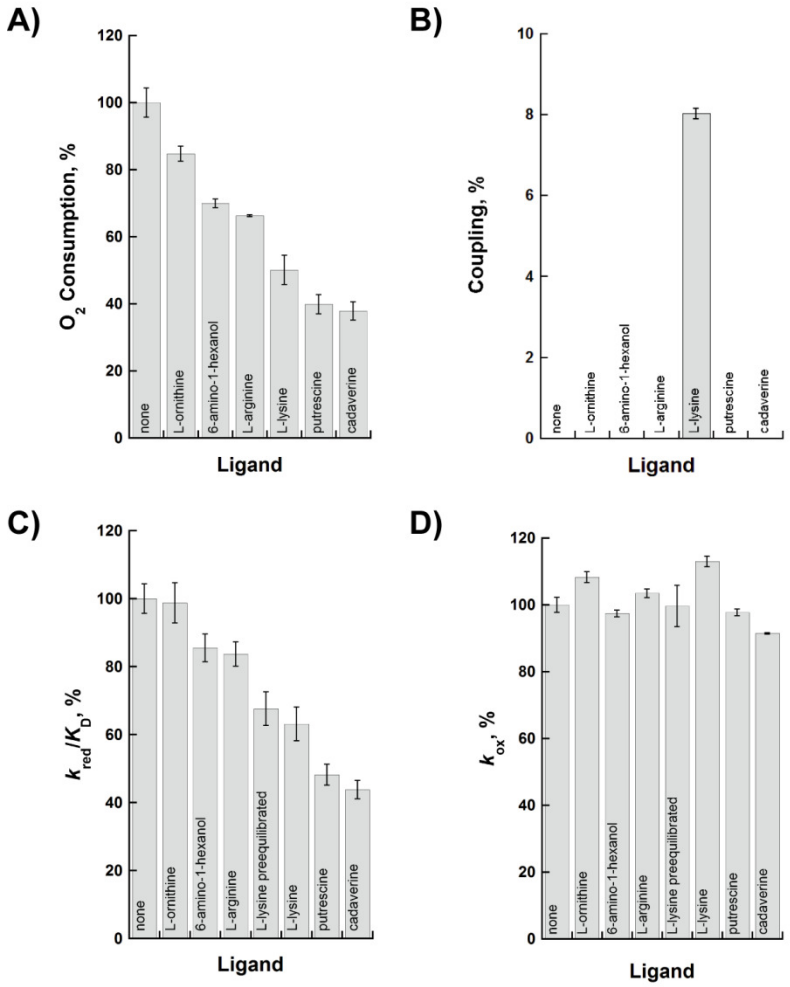

Figure 9.8 Effect of ligand binding to MbsG. All experiments were normalized to the values obtained in the absence of ligand with the exception of the hydroxylation experiment where all values were normalized to the value obtained with L-lysine. (A) Normalized effect on oxygen consumption. (B) Coupling of MbsG (oxygen consumption to L-lysine hydroxylation). (C) Normalized effect on flavin reduction. (D) Normalized effect on flavin oxidation. 5 mM NADH and 10 mM ligand were used in the oxygen consumption and hydroxylation experiments. NADH was varied between 1 and 5 mM while ligands were used at 10 mM in the flavin reduction experiment. 300 μM oxygen and 10 mM ligand were used in the flavin oxidation experiment.

3.6 Solvent kinetic isotope effects. The solvent kinetic isotope effect was measured in order to determine if protons are exchanged with solvent in a rate-limiting transition state. The pL profile indicated that the kinetic parameters were independent at pL values equal to or greater than 7.5 (Fig. 9.5A). The k_{cat}/K_m pD profile for NAD(P)H shows a pK_a value of 6.25 ± 0.07 (Fig. 9.5A

open circles). The solvent kinetic isotope effect determined at pL 7.5, resulted in a $^{D_2O}k_{cat}$ value of 1.36 ± 0.03 and a $^{D_2O}(k_{cat}/K_m)$ value of 0.93 ± 0.03 (Fig. 9.5B). The low $^{D_2O}k_{cat}$ value possibly indicates one or more solvent exchangeable protons in flight during a partially rate-limiting transition state, possibly flavin oxidation. A possible explanation for the slight inverse solvent kinetic isotope effect on k_{cat}/K_m is the presence of an isomerization step that is enhanced due to the higher viscosity of D_2O.

3.7 Solvent viscosity effects. Results from the solvent kinetic isotope effect experiments provided clues of the presence of an isomerization step in MbsG. To test this possibility, the effect of solvent viscosity was determined as a function of NADH in the presence of 3 mM L-lysine at both pH 7.5 and pH 5.6. In a plot of normalized k_{cat} versus relative glycerol viscosity, a slope of 0.10 was calculated at pH 7.5 (Fig. 9.9A). This indicates that product release is partially rate-limiting in the reaction at pH 7.5. Calculation of k_{cat} values at pH 7.5 required less extrapolation due to the relatively low Michaelis constant (~2 mM) in the presence of glycerol at this pH (data not shown). A plot of normalized k_{cat} could not be calculated at pH 5.6 due to the inability to saturate with NADH at lower pH, thus, only the k_{cat}/K_m was analyzed. In a plot of normalized k_{cat}/K_m versus relative viscosity, a slope of -0.13 was calculated at pH 7.5 (Fig. 9.9B closed circles). A plot of normalized k_{cat}/K_m versus relative viscosity at pH 5.6 results in a slope of 0.10 instead of a negative slope (Fig. 9.9B open circles). An inverse effect on solvent viscosity has also been reported in other flavoenzymes, where it has been interpreted as the participation of a viscosity sensitive isomerization or conformational change in the reaction [31, 32]. The data is consistent with a conformational change that is favored in solutions of higher viscosity at a pH of 7.5. At pH 5.6, this conformational change is no longer sensitive to solvent viscosity and the

reaction decreases as a function of increasing glycerol concentration suggesting that NADH binding is more rate-limiting under these conditions.

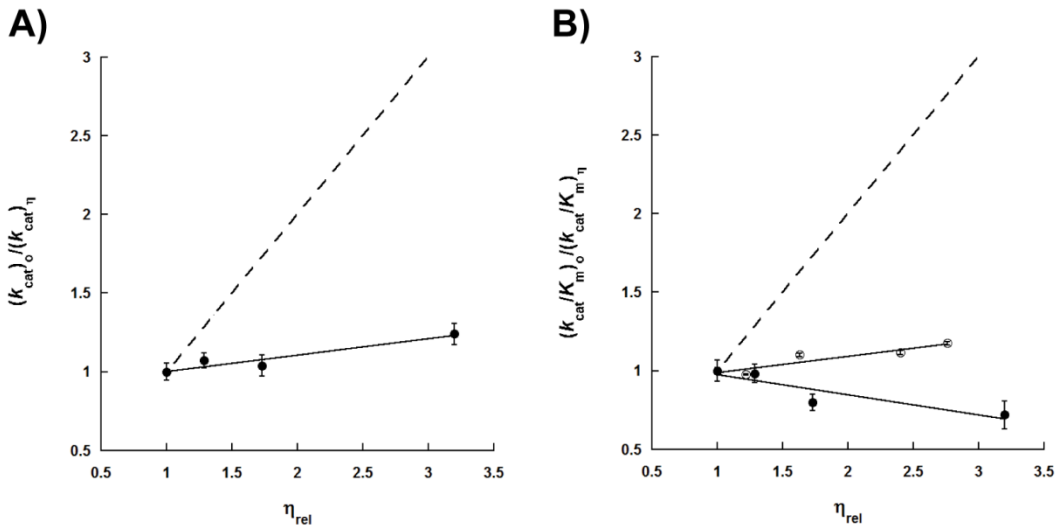

Figure 9.9 Effect of solvent viscosity on MbsG. Effect of solvent viscosity on (A) k_{cat} at pH 7.5 and (B) on k_{cat}/K_m at pH 7.5 (●) and pH 5.6 (○). Steady-state values were normalized to the values calculated for 0% glycerol. The k_{cat}/K_m values are those calculated for NADH at various concentrations of glycerol in the presence of 3 mM L-lysine. The dashed line with a slope of one describes a case in which the reaction is completely diffusion-controlled.

4. Discussion

The two most comprehensively studied NMOs to date are the L-ornithine monooxygenases, SidA and PvdA. These enzymes are capable of stabilizing long-lived C4a-hydroperoxyflavin intermediates, which is a common characteristic of members of the Class B flavin monooxygenases (Scheme 9.1C) [17, 18, 33-35]. Stabilization of this intermediate is required to ensure coupling of oxygen activation to formation of hydroxylated product, rather than the release of hydrogen peroxide or other reactive oxygen species [20, 36, 37]. MbsG is an NMO that does not function like related Class B flavin monooxygenases. This L-lysine

monooxygenase is highly uncoupled, producing high levels of reactive oxygen species during turnover (Table 9.2) [21].

Table 9.2 Activity of MbsG following L-lysine hydroxylation, superoxide, and hydrogen peroxide formation.

	NADH		NADPH	
	no L-lysine	**3 mM L-lysine**	**no L-lysine**	**3 mM L-lysine**
$k_{hydroxylation}$, s^{-1}	-	0.075 ± 0.002	-	0.070 ± 0.002
$k_{superoxide}$, s^{-1}	0.50 ± 0.04	0.024 ± 0.001	0.16 ± 0.04	0.028 ± 0.002
$k_{hydrogen\ peroxide}$, s^{-1}	0.30 ± 0.15	0.07 ± 0.02	0.14 ± 0.05	0.014 ± 0.001

Conditions: Reactions were performed in 100 mM sodium phosphate at pH 7.5 and 25 ºC.

Various mechanisms of regulation for flavin monooxygenases have been determined. For *p*-hydroxybenzoate hydroxylase (PHBH), a member of the Class A flavin monooxygenases, the activity is regulated in the reductive half reaction. In this enzyme, deprotonation of the hydroxyl group of *p*-hydroxybenzoate triggers movement of the flavin isoalloxazine ring from an *in* position to an *out* position, enhancing the reaction with NADPH by ~10^5 fold [38, 39]. The reduced flavin swings back into the active site where it is protected from solvent and reacts with molecular oxygen forming the C4a-hydroperoxyflavin, which is the hydroxylating species. Thus, the activity of PHBH is regulated by binding of substrate, which *enhances* reduction of the flavin. Class B flavin monooxygenases utilize a different mechanism of regulation. In this group of enzymes, the catalytic cycle has been well characterized in bacterial and mammalian flavin monooxygenase (FMOs), phenylacetone monooxygenase (PAMO), and in the ornithine monooxygenase, SidA. In these enzymes, the reaction of oxidized flavin with NADPH is independent of binding of the hydroxylatable substrate yielding reduced enzyme in complex with

$NADP^+$. This complex reacts with molecular oxygen to form a C4a-(hydro)peroxyflavin, which is stabilized in some cases for more than 1 hr [18, 33, 37, 40-42]. The presence of $NADP^+$ is absolutely necessary for stabilization of the C4a-(hydro)peroxyflavin. Only upon binding of the hydroxylatable substrate is rapid turnover observed (i.e., ornithine increases turnover of SidA by ~80-fold) [43]. This mechanism has been referred to as the "cocked-gun mechanism" where the stable C4a-(hydro)peroxyflavin is ready to react with an appropriate substrate [41].

As mentioned, MbsG does not function as other flavin-dependent monooxygenases. In addition to being highly uncoupled, the presence of L-lysine and other ligands results in a decrease in the rate of oxygen consumption. Here, we show that the k_{red} value decreases in the presence of L-lysine and non-hydroxylatable analogs (Figs. 9.1 and 9.8C). Pre-incubation of MbsG with L-lysine before reaction with NADH or reaction of MbsG with NADH/ L-lysine results in a similar decrease in the k_{red} value. This is consistent with rapid equilibrium binding of L-lysine, most likely before NAD(P)H binding. The down regulation on the rate of flavin reduction by substrate binding has not been reported for any other flavin monooxygenase.

Stopped-flow experiments on the oxidation step show that the reaction of reduced MbsG with oxygen occurs in a one-step process without the observation of a C4a-hydroperoxyflavin intermediate (Fig. 9.3). This is in stark contrast to SidA where the half-life of the C4a-hydroperoxyflavin is ~30 minutes [18, 20, 44]. The lack of stabilization of this intermediate is consistent with the high level of uncoupling in MbsG (Table 9.2). Furthermore, in the related NMOs SidA and PvdA, as well as other Class B monooxygenases, addition of substrate enhances flavin oxidation [17, 19]. Our results clearly indicate that MbsG does not utilize the same mechanism of stabilization, as the oxidation step is not affected by the addition of L-lysine or non-hydroxylatable analogs (Figs. 9.3 and 9.8D).

Probing the hydride transfer step by measuring the primary deuterium KIE showed that this step is partially rate-limiting at pH 7.5 since the effect on the $^{D}(k_{cat}/K_m)$ value is only 1.4 ± 0.1. The magnitude of the isotope effect is significantly different between MbsG and other Class B flavin-dependent monooxygenases where hydride transfer is the rate-determining step with KIE values of 3 – 6; however, the *pro*-(*R*)-stereoselectivity is conserved [18, 35, 36].

To gain further insight into the catalytic cycle of MbsG, pH studies were conducted. The results showed that as the pH decreases, the k_{cat}/K_m values increase. Fitting the data to Eq. 4 results in a pK_a value of ~6 for a group(s) that need(s) to be protonated for activity (Fig. 9.5A). Similar results were obtained when the k_{red}/K_D pH profile was determined, indicating that the pH sensitive step occurs during or before flavin reduction. pH studies on the oxidative half-reaction indicate that reaction with molecular oxygen is independent of pH (Fig. 9.6B). In other flavin monooxygenase systems, the rate of oxidation increases as a group with a pK_a value > 9 becomes deprotonated [44, 45]. This was proposed to be due to deprotonation of the N5 atom of the flavin, or due to a residue that is involved in hydrogen peroxide elimination from the C4a-hydroperoxyflavin. Thus, the degree of coupling decreases at higher pH in these enzymes as the C4a-hydroperoxyflavin becomes less stable. The mechanism by which MbsG achieves optimal coupling appears to be very different from other studied systems. While the rate of lysine hydroxylation is largely unchanged by pH, the rates of formation of reactive oxygen species increases ~10-fold at low pH when compared to more basic pH values (Fig. 9.7).

The viscosity and solvent kinetic isotope effect results on k_{cat}/K_m are consistent with the presence of a conformational change in the catalytic cycle of MbsG. A solution viscosity sensitive conformational change has been reported in other flavoenzyme systems; however, MbsG is the first monooxygenase [31, 32]. The fact that hydride transfer or flavin oxidation are

not significantly rate-limiting suggests that perhaps the conformational change is the slow step in the reaction. Furthermore, based on the pH results, we hypothesized that the conformational change might be pH sensitive, becoming faster at lower pH values. To test this hypothesis, the viscosity effects were performed at pH 5.6. In contrast to the observed increase in the k_{cat}/K_m values at pH 7.5, the k_{cat}/K_m values at pH 5.6 decrease as a function of increasing concentrations of glycerol. We interpret these data to indicate a change in the rate-limiting step in the reaction, with a conformational change being rate-limiting at pH 7.5 and becoming less rate-limiting as pH decreases. To further test if a pH sensitive conformational change controls the reaction of MbsG, we measured the KIE at pH 5.6. A $^{D}(k_{cat}/K_m)$ value of 2.0 ± 0.1 was determined at pH 5.6, which is significantly higher than the value of 1.4 ± 0.1 measured at pH 7.5. These results further support our hypothesis that a conformational change limits the reaction of MbsG at pH >7.5, while at lower pH values this step becomes less rate-limiting.

In summary, the mechanism of regulation of MbsG is unusual among flavin-dependent monooxygenases (Scheme 9.2). In MbsG, L-lysine binding *decreases* the rate of flavin reduction while having no effect on flavin oxidation. The pH studies show that isomerization of an MbsG-lysine-NADPH complex is pH sensitive, where at high pH (>7.5) the enzyme has a lower rate of flavin reduction, but is more coupled. At acidic pH, MbsG reacts faster with NAD(P)H; however, the increased rate mainly channels oxygen consumption towards formation of superoxide and hydrogen peroxide. Thus, it appears that slowing the conformational change prior to reduction increases the efficiency of lysine hydroxylation. Recent structural investigations on related Class B flavin monooxygenases have provided clues about the mechanism of stabilization of the C4a-hydroperoxyflavin. It has been shown that after flavin reduction, $NADP^+$ moves into a conformation that is essential for stabilization of the C4a-hydroperoxyflavin [33, 41, 46]. This

ensures efficient hydroxylation of the substrate and prevents the futile utilization of NADPH. In MbsG, L-lysine binding might induce conformational changes that primes the active site for proper interaction with NAD(P)H, such that reduction is slightly decreased, but activation of molecular oxygen does not yield excess reactive oxygen species.

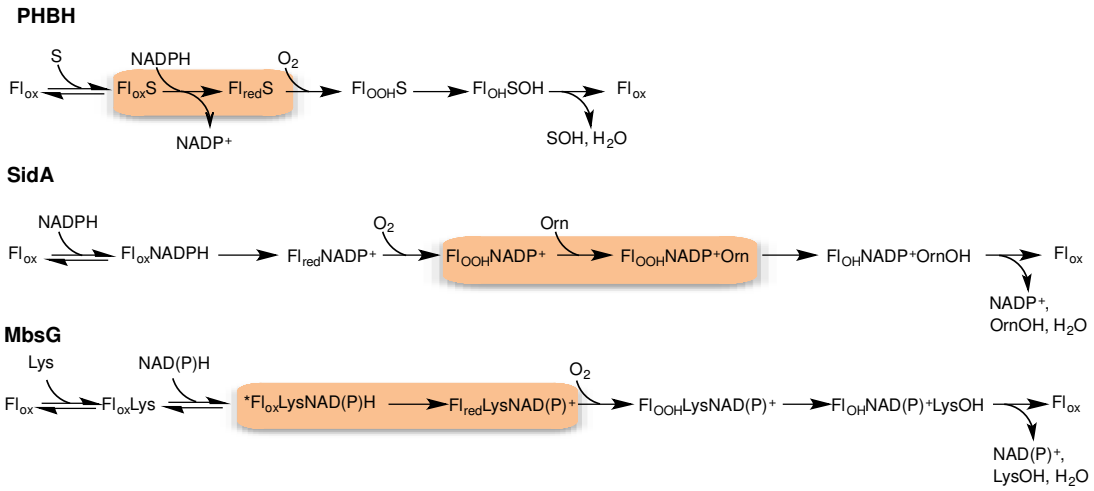

Scheme 9.2 Kinetic mechanisms of flavin monooxygenases. The regulatory steps modulated by substrate binding are highlighted in apricot colored boxes. In PHBH, substrate binds before reaction with NADPH, which results in an increase in the rate of flavin reduction. SidA stabilizes a long-lived C4a-hydroperoxyflavin intermediate, which is ready to hydroxylate L-ornithine upon binding. Here, L-ornithine enhances the oxidation of the flavin (similar mechanisms apply to FMO, PAMO, and PvdA). In MbsG, L-lysine binds before NAD(P)H. L-lysine binding induces a conformational change that decreases the flavin reduction step and the production of reactive oxygen species.

5. Acknowledgements

This work was supported by a grant from the National Science Foundation (MCB 1021384).

6. References

[1] J.L. Pierre, M. Fontecave, Biometals 12 (1999) 195-199.
[2] S.C. Andrews, A.K. Robinson, F. Rodriguez-Quinones, FEMS Microbiol Rev 27 (2003) 215-237.

[3] R.S. Eisenstein, Annu Rev Nutr 20 (2000) 627-662.
[4] P.P. Ward, S. Uribe-Luna, O.M. Conneely, Biochem Cell Biol 80 (2002) 95-102.
[5] J.B. Neilands, Annu Rev Biochem 50 (1981) 715-731.
[6] R.C. Hider, X. Kong, Nat Prod Rep 27 (2010) 637-657.
[7] A.H. Hissen, A.N. Wan, M.L. Warwas, L.J. Pinto, M.M. Moore, Infect Immun 73 (2005) 5493-5503.
[8] H. Takase, H. Nitanai, K. Hoshino, T. Otani, Infect Immun 68 (2000) 1834-1839.
[9] J.J. De Voss, K. Rutter, B.G. Schroeder, H. Su, Y. Zhu, C.E. Barry, 3rd, Proc Natl Acad Sci U S A 97 (2000) 1252-1257.
[10] C.A. Madigan, T.Y. Cheng, E. Layre, D.C. Young, M.J. McConnell, C.A. Debono, J.P. Murry, J.R. Wei, C.E. Barry, 3rd, G.M. Rodriguez, I. Matsunaga, E.J. Rubin, D.B. Moody, Proc Natl Acad Sci U S A 109 (2012) 1257-1262.
[11] P. Visca, A. Ciervo, N. Orsi, J Bacteriol 176 (1994) 1128-1140.
[12] L.E. Quadri, J. Sello, T.A. Keating, P.H. Weinreb, C.T. Walsh, Chem Biol 5 (1998) 631-645.
[13] M. Herrero, V. de Lorenzo, J.B. Neilands, J Bacteriol 170 (1988) 56-64.
[14] D. Lynch, J. O'Brien, T. Welch, P. Clarke, P.O. Cuiv, J.H. Crosa, M. O'Connell, J Bacteriol 183 (2001) 2576-2585.
[15] H.Y. Kang, T.J. Brickman, F.C. Beaumont, S.K. Armstrong, J Bacteriol 178 (1996) 4877-4884.
[16] F. Barona-Gomez, U. Wong, A.E. Giannakopulos, P.J. Derrick, G.L. Challis, J Am Chem Soc 126 (2004) 16282-16283.
[17] S.W. Chocklett, P. Sobrado, Biochemistry 49 (2010) 6777-6783.
[18] E. Romero, M. Fedkenheuer, S.W. Chocklett, J. Qi, M. Oppenheimer, P. Sobrado, Biochim Biophys Acta 1824 (2012) 850-857.
[19] K.M. Meneely, E.W. Barr, J.M. Bollinger, Jr., A.L. Lamb, Biochemistry 48 (2009) 4371-4376.
[20] J.A. Mayfield, R.E. Frederick, B.R. Streit, T.A. Wencewicz, D.P. Ballou, J.L. DuBois, J Biol Chem 285 (2010) 30375-30388.
[21] R. Robinson, P. Sobrado, Biochemistry 50 (2011) 8489-8496.
[22] T. Csaky, Acta Chem Scand 2 (1948) 450-454.
[23] C.M. Harris, V. Massey, J Biol Chem 272 (1997) 8370-8379.
[24] S.S. Jeong, J.E. Gready, Anal Biochem 221 (1994) 273-277.
[25] J. Sucharitakul, P. Chaiyen, B. Entsch, D.P. Ballou, Biochemistry 44 (2005) 10434-10442.
[26] R.E. Viola, P.F. Cook, W.W. Cleland, Anal Biochem 96 (1979) 334-340.
[27] R. Dhatwalia, H. Singh, L.M. Solano, M. Oppenheimer, R.M. Robinson, J.F. Ellerbrock, P. Sobrado, J.J. Tanner, J Am Chem Soc 134 (2012) 18132-18138.
[28] R.M.C. Dawson, D.C. Elliot, W.H. Elliot, K.M. Jones, Data for Biochemical Research, 3rd ed., Oxford University Press, New York, NY, 1986, p. 427.
[29] K.B. Schowen, R.L. Schowen, Methods Enzymol 87 (1982) 551-606.
[30] R.C. Weast, Handbook of Chemistry and Physics 1982-1983, 63rd ed., CRC Press, Boca Raton, FL, 1982, pp. D239-D240.
[31] P. Sobrado, S.C. Daubner, P.F. Fitzpatrick, Biochemistry 40 (2001) 994-1001.
[32] G. Gadda, P.F. Fitzpatrick, FEBS Lett 587 (2013) 2785-2789.

[33] S. Franceschini, M. Fedkenheuer, N.J. Vogelaar, H.H. Robinson, P. Sobrado, A. Mattevi, Biochemistry 51 (2012) 7043-7045.
[34] J. Olucha, K.M. Meneely, A.S. Chilton, A.L. Lamb, J Biol Chem 286 (2011) 31789-31798.
[35] W.J. van Berkel, N.M. Kamerbeek, M.W. Fraaije, J Biotechnol 124 (2006) 670-689.
[36] D.E. Torres Pazmino, B.J. Baas, D.B. Janssen, M.W. Fraaije, Biochemistry 47 (2008) 4082-4093.
[37] R. Orru, D.E. Pazmino, M.W. Fraaije, A. Mattevi, J Biol Chem 285 (2010) 35021-35028.
[38] B.A. Palfey, C.A. McDonald, Arch Biochem Biophys 493 (2010) 26-36.
[39] B.A. Palfey, G.R. Moran, B. Entsch, D.P. Ballou, V. Massey, Biochemistry 38 (1999) 1153-1158.
[40] R. Orru, H.M. Dudek, C. Martinoli, D.E. Torres Pazmino, A. Royant, M. Weik, M.W. Fraaije, A. Mattevi, J Biol Chem 286 (2011) 29284-29291.
[41] A. Alfieri, E. Malito, R. Orru, M.W. Fraaije, A. Mattevi, Proc Natl Acad Sci U S A 105 (2008) 6572-6577.
[42] N.B. Beaty, D.P. Ballou, J Biol Chem 255 (1980) 3817-3819.
[43] R. Robinson, S. Badieyan, P. Sobrado, Biochemistry 52 (2013) 9089-9091.
[44] E. Romero, D. Ávila, P. Sobrado, In S. Miller, R. Hille, B. Palfey (eds.) Flavins and Flavoproteins 2011, Lulu, Raleigh, NC, 2013, pp. 289-294.
[45] N. Ruangchan, C. Tongsook, J. Sucharitakul, P. Chaiyen, J Biol Chem 286 (2011) 223-233.
[46] I.A. Mirza, B.J. Yachnin, S. Wang, S. Grosse, H. Bergeron, A. Imura, H. Iwaki, Y. Hasegawa, P.C. Lau, A.M. Berghuis, J Am Chem Soc 131 (2009) 8848-8854.

CHAPTER 10

An unprecedented NADPH domain conformation in lysine monooxygenase NbtG provides insights into uncoupling of oxygen consumption from substrate hydroxylation

Under Review in The Journal of Biological Chemistry, Binda, C., Robinson, R. M., Martin del Campo, J. S., Keul, N. D., Rodriguez, P. J., Robinson, H. H., Mattevi, A., and Sobrado, P. "An unprecedented NADPH domain conformation in Lysine Monooxygenase NbtG provides insights into uncoupling of oxygen consumption from substrate hydroxylation" in press: *The Journal of Biological Chemistry*. 2015 (ID 10.1074/jbc.M114.629485).

Author Contributions:
*Claudia Binda solved and refined the structure of NbtG and help write the article.

*Reeder M. Robinson performed all stopped-flow experiments, crystallized NbtG, and helped write the article.

Julia S. Martin del Campo performed the HPLC assay to detect N^6-hydroxy-Lys.

Nicholas D. Keul performed the steady-state assays with wild-type.

Pedro J. Rodriguez performed the steady-state assays with K64A.

Howard H. Robinson collected diffraction data on the NbtG crystals.

Andrea Mattevi oversaw the solving and refinement of the structure of NbtG and helped write the article

Pablo Sobrado oversaw and directed the research, and helped write the article.

*Claudia Binda and Reeder M. Robinson contributed equally to this study.

Abstract

N-Hydroxylating monooxygenases (NMOs) are involved in the biosynthesis of iron-chelating hydroxamate-containing siderophores that play a role in microbial virulence. These flavoenzymes catalyze the NADPH- and oxygen-dependent hydroxylation of amines, such as

those found on the side chains of lysine and ornithine. In this work we report the biochemical and structural characterization of *Nocardia farcinica* Lys monooxygenase (NbtG), which has similar biochemical properties to mycobacterial homologs. NbtG is also active on D-Lys although it binds L-Lys with a higher affinity. Differently from the ornithine monooxygenases PvdA, SidA and KtzI, NbtG can use both NADH and NADPH and is highly uncoupled, producing more superoxide and hydrogen peroxide than hydroxylated Lys. The crystal structure of NbtG solved at 2.4 Å resolution revealed an unexpected protein conformation with a 30 ° rotation of the NAD(P)H domain with respect to the FAD domain that precludes binding of the nicotinamide cofactor. This "occluded" structure may explain the biochemical properties of NbtG, specifically with regard to the substantial uncoupling and limited stabilization of the C4a-hydroperoxyflavin intermediate. Biological implications of these findings are discussed.

1. Introduction

Flavin-dependent *N*-hydroxylating monooxygenases (NMOs) are involved in the biosynthesis of hydroxamate-containing siderophores. These enzymes catalyze the NADPH- and oxygen-dependent hydroxylation of amine groups on the side chains of L-ornithine (L-Orn), L-lysine (L-Lys), and some primary aliphatic diamines (1-6). Many of these NMOs are linked to virulence in pathogenic bacteria. For instance, gene deletion experiments have shown that the L-Orn monooxygenases SidA from *Aspergillus fumigatus* and PvdA from *Pseudomonas aeruginosa* as well as the L-Lys monooxygenases, MbtG from *Mycobacterium tuberculosis* and MbsG from *Mycobacterium smegmatis,* are essential for functional siderophore biosynthesis and virulence (7-9). It is possible that these enzymes would make promising drug targets for various

infectious diseases because of their requirement for the production of virulence-conferring siderophores and the lack of any human homologs.

Substantial mechanistic and structural data has been obtained in recent years on the L-Orn monooxygenases SidA, PvdA, and, more recently, on *Kutzneria* sp. 744 L-Orn monooxygenase (KtzI) (10-12). These enzymes are very selective for L-Orn and are highly coupled, producing little or no hydrogen peroxide during catalysis (1,13) as they stabilize the C4a-hydroperoxyflavin (FAD_{OOH}) intermediate long enough to allow effective hydroxylation of L-Orn (14-16). A different strategy for oxygen consumption regulation was found in KtzI where flavin movement from an "out" to "in" conformation controls the oxidized/reduced state of the cofactor, similarly to what happens in Class A monooxygenases such as *p*-hydroxybenzoate hydroxylase (PHBH). Despite this difference, the structures of SidA, PvdA and KtzI all share a similar overall fold to other Class B flavin monooxygenases and a similar binding conformation for $NADP^+$, which is important for stabilization of the FAD_{OOH} (6,10,17,18).

Comparison of the structures of SidA in complex with L-Orn and L-Lys revealed the mechanism of substrate selectivity where the *N*ε of L-Orn is in a favorable position for hydroxylation by the distal oxygen of the FAD_{OOH}. In contrast, L-Lys protrudes further into the active site in a sub-optimal position, which causes breakdown of the FAD_{OOH} resulting in production of high levels of hydrogen peroxide and low levels of hydroxylated L-Lys (10).

In contrast to the significant mechanistic and structural data of L-Orn monooxygenases, relatively little is known about L-Lys monooxygenases. IucD from *Escherichia coli* was the first L-Lys monooxygenase characterized. IucD shares similar mechanistic features to SidA and PvdA, as this enzyme has been shown to be highly coupled and specific for NADPH and L-Lys (3,19). Recently, characterization of the L-Lys monooxygenase MbsG from *Mycobacterium*

smegmatis showed that this enzyme can use both NADH and NADPH and is highly uncoupled, making more superoxide and hydrogen peroxide than hydroxylated Lys (20,21). Also, unlike other NMOs where substrate binding accelerates turnover, L-Lys binding decreases the activity of MbsG ~2-fold by regulating the reaction with NAD(P)H (21). These results suggest that there is a higher degree of mechanistic variability among NMOs than previously thought.

The biosynthesis of the siderophore nocobactin in *Nocardia farcinica* requires functioning of NbtG, a L-Lys monooxygenase that shares more than 50% of sequence identity with MbsG (Scheme 10.1) (22). The *Nocardia* genus comprises parasitic bacteria, which can infect both plants and animals, including humans, and has a high mortality rate due to antibiotic resistance (22). Here, we present a thorough biochemical and structural characterization of NbtG. The enzyme is an effective L-Lys monooxygenase that is also able to hydroxylate D-Lys. NbtG is unable to stabilize the FAD_{OOH} intermediate, which results in production of hydrogen peroxide and superoxide. The structure of NbtG was solved by X-ray crystallography and the results show an unexpected and unprecedented protein conformation that can rationalize the biochemical properties of NbtG, specifically with regard to the substantial uncoupling and limited stabilization of FAD_{OOH}.

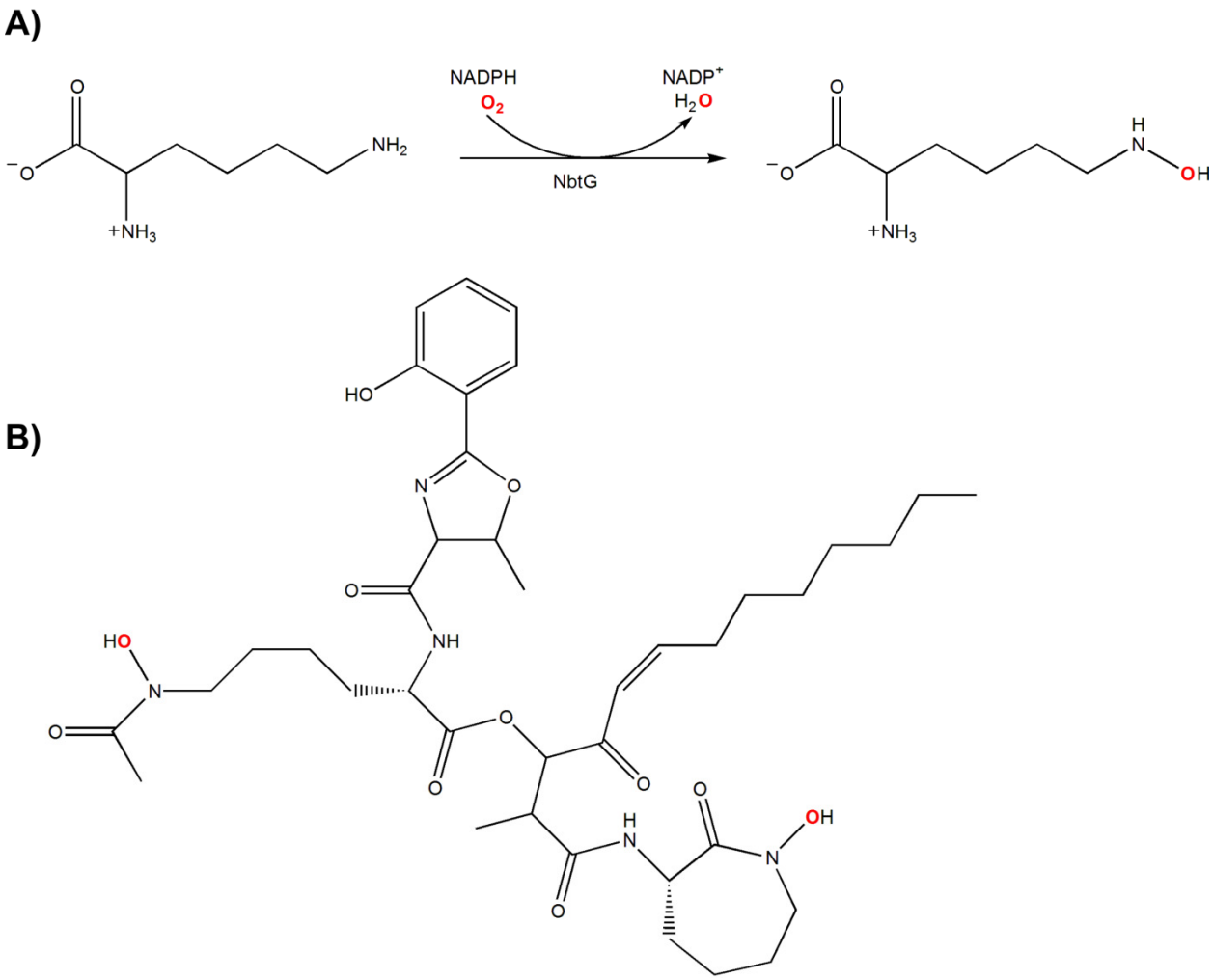

Scheme 10.1 (A) Reaction catalyzed by NbtG. NbtG utilizes NADPH and molecular oxygen (shown in red) to hydroxylate the N^6-atom of L-Lys. $NADP^+$ and H_2O are by-products of the catalytic cycle. B) Siderophore nocobactin produced by *Nocardia farcinica*. N^6-hydroxy-L-lysines are incorporated into the backbone of nocobactin (oxygens inserted by NbtG are shown in red).

2. Materials and Methods

2.1 Materials. The synthetic gene encoding for NbtG from *Nocardia farcinica* IFM 10152 was obtained from GenScript (Piscataway, NJ). *Pme*I and *Sgf*I were from Promega (Madison, WI). *Escherichia coli* TOP10 and BL21-T1^R chemically competent cells were from Invitrogen (Grand Island, NY). pVP56K was obtained from the Center for Eukaryotic Structural Genomics (University of Wisconsin, Madison, WI). DNA sequencing was performed at the DNA

sequencing facility of the Virginia Bioinformatics Institute (Blacksburg, VA). Protein purification was performed on an ÄKTA Prime Plus FPLC (GE Healthcare). L-Lys, D-Lys, NADPH, $NADP^+$, buffers, and salts were from Fisher Scientific (Pittsburgh, PA). Amino acid analysis was performed using an Acquity Ultraperformance Liquid Chromatography (UPLC) system (Waters, Milford, MA). Oxygen consumption studies were performed on a Hansatech Oxygraph (Norfolk, UK). WST-1, used for superoxide quantification, was from Dojindo Molecular Technologies, Inc. (Rockville, MD). Alcohol dehydrogenase from *Thermoanaerobium brockii* was obtained from Sigma-Aldrich (St. Louis, MO). Glucose oxidase was from MP Biomedical (Solon, OH). Rapid-reaction studies were performed on an Applied Photophysics SX20 stopped-flow spectrophotometer (Leatherhead, UK) housed in a Coy Glove Box (Grass Lake, MI).

2.2 Cloning. To subclone the NbtG gene into the expression vector pVP56K, the pUC57:*nbtG* plasmid was incubated with *Pme*I and *Sgf*I restriction endonucleases at 37 °C for 2 h. After digestion, the restriction endonucleases were inactivated by incubation at 65 °C for 30 min. The digested gene was then ligated into pVP56K, which was previously treated with *Pme*I and *Sgf*I. The ligation reaction was then transformed into *E. coli* TOP10 cells. Five colonies were grown for plasmid purification and sequenced to determine proper ligation of *nbtG* into pVP56K.

2.3 Site–directed mutagenesis. Mutagenesis was performed using the QuikChange (Agilent Technologies) method following the manufacturer's instructions. The wild-type NbtG gene, subcloned into the pVP56K plasmid, was used as the template. The mutations were confirmed by DNA sequencing at Virginia Bioinformatics Core Sequencing Facility.

2.4 Protein expression and purification. A single colony of *E. coli* BL21-T1^{R} transformed with pVP56K:*nbtG* was used to inoculate a 50 mL overnight LB culture flask (supplemented with 50 µg/mL kanamycin). After overnight incubation at 37 °C, 6 flasks containing 1 L each of autoinduction media (23) (supplemented with 50 µg/mL kanamycin) were each inoculated with 10 mL of the overnight culture and grown at 37 °C with agitation at 250 rpm. When the optical density at 600 nm reached a value of ~3, the temperature was lowered to 18 °C. After overnight incubation, the cells were harvested by centrifugation and the cell pellet was stored at −80 °C. All subsequent steps were performed at 4 °C. Cell paste (50 g) was resuspended in 150 mL of buffer A (25 mM HEPES, 300 mM NaCl, 25 mM imidazole, 5% glycerol, pH 7.5) containing 1 mM phenylmethanesulfonyl fluoride (PMSF), 100 µM FAD, and 25 µg/mL each of DNase, RNase, and lysozyme. The solution was stirred for 30 min. Cells were lysed by sonication using a Fisher Scientific Sonic Dismembrator Model 500 at 70% amplitude for 10 minutes (5 second pulses with 15 second delays). Next, the lysate was centrifuged at 35,000 *g* for 1 h. The resulting supernatant was loaded at 5 mL/min onto three in-tandem 5 mL HisTrap FF crude columns (GE Healthcare) previously equilibrated with buffer A. After loading, the column was washed with buffer A followed by 100 mL of buffer A containing 75 mM imidazole. Bound His_8-MBP-NbtG was eluted with 150 mL of buffer A containing 500 mM imidazole. Fractions were analyzed by sodium-dodecyl sulfate polyacrylamide gel electrophoresis (SDS-PAGE) and those containing His_8-MBP-NbtG were combined. To liberate NbtG from the His_8-MBP, 10 mg of tobacco etch virus (TEV) protease was added and the solution was then transferred to a 4000 MWCO dialysis bag and dialyzed in 2 L of buffer A. The next day, the solution was loaded at 3 mL/min onto three in-tandem 5 mL HisTrap FF crude columns previously equilibrated with buffer A. In this step His_8-MBP, His_8-TEV, and any uncleaved His_8-MBP-NbtG remain bound to the column

while NbtG elutes in the flow-through. SDS-PAGE analysis of the flow-through showed highly pure NbtG, however, small amounts of His_8-MBP-NbtG were still present. To remove the fusion from free NbtG, the sample was loaded at 3 mL/min onto two in-tandem 5 mL MBPTrap HP columns equilibrated in buffer B (25 mM HEPES, 500 mM NaCl, pH 7.5). The flow-through contained NbtG and was determined to be > 95% pure by SDS-PAGE. The sample (~20 mL) was dialyzed for 3 h in 1 L of storage buffer (100 mM sodium phosphate, 50 mM NaCl, pH 7.5) then dialyzed in 1 L of fresh storage buffer overnight. Dialyzed NbtG was concentrated to ~300 μM, aliquoted (in ~60 μL drops), and frozen in liquid nitrogen prior to storage at −80 °C. NbtG K184A Se-Met was produced using the metabolic inhibition method (24). Both Se-Met labeled NbtG K184A and unlabeled enzymes were purified as described above.

2.5 Characterization of the flavin cofactor. A solution of NbtG (25 μM) was heated at 95 °C for 10 min. After incubation on ice for 5 min, the denatured protein was precipitated by centrifugation at 15,000 *g* for 10 min. The supernatant containing the flavin cofactor was used for mass spectroscopy analysis as previously described (20,21). The extinction coefficient of the bound FAD to NbtG was determined by addition of 5% SDS and incubation at room temperature for 5 min. The spectrum of the liberated FAD was recorded and an extinction coefficient at 452 nm of 12,600 M^{-1} cm^{-1} was calculated using the extinction coefficient for free FAD of 11,300 M^{-1} cm^{-1}.

2.6 $NADP^+$ binding. The binding of $NADP^+$ to oxidized NbtG was monitored by recording the change in the flavin spectra at increasing concentrations of $NADP^+$. Each solution consisted of 100 μL of 100 mM sodium phosphate pH 7.5, NbtG (60 μM) and $NADP^+$ (0-10 mM). The

solutions were incubated on ice for 10 min before data collection. The spectra of $NADP^+$ alone were subtracted from spectra of $NADP^+$/NbtG, at each $NADP^+$ concentration. The absorbance differences showed the largest decrease at 395 nm. An extinction coefficient of 1300 $M^{-1}cm^{-1}$ for this change in absorbance at 395 nm was determined and used to calculate the concentrations of NbtG–$NADP^+$ complex.

2.7 Oxygen consumption assay. Oxygen consumption was monitored in 1 mL reactions of 100 mM sodium phosphate, pH 7.5. NAD(P)H was varied between 0.1 – 5 mM, L-Lys was varied between 0 – 5 mM, and D-Lys was varied between 0 – 100 mM. For assays where NAD(P)H was varied, no Lys, 2 mM L-Lys, or 10 mM D-Lys were present. In assays where Lys was varied, NAD(P)H was held constant at 2 mM. Assays were initiated with 1 μM NbtG and monitored on a Hansatech Oxygraph system at 25 °C under constant stirring.

2.8 Product formation assay. To determine if L-Lys was hydroxylated, NbtG (8 μM) was mixed with 5 mM NADPH and 1 mM L-Lys in 100 μL of 50 mM Tris-Cl, 100 mM NaCl, pH 8.0. At 0.5, 1, 2, and 3 min the reaction was quenched with 200 μL of 100% acetonitrile and centrifuged at 13,000 rpm for 1 min. The supernatant was withdrawn and combined with 25 μL of 200 mM borate (pH 8.0). L-Lys was derivatized by adding 3.4 μL of 9-fluorenylmethoxycarbonyl chloride (FMOC-Cl, 150 mM) to 130 μL of the quenched reaction. This was allowed to incubate for 5 min at 25 °C. To remove any remaining derivatizing reagent, 158 μL of 1-aminoadamantane (ADAM, 53 mM) was added and incubated at room temperature for an additional 15 min.The sample was analyzed by reverse phase UPLC by loading 2 μL onto a C18 AcQuity column (2.1 mm x 100 mm) equilibrated in 70 % eluent A (0.1 % trifluoroacetic acid in water) at 0.5

min/mL. The samples were eluted with a linear gradient from 30 to 100% eluent B (0.1% trifluoroacetic acid in acetonitrile) at 0.5 min/mL, samples were monitored at 263 nm. The elution profiles of derivatized L-Lys and L-Lys-OH were consistent with previously published data (25).

Hydroxylated Lys was quantified by a variation of the Csaky iodine oxidation assay as previously described (20,26). Each reaction consisted of 104 µL of 100 mM sodium phosphate, pH 7.5. NAD(P)H was varied between 0.1 − 10 mM, L-Lys was varied between 0.1 − 5 mM, and D-Lys was varied between 0 − 10 mM. In assays where NAD(P)H was varied, 2 mM L-Lys or 10 mM D-Lys were used. For reactions with varying concentrations of D/L-Lys, 2 mM NAD(P)H was used. Reactions were initiated with 2 µM NbtG and allowed to proceed at 25 °C for 10 min while shaking at 750 rpm.

2.9 Hydrogen peroxide formation assay. Hydrogen peroxide formed during the reaction was measured using the Pierce Hydrogen Peroxide Detection Kit as described previously (20,21). Each reaction consisted of 104 µL of 100 mM sodium phosphate, pH 7.5. NAD(P)H was varied between 0.1 − 10 mM in the absence of D/L-Lys or with L-Lys or D-Lys held constant at 2 mM and 10 mM, respectively. Reactions were initiated with 2 µM NbtG and allowed to proceed at 25 °C for 10 minutes under constant orbital shaking at 750 rpm.

2.10 Superoxide formation assay. Superoxide formed during the reaction was measured by coupling the reaction with WST-1 as described previously (20,21). Each reaction consisted of 200 µL of 100 mM sodium phosphate, pH 7.5. NAD(P)H was varied between 0.1 − 10 mM in the absence of D/L-Lys or with L-Lys or D-Lys held constant at 2 mM and 10 mM, respectively.

Reactions were initiated with 2 μM NbtG and allowed to proceed at 25 °C for 10 minutes while shaking at 750 rpm.

2.11 Flavin reduction. Flavin reduction was monitored at 25 °C in 100 mM sodium phosphate, pH 7.5 in a stopped-flow spectrophotometer in single mixing mode. The stopped-flow spectrophotometer system and buffers were made anaerobic as described previously (21). Oxidized NbtG (15 μM after mixing) was mixed with various concentrations of NADPH (0.025 mM – 5 mM after mixing). The reaction was monitored with a photodiode array spectrophotometer until flavin reduction was complete. This was repeated with L-Lys or D-Lys at 2 mM and 10 mM (after mixing), respectively.

2.12 Flavin oxidation. Flavin oxidation was monitored at 25 °C in 100 mM sodium phosphate, pH 7.5 in a stopped-flow spectrophotometer in double mixing mode. In the first mixing step, 30 μM of NbtG (after mixing) was allowed to react with a stoichiometric concentration of NADPH (30 μM after mixing) for 500 s. In the second mixing step, reduced NbtG was reacted with various concentrations of molecular oxygen (100 – 600 μM after mixing). The reaction was monitored using a photodiode array spectrophotometer until flavin oxidation was complete. Oxygen saturated buffer (1.2 mM) was obtained by bubbling 100 % oxygen for 30 min at 25 °C. Various oxygen concentrations were obtained by mixing with appropriate volumes of anaerobic buffer. Experiments with L-Lys or D-Lys contained 2 mM and 10 mM, respectively. To determine if excess $NADP^+$ was required to stabilized the FAD_{OOH} intermediate, $NADP^+$ was added to the second mix (0 – 10 mM after mixing) during oxidation.

2.13 Synthesis of deuterated NADPH. *R*-4H^2-NADPH was synthesized by the method of Jeong with some minor modifications as previously described (27,28). Briefly, 25 mg of $NADP^+$ (5.6 mM final concentration), 480 μL 2-propanol-*d*8 (1 M final concentration), and 50 units of alcohol dehydrogenase (*Thermoanaerobium brockii*) were added to 6 mL of 25 mM Tris-Cl pH 9.0. The reaction was allowed to proceed for 30 min at 40 ºC with light agitation until the A_{260}/A_{340} ratio reached a value of ~ 2.5.

2.14 Data analysis. The kinetic data were fit using KaleidaGraph (Synergy Software, Reading, PA). Steady-state kinetic data were fit to the Michaelis-Menten equation. Data that exhibited substrate inhibition were fit to eq. 1, to obtain the turnover number (k_{cat}), the Michaelis constant (K_M) and the substrate inhibition constant (K_{is}). The decrease in absorbance at 452 nm was fit to a double exponential decay equation (eq. 2) and the resulting k_{obs} values were plotted as a function of NADPH concentration. These data were fit using eq. 3 to determine the maximum rate of flavin reduction (k_{red}) and K_D values. The rate of flavin oxidation was determined by fitting the increase in absorbance at 452 nm to a single exponential rise equation (eq. 4). The resulting k_{obs} values were plotted as a function of oxygen concentration and fit to a linear equation to determine the bimolecular rate constant for flavin oxidation (k_{ox}).

$$v = \frac{k_{cat}[S]}{K_M + [S] + [S^2]/K_{is}} \quad (1)$$

$$v = C + A_1 e^{-(kobs_1 t)} + A_2 e^{-(kobs_2 t)} \quad (2)$$

$$k_{obs} = \frac{k_{red} \times [S]}{K_D + [S]} \quad (3)$$

$$v = C + A_1(1 - e^{-(kobst)}) \quad (4)$$

2.15 Crystallization and structure determination. Purified samples of NbtG (6 mg/mL) in 25 mM HEPES/NaOH pH 7.5, 500 mM NaCl, 5 mM $NADP^+$, in the presence of either L-Lys or D-Lys (various concentrations ranging from 5 to 100 mM) were used for crystallization screenings. As no crystals were obtained in these initial trials, surface mutagenesis experiments were carried out. Using the surface entropy reduction prediction server (SERp Server) (29), K184, K200, and K202 where selected and mutated to Ala. After initial screening, promising conditions were found only with the K184A mutant. As shown by the crystal structure, Lys184 is on a loop, which is fully exposed to the solvent at >20 Å distance from the flavin ring. Moreover, the kinetic properties were very similar to those of the wild-type (data not shown). Yellow crystals of the K184A NbtG mutant grew in 3-4 days at 20 °C using the hanging drop vapor diffusion method by mixing 1 µL of protein solution with an equal volume of a reservoir containing 10% w/v PEG 6,000, 5% v/v 2,4-methylpentanediol (MPD), and 0.1 M HEPES/NaOH pH 7.5. Optimization was achieved by the micro-seeding technique using a seed stock generated by vortexing crystals for 90 seconds in a seed bead tube. Crystallization experiments were then performed by adding 0.3 µL of a 100-fold diluted seed stock solution into a drop with a 2:1 ratio of protein to reservoir solution. Similar procedures were followed to crystallize a SeMet-labeled sample of K184A NbtG.

For X-ray data collection, NbtG crystals were soaked in a cryo solution containing 16% w/v PEG 6,000, 14% v/v 2,4-methylpentanediol (MPD), 0.1 M HEPES/NaOH pH 7.5, 5 mM $NADP^+$, D/L-Lys (at the concentration used for crystallization), 20% v/v glycerol, and flash-cooled in liquid nitrogen. Many crystals were screened for X-ray diffraction at the beamlines ID23-EH1 (ESRF, Grenoble, France), X06SA (SLS, Villigen, Switzerland) and X29 (NSLS, Upton, NY). Data processing and scaling were performed using MOSFLM (30) and programs of

the CCP4 package (31). Final statistics of the collected datasets are reported in Table 10.1. The NbtG structure was solved by single-wavelength anomalous diffraction (SAD) on the Se-edge using the program SHELX (32). Because the crystals were highly isomorphous, it was possible to merge two datasets at 2.7 and 2.9 Å resolution to increase redundancy. The eight Se sites (including that of the N-terminal methionine which is left in the recombinant protein after His-tag cleavage) were identified and used for phasing with the program PHENIX (33). The quality of the initial electron density map was poor (figure of merit = 0.27), but a significant improvement was obtained after PHENIX density modification (averaging among the 4 molecules present in the asymmetric unit). This allowed us to perform autobuilding which yielded good statistics (model-map CC = 62%, R_f = 36%, free R_f = 41%), although a large portion of the protein needed to be manually traced by COOT (34). Refinement was carried out using a native data set at 2.4 Å resolution with the program REFMAC5 (35). Figures were produced by CCP4mg (36).

Table 10.1 Data collection and refinement statistics for the NbtG structure.

	SeMet (crystal 1)	SeMet (crystal 2)	Native
PDB code	-	-	4d7e
Space group	$P2_1$	$P2_1$	$P2_1$
a (Å)	80.3	80.4	80.6
b (Å)	121.5	122.1	121.9
c (Å)	92.2	92.6	91.9
β (°)	97.7	97.6	97.7
Wavelength (Å)	0.98	0.98	1.07
Resolution (Å)	2.7	2.9	2.4
R_{sym}[a,b] (%)	10.1 (96.8)	10.8 (99.5)	7.6 (98.4)
$CC_{1/2}$[b,c]	0.997 (0.423)	0.997 (0.627)	0.999 (0.563)
Completeness[b] (%)	85.4 (79.9)	100.0 (99.9)	99.2 (98.5)
Anomalous completeness[b] (%)	82.3 (78.3)	99.6 (99.0)	-
Redundancy	6.1 (6.4)	7.1 (7.1)	6.5 (6.3)
Anomalous redundancy	3.0 (3.1)	3.6 (3.6)	-
Unique reflections	40862	39427	68260
I/σ[b]	13.4 (1.4)	14.2 (1.8)	12.3 (1.0)
Protein/FAD atoms (*N*)	-	-	11431/53x4
Water atoms (*N*)	-	-	239
Average B value (Å^2)	-	-	43.5
R_{cryst}[d] (%)	-	-	20.7
R_{free}[d] (%)	-	-	28.2
Rms bond length (Å)	-	-	0.013
Rms bond angles (°)	-	-	1.7

[a] $R_{sym}=\sum|I_i-<I>|/\sum I_i$, where I_i is the intensity of i^{th} observation and <I> is the mean intensity of the reflection.

[b] Values in parentheses are for reflections in the highest resolution shell.

[c] A cut-off criterion for resolution limits was applied on the basis of the mean intensity correlation coefficient of half-subsets of each dataset ($CC_{1/2}$) (43).

[d] $R_{cryst}=\sum|F_{obs}-F_{calc}|/\sum|F_{obs}|$ where F_{obs} and F_{calc} are the observed and calculated structure factor amplitudes, respectively. R_{cryst} and R_{free} were calculated using the working and test sets, respectively.

3. Results

3.1 Purification of wild-type NbtG and mutant variants. Wild-type NbtG and the K184A isoform used for crystallography were expressed as a fusion to His_8-MBP in pVP56K. This was critical to obtaining soluble active enzymes as expression with only a His_8 tag, produced insoluble protein. Overall, a yield of ~30 mg of purified NbtG was obtained per liter of growth media with a flavin incorporation of ~75%. High-resolution MALDI-TOF of the extracted flavin from the active site of NbtG yielded an *m/z* value of 784.15, which is consistent with flavin adenine dinucleotide (FAD) (data not shown). The flavin spectrum of NbtG displayed characteristic absorbance maxima at 380 and 452 nm for oxidized FAD (Fig. 10.1). The extinction coefficient at 452 nm was 12,600 $M^{-1}cm^{-1}$. The same results were obtained for the NbtG P238R and K64A variants.

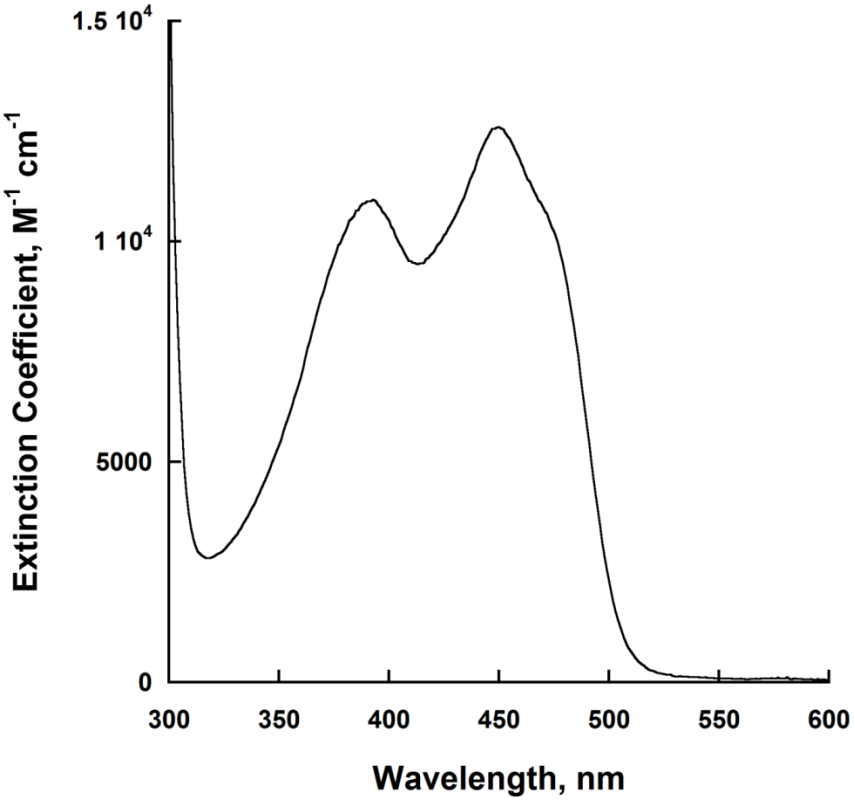

Figure 10.1 UV−visible spectrum of the flavin bound to NbtG, which has absorbance peaks at 380 nm and 452 nm.

3.2 Oxygen consumption. The activity of NbtG was monitored by measuring the rate of oxygen consumption with either NADPH or NADH (Table 10.2). NbtG is highly active in the absence of L-Lys, having ~2-fold higher activity with NADPH as compared to NADH. Under these conditions, NbtG functions as an oxidase, since no hydroxylation occurs. With NADPH, in the presence of L-Lys a ~2-fold increase in the k_{cat} value was determined, and a ~5-fold increase when D-Lys was used as substrate. When NADH was used as the coenzyme, the k_{cat} values increased ~4 and ~8-fold in the presence of L-Lys and D-Lys, respectively. In the presence of L-Lys the k_{cat}/K_{NADPH} was only 2-fold higher than for k_{cat}/K_{NADH}. In the presence of D-Lys the k_{cat}/K_{NADPH} value was ~4-fold higher. Thus, NbtG does not have significant coenzyme selectivity, in contrast to other Class B flavin monooxygenases which are all highly selective for NADPH (1,37-39).

Table 10.2 Activity of NbtG following oxygen consumption.

NADPH			
	No Lys	**L-Lys**	**D-Lys**
k_{cat} (s^{-1})	0.58 ± 0.02	1.08 ± 0.01	2.9 ± 0.1
K_{NADPH} (mM)	0.20 ± 0.02	0.14 ± 0.01	0.51 ± 0.06
k_{cat}/K_{NADPH} ($M^{-1}s^{-1}$)	2900 ± 300	7700 ± 500	5600 ± 700
NADH			
	No Lys	**L-Lys**	**D-Lys**
k_{cat} (s^{-1})	0.32 ± 0.01	1.29 ± 0.04	2.5 ± 0.1
K_{NADH} (mM)	0.36 ± 0.05	0.40 ± 0.04	1.6 ± 0.2
k_{cat}/K_{NADH} ($M^{-1}s^{-1}$)	900 ± 100	3300 ± 400	1500 ± 200

Conditions: 100 mM sodium phosphate pH 7.5, 25 °C. L-Lys and D-Lys were present at saturating concentration (2 mM for L-Lys and 10 mM for D-Lys).

3.3 Lysine hydroxylation. NbtG displayed significant activity as measured by the oxygen consumption assay. To determine if hydroxylation of L-Lys was taking place, NbtG was reacted

with NADPH in excess and 1 mM L-Lys and the reaction was monitored by UPLC after derivatization of the amino acid as described in the materials and methods. The results clearly show that NbtG is able to produced L-Lys-OH (Fig. 10.2). In order to quantitate the amount of L-Lys-OH produced, the Csaky iodine oxidation assay was performed. The reaction was initially done using NADPH as the reducing substrate (Table 10.3). Under fully coupled conditions, one equivalent of hydroxylated D/L-Lys should be produced for every one equivalent of oxygen consumed. Very similar k_{cat} values were determined for hydroxylation of D/L-Lys; however, the values were ~ 3-7-fold lower than the k_{cat} values obtained in the oxygen consumption assay. These results suggest that NbtG is highly uncoupled, producing oxygen reactive species in addition to hydroxylated D/L-Lys. Substrate inhibition was observed when NADPH was varied in the presence of saturating levels of either D- or L-Lys, with a lower $K_{I(NADPH)}$ value with L-Lys. The k_{cat}/K_M value for L-Lys was ~6-fold higher than for D-Lys, which originates mainly from a lower K_M value for L-Lys. Weak substrate inhibition was observed with L-Lys, which is a common feature observed in other NMOs. With D-Lys, no substrate inhibition was observed, most likely because of the lower affinity. Very similar results were observed when NADH was used as the coenzyme (Table 10.3).

Table 10.3 Activity of NbtG following Lys hydroxylation.

	NADPH		NADH	
	L-Lys	**D-Lys**	**L-Lys**	**D-Lys**
k_{cat} (s^{-1})	0.32 ± 0.02	0.41 ± 0.03	0.62 ± 0.08	0.31 ± 0.02
$K_{NAD(P)H}$ (mM)	0.7 ± 0.2	0.5 ± 0.1	0.6 ± 0.1	3.8 ± 2.4
$K_{I\,(NAD(P)H)}$ (mM)	2.4 ± 0.6	35 ± 24	5.7 ± 1.7	2.1 ± 1.5
$k_{cat}/K_{NAD(P)H}$ ($M^{-1}s^{-1}$)	460 ± 130	520 ± 120	1100 ± 300	80 ± 50
K_{Lys} (mM)	0.35 ± 0.05	2.6 ± 0.3	0.9 ± 0.3	4.2 ± 0.6
$K_{I\,(Lys)}$ (mM)	15 ± 3	-	6.3 ± 2.5	-
$k_{cat}/K_{m\,(Lys)}$ ($M^{-1}s^{-1}$)	910 ± 140	100 ± 20	580 ± 230	70 ± 10
Uncoupling (%)	70	86	52	92

Conditions: 100 mM sodium phosphate pH 7.5, 25 °C. The final concentration of L-Lys was 2 mM and of D-Lys was 10 mM. Uncoupling was calculated using the following equation, $(1-k_{cat(N\text{-}OH)}/k_{cat\,(O2)})*100$, where $k_{cat(N\text{-}OH)}$ is the k_{cat} calculated measuring hydroxylated D/L-Lys and $k_{cat\,(O2)}$ the k_{cat} from the oxygen consumption assay.

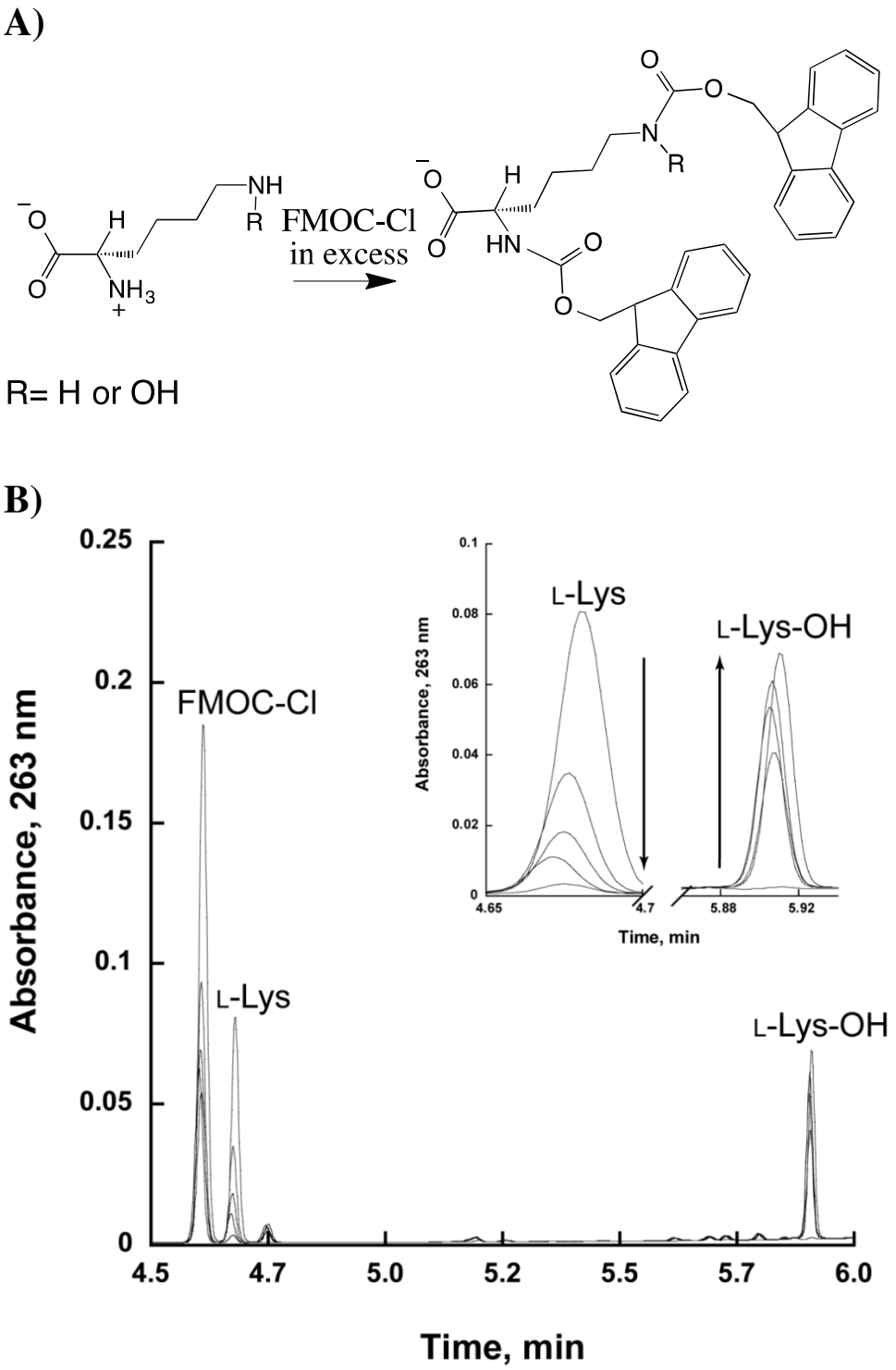

Figure 10.2 Production of hydroxylated lysine (L-Lys-OH) by NbtG**.** (A) Scheme of the derivatization reaction of L-Lys with FMOC-Cl. FMOC-Cl can react with the amino groups of either L-Lys or L-Lys-OH. (B) UPLC chromatogram (263 nm) showing the elution of L-Lys and L-Lys-OH derivatized with FMOC-Cl. The inset shows a zoomed in view of the L-Lys peak decreasing and the L-Lys-OH peak increasing between 0 and 3 min.

3.4 Reactive oxygen species production. By comparing the k_{cat} values measured in the oxygen consumption assay (in the presence of either L- or D-Lys) with the k_{cat} values measured in the hydroxylation assay, it was determined that there was a substantial degree of uncoupling (less than one hydroxylated D/L-Lys per oxygen consumed) in the reaction catalyzed by NbtG. In general, coupling was higher with L-Lys than with D-Lys and did not significantly vary if NADPH or NADH were used (Table 10.3).

With enzymatic assays highlighting such a substantial uncoupling, we next asked the question as to the type of product generated since flavoenzymes can produce both hydrogen peroxide and superoxide upon reacting with oxygen. The kinetic analysis indicated that the oxidase activity of NbtG partly produces superoxide and hydrogen peroxide, which were detected using both NADPH and NADH either in the absence or presence of D/L-Lys (Table 10.4). In summary, NbtG is rather inefficient in Lys hydroxylation because flavin reoxidation can efficiently occur through the direct generation of hydrogen peroxide and/or superoxide. This finding warranted a more in-depth kinetic and structural analysis to understand the features underlying such a functional property.

Table 10.4 Oxygen reactive species produced during oxidation of NbtG.

Hydrogen peroxide	k_{cat} (s^{-1})		
	No Lys	**2 mM L-Lys**	**10 mM D-Lys**
NADPH	0.31 ± 0.1	0.20 ± 0.04	0.40 ± 0.05
NADH	0.27 ± 0.02	0.32 ± 0.05	0.40 ± 0.04
Superoxide	k_{cat} (s^{-1})		
	No Lys	**2 mM L-Lys**	**10 mM D-Lys**
NADPH	0.30 ± 0.02	0.30 ± 0.02	0.23 ± 0.01
NADH	0.22 ± 0.02	0.17 ± 0.004	0.34 ± 0.02

Conditions: 100 mM sodium phosphate pH 7.5, 25 °C. The final concentration of L-Lys was 2 mM and of D-Lys 10 mM.

3.5 Flavin reduction. Flavin reduction was monitored as a function of NADPH in both the presence and absence of L-Lys (Fig. 10.3). The reaction was monitored by measuring the decrease in absorbance at 452 nm in the stopped-flow spectrophotometer. Two kinetic phases were observed in this reduction of NbtG. The first phase was ~10-fold faster than the second and both were dependent on NADPH concentration. The slow phase might originate from a small population of less active enzyme in our sample. Binding of either L-Lys or D-Lys did not change the rate of flavin reduction or the binding affinity for NADPH (Table 10.5).

Table 10.5 Rapid reaction kinetic parameters for NbtG with NADPH.

	No Lys	
	fast phase	**slow phase**
k_{red}, s^{-1}	1.00 ± 0.03	0.120 ± 0.002
K_D , mM	0.20 ± 0.03	0.23 ± 0.03
k_{red}/K_D, $M^{-1}s^{-1}$	5000 ± 760	520 ± 70
	L-Lys	
k_{red}, s^{-1}	0.92 ± 0.03	0.106 ± 0.003
K_D, mM	0.26 ± 0.04	0.28 ± 0.04
k_{red}/K_D, $M^{-1}s^{-1}$	3540 ± 560	380 ± 60
	D-Lys	
k_{red}, s^{-1}	1.00 ± 0.02	0.120 ± 0.001
K_D, mM	0.20 ± 0.01	0.19 ± 0.006
k_{red}/K_D, $M^{-1}s^{-1}$	5000 ± 270	620 ± 20

Conditions: 100 mM sodium phosphate pH 7.5, 25 °C.

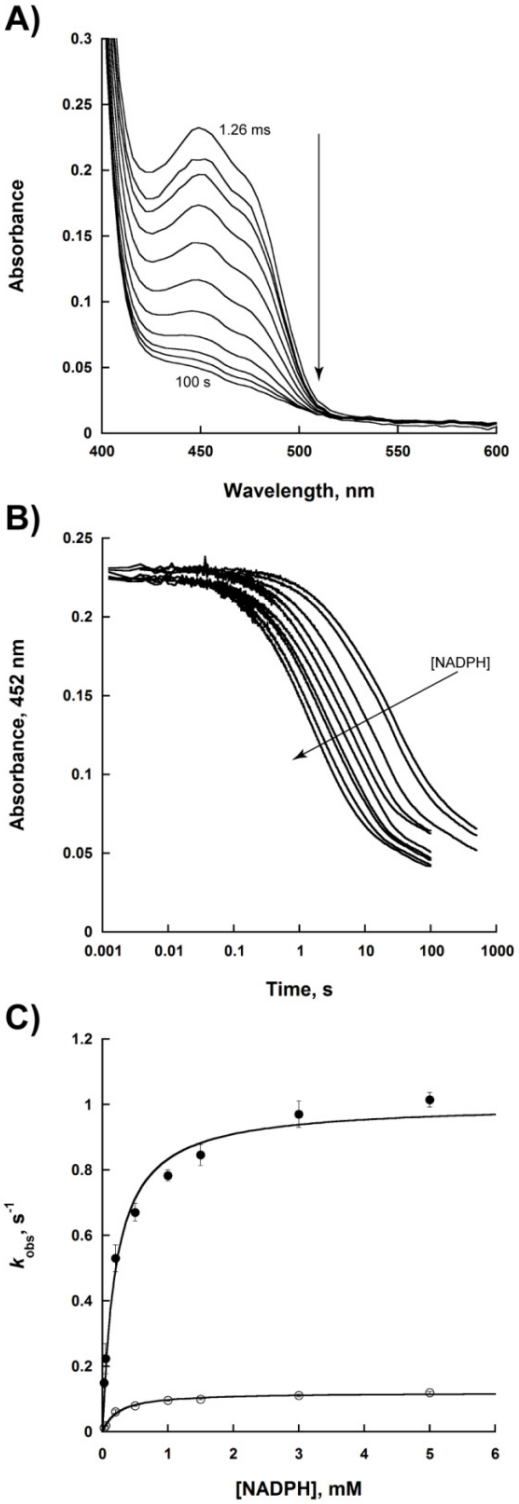

Figure 10.3 Flavin reduction with NADPH. (A) Spectra of reduction with 3 mM NADPH monitored over 100 s. (B) Change in the flavin absorbance at 452 nm at various concentrations of NADPH (0.025 – 5 mM). The changes in absorbance at 452 nm were fit to eq. 2 to obtain the k_{obs} values of the two phases. (C) Dependence of the k_{obs} values as a function of NADPH for the fast phase (●) and slow phase (○) The data were fit to eq. 3.

3.6 Kinetic isotope effects. The hydride transfer step was probed using deuterium kinetic isotope effects (KIEs). KIEs were calculated by measuring the ratio of the kinetic values determined with NADPH and to those determined with *R*-[4^{2}H]-NADPH. Under steady-state conditions a $^{D}k_{cat}$ value of 1.58 ± 0.03 and a $^{D}k_{cat}/K_m$ value of 1.0 ± 0.1 were obtained. Under rapid reaction conditions, a kinetic isotope effect for flavin reduction was observed for both phases with $^{D}k_{red}$ values being 1.5 ± 0.1 and 1.4 ± 0.1, for the fast and slow phase, respectively. A $^{D}k_{red}/K_D$ value of 0.7 ± 0.2 was measured for the fast phase and a $^{D}k_{red}/K_D$ value of 1.0 ± 0.3 was measured for the slow phase. These data are consistent with the hydride transfer step being only partially rate-limiting. Solvent kinetic isotope effects were measured to determine if a proton transfer occurs in the rate-limiting step in the reaction catalyzed by NbtG. A $^{D2O}k_{cat}$ value of 2.43 ± 0.03 was determined, which indicates that the proton transfer step is significantly rate-limiting.

3.7 Flavin oxidation. Flavin oxidation was monitored as a function of molecular oxygen concentration. NbtG oxidation occurs in a single step process, without the stabilization of a FAD_{OOH} intermediate. In the absence of D/L-Lys, a rate of 3,100 ± 200 M^{-1} s^{-1} was determined. In the presence of L-Lys, this value increased to 3,900 ± 100 M^{-1} s^{-1} whereas the rate was 5,400 ± 400 M^{-1} s^{-1} in the presence of D-Lys (Fig. 10.4). The effect of excess $NADP^+$ on flavin oxidation was also determined. Addition of 0.5 − 10 mM $NADP^+$ did not change the rate of flavin oxidation nor was there evidence of the spectra for the FAD_{OOH} intermediate (Fig. 10.4C).

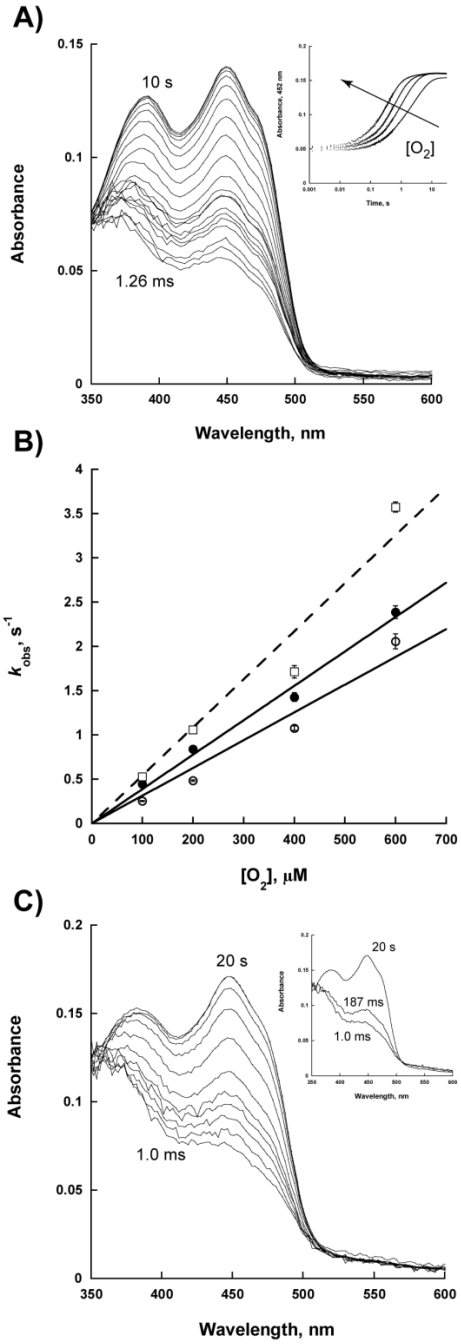

Figure 10.4 Flavin oxidation of NbtG. (A) Spectra changes of the reaction of reduced NbtG with 270 μM O_2. The inset shows the changes in absorbance at 452 nm as a function of oxygen concentration (100, 200, 400, and 600 μM O_2). The data was fit to eq 4. (B) k_{obs} values as a function of O_2 without Lys (open circles), with 2 mM L-Lys (solid circles), and with 10 mM D-Lys (open squares, dashed line). (C) Spectra of NbtG flavin oxidation with 3 mM $NADP^+$. The spectra of flavin oxidation were subtracted from the spectrum of 3 mM $NADP^+$ alone. The inset shows the deconvoluted flavin spectra. The data was fit to a two-step process in order to determine if a transient C4a-hydroperoxyflavin is present. Pro-K (Applied Photophysics) was used in order to deconvolute the flavin spectra.

3.8 $NADP^+$ binding. It has been determined that $NADP^+$ is essential for stabilization of the FAD_{OOH} intermediate in members of Class B flavin-dependent monooxygenases. In PvdA and SidA, $NADP^+$ has similar affinity to NADPH. Using the spectral perturbation methods, a K_D value of 2.0 ± 0.5 mM was determined for $NADP^+$ binding to oxidized NbtG (Fig. 10.5). Thus, for NbtG, the K_D for $NADP^+$ is ~10-fold higher than the K_D for NADPH (Table 10.5)

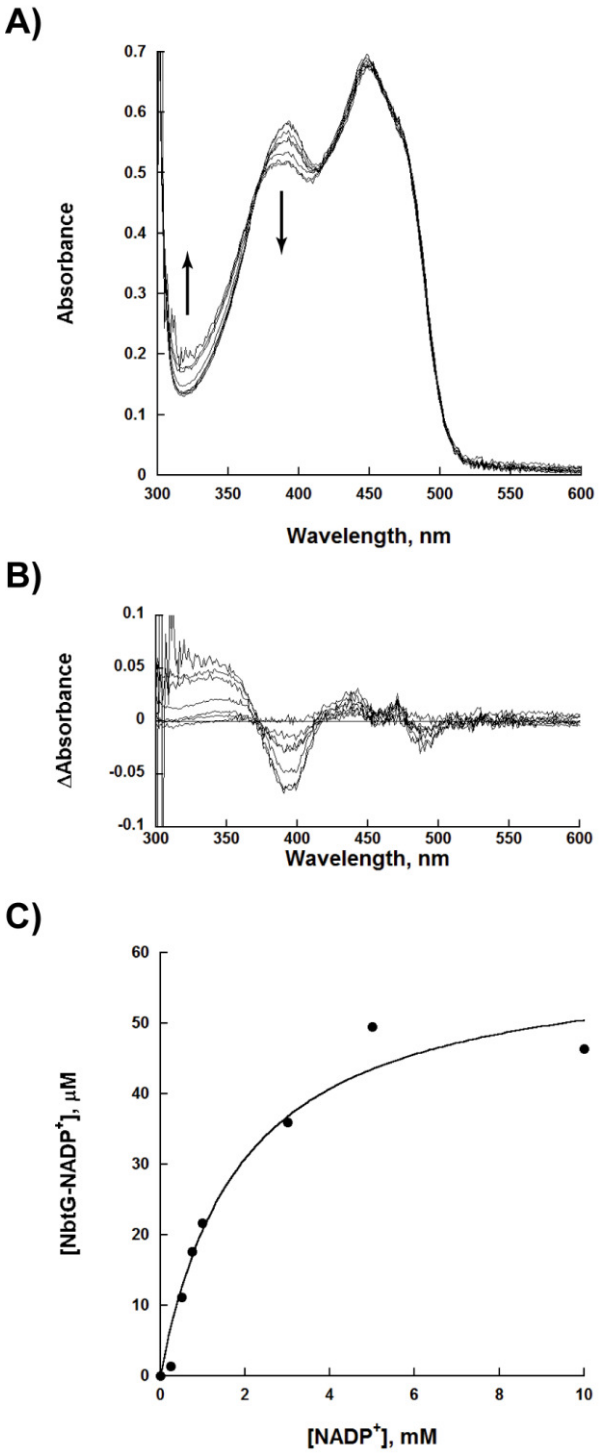

Figure 10.5 $NADP^+$ binding to NbtG. (A) Flavin spectra changes as a function of increasing concentrations of $NADP^+$ (0 – 10 mM). The spectral changes show an increase in absorbance at 340 nm and a decrease in absorbance at 395 nm. (B) Spectra differences after subtracting the spectrum of NbtG with 0 mM $NADP^+$. (C) Determination of the K_D value of $NADP^+$. The concentration of the NbtG-$NADP^+$ complex was plotted as a function of $NADP^+$ in order to determine a K_D value.

3.9 Three-dimensional structural analysis of NbtG. The crystal structure of NbtG was solved by SAD at the selenium edge and refined at 2.4 Å resolution (Table 10.1). The four NbtG molecules present in the asymmetric unit form a compact tetramer with the same arrangement observed in the L-Orn monooxygenases SidA (10) and PvdA (11) (their monomeric and dimeric structures, respectively, form a tetramer through application of crystallographic symmetry operators); in KtzI a similar but not identical tetramer was observed (12). The NbtG subunit folds into a two-domain topology similar to that of other NMOs: the FAD-binding domain (residues 1-178 and 337-429), including the non-covalently bound FAD cofactor (Fig. 10.6B), and the NADPH-binding domain (residues 179-336). Nearly all 429 residues of the protein could be modeled for each of the four polypeptide chains present in the asymmetric unit except for monomer D, in which one-third of the molecule (i.e. most of the $NADP^+$ domain) lacks clear electron density (Fig. 10.6A).

A)

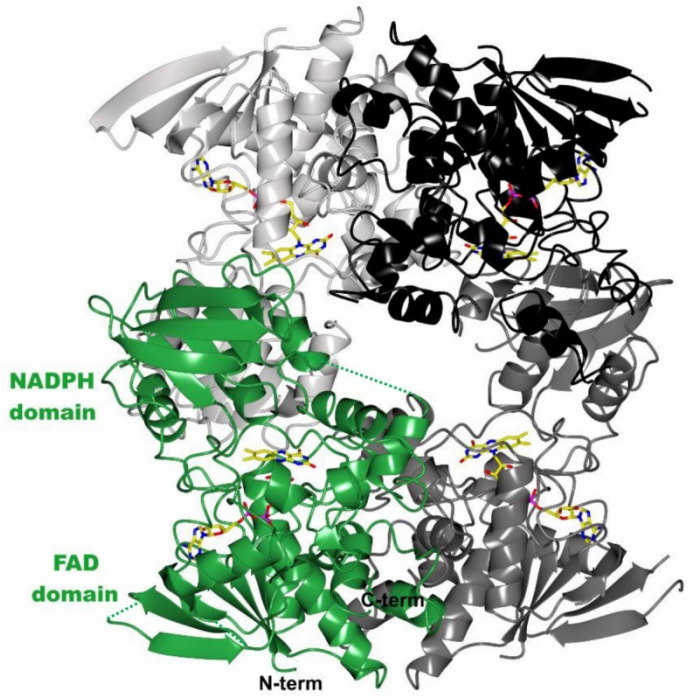

B)

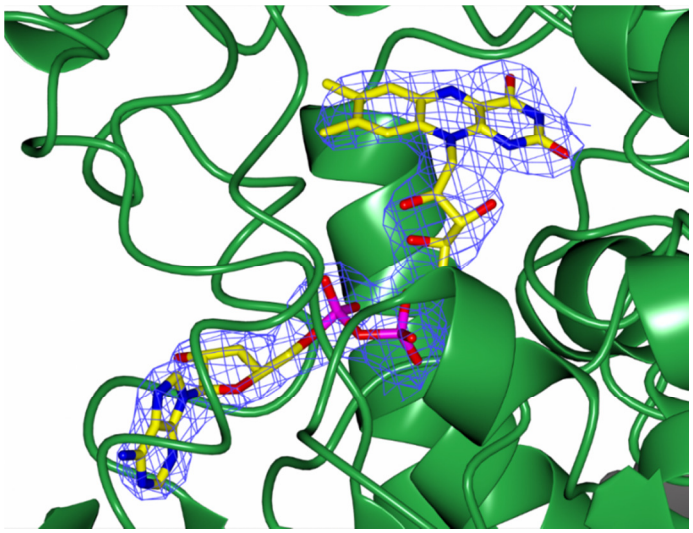

Figure 10.6 Crystal structure of NbtG. (A) Ribbon diagram of the crystallographic tetramer of NbtG observed in the asymmetric unit. Monomers A, B, C, and D of the tetramer are represented in green, light gray, dark gray and black, respectively. The FAD cofactor is drawn as sticks for each monomer, with carbon, oxygen, nitrogen and phosphorus atoms colored in yellow, red, blue, and magenta, respectively. For the sake of clarity, flexible regions which lack electron density, are indicated only for monomer A as green dashed lines (residues 143-149, 158-160, 241-247; the C-terminal 414-429 residues could not be included in the final model). (B) Close-up view (same orientation as Fig. 10.6A) of FAD bound to monomer A with its refined weighted 2Fo-Fc electron density contoured at 1.2 σ.

The structures of the homologous SidA (10) and PvdA (11) NMOs were elucidated in complex with L-Orn and $NADP^+$, whereas, despite extensive screening of NbtG crystals grown in the presence of either $NADP^+/NAD^+$ or NADPH/NADH and/or D/L-Lys, no electron density for any ligand except for the FAD cofactor could be detected. NbtG shares about 20% sequence identity and the same domain topology with SidA, PvdA and KtzI. However, comparison of NbtG structure with those of SidA, PvdA and KtzI reveals a large change in domain orientation. More specifically, the program DynDom (40) indicates that the NADPH domain of NbtG is rotated by 33° with respect to the same domain of SidA using the superimposed FAD domains as reference. Such a rotation occurs through an axis passing through the residues (175-178 and 335-337 in NbtG) linking the two protein domains (Fig. 10.7A). This finding provides a rationale for the unsuccessful attempts to obtain the $NADP^+$ and D/L-Lys bound to NbtG in this crystalline form. The domain rotation found in the NbtG structure makes the nicotinamide-binding site in front of the FAD ring become occluded by an α-helical segment, preventing NADP(H) binding (Figs. 10.7B and 10.8). Likewise, structural comparison shows that the residues responsible for binding the L-Orn backbone group in SidA are conserved in NbtG (Lys64, Asn252, Ser402) but their relative positions are modified (Fig. 10.8). In essence, the domain rotation featured by the NbtG structure drastically alters the active site geometry and accessibility. Differences in the $NAD(P)^+$ binding site may explain also the lack of $NAD^+/NADP^+$ specificity found in NbtG. In SidA the position of the $NADP^+$ adenine-ribose moiety is stabilized by a network of interactions that also involve the phosphate. In particular, the ribose 3'-OH is H-bonded to both the side chain and the peptidic nitrogen of Ser254, whereas the phosphate interacts with Ser325 and with Arg279 (37). In NbtG, Arg279 is substituted by Pro238 and Ser325 by Asp277 whose longer side chain is likely to interact with the ribose rather than with the phosphate. All of these NbtG

residues are also conserved in MbsG, which is consistent with the similar cofactor specificity properties of the mycobacterial enzyme.

A)

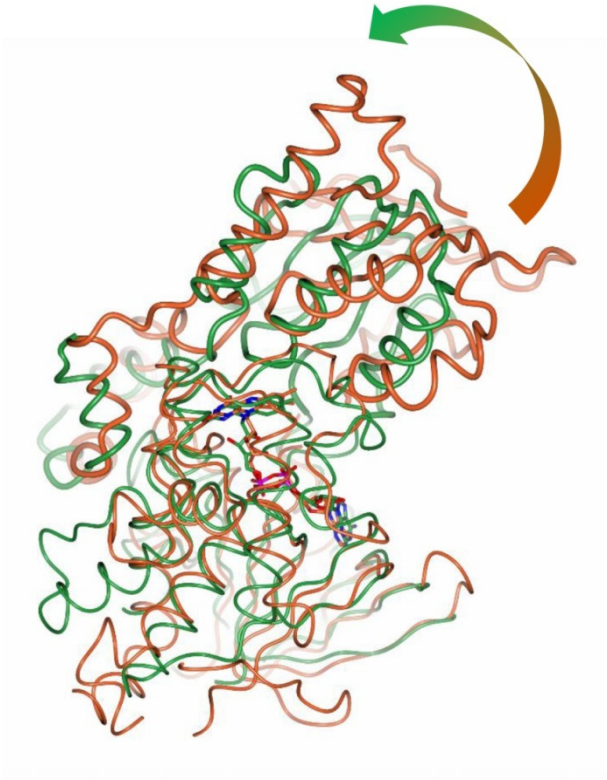

B)

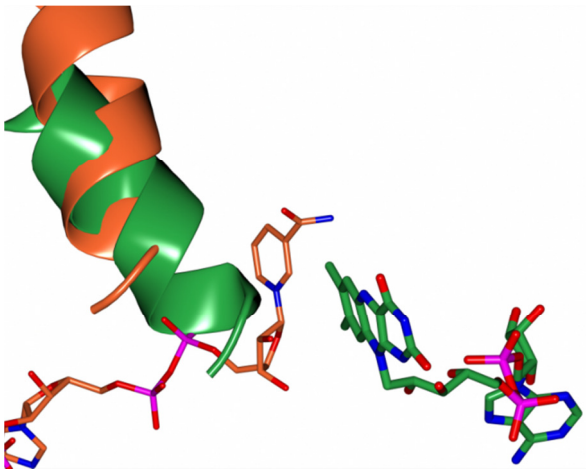

Figure 10.7 Comparison of SidA (PDB code 4b64; $NADP^+$ complex)[14] and NbtG. (A) The large change in the orientation of the NADPH-binding domains is visualized by superimposing NbtG (green) and SidA (orange) structures using their respective FAD-binding domains (rmsd = 2.5 Å for the equivalent Cα atoms). The shaded arrow outlines the additional 33° rotation, which is needed for the optimal superposition of the $NADP^+$-binding domains (highlighted as bold worms). (B) Close-up view of the flavin site in NbtG (green) and SidA (orange). Because of the domain rotation, the nicotinamide-ribose site in NbtG is physically occluded by an α-helix (residues 215-229) of the $NADP^+$-binding domain.

3.10 Steady-state kinetic properties of P238R. To determine if replacing Pro at position 238 to Arg resulted in a higher affinity and specificity for NADPH, the NbtG P238R mutant was created. The steady-state kinetic parameters were determined by monitoring oxygen consumption and lysine hydroxylation. Oxygen consumption data shows that in the presence of L-Lys the k_{cat} value is only ~2-fold lower and the K_{NADPH} value is ~5-fold higher than wild-type, however, no activity was observed with NADH (Table 10.6). Similar results were obtained when lysine hydroxylation was monitored. The levels of uncoupling are very similar to those calculated for the wild-type enzyme.

Table 10.6 Steady-state kinetic parameters for NbtG P238R.

	O_2 Consumption	**L-Lys Hydroxylation**
k_{cat} (s^{-1})	0.60 ± 0.04	0.146 ± 0.009
K_{NADPH} (mM)	0.8 ± 0.2	0.7 ± 0.2
k_{cat}/K_{NADPH} ($M^{-1}s^{-1}$)	790 ± 170	210 ± 60
$K_{I\ (NADPH)}$ (mM)	-	1.6 ± 0.4
Uncoupling (%)	-	76

Conditions: 100 mM sodium phosphate pH 7.5 with 2 mM D/L-Lys. Uncoupling was calculated using the following equation, $(1- k_{cat(N\text{-}OH)}/k_{cat\ (O2)})*100$, where $k_{cat(N\text{-}OH)}$ is the k_{cat} calculated measuring hydroxylated L-Lys and $k_{cat\ (O2)}$ the k_{cat} from the oxygen consumption assay.

3.11 Steady-state kinetic properties of K64A. Although the structure of NbtG did not contain electron density for Lys, the amino acids involved in L-Orn binding in SidA, PvdA, and KtzI are conserved in NbtG (Fig. 10.8). We probed the role of K64 in L- and D-Lys binding by mutating it to Ala. The steady-state lysine hydroxylation data clearly show that the major effect is on the K_m value for L- and D – Lys. The $K_{L\text{-}Lys}$ value increased ~40-fold while the $K_{D\text{-}Lys}$ value increased ~15-20-fold. In contrast, the k_{cat} values decreased only ~3-13-fold (Table 10.7). The uncoupling values for K64A are similar to the values obtained for the wild-type enzyme (Table 10.7). This

data indicates that K64A is primarily involved in Lys binding in NbtG as predicted from the three-dimensional structure.

Table 10.7 Steady-state kinetic parameters for NbtG K64A.

	NADPH		**NADH**	
	L-Lys	D-Lys	L-Lys	D-Lys
k_{cat}, s^{-1}	0.34 ± 0.01	0.130 ± 0.004	0.180 ± 0.005	0.021 ± 0.001
K_{Lys}, mM	13 ± 1	49 ± 4	40 ± 3	62 ± 5
k_{cat}/K_{Lys}, $M^{-1}s^{-1}$	27 ± 3	2.7 ± 0.2	4.4 ± 0.4	0.38 ± 0.03
Uncoupling, %	78	89	69	94

Conditions: 100 mM sodium phosphate pH 7.5 with 2 mM NAD(P)H. Uncoupling was calculated using the following equation, (1- $k_{cat(N\text{-}OH)}/k_{cat\ (O2)}$)*100, where $k_{cat(N\text{-}OH)}$ is the k_{cat} calculated measuring hydroxylated D/L-Lys and $k_{cat\ (O2)}$ the k_{cat} from the oxygen consumption assay.

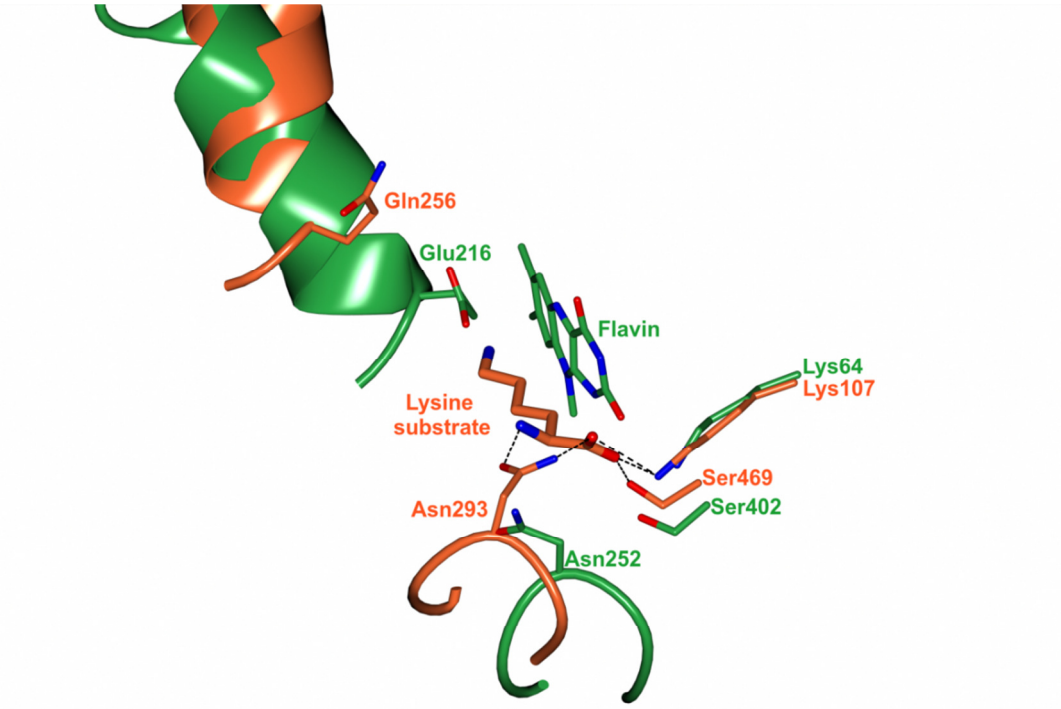

Figure 10.8 Comparison of NbtG (green) and SidA (orange) active sites. For the sake of clarity, only the flavin ring of NbtG is drawn. Equivalent residues surrounding the flavin site of the two enzymes and the position of the L-Lys substrate bound to the SidA active site are drawn (dashed lines indicate hydrogen bonds, which stabilize substrate binding). Loop 276-279 of NbtG and loop 321-324 of SidA are shown to highlight the different conformation.

4. Discussion

NMOs represent a class of flavin monooxygenases involved in the biosynthesis of hydroxamate-containing siderophores, whose iron-chelating properties are responsible for the virulence of microbes that secrete them. The L-Lys monooxygenase NbtG from *Nocardia farcinica* catalyzes the hydroxylation of L-Lys in the pathway leading to the production of the siderophore nocobactin (Scheme 10.1), similar to what occurs in mycobacteria for mycobactin biosynthesis by the MbsG and MbtG proteins (20). Homologous enzymes are represented by L-Orn monooxygenases such as SidA (13), PvdA (11), and KtzI (12) which specifically hydroxylate L-Orn to generate siderophores. Like other flavin monooxygenases, the NMOs catalytic process begins with binding of NADPH, which reduces the flavin cofactor that, in turn, reacts with molecular oxygen generating the FAD_{OOH} intermediate capable of donating the distal oxygen to the substrate.

We first studied the NbtG reaction by probing the enzyme cofactor specificity. In contrast to L-Orn monooxygenases, which show a clear preference for NADPH, NbtG can also use NADH as a reducing agent, though at a lower efficiency. The same was observed for MbsG where, nevertheless, the K_M values for both cofactors are higher than those measured with NbtG: for the mycobacterial enzyme K_{NADPH} and K_{NADH} are 12.0 mM and 7.0 mM, respectively, whereas values of 0.20 mM and 0.36 mM were determined with NbtG (Table 10.2) (21). In either case, the presence of the L-Lys substrate does not significantly alter the affinity for the coenzymes. Comparative analysis of NbtG and SidA structures show that the interactions in SidA that stabilize the NADPH 2'-OH-phosphate during binding (Arg279 and Ser325 side chains) do not form in NbtG (and neither in MbsG) because these residues are not conserved and, therefore, either NADH or NADPH would indifferently bind to these Lys monooxygenases.

Substitution of Pro to an Arg at position 238 (the corresponding position for Arg279 in SidA), converted NbtG into a NADPH specific monooxygenase, but increased the K_M value for NADPH. Furthermore, the P238R enzyme was as uncoupled as wild-type NbtG. These results suggest that the mode of binding of NADP(H) in NbtG is different from what is observed in SidA and PvdA.

The kinetics of the NbtG reaction were investigated by measuring the O_2 consumption rate under steady-state conditions by using an Oxygraph. A k_{cat} value of 0.58 s^{-1} was determined for NADPH and a ~2-fold increase was obtained in the presence of L-Lys, with this substrate effect being even more pronounced with NADH. We also probed the substrate stereospecificity of NbtG and we found that the enzyme is also active on D-Lys although it binds L-Lys with a higher affinity. The results of the K64A mutant support a conserved amino acid substrate binding site among members of the NMO group of enzymes.

We then investigated the overall reaction leading to substrate hydroxylation by isotope effect analysis and by quantifying the final product using the Csaky assay. Flavin reduction occurs through two phases, one being ~10-times faster than the other and both dependent on NADPH concentration. While hydride transfer has been shown to be the rate-limiting step in SidA, isotope effect experiments showed that in NbtG this step is only partially rate-limiting. The large solvent kinetic isotope effect suggests that a proton exchangeable step is the slow step in the reaction. Similar to MbsG, we found that the k_{cat} of D/L-Lys hydroxylation is significantly lower than that of O_2 consumption even in the presence of the substrate and production of superoxide and hydrogen peroxide was also detected using both NADPH and NADH (Table 10.4). This means that NbtG undergoes a number of unproductive catalytic cycles with an uncoupling level of 70% for L-Lys hydroxylation from O_2 consumption using NADPH as the

reducing agent and 52% in the case of NADH (Table 10.3). Even more pronounced uncoupling effects were detected with D-Lys as the substrate.

NbtG represents the first crystal structure of an L-Lys monooxygenase (Fig. 10.6A). Structural comparison with L-Orn monooxygenases revealed that, while the NADPH domain is individually very similar to those of SidA and PvdA, in NbtG it is differently oriented by about 30° with respect to the FAD domain. Importantly, such a domain rotation alters the NADPH-binding site, which becomes physically inaccessible to the dinucleotide cofactor. Although domain rotations have been found among members of this family of flavoenzymes (41) (including NMOs, Baeyer-Villiger enzymes, and flavin-containing monooxygenases), such a large change so drastically affecting the active center has not been observed thus-far. Combining these findings with the enzymological data, we hypothesize that in NbtG the catalytic uncoupling of O_2 consumption from substrate hydroxylation is related to this peculiar NADPH domain conformation. After reduction of the flavin by NADPH, the enzyme might quickly release $NADP^+$ and adopt the "occluded" conformation observed in the crystal structure. Along with this, flavin re-oxidation will occur without any stable formation of the FAD_{OOH}, whose stability requires bound $NADP^+$ (16,42). Alternatively, the FAD_{OOH} might form but will quickly decay upon release of $NADP^+$. In either case, flavin reoxidation occurs without stable formation of the FAD_{OOH}, which is fully consistent with the low $NADP^+$ affinity, lack of a detectable intermediate in flavin reoxidation, and the substantial uncoupling featured by the enzyme (Fig. 10.4 and Table 10.3).

These findings raise the intriguing question as to the biological significance of these functional and structural features. The possibility exists that NbtG and the homologous mycobacterial MbsG are uncoupled because they dually function as both Lys hydroxylases and

NADPH oxidases, with this second activity possibly being involved in ROS generation and signaling. Alternatively, these properties might be instrumental in enzyme regulation by yet-unknown factors that control the oxidase *versus* the hydroxylase activities for instance through stabilization of the functionally distinct enzyme conformations.

5. Acknowledgments

This work was supported in part by a grant from the National Science Foundation MCB-1021384 (to PS). JSMC was supported by a Postdoctoral fellowship from the National Council of Science and Technology of Mexico (CONACYT). We thank the European Synchrotron Radiation Facility (ESRF) and the Swiss Light Source (SLS) for providing beamtime and assistance, and the BioStruct-X program (project n. 5275) for funding synchrotron trips. Support for the work at the National Synchrotron Light comes principally from the Offices of Biological and Environmental Research and of Basic Energy Sciences of the US Department of Energy, and from the National Center for Research Resources (P41RR012408) and the National Institute of General Medical Sciences (P41GM103473) of the National Institutes of Health. We would also like to thank the anonymous reviewers for their suggestions.

6. References

1. Meneely, K. M., and Lamb, A. L. (2007) Biochemical characterization of a flavin adenine dinucleotide-dependent monooxygenase, ornithine hydroxylase from Pseudomonas aeruginosa, suggests a novel reaction mechanism. *Biochemistry* **46**, 11930-11937
2. Kang, H. Y., Brickman, T. J., Beaumont, F. C., and Armstrong, S. K. (1996) Identification and characterization of iron-regulated Bordetella pertussis alcaligin siderophore biosynthesis genes. *J. Bacteriol.* **178**, 4877-4884
3. Macheroux, P., Plattner, H. J., Romaguera, A., and Diekmann, H. (1993) FAD and substrate analogs as probes for lysine N6-hydroxylase from Escherichia coli EN 222. *Eur. J. Biochem.* **213**, 995-1002

4. Barona-Gomez, F., Wong, U., Giannakopulos, A. E., Derrick, P. J., and Challis, G. L. (2004) Identification of a cluster of genes that directs desferrioxamine biosynthesis in Streptomyces coelicolor M145. *J. Am. Chem. Soc.* **126**, 16282-16283
5. Lynch, D., O'Brien, J., Welch, T., Clarke, P., Cuiv, P. O., Crosa, J. H., and O'Connell, M. (2001) Genetic organization of the region encoding regulation, biosynthesis, and transport of rhizobactin 1021, a siderophore produced by Sinorhizobium meliloti. *J. Bacteriol.* **183**, 2576-2585
6. Olucha, J., and Lamb, A. L. (2011) Mechanistic and structural studies of the N-hydroxylating flavoprotein monooxygenases. *Bioorg. Chem.* **39**, 171-177
7. Hissen, A. H., Wan, A. N., Warwas, M. L., Pinto, L. J., and Moore, M. M. (2005) The Aspergillus fumigatus siderophore biosynthetic gene sidA, encoding L-ornithine N5-oxygenase, is required for virulence. *Infect. Immun.* **73**, 5493-5503
8. Takase, H., Nitanai, H., Hoshino, K., and Otani, T. (2000) Impact of siderophore production on Pseudomonas aeruginosa infections in immunosuppressed mice. *Infect. Immun.* **68**, 1834-1839
9. De Voss, J. J., Rutter, K., Schroeder, B. G., Su, H., Zhu, Y., and Barry, C. E., 3rd. (2000) The salicylate-derived mycobactin siderophores of Mycobacterium tuberculosis are essential for growth in macrophages. *Proc. Nat. Acad. Sci.U S A* **97**, 1252-1257
10. Franceschini, S., Fedkenheuer, M., Vogelaar, N. J., Robinson, H. H., Sobrado, P., and Mattevi, A. (2012) Structural insight into the mechanism of oxygen activation and substrate selectivity of flavin-dependent N-hydroxylating monooxygenases. *Biochemistry* **51**, 7043-7045
11. Olucha, J., Meneely, K. M., Chilton, A. S., and Lamb, A. L. (2011) Two structures of an N-hydroxylating flavoprotein monooxgenase: the ornithine hydroxylase from Pseudomonas aeruginosa. *J. Biol. Chem.* **286**. 31780-31798.
12. Setser, J. W., Heemstra, J. R., Jr., Walsh, C. T., and Drennan, C. L. (2014) Crystallographic Evidence of Drastic Conformational Changes in the Active Site of a Flavin-Dependent N-Hydroxylase. *Biochemistry* **53**, 606063-6077.
13. Chocklett, S. W., and Sobrado, P. (2010) Aspergillus fumigatus SidA is a highly specific ornithine hydroxylase with bound flavin cofactor. *Biochemistry* **49**, 6777-6783
14. Meneely, K. M., Barr, E. W., Bollinger, J. M., Jr., and Lamb, A. L. (2009) Kinetic mechanism of ornithine hydroxylase (PvdA) from Pseudomonas aeruginosa: substrate triggering of O2 addition but not flavin reduction. *Biochemistry* **48**, 4371-4376
15. Mayfield, J. A., Frederick, R. E., Streit, B. R., Wencewicz, T. A., Ballou, D. P., and DuBois, J. L. (2010) Comprehensive spectroscopic, steady state, and transient kinetic studies of a representative siderophore-associated flavin monooxygenase. *J. Biol. Chem.* **285**, 30375-30388
16. Romero, E., Fedkenheuer, M., Chocklett, S. W., Qi, J., Oppenheimer, M., and Sobrado, P. (2012) Dual role of NADP(H) in the reaction of a flavin dependent N-hydroxylating monooxygenase. *Biochim. Biophys. Acta* **1824**, 850-857
17. Alfieri, A., Malito, E., Orru, R., Fraaije, M. W., and Mattevi, A. (2008) Revealing the moonlighting role of NADP in the structure of a flavin-containing monooxygenase. *Proc. Nat. Acad. Sci. U S A* **105**, 6572-6577
18. Malito, E., Alfieri, A., Fraaije, M. W., and Mattevi, A. (2004) Crystal structure of a Baeyer-Villiger monooxygenase. *Proc. Nat. Acad. Sci. U S A* **105**, 6572-6577

19. Plattner, H. J., Pfefferle, P., Romaguera, A., Waschutza, S., and Diekmann, H. (1989) Isolation and some properties of lysine N6-hydroxylase from Escherichia coli strain EN222. *Biol. Met.* **2**, 1-5
20. Robinson, R., and Sobrado, P. (2011) Substrate binding modulates the activity of Mycobacterium smegmatis G, a flavin-dependent monooxygenase involved in the biosynthesis of hydroxamate-containing siderophores. *Biochemistry* **50**, 8489-8496
21. Robinson, R. M., Rodriguez, P. J., and Sobrado, P. (2014) Mechanistic studies on the flavin-dependent N(6)-lysine monooxygenase MbsG reveal an unusual control for catalysis. *Arch. Biochem. Biophys.* **550-551**, 58-66
22. Hoshino, Y., Chiba, K., Ishino, K., Fukai, T., Igarashi, Y., Yazawa, K., Mikami, Y., and Ishikawa, J. (2011) Identification of nocobactin NA biosynthetic gene clusters in Nocardia farcinica. *J. Bacteriol.* **193**, 441-448
23. Fox, B. G., and Blommel, P. G. (2009) Autoinduction of protein expression. *Curr. Protoc. Protein Sci.* **Chapter 5**, Unit 5 23
24. Doublie, S. (1997) Preparation of selenomethionyl proteins for phase determination. *Methods Enzymol.***276**, 523-530
25. Heemstra, J. R., Jr., Walsh, C. T., and Sattely, E. S. (2009) Enzymatic tailoring of ornithine in the biosynthesis of the Rhizobium cyclic trihydroxamate siderophore vicibactin. *J. Am. Chem. Soc.* **131**, 15317-15329
26. Csaky, T. (1948) On the Estimation of Bound Hydroxylamine in Biological Materials. *Acta Chem. Scand.* 450-454
27. Jeong, S. S., and Gready, J. E. (1994) A method of preparation and purification of (4R)-deuterated-reduced nicotinamide adenine dinucleotide phosphate. *Anal. Biochem.* **221**, 273-277
28. Dhatwalia, R., Singh, H., Solano, L. M., Oppenheimer, M., Robinson, R. M., Ellerbrock, J. F., Sobrado, P., and Tanner, J. J. (2012) Identification of the NAD(P)H binding site of eukaryotic UDP-galactopyranose mutase. *J. Am. Chem. Soc.* **134**, 18132-18138
29. Goldschmidt, L., Cooper, D. R., Derewenda, Z. S., and Eisenberg, D. (2007) Toward rational protein crystallization: A Web server for the design of crystallizable protein variants. *Protein Sci.* **16**, 1569-1576
30. Battye, T. G., Kontogiannis, L., Johnson, O., Powell, H. R., and Leslie, A. G. (2011) iMOSFLM: a new graphical interface for diffraction-image processing with MOSFLM. *Acta. Acta Crystallogr. D* **67**, 271-281
31. Winn, M. D., Ballard, C. C., Cowtan, K. D., Dodson, E. J., Emsley, P., Evans, P. R., Keegan, R. M., Krissinel, E. B., Leslie, A. G., McCoy, A., McNicholas, S. J., Murshudov, G. N., Pannu, N. S., Potterton, E. A., Powell, H. R., Read, R. J., Vagin, A., and Wilson, K. S. (2011) Overview of the CCP4 suite and current developments. *Acta Crystallogr. D* **67**, 235-242
32. Pape, T., Schneider, T.R. . (2004) HKL2MAP: a graphical user interface for phasing with SHELX programs. *J. Appl. Cryst.* **37**, 843-884
33. Adams, P. D., Afonine, P. V., Bunkoczi, G., Chen, V. B., Davis, I. W., Echols, N., Headd, J. J., Hung, L. W., Kapral, G. J., Grosse-Kunstleve, R. W., McCoy, A. J., Moriarty, N. W., Oeffner, R., Read, R. J., Richardson, D. C., Richardson, J. S., Terwilliger, T. C., and Zwart, P. H. (2010) PHENIX: a comprehensive Python-based system for macromolecular structure solution. *Acta Crystallogr. D* **66**, 213-221

34. Emsley, P., and Cowtan, K. (2004) Coot: model-building tools for molecular graphics. *Acta Crystallogr. D* **60**, 2126-2132
35. Murshudov, G. N., Vagin, A. A., and Dodson, E. J. (1997) Refinement of macromolecular structures by the maximum-likelihood method. *Acta Crystallogr. D* **53**, 240-255
36. McNicholas, S., Potterton, E., Wilson, K. S., and Noble, M. E. (2011) Presenting your structures: the CCP4mg molecular-graphics software. *Acta Crystallogr. D* **67**, 386-394
37. Robinson, R., Franceschini, S., Fedkenheuer, M., Rodriguez, P. J., Ellerbrock, J., Romero, E., Echandi, M. P., Martin Del Campo, J. S., and Sobrado, P. (2014) Arg279 is the key regulator of coenzyme selectivity in the flavin-dependent ornithine monooxygenase SidA. *Biochim. Biophys. Acta* **1844**, 778-784
38. Dudek, H. M., Torres Pazmino, D. E., Rodriguez, C., de Gonzalo, G., Gotor, V., and Fraaije, M. W. (2010) Investigating the coenzyme specificity of phenylacetone monooxygenase from Thermobifida fusca. *Appl. Microbiol. Biotechnol.* **88**, 1135-1143
39. Torres Pazmino, D. E., Baas, B. J., Janssen, D. B., and Fraaije, M. W. (2008) Kinetic mechanism of phenylacetone monooxygenase from Thermobifida fusca. *Biochemistry* **47**, 4082-4093
40. Hayward, S., and Berendsen, H. J. (1998) Systematic analysis of domain motions in proteins from conformational change: new results on citrate synthase and T4 lysozyme. *Proteins* **30**, 144-154
41. Mirza, I. A., Yachnin, B. J., Wang, S., Grosse, S., Bergeron, H., Imura, A., Iwaki, H., Hasegawa, Y., Lau, P. C., and Berghuis, A. M. (2009) Crystal structures of cyclohexanone monooxygenase reveal complex domain movements and a sliding cofactor. *J. Am. Chem. Soc.* **131**, 8848-8854
42. Orru, R., Dudek, H. M., Martinoli, C., Torres Pazmino, D. E., Royant, A., Weik, M., Fraaije, M. W., and Mattevi, A. (2011) Snapshots of enzymatic baeyer-villiger catalysis: oxygen activation and intermediate stabilization. *J. Biol. Chem.* ***286****, 29284-29291.*
43. Karplus, P. A., and Diederichs, K. (2012) Linking crystallographic model and data quality. *Science* **336**, 1030-1033

CHAPTER 11

Conclusions

This dissertation presents detailed mechanistic and structural studies on the L-ornithine monooxygenase SidA and the L-lysine monooxygenases NbtG and MbsG. These enzymes are members of the microbial *N*-hydroxylating monooxygenases (NMOs) and are critical in the biosynthesis of hydroxamate-containing siderophores which competitively chelate Fe^{III}. NMOs are potential drug targets in a number of pathogenic organisms such as *Aspergillus fumigatus*, *Mycobacterium tuberculosis*, and *Pseudomonas aeruginosa* among others as disruption of their biochemical function would lead to the inability of the invading pathogen to uptake Fe^{III} which is an essential nutrient.

The detailed chemical mechanism of flavin oxidation in SidA was determined (Chapters 3, 4). Protonation of the C4a-hydroperoxyflavin in SidA occurs through the 2'-OH of the nicotinamide ribose. This 2'-OH group is part of a water and phosphate mediated proton shuttle network that connects to bulk solvent and allows for reprotonation of the 2'-OH after proton transfer to the intermediate. After formation of the C4a-hydroperoxyflavin, L-ornithine binds where the N^5 is deprotonated by an altered pK_a value in the active site of SidA. This allows for electrophilic oxygenation by the distal oxygen of the C4a-hydroperoxyflavin to the nucleophilic terminal amine group of L-ornithine. The resulting C4a-hydroxyflavin is then dehydrated through a partially rate-limiting single proton transfer from the N5 of the flavin. This is similar to the chemical steps of hydrogen peroxide elimination where a proton is also transferred from the N5 of the flavin. In the C4a-hydroperoxyflavin form, the N5 proton forms a hydrogen bond to the carbonyl of the nicotinamide ribose which makes it unavailable for transfer to the hydroperoxide group, contributing to the stability of the C4a-hydroperoxyflavin.

Mutagenesis of active site residues in SidA were performed in order to determine important residues involved in substrate binding and catalysis. Chapter 5 provides data which highlights the importance of the electrostatic interaction provided by Arg279 to the phosphate of NADPH in coenzyme selectivity. This provides a ~70-fold selectivity for NADPH over NADH and a K_D value for NADPH of ~1 μM. Four residues (Lys107, Asn293, Asn323, and S469) coordinate binding of L-ornithine in the active site (Chapter 6). Lys107, Asn293, and S469 interact with the α-amino and α-carboxylate groups of L-ornithine which provide specificity for L-ornithine over D-ornithine. Asn323 hydrogen bonds with the N^5 of L-ornithine and properly positions the N^5 for oxygen transfer. Asn323 also helps to control the "sliding" of NADPH as it interacts with the 3'-OH of the nicotinamide ribose.

Chapter 7 provides data which show that three residues, Met101, Gln102, and Arg144 are important for flavin oxidation in SidA. Met101 properly positions the isoalloxazine ring of the flavin to efficiently hydroxylate L-ornithine. Removal of this interaction results in the isoalloxazine ring of the flavin to be flipped to an "out" position and prevents oxygen transfer from the C4a-hydroperoxyflavin. Gln102 is part of a hydrogen bonding network with $NADP^+$ and the C4a-hydroperoxyflavin which contributes to its stability. Arg144 has two functions, both of which contribute to efficient hydroxylation and flavin oxidation. Arg144 positions the amide group of $NADP^+$ to hydrogen bond with the N5 proton so that it is unavailable for hydrogen peroxide elimination. Also, this positioning allows for the amide group to act as a proton shuttle mediator in the chemical steps of flavin dehydration. This data helps to highlight the complexity of the active site in SidA and the numerous interactions which provide for a stable C4a-hydroperoxyflavin.

Despite the similar function of SidA to NbtG and MbsG, there is a divergence in the details of the mechanism with the L-lysine monooxygenases. First, hydride transfer is rate-limiting in SidA, typical of Class B monooxygenases; whereas in NbtG and MbsG, hydride transfer is only partially rate-limiting (Chapters 9, 10). Another difference is SidA displays a clear preference for NADPH over NADH, while NbtG and MbsG utilize either cofactor indiscriminately. Probably the most drastic disparity observed in this study is the differences in stabilities of the C4a-hydroperoxyflavins. In SidA, this intermediate is very stable leading to efficient hydroxylation (~100% coupled) and minimal production of reactive oxygen species. In NbtG and MbsG however, this intermediate is transient where more hydrogen peroxide and superoxide are produced than hydroxylated lysine (~30% coupled).

The first structure of an L-lysine monooxygenase (NbtG) is presented in this dissertation and helps to provide some clarity among these mechanistic discrepancies (Chapter 10). The structure of NbtG shows that the NAD(P)H-binding domain is rotated 30 º relative to the NADPH-binding domain in SidA. This might rationalize the differences in the observed kinetic isotope effects for hydride transfer in flavin reduction. In SidA after NADPH binding, there is no evidence of any large domain movements that are important for flavin reduction to occur. In NbtG however, this domain would need to rotate in order to allow for NADPH to bind and transfer a hydride equivalent. Therefore, this conformational change in NbtG, and possibly MbsG, might be the rate-limiting step in catalysis.

Along with providing for a different rate-limiting step in the L-lysine monooxygenases, the NAD(P)H-binding domain in NbtG could also justify the lack of a stable C4a-hydroperoxyflavin. In Class B monooxygenases, proper interaction by $NADP^+$ is essential for the stabilization of the C4a-hydroperoxyflavin. In SidA, $NADP^+$ shields the C4a-hydroperoxyflavin

from bulk solvent and provides interaction with the distal oxygen and N5 of the C4a-hydroperoxyflavin, preventing hydrogen peroxide elimination. The rotation of the NAD(P)H-binding domain would block the adoption of this conformation in NbtG. Furthermore, the weakened affinity for NAD(P)H when compared to SidA, might cause for release of NAD(P)H in the L-lysine monooxygenases after reduction. This would account for the transience of the C4a-hydroperoxyflavins in NbtG and MbsG.

A direct result of the lack of stable intermediates in the L-lysine monooxygenases is the production of hydrogen peroxide and superoxide. Intracellular relevance for this oxidase activity is currently unknown, but it could be important in reactive oxygen species generation and signaling. Also, there exists the possibility this oxidase activity is not even important as enzymes such as catalase and superoxide dismutase scavenge for reactive oxygen species and have k_{cat} values several orders of magnitude faster than MbsG or NbtG. Lastly, another protein *in vivo* could interact with these L-lysine monooxygenases and channel activity towards hydroxylation. Future studies will need to be performed in order to explain the role of the oxidase activities observed here and provide merit to any of these hypotheses.

In summary, this dissertation advances the knowledge of the mechanisms and structures of NMOs. Future efforts are needed in order to justify the mechanistic and structural discrepancies raised here among this family. This could be accomplished by studying other members from this family as well as the generation of more structures, particularly L-lysine monooxygenases with $NAD(P)^+$ and L-lysine bound. Also, more work needs to be performed in identifying inhibitors of NMOs. Our lab has developed a high throughput screening assay for chemical libraries in SidA which can be used to identify potential inhibitors of NMOs. The discovery of a molecular "scaffold" could then be improved upon rationally by the work

presented here. This, and future studies hopefully will someday result in the development of drugs to treat among other infections, aspergillosis and tuberculosis.